

ASSESSING METHODS FOR PREDICTING RETROFIT ENERGY SAVINGS IN BUILDINGS: CASE STUDY OF A NORWEGIAN SCHOOL

by

Elizabeth Ricker

B.S., Mechanical Engineering
Tufts University, 2006

Submitted to the Department of Mechanical Engineering
In Partial Fulfillment of the Requirements for the Degree of
Master of Science in Mechanical Engineering

at the

Massachusetts Institute of Technology

June 2008

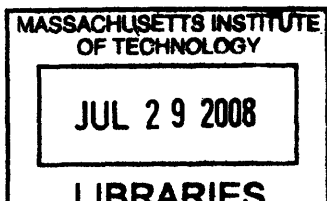
© 2008 Massachusetts Institute of Technology
All rights reserved

Signature of Author.....
Department of Mechanical Engineering
May 9, 2008

Certified by
Leon Glicksman
Professor of Building Technology and Mechanical Engineering

Certified by
Leslie Norford
Professor of Building Technology

Accepted by
Lallit Anand
Chairman, Department Committee on Graduate Students



ARCHIVES

ASSESSING METHODS FOR PREDICTING RETROFIT ENERGY SAVINGS IN
BUILDINGS: CASE STUDY OF A NORWEGIAN SCHOOL

by

Elizabeth Ricker

Submitted to the Department of Mechanical Engineering
on May 9th, 2008 in Partial Fulfillment of the
Requirements for the Degree of Master of Science in
Mechanical Engineering

at the

Massachusetts Institute of Technology

June 2008

© Massachusetts Institute of Technology
All rights reserved

ABSTRACT

This work investigates methods for predicting retrofit energy savings in existing Norwegian buildings. A case study is performed on a 30 year old primary school in Trondheim, Norway. The energy consumption in the school is simulated with the EnergyPlus computer software and calibrated against measured utility data. Two simulation calibration techniques are investigated: manual calibration and Latin Hypercube Monte Carlo (LHMC) analysis. LHMC is a statistical technique for calibrating building energy simulations, whereas manual calibrations are tuned by the modeler. Calibrated simulations are then used to predict the potential for energy savings under a number of retrofit conditions. Methods of quantifying the uncertainty in energy savings predictions are also investigated.

The LHMC is shown to be most appropriate for models with a high number of uncertain building simulation inputs and when monthly utility data is available. However, manual calibration is found to be more suitable for simulations with fewer uncertain inputs and when hourly utility data is available. The retrofit analysis with the manually calibrated model predicted savings of up to 55% of the 173 kWh/m² base-year energy consumption in the case study building.

Thesis Supervisor: Leon Glicksman

Supervisor Title: Professor of Building Technology and Mechanical Engineering

Acknowledgements

I would like to thank my professors and colleagues in the Building Technology Department at MIT. Their knowledge, patience, and good humor have been exceptional resources.

I would especially like to thank Professors Leon Glicksman, Les Norford, and Steve Connors for their guidance and support over the course of this project.

I am extremely grateful to Professor Anne Grete Hestnes at NTNU, and Bjørn Bakken and Bjørn Wachenfeldt at SINTEF. Their insight and guidance during my stay in Norway, and throughout this work, were fundamental to the success of this project.

I would like to extend a very sincere thank you to Igor Sartori of NTNU. He was a tremendous asset to me throughout this work, and I am very appreciative of his willingness to share his knowledge and experience.

I would like to thank my friends and family whose support and encouragement have kept me buoyed through some of the more challenging parts of this project.

I would especially like to thank Dave whose patience, love, and support were more than I could have asked for.

This work is dedicated to Brian Wrigley.

Table of Contents

1	Introduction.....	24
1.1	Motivation.....	24
1.2	Problem Statement.....	24
1.3	Outline of Work.....	25
2	Background on Norway.....	26
2.1	Geography and Topography.....	26
2.2	People and Government.....	26
2.3	Economy.....	27
2.4	Energy Supply and Demand.....	28
2.5	Norwegian Building Codes.....	30
2.6	Energy Performance in Buildings Directive (EPBD).....	35
3	Procedures for Evaluating Energy and Demand Savings.....	38
3.1	General Energy Savings Evaluation Procedures.....	38
3.2	Calibrated Simulations and Energy Conservation Measure (ECM) Savings Estimation 41	
3.3	ASHRAE RP-1051 [Reddy 2006].....	69
4	Retrofit Analysis: Case Study.....	75
4.1	Selection of a Case Study Building.....	76
4.2	Presentation of Case Study: Steindal School.....	82
5	Data Collection.....	84
5.1	Collected Data.....	85
5.2	Summary of Collected Data.....	132
5.3	Sources of Uncertainty.....	135
6	Simple Estimates and Input Verification.....	138
6.1	Annual Steady-State Energy Consumption.....	138
6.2	Infiltration Rates: Qualitative Assessment.....	153
6.3	Lessons Learned.....	164
7	Calibration.....	165
7.1	Metrics for Calibration.....	165
7.2	Manual Calibration.....	168
7.3	Latin Hypercube Monte Carlo Analysis.....	187
7.4	Lessons Learned: Calibration.....	202
8	Retrofits.....	204
8.1	Base-year Adjustments.....	206
8.2	Retrofit Identification and Overview.....	210
8.3	Individual Retrofit Analysis.....	231
8.4	Parametric Analysis.....	265
8.5	Lessons Learned.....	276

9	Conclusions	278
9.1	Steindal School Case Study: Implications of Energy Savings Results.....	282
10	General Procedure for Performing Energy Conservation Measure (ECM) Evaluations with Calibrated Simulations	284
10.1	Input.....	286
10.2	Calibration.....	286
10.3	Retrofit.....	289
11	Future Work	291
Appendix A	Considerations in Building Energy Simulation: Steady-state vs. Transient Building Models	292
A.1	Thermal Mass Analysis.....	292
A.2	Lessons Learned.....	306
Appendix B	Supplementary Information	307
B.1	Preliminary EPBD Certification Values	307
B.2	Additional Retrofit Results	308
Appendix C	Calculations	312
C.1	UA-Value of the heating coil.....	312
C.2	Heating Contribution from Thermal Mass.....	314
C.3	Ground Heat Loss Calculation.....	322
References	326

List of Figures

Figure 2-2: Gross domestic product (GDP) per capita of selected countries reported for 2004-2007 (USD/person) [Factbook 2008a].....	27
Figure 2-3: Annual domestic energy demand in Norway by energy carrier from.....	28
Figure 2-4: Annual electricity supply in Norway, by energy supplier, 1989-2005 (TWh) [Statbank 2007].....	29
Figure 2-5: Domestic energy consumption in Norway by consumer type (TWh). “Other consumers” is comprised largely of commercial buildings [Statbank 2007].....	29
Figure 2-6: Minimum energy consumption requirements for new constructions and major renovations in houses, building blocks, kindergartens, offices, schools, university buildings, hospitals, nursing homes, hotels, sports facilities, business buildings, cultural buildings, and industrial buildings in Norway [Gustavsen 2007]. All values are given in energy consumption per unit of conditioned floor area (kWh/m ² -year).....	34
Figure 2-7: Example EPBD certificate for Norwegian buildings [Wigenstad 2005].....	35
Figure 3-1: Summary of recommended procedures for evaluating ECM energy savings according to ASHRAE Guideline 14 [ASHRAE 14 2002] and the IPMVP [IPMVP 2002].	39
Figure 3-2: Energy savings uncertainty at 95% confidence and 5% (solid), 10% (short dash), and 15% (long dash) CVRMSE [ASHRAE 14 2002].	64
Figure 3-3: Energy savings uncertainty at 90% confidence and 5% (solid), 10% (short dash), and 15% (long dash) CVRMSE [ASHRAE 14 2002].	65
Figure 3-4: Energy savings uncertainty at 80% confidence and 5% (solid), 10% (short dash), and 15% (long dash) CVRMSE [ASHRAE 14 2002].	65
Figure 3-5: Energy savings uncertainty at 68% confidence and 5% (solid), 10% (short dash), and 15% (long dash) CVRMSE [ASHRAE 14 2002]. The red line indicates the maximum uncertainty for	66
Figure 3-6: Procedure for calibrating building energy simulations recommended in ASHRAE RP-1051 [Reddy 2006].	70
Figure 4-1: Steps that were taken in performing the case study.	75
Figure 4-2: Energy consumption in the Norwegian building stock by building type [Sartori 2008a]. Schools and Offices are the slices that are removed from the pie. Holiday houses are vacation homes that are occupied intermittently.....	79
Figure 4-3: Image of the Steindal School, looking at the North façade of the building.	82

Figure 5-1: Cumulative weekly energy consumption in the Steindal School from 2004 through 2006.....	86
Figure 5-2: Location of weather stations for collecting data to describe the conditions at the Steindal School [MET 2007],[Bioforsk 2007],[Factbook 2008a].	88
Figure 5-3: Global radiation data from Trondheim, Oslo, and Bergen in Norway and Ostersund in Sweden.....	89
Figure 5-4: North and South façades of the Steindal School. Note the shading from the three entrance wardrobes on the South façade [Hestnes 2007b].	90
Figure 5-5: Building floor plan, taken from as-built documents	92
Figure 5-6: Simplified layout of the Steindal School’s floor plan, including dimensions. All dimensions are in meters. The brown areas indicate ground and the black hatched area indicates the building roof.	93
Figure 5-7: Window dimensions for those windows on the North and South façades of the Steindal School. Drawing not to scale.	94
Figure 5-8: Layout of building zones based on building usage. The Underroof is directly above the North half of the 1st Floor (classrooms) and Gym. The hatched black area indicates the roof of the building.	95
Figure 5-9: North and South wall constructions in the Main building and Annex of the Steindal School. Applicable Main building walls are highlighted in red, while the Annex walls are highlighted in magenta.....	101
Figure 5-10: East and West wall constructions in the Main building and Annex. Applicable Main building walls are highlighted in red, while the Annex walls are highlighted in magenta.	102
Figure 5-11: South roof ridge wall construction. Applicable Main building walls are highlighted in red, while the Annex walls are highlighted in magenta.....	102
Figure 5-12: Ground wall construction. Applicable Main building walls are highlighted in red, while the Annex walls are highlighted in magenta.	103
Figure 5-13: Roof constructions in the Main building and Annex. Main building roofs are highlighted in red (South) and blue (North), Annex roofs are highlighted in magenta, and Wardrobe roofs are highlighted in orange.	103
Figure 5-14: Location of roof constructions in the Steindal School. Main building roofs are highlighted in red (South) and blue (North), Annex roofs are highlighted in magenta, and Wardrobe roofs are orange.....	104

Figure 5-15: Vertical cross-section of Steindal School showing the Offices, Bomb Shelter, 1 st Floor, and Underroof. The location of the mineral wool in the North roof over the 1 st Floor classrooms is indicated.	104
Figure 5-16: Window locations in the Steindal School. Solid red circles and lines indicate the location of the North windows, dashed red lines and circles indicate the location of the South windows, and magenta lines and circles indicate the location of the Annex windows.	106
Figure 5-17: Schematic layout for a generic rotary wheel heat recovery unit.....	124
Figure 5-18: Main ventilation system heat recovery effectiveness measurements from Municipality data. The data are split into measurements taken in the Spring (filled diamonds) and Fall (unfilled triangles).....	126
Figure 5-19: Annex ventilation system heat recovery effectiveness measurements from Municipality data. All measurements were made between February and March in 2007 [Municipality 2007b].	127
Figure 5-20: Cross-section of the Main ventilation system heat recovery layout. Note the placement of the temperature probe. Drawing not to scale.....	128
Figure 6-1: Energy balance in the Steindal School. This balance accounts for all heat flows into and out of the interior of the building.	139
Figure 6-2: Annual energy consumption in typical Norwegian schools and the Steindal School. The results of the annual steady-state calculation and the 2006 measured electricity consumption in the Steindal School are both shown.	152
Figure 6-3: Heating contribution from thermal mass on weekends in the Steindal School. The calculated heating contribution from the interior thermal mass in the Steindal School is shown. Also shown is the measured hourly energy consumption for all data points occurring from 5 p.m. (0 th hour, x-axis) on Friday through midnight (55 th hour, x-axis) on Sunday when $T_{\text{outdoor}} = 0\pm 2^{\circ}\text{C}$ and windspeed < 2 m/s at the Steindal School in 2006. “Total” refers to all walls, ceilings, and floors that are made of thermal massive materials and are located on the inside of the building. “Internal” refers only to those building surfaces that separate building zones. “External” refers to all walls, roofs, and floors that are located on the exterior surfaces of the building, but that face the interior space. These surfaces are discussed in detail in section C.2 of Chapter Appendix C.....	156
Figure 6-4: Energy demand (kW) versus wind speed (m/s) at outdoor temperatures of $0^{\circ}\text{C}+1^{\circ}\text{C}$ during the night time hours on Saturdays and Sundays in the Steindal School in 2006. Wind data was from Kvithamar, Norway.....	158
Figure 6-5: Energy demand (kW) versus wind speed (m/s) at outdoor temperatures of $5^{\circ}\text{C}+1^{\circ}\text{C}$ during the night time hours on Saturdays and Sundays in the Steindal School in 2006. Wind data was from Kvithamar, Norway.....	159

Figure 6-6: Energy demand (kW) versus wind speed (m/s) at outdoor temperatures of $-5^{\circ}\text{C}/+1^{\circ}\text{C}$ during the night time hours on Saturdays and Sundays in the Steindal School in 2006. Wind data was from Kvithamar, Norway..... 159

Figure 6-7: Map of weather stations near the Steindal School where wind data was collected 161

Figure 6-8: Average daily wind speed in 2006 at Kvithamar, Skjetlein, Frosta, Rissa, and Mære weather stations (m/s). 162

Figure 6-9: Energy demand (kW) versus wind speed (m/s) with 2006 wind data from various weather stations near the Steindal School. All data shown had an outdoor temperature of $0^{\circ}\text{C}/+1^{\circ}\text{C}$ and occurred during the night time hours on Saturdays and Sundays in the Steindal School in 2006. (a) Skjetlein; (b) Frosta; (c) Mære; (d) Rissa..... 163

Figure 7-1: Fit between simulated and measured energy consumption for June (hours 3625-4344 in 2006). The Original calibrated model is shown by the dashed red line and the measured hourly utility data is shown by the solid black line. The hour of the year is along the x-axis (h), while the hourly energy consumption (kWh/h) is along the y-axis. 171

Figure 7-2: Fit between simulated and measured energy consumption for February (hours 745-1417 in 2006). The Original calibrated model is shown by the dashed red line and the measured hourly utility data is shown by the solid black line. The hour of the year is along the x-axis (h), while the hourly energy consumption (kWh/h) is along the y-axis..... 175

Figure 7-3: Fit between simulated and measured energy consumption for November (hours 7927-8647 in 2006). The Original calibrated model is shown by the dashed red line and the measured hourly utility data is shown by the solid black line. The hour of the year is along the x-axis (h), while the hourly energy consumption (kWh/h) is along the y-axis..... 175

Figure 7-4: Monthly fit between simulated and measured energy consumption in 2006. The Original calibrated model is shown by the dashed red line and the measured utility data is shown by the solid black line. The month is along the x-axis, while the monthly energy consumption (kWh) is along the y-axis. 177

Figure 7-5: Weekly fit between simulated and measured energy consumption in 2006. The Original calibrated model is shown by the solid grey line, the Corrected model is shown by the dashed red line, and the measured utility data is shown by the solid black line. The week is numbered along the x-axis, while the weekly energy consumption (kWh) is along the y-axis. 180

Figure 7-6: Weekly fit between simulated and measured peak power demand in 2006. The Original calibrated model is shown by the solid grey line, the Corrected model is shown by the dashed red line, and the measured utility data is shown by the solid black line. The week is numbered along the x-axis, while the peak power consumption (kW) is along the y-axis. 180

Figure 7-7: Hourly profiles for Original and Corrected manually calibrated models for January 23rd through January 27th, 2006. The Original calibrated model is shown by the solid grey

line, the Corrected model is shown by the dashed red line, and the measured utility data is shown by the solid black line. The hour of the year is numbered along the x-axis, while the hourly energy consumption (kWh) is along the y-axis. 181

Figure 7-8: Hourly energy consumption profiles from the Original and Corrected manually calibrated models for April 24th through April 30th, 2006. The Original calibrated model is shown by the solid grey line, the Corrected model is shown by the dashed red line, and the measured utility data is shown by the solid black line. The hour of the year is numbered along the x-axis, while the hourly energy consumption (kWh) is along the y-axis..... 181

Figure 7-9: Hourly profiles for Original and Corrected manually calibrated models for July 31st through August 6th, 2006. The Original calibrated model is shown by the solid grey line, the Corrected model is shown by the dashed red line, and the measured utility data is shown by the solid black line. The hour of the year is numbered along the x-axis, while the hourly energy consumption (kWh) is along the y-axis. 182

Figure 7-10: Hourly profiles for Original and Corrected manually calibrated models for October 16th through October 22nd, 2006. The Original calibrated model is shown by the solid grey line, the Corrected model is shown by the dashed red line, and the measured utility data is shown by the solid black line. The hour of the year is numbered along the x-axis, while the hourly energy consumption (kWh) is along the y-axis. 182

Figure 7-11: Annual end-use specific energy and peak power distribution resulting from manual calibration of the Original and Corrected models. The specific energy consumption and peak annual power demand are shown along the x-axes for each model (y-axis). The specific energy consumption was calculated as the total annual energy consumption, divided by the 4,400 m² of conditioned floor area..... 184

Figure 7-12: Comparison of the annual specific energy consumption in the Original model, Corrected model, Simple model, typical Norwegian schools, and the 2006 measured utility data in the Steindal School. The specific energy consumption is shown along the x-axis for each model (y-axis). The specific energy consumption was calculated as the total annual energy consumption, divided by the 4,400 m² of conditioned floor area. 185

Figure 7-13: Monthly end-use load distributions resulting from the manually calibrated Original and Corrected building models. The specific energy consumption is shown along the x-axis for each model (y-axis). The specific energy consumption was calculated as the total annual energy consumption, divided by the 4,400 m² of conditioned floor area. 186

Figure 7-15: Floor plan of the Steindal School, including zone labels..... 189

Figure 7-16: Goodness-of-fit (GOF) vs. Normal Mean Bias Error (NMBE) for the LHMC calibrated Detailed-Corrected, Detailed-Original, and Simple models run with 500 simulations (left) and 2000 simulations (right). The grey dot indicates the manually calibrated solution in the Detailed-Original and Detailed-Corrected models and the original “best guess” simulation in the Simple model. All results are for 2006. 195

- Figure 7-17: Energy (kWh, left) and Power (kW, right) vs. month of the year. The “best guess” is shown by the solid grey line, the best calibrated model (lowest GOF) is shown by the dashed black line, and the measured utility data is shown by the solid black line. All results are for the year 2006. 196
- Figure 7-18: Distribution of parameter states for the Detailed-Corrected, Detailed-Original, and Simple LHMC calibrated models. The distribution of all of the calibrated candidates (“all candidates”, left graph) and Top 20 solutions (“Top 20 GOF”, right graph) are shown for each model. Results are from the 2000 LHMC runs..... 199
- Figure 8-1: Steps followed in performing the retrofit analysis of the Steindal School. 204
- Figure 8-2: Monthly energy consumption of the four models that were developed in each step of the base-year model definition (kWh/m²). The monthly utility data from 2006 and 2007 are also shown. The results are for the Corrected building model..... 209
- Figure 8-3: Monthly CVRMSE (%) vs. annual energy savings, F (%). The black line indicates combinations of the CVRMSE and F that result in 50% uncertainty in retrofit energy savings prediction at 68% confidence, as calculated with Equation 8-3. Similarly, the dashed grey line equates to 25% uncertainty at 68% confidence and the solid grey line represents 50% uncertainty at 95% confidence. The dashed red line indicates the threshold monthly CVRMSE for calibrated simulations, as per ASHRAE Guideline 14 [ASHRAE 14 2002]. The orange line indicates the 5% minimum energy savings required for acceptable retrofit energy savings in RP-1051[Reddy 2006], while the yellow line indicates the recommended 10% energy savings for acceptable retrofit energy savings in RP-1051 [Reddy 2006]. The grey area highlights the plausible retrofit space defined in ASHRAE Guideline 14 [ASHRAE 14 2002], while the green areas indicate the plausible retrofit areas (light green – maximum solution space, dark green – recommended solution space) defined in RP-1051[Reddy 2006]. The retrofit energy savings data points shown by the various colored diamonds, squares, circles, and triangles are from the low-energy Individual Retrofit of the Corrected model of the Steindal School..... 234
- Figure 8-4: Hourly CVRMSE (%) vs. annual energy savings, F (%). The black line indicates combinations of the CVRMSE and F that result in 50% uncertainty in retrofit energy savings prediction at 68% confidence, as calculated with Equation 8-3. Similarly, the solid grey line represents 50% uncertainty at 68% confidence, as calculated with Equation 8-4 with n’ equal to 318. The dashed red line indicates the threshold monthly CVRMSE for calibrated simulations, as per ASHRAE Guideline 14 [ASHRAE 14 2002]. The retrofit energy savings data points shown by the various colored diamonds, squares, circles, and triangles are from the low-energy Individual Retrofit of the Corrected model of the Steindal School. 238
- Figure 8-5: Monthly goodness-of-fit (%) vs. predicted annual energy savings (%) from the temperature setback retrofit, as simulated with the manually calibrated Original and Corrected models and the Top 20 solutions of the Detailed-Original, Detailed-Corrected, and Simple LHMC calibrated models. The manually calibrated models are bounded by their savings uncertainty (U*F). Increasingly negative energy savings indicate increased

energy savings from the base-year. Increasing GOF indicates a poorer fit between the calibrated model and measured utility data..... 245

Figure 8-6: Monthly goodness-of-fit (%) vs. predicted annual energy savings (%) from the ventilation rate retrofit, as simulated with the manually calibrated Original and Corrected models and the Top 20 solutions of the Detailed-Original, Detailed-Corrected, and Simple LHMC calibrated models. The manually calibrated models are bounded by their savings uncertainty (U*F). Increasingly negative energy savings indicate increased energy savings from the base-year. Increasing GOF indicates a poorer fit between the calibrated model and measured utility data. 247

Figure 8-7: Monthly goodness-of-fit (%) vs. predicted annual energy savings (%) from the occupant controlled ventilation retrofit, as simulated with the manually calibrated Original and Corrected models and the Top 20 solutions of the Detailed-Original, Detailed-Corrected, and Simple LHMC calibrated models. The manually calibrated models are bounded by their savings uncertainty (U*F). Increasingly negative energy savings indicate increased energy savings from the base-year. Increasing GOF indicates a poorer fit between the calibrated model and measured utility data..... 247

Figure 8-8: Ventilation rate retrofit annual energy consumption and load distribution (kWh/m²/year). The mean load distribution of the Top 20 solutions from the Simple and Detailed-Original LHMC calibrated models are shown. 249

Figure 8-9: Occupant controlled ventilation retrofit annual energy consumption and load distribution (kWh/m²/year). The mean load distribution of the Top 20 solutions from the Simple and Detailed-Original LHMC calibrated models are shown. 249

Figure 8-10: Monthly goodness-of-fit (%) vs. predicted annual energy savings (%) from the heat recovery effectiveness retrofit, as simulated with the manually calibrated Original and Corrected models and the Top 20 solutions of the Detailed-Original, Detailed-Corrected, and Simple LHMC calibrated models. The manually calibrated models are bounded by their savings uncertainty (U*F). Increasingly negative energy savings indicate increased energy savings from the base-year. Increasing GOF indicates a poorer fit between the calibrated model and measured utility data..... 250

Figure 8-11: Monthly goodness-of-fit (%) vs. predicted annual energy savings (%) from the infiltration rate retrofit, as simulated with the manually calibrated Original and Corrected models and the Top 20 solutions of the Detailed-Original, Detailed-Corrected, and Simple LHMC calibrated models. The manually calibrated models are bounded by their savings uncertainty (U*F). Increasingly negative energy savings indicate increased energy savings from the base-year. Increasing GOF indicates a poorer fit between the calibrated model and measured utility data. 252

Figure 8-12: Electricity billing production tariffs from the Steindal School for the periods from January 2004-August 2007 (NOK/kWh) [Skjennald 2007]. 256

Figure 8-13: Monthly utility billing (NOK) and electricity consumption (kWh) from the Steindal School for the period from January 2004 through December 2007..... 257

Figure 8-14: Total annual cost of all Individual Retrofits at their moderate retrofit state. Total annual costs are shown at a 1%, 2%, 4%, 7%, and 10% interest rate. All results are from the manually calibrated Corrected model (NOK/year).....	262
Figure 8-15 : Total annual cost of all Individual Retrofits at their low-energy retrofit state. Total annual costs are shown at a 1%, 2%, 4%, 7%, and 10% interest rate. All results are from the manually calibrated Corrected model (NOK/year).....	263
Figure 8-16: Annual energy savings (%) and total annual cost (NOK/year) of all Individual Retrofits at their moderate retrofit state. The interest rate was 4%; all results are from the Corrected model.....	264
Figure 8-17: Annual energy savings (%) and total annual cost (NOK/year) of all Individual Retrofits at their low-energy retrofit state. The interest rate was 4%; all results are from the Corrected model.....	265
Figure 8-18: Results of the Parametric Retrofit analysis with the temperature setback, ventilation rate, occupant controlled ventilation, heat recovery effectiveness, and infiltration rates retrofits. All results are from the manually calibrated Corrected model.	268
Figure 8-19: Annual energy consumption (kWh/m ² /year) and total annual cost (NOK/year) for a number of retrofits from the Parametric Analysis. The annual energy consumption in the base-year of the Corrected model and a typical Norwegian school are also shown.....	272
Figure 10-1: Recommended procedure for performing future retrofit analyses.....	285
Figure A-1: Geometry of building for thermal mass analysis.	293
Figure A-2: Summary of input conditions for the building façade in the thermal mass analysis. The green values are for the poor energy performance, or “Old”, scenario; the white boxes highlight the excellent energy performance, or “New”, scenario.....	294
Figure A-3: Outdoor temperature and indoor temperature variation, with vs. without thermal mass.....	298
Figure A-4: Total energy consumption resulting from the thermal mass analysis.....	299
Figure A-5: Difference in the required power for heating and cooling in the thermal mass analysis.....	300
Figure A-6: Change in indoor temperature due to increased temperature setback (from 2 to 6 °C). The graph refers to the case with thermal mass.....	302
Figure A-7: Change in heating energy due to increased temperature setback (from 2 to 6 °C).	303
Figure A-8: Change in heating power demand due to increased temperature setback (from 2 to 6 °C).....	304

Figure A-9: Change in heating and cooling energy with variation of thermal mass. Changes to thermal mass are made in the thickness. 305

Figure A-10: Change in heating and cooling peak power demand with variation of thermal mass. Changes to thermal mass are made in the thickness. 305

Figure A-11: Indoor air temperature for various volumes of thermal mass. 306

Figure C-1: Heating contribution of the internal thermal mass in the Steindal School, expressed as energy released (kWh) vs. time (hr). “INTERNAL” represents the heating contribution from internal building surfaces, while “EXTERNAL” represents the heating contribution from all exterior building surfaces. “TOTAL” is the sum of the two heating contributions. 321

List of Tables

Table 2-1: Envelope U-value and window area requirements from the energy section of the.....	30
Table 2-2: Wind exposure coefficients for infiltration calculations [NS3031 2007].	31
Table 2-3: Outdoor airflow requirements for acceptable indoor air quality.....	31
Table 2-4: Minimum outdoor air flow rates from European standards, EN 13779 [EN13779 2004].	32
Table 2-5: Minimum outdoor air flow rates from ASHRAE Standard 62-2004 [ASHRAE 62 2004]. The number of expected people per m ² should only be used when the actual occupancy is unknown.	33
Table 2-6: Temperature setpoints and schedules for typical houses, building blocks, kindergartens, offices, schools, and university buildings in Norway [Gustavsen 2007],[NS3031 2007].	33
Table 2-7: Recommended values for temperature independent loads and internal gains in houses, building blocks, kindergartens, offices, schools, and university buildings in Norway [NS3031 2007]......	34
Table 2-8: Energy consumption requirements for obtaining various EPBD ratings	36
Table 2-9: Modification factors to account for various primary energy sources when calculating the EPBD rating for Norwegian buildings [Wigenstad 2005].	37
Table 3-1: Summary of methods for estimating retrofit energy savings. All data was taken from ASHRAE Guideline 14 [ASHRAE 14 2002], except where indicated (IPMVP) [IPMVP 2002].	40
Table 3-2: Procedure for calibrating whole building simulations, as recommended by	41
Table 3-3: Summary of building energy simulation articles [Norford 1994],[Pan 2006],[Pedrini 2002],[Westphal 2005],[Yoon 2003],[Zhu 2006], [Tamburrini 2003],.....	42
Table 3-4: Measurement techniques for defining building energy	45
Table 3-5: Six levels of simulation input data quality from RP-1051[REDDY 2006]......	47
Table 3-6: Summary of commonly used building energy simulation software [EERE 2008A]. .	49
Table 3-7: Threshold values of the NMBE and CVRMSE statistics required to accept simulations to be calibrated on a monthly basis [ASHRAE 14 2002].	53
Table 3-8: Influence and sensitivity coefficients for quantifying the impact of a parameter on a building energy model [Lam 1996]. ΔOP is the change in the output of interest, OP_{bc} is the	

base case value of the output, ΔIP is the change in the input, and IP_{bc} is the base case value of the input.	57
Table 3-9: Values of the t-statistic for quantifying confidence in retrofit energy savings predictions during uncertainty analysis. Where, $p = 1$ for calibrated simulations and n is the number of time steps in the simulation period [ASHRAE 14 2002].	64
Table 3-10: Values of the χ^2 statistic, organized according to confidence interval. D.f. stands for the number of degrees of freedom, equal to the number of parameter states (n), less 1 ($n-1$).	72
Table 3-11: Example input vectors for running a fine grid search during LHMC calibration.	73
Table 4-1: Desirable features of a case study building.	76
Table 4-2: Candidate office buildings for case study. Each building is labeled according to the first letter in the location and the year of construction [TEV 2007A],[EC Dahls 2007],[ENOVA 2007]. The specific energy is the energy consumed at the building site...	80
Table 4-3: Candidate school buildings for case study [TEV 2007a],[Arentz 2007]. The specific energy is the energy consumed at the building site.	81
Table 5-1: Window distribution between North, East, South, and West facades on the ground and 1 st floors. The percent of the wall area is the fraction of the wall area that is glazed. The parent surface for each set of windows is given in the left hand column of the table.	94
Table 5-2: Utility floor area, conditioned floor area, and volume of each building zone in the Steindal School. Conditioned spaces are those with ventilation and/or heating.	96
Table 5-3: Summary of materials, with properties, that were present in the walls, roof, and floors of the Steindal School [EPLUS 2007E],[NS3031 1987].	97
Table 5-4: Summary of glazing material, and properties, that were present windows of the Steindal School [EPlus 2007e].	98
Table 5-5: Summary of gases that were present between the two panes of glass in the windows of the Steindal School [EPlus 2007e].	98
Table 5-6: Ground floor construction.	105
Table 5-7: Thermal and radiation properties of the windows in the Steindal School, as per data provided by the manufacturer [PILKINGTON 2007].	106
Table 5-8: Summary of constructions used in the interior ceilings, floors, walls, and other internal mass in the Steindal School.	107
Table 5-9: Recommended infiltration rates for Norwegian buildings from the	108
Table 5-10: Estimated infiltration rates for each zone in the Steindal School.	109

Table 5-11: Maximum number of occupants per zone. Fractional schedules were used to modify the number of occupants in each zone throughout the day [Kringstad 2007].	110
Table 5-12: Daily occupancy schedules for the Classrooms, Offices, Annex, and Gym in the Steindal School [Kringstad 2007],[Skjennald 2007].	112
Table 5-13: Scheduled vacations for students and teachers in the Steindal School. Specific dates correspond to the 2006 schedules from the Steindal School [Skjennald 2007].	113
Table 5-14: Interior lighting distribution in the Steindal School [EERE 2008B],[Steindal 2007],[WIGENSTAD 2005].	114
Table 5-15: Installed plug load capacity and distribution in the Steindal School	116
Table 5-16: Estimated domestic hot water capacity in the Steindal School [Steindal 2007],[Wigenstad 2005].	117
Table 5-17: Installed heating capacity in the Steindal School [Steindal 2007].	118
Table 5-18: Daily schedule of temperature setpoints in the Steindal School, divided by building zone [Municipality 2007b].	119
Table 5-19: Measurements of the supply ventilation flow rates in the Steindal School, made with a hand-held anemometer during site visits in May, 2007.	121
Table 5-20: Measurements of the exhaust ventilation flow rates in the Steindal School, made with a hand-held anemometer during site visits in May, 2007.	122
Table 5-21: Ventilation flow rates in each zone of the Steindal School in 2006 [Steindal 2007].	122
Table 5-22: Daily ventilation schedules in the Main and Annex ventilation systems in 2006...	131
Table 5-23: Daily schedule of ventilation air supply during weeks 28-32 (summer vacation) in 2006 [Municipality 2007b].	132
Table 5-24: Summary of data collection resources that were used to define the energy consumption characteristics of the Steindal School.	133
Table 5-25: Summary of weather, envelope, occupancy, lighting, plug load, and domestic hot water energy consumption characteristics from the Steindal School in 2006.	134
Table 5-26: Summary of heating and ventilation energy consumption characteristics from the Steindal School in 2006.	135
Table 5-27: Summary of uncertain data from collected information on the energy consumption in the Steindal School in 2006.	136

Table 6-1: Solar heat gained through a clear, single paned, windows on the 21 st day of each month	140
Table 6-2: Properties for calculating the solar heat gain through the windows in the Steindal school. The solar coefficient and window area for all four building facades were taken from Chapter 5.....	140
Table 6-3: Annual solar heat gain per façade in the Steindal School. Calculated according to the solar heat gain factor (SHGF) method.....	141
Table 6-4: Occupied and unoccupied temperature setpoints and hours of operation in the.....	145
Table 6-5: Properties for calculating the steady-state heat loss via transmission through exterior walls, roofs, and windows. The U-value for the windows was the area-weighted average of the three difference window types in the building.....	146
Table 6-6: Material properties for calculating the heat loss via transmission through ground walls and floors.	148
Table 7-1: Monthly ground temperatures resulting from the calibration of the Original building model of the Steindal School.	174
Table 7-2: Average annual infiltration rates resulting from the calibration of the calibration of the Original building model of the Steindal School.	174
Table 7-3: Monthly and weekly NMBE and CVRMSE values resulting from the manual calibration of the Original building simulation.....	176
Table 7-4: List of temperature independent load adjustments from the Original to Corrected model. These included properly defining the “baseload”, and improving the lighting, domestic hot water, and fan pressure (Main ventilation system) inputs.....	179
Table 7-5: Annual, monthly, weekly, daily, and hourly CVRMSE and NMBE resulting from the calibration of the Original and Corrected models.....	183
Table 7-6: List of values for the 15 parameters adopted in the Detailed-Corrected LHMC analysis. Values apply to all 2006 models except values in brackets - () and {} - which are used in the Simple and Detailed-Original models, respectively. HVAC and SFP are abbreviations for Heating, Ventilation and Air Conditioning and Specific Fan Power, respectively. The U-values shown result from calculations in EnergyPlus of windows with properties intended to match as closely as possible the configurations given in the manufacturer’s specifications with frames and dividers included.....	191
Table 7-7: Summary of CVRMSE, NMBE, and GOF values resulting from the LHMC calibration. Results are shown for 2004, 2005, and 2006 data. Additionally, the resulting GOF values from the fine grid search and the “freezing” of strong parameters are shown.	197

Table 7-8: Summary of monthly weekly, daily, and hourly NMBE, CVRMSE, and GOF of the “best” calibrations (those with the lowest GOF) from the Detailed-Corrected, Detailed-Original, and Simple models. All results are for the year 2006.....	198
Table 8-1: Calibrated models with which the retrofit analysis of the Steindal School was performed.....	205
Table 8-2: Monthly CVRSME, NMBE and GOF resulting from the comparison between the five 2006 calibrated models (with increased temperature setpoints) and the 2007 utility data.	207
Table 8-3: List of candidate retrofits for possible installation in the Steindal School.....	210
Table 8-4: Definition of the moderate and low-energy temperature setback retrofit with ramping. The ramping gradient was 2 degrees/hour.	212
Table 8-5: Definition of the occupant controlled ventilation retrofit. Both the schedules of operation	214
Table 8-6: Estimated cost of installing the occupant controlled ventilation retrofit in the Steindal School. Cost estimates are shown from both US and Norwegian databases [Means Mech. 2007],[FDV 2007].....	215
Table 8-7: Definition of the moderate and low-energy ventilation flow rate retrofit states (L/m ² /sec).....	215
Table 8-8: Estimated cost of installing the ventilation rate retrofit in the Steindal School. Cost estimates are shown from both US and Norwegian databases [Means Fac. 2007],[FDV 2007].	216
Table 8-9: Definition of the moderate and low-energy heat recovery effectiveness retrofit values for the Main ventilation system (%).	216
Table 8-10: Estimated cost of installing the heat recovery ventilation retrofit in the Steindal School. Cost estimates are shown from both US and Norwegian databases [Means Mech. 2007],[Means Fac. 2007],[FDV 2007].	217
Table 8-11: Definition of the moderate and low-energy window U-value retrofit states (W/m ² K).	218
Table 8-12: Estimated cost of installing the window U-value retrofits in the Steindal School. Cost estimates are shown from both US and Norwegian databases [Means Mech. 2007],[Means Fac. 2007],	218
Table 8-13: Definition of the moderate and low-energy wall U-value retrofit states (W/m ² K).	219
Table 8-14: Estimated cost of installing the wall U-value retrofit in the Steindal School. Cost estimates are shown from both US and Norwegian databases [Means Mech. 2007][Means Fac. 2007],[Means LC 2007],[FDV 2007].	219

Table 8-15: Moderate and low-energy roof U-value retrofit states (W/m^2K).	220
Table 8-16: Estimated cost of installing the North roof in the Main building U-value retrofit in the Steindal School. Cost estimates are shown from both US and Norwegian databases [Means Mech. 2007],[Means Fac. 2007],[HOLTE 2007],[MEANS LC 2007].....	221
Table 8-17: Estimated cost of installing the South roof in the Main building and the Annex roof U-value retrofits in the Steindal School. Cost estimates are shown from both US and Norwegian databases [Means Mech. 2007],[Means Fac. 2007],[HOLTE 2007],[MEANS LC 2007].	221
Table 8-18: Estimated cost of installing <i>all</i> roof U-value retrofits in the Steindal School. Cost estimates are shown from both US and Norwegian databases [Means Mech. 2007],[Means Fac. 2007],[HOLTE 2007],[MEANS LC 2007].....	221
Table 8-19: Moderate and low-energy ground floor and ground wall U-value retrofit states (W/m^2K).....	222
Table 8-20: Estimated cost of installing the ground floor U-value retrofit in the Steindal School. Cost estimates are shown from both US and Norwegian databases [Means LC 2007],[Holte 2007].	223
Table 8-21: Estimated cost of installing the ground wall U-value retrofit in the Steindal School. Cost estimates are shown from both US and Norwegian databases [Means Mech. 2007][Means LC 2007],[Holte 2007].	223
Table 8-22: Moderate and low-energy infiltration rate retrofit states (ACH).	224
Table 8-23: Estimated cost of installing the infiltration rate retrofit in the Steindal School. Cost estimates are shown from both US and Norwegian databases [Means Mech. 2007][Means Fac. 2007],[FDV 2007].....	225
Table 8-24: Moderate and low-energy lighting density retrofit states (W/m^2).....	225
Table 8-25: Estimated cost of installing the lighting density retrofit in the Steindal School. Cost estimates are shown from both US and Norwegian databases [Means Mech. 2007][Means Fac. 2007],[FDV 2007].....	226
Table 8-26: Required oil boiler retrofit heating capacity (kW) and efficiency (%).	227
Table 8-27: Estimated cost of installing the oil boiler and hydronic heating system retrofit in the Steindal School. Cost estimates are shown from both US and Norwegian databases [Means SF 2007],.....	227
Table 8-28: Required district heating retrofit heating capacity (kW) and efficiency (%).	227

Table 8-29: Estimated cost of installing the district heating and hydronic heating system retrofit in the Steindal School. Cost estimates are shown from both US and Norwegian databases costs [Means SF 2007],.....	228
Table 8-30: Summary of moderate and low-energy retrofit states for all energy conservation retrofits.	229
Table 8-31: Summary of moderate and low-energy retrofit states for the hydronic heating retrofit with an oil boiler and district heating.	230
Table 8-32 Summary of investment costs of all energy conservation measure retrofits. All costs are given in NOK. M and L are abbreviations for “moderate” and “low-energy”.	230
Table 8-33: Summary of investment and annual investment costs of alternative heating supply retrofits. All costs are given in NOK.	231
Table 8-34: Predicted energy savings from the Individual Retrofit analysis with all retrofits at their moderate retrofit state. The % +/- savings indicates the energy savings uncertainty as a percent of the base-year energy consumption. This was calculated from Equation 8-3 for the manually calibrated models and is equal to twice the standard deviation of the Top 20 solutions for each of the LHMC calibrated models.	240
Table 8-35: Predicted energy savings from the Individual Retrofit analysis with all retrofits at their low-energy retrofit state. The % +/- savings indicates the energy savings uncertainty as a percent of the base-year energy consumption. This was calculated from Equation 8-3 for the manually calibrated models and is equal to twice the standard deviation of the Top 20 solutions for each of the LHMC calibrated models.	241
Table 8-36: Predicted peak annual power demand savings from the Individual Retrofit analysis at the moderate retrofit state. Only those retrofits with energy savings $\geq 5\%$ are shown. The % +/- savings indicates the energy savings uncertainty as a percent of the base-year energy consumption. This was calculated from Equation 8-3 for the manually calibrated models and is equal to twice the standard deviation of the Top 20 solutions for each of the LHMC calibrated models.	242
Table 8-37: Predicted peak annual power demand savings from the Individual Retrofit analysis at the low-energy retrofit state. Only those retrofits with energy savings $\geq 5\%$ are shown. The % +/- savings indicates the energy savings uncertainty as a percent of the base-year energy consumption. This was calculated from Equation 8-3 for the manually calibrated models and is equal to twice the standard deviation of the Top 20 solutions for each of the LHMC calibrated models.	243
Table 8-38: Electricity billing distribution tariffs from the Steindal School for the periods from January 2004–August 2007 [Skjennald 2007]. In 2004 the power tariffs and consumption tax increased starting with the August utility bill.	255

Table 8-39: Monthly oil tariffs (NOK/m ³) and costs (NOK/kWh) and seasonal cost factors for schools in the Trondheim Municipality from January through September, 2007. The Cost of Oil includes the MVA, or tax.....	258
Table 8-40: Monthly district heating tariffs (NOK/kWh) for schools in the Trondheim Municipality from January through September, 2007. The Cost of District Heating includes the MVA, or tax.	259
Table 8-41: Simulated utility bill savings, expressed as a percentage of the base-year utility costs, for the temperature setback, ventilation rate, occupant controlled ventilation, heat recovery effectiveness, and infiltration rate retrofits, as simulated with the Corrected building model. Negative savings equate to a decrease in utility costs from the base-year.	260
Table 8-42: Modification factors for calculating the EPBD rating of Norwegian buildings. Modification factors for electricity, district heating, and an oil boiler are all given.	267
Table 8-43: EPBD ratings for various retrofits combinations from the Parametric Retrofit analysis. Ratings are shown with each of the three alternative heating systems: electricity, oil, and district heating.....	270
Table 8-44: Calculated savings for two-retrofit, low-energy, combinations. Grey indicates Individual Retrofit results, while white indicates simulations with two retrofits in combination.....	273
Table 8-45: Calculated retrofits energy savings, equal to the sum of the energy savings of each Individual Retrofit.....	274
Table 8-46: % Error in the calculated vs. simulated savings for various retrofit pairings.	274
Table A-1: Overview of variables for thermal mass analysis.....	292
Table A-2: Summary of inputs to the thermal mass analysis.	294
Table B-1: Annual peak power demand savings under moderate retrofit conditions from the Individual Retrofit analysis in Chapter 8	308
Table B-2: Annual peak power demand savings under low-energy retrofit conditions from the Individual Retrofit analysis in Chapter 8.....	309
Table B-3: Utility bill savings under moderate retrofit conditions from the Individual Retrofit analysis in Chapter 8.....	310
Table B-4: Utility bill savings under low-energy retrofit conditions from the Individual Retrofit analysis in Chapter 8.....	311
Table C-1: Internal ceiling, floor, and thermal mass constructions.....	314

Table C-2: Values of ζ_1 and C_1 for the 1 st term approximation of heat transfer in a plane wall [Incropera 2001].....	319
Table C-3: Inputs for calculating the heating energy in the thermal mass in the Steindal School.	320
Table C-4: Inputs for ground heat transfer calculation [ASHRAE 2005].	323
Table C-5: Calculation of ground heat transfer in the Steindal School.	325

1 Introduction

1.1 Motivation

The work in this thesis was performed under the auspices of the “Alternatives to the Transition to Sustainable Energy Services in Northern Europe” (TRANSES) project, which was a collaboration between researchers at the Massachusetts Institute of Technology (MIT) in the United States, the Norwegian Institute of Technology (NTNU) and the Foundation for Scientific and Industrial Research (SINTEF) in Norway, and Chalmers University of Technology in Sweden. The objective of TRANSES was to “aid governments, industries and communities to meet their future energy service needs in a cost-effective and sustainable manner” [SINTEF 2007]. Strategies for achieving this included the investigation of long-term policies for meeting future energy needs, the development of a “toolbox” of methods, computational tools, and databases for improving the information available to decision makers, and the creation of an international forum for the discussion and exchange of ideas and results.

Previous TRANSES projects investigated both the supply and demand sides of energy planning. Research areas have included renewable energy, energy production, energy markets, and energy consumption. The work performed here focused on energy consumption in Norwegian buildings, specifically, on tools for modeling current and future energy needs.

1.2 Problem Statement

This project investigated methods of identifying energy saving retrofits for Norwegian buildings. The procedures under consideration identified retrofit options from a list of candidates. Such procedures are necessary when a number of retrofits that influence different building systems are under consideration as potential installations.

This work focused on predicting retrofit energy savings with calibrated computer simulations. This method of retrofit evaluation allowed retrofit energy savings to be predicted prior to retrofit installation. This work was performed through a case study of a Norwegian school building.

Existing buildings were the focus of this work because (1) the turnover in the Norwegian building sector is low and (2) buildings in Norway may last anywhere from 30 to 100 years, while their components may last only 10-30 years, making retrofit a fundamental part of the life

cycle of any building. Additionally, the retrofit of existing Norwegian buildings to decrease energy consumption is expected to become increasingly important in the coming years with the implementation of the Energy Performance in Buildings Directive (EPBD) rating system in which all new constructions and major renovations are expected to meet certain energy consumption standards.

1.3 Outline of Work

Chapter 2 provides general information about Norway and the state of energy consumption and building practice there, while Chapter 3 presents a review of previous work on retrofit energy savings analysis. Chapter 4 introduces the case study building and Chapter 5 provides a detailed description of the building's energy consumption characteristics. Chapter 5 also identifies a number of uncertain inputs before proceeding with simple estimates and simulated model calibration in Chapter 6 and Chapter 7, respectively. Chapter 7 contrasts two methods of calibrating simulations: manual and Latin Hypercube Monte Carlo (LHMC) analysis. Chapter 8 presents the results of the energy conservation measure (ECM) analysis in addition to several methods of quantifying the uncertainty in the predicted energy savings. Chapter 9 summarizes the observations from Chapters 5 through 8, and Chapter 10 proposes a set of guidelines for performing future ECM analyses.

2 Background on Norway

The purpose of this chapter is to provide an understanding of the need for energy reduction in Norwegian buildings. Therefore, this chapter opens with a geographic, economic, and political description of the country of Norway, followed by an introduction to the current and past state of energy supply and demand. Information on energy consumption in buildings is provided, as is a summary of the energy-related requirements that were included in the 2007 revision of the Norwegian Building Codes (NBC). A description of the Energy Performance in Buildings Directive (EPBD), as it pertains to Norwegian buildings, is also provided.



Figure 2-1: Map of Norway
[Factbook 2008a]

2.1 Geography and Topography

The country of Norway is located in northern Europe and is bordered by Sweden, Finland, and Russia to the east, the Norwegian Sea to the west, the North Sea to the south, and the Barents Sea to the north. The topography is highly glaciated, with deep fjords, tall peaks, fertile farmland, and arctic tundra in the western, eastern, southern, and northern regions of the country, respectively. The total land and freshwater holdings in Norway amount to more than 320,000 km² (123,000 sq. miles) [Factbook 2008a]. The country's North is considered a cold climate, while the South is much more temperate, due largely to the warm North Atlantic Ocean current. The average temperature in the capital city of Oslo, located in southern Norway (59° 55" N, 10° 45" E), is 6°C (50°F) [MET 2007].

2.2 People and Government

The population of Norway has shown steady growth in the last decade, bolstered by increased immigration rates. The country is currently home to nearly 4.9 million people. Norway has been governed intermittently by both the Swedes and Danes since the demise of the Vikings in the 14th century. Most recently, Norway was a part of

the kingdom of Sweden, under whose control it remained until gaining independence in 1905. Since then, Norway has been ruled by a parliamentary government. The presiding monarch is King Harald V, who has reigned since 1991. Prime Minister Jens Stoltenberg has presided over the Norwegian parliament, or Storting, since his election by popular vote in 2004 [Factbook 2008a].

2.3 Economy

The economic system in Norway is based on a welfare capitalism ideology, with several key industries, such as petroleum, under government control. Historically, the Norwegian economy was based on fishing, farming, and timber. All three remain staples in Norwegian life, although the discovery of oil and gas offshore in the 1960's initiated an economic boom, and led Norway to become the 3rd largest exporter of petroleum products in the world [Factbook 2008a]. The strength of the Norwegian economy and its relatively small population combine to give Norway the 6th highest per capita gross domestic product (GDP) in the world.

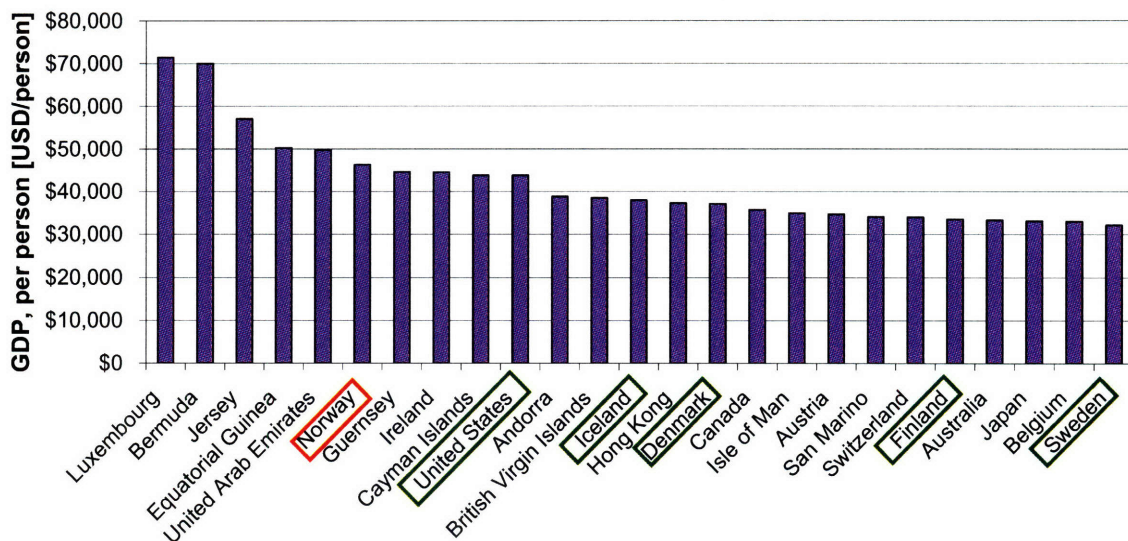


Figure 2-2: Gross domestic product (GDP) per capita of selected countries reported for 2004-2007 (USD/person) [Factbook 2008a].

Twice, Norway has narrowly rejected membership in the European Union (EU) by popular vote; first in 1972 and again in 1994. However, as a member of the European Economic Area (EEA), Norway can engage in free trade with all other EEA and EU member states [EC 2008].

2.4 Energy Supply and Demand

Petroleum is one of several energy carriers that satisfy the more than 222 trillion watt-hours (TWh) of domestic energy demands in Norway each year [Statbank 2007]. Others include solid fuel, district heating, and electricity. Historically, electricity has supplied more than 50% of the domestic energy demand in Norway (Figure 2-3).

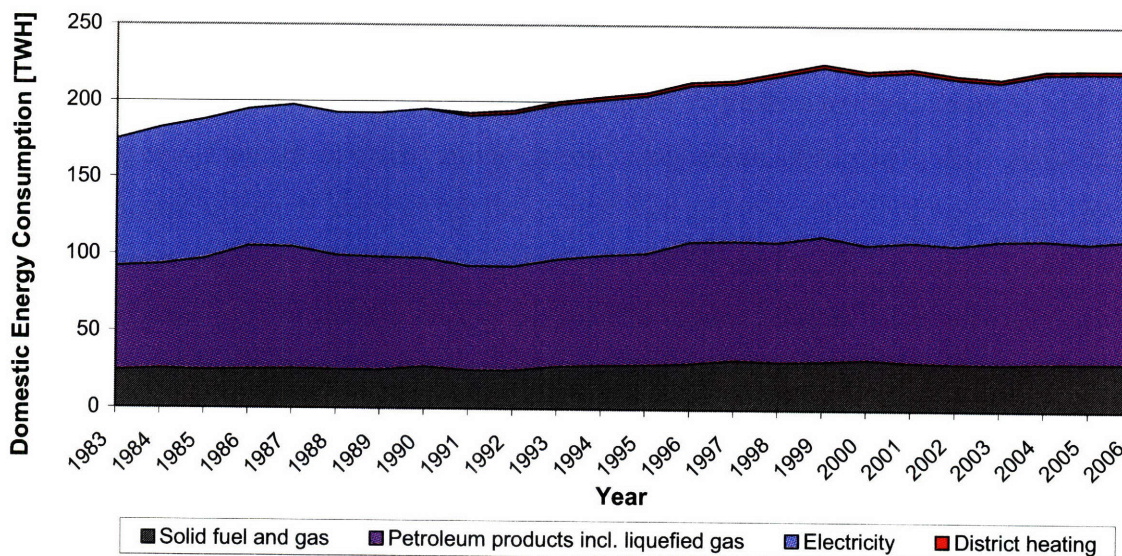


Figure 2-3: Annual domestic energy demand in Norway by energy carrier from 1983-2006 (TWh) [Statbank 2007].

This is likely due to the plentiful supply of electricity, 98% of which is generated by hydroelectric power plants [Statbank 2007]. In the past, the abundance of this resource has made Norway a net exporter of electric energy. Recently, however, increased population growth and the extensive use of electricity for heating in buildings has led Norway to become a net importer of electricity (Figure 2-4). As a result, Norway has relied on electricity from both Sweden and Denmark to meet the excess demand. Wind turbines have been installed in several areas of Norway, but as of July 2007, less than 1% of Norway's electricity was supplied by wind power [Statbank 2007].

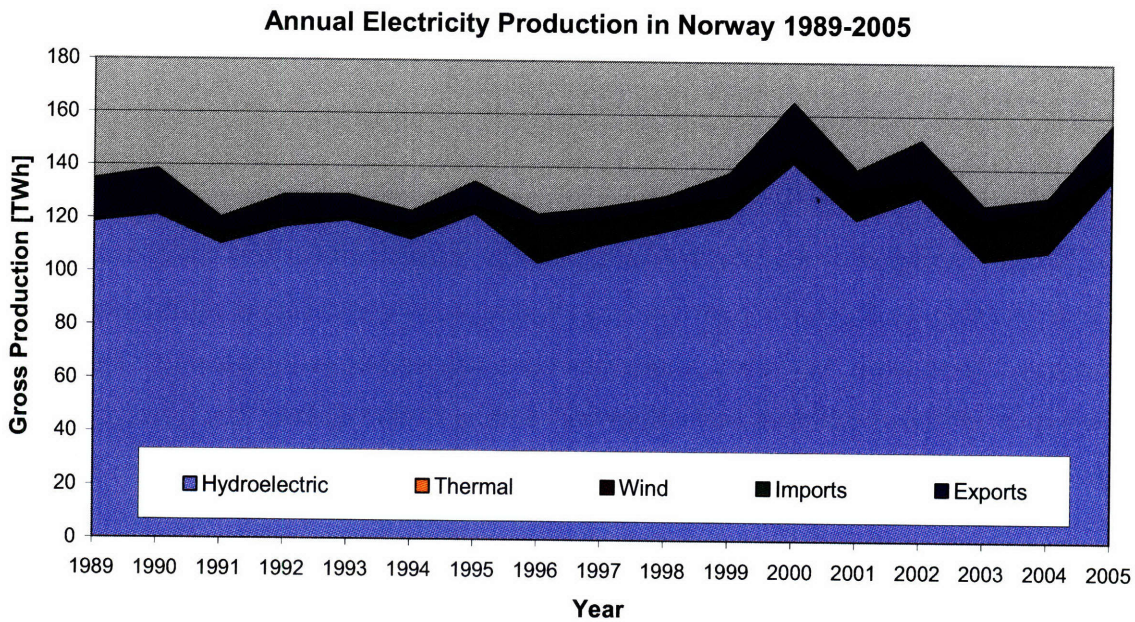


Figure 2-4: Annual electricity supply in Norway, by energy supplier, 1989-2005 (TWh) [Statbank 2007].

The annual energy demand in Norway is divided among several services, of which, manufacturing, mining, transportation, and households account for the majority of the domestic energy consumption.

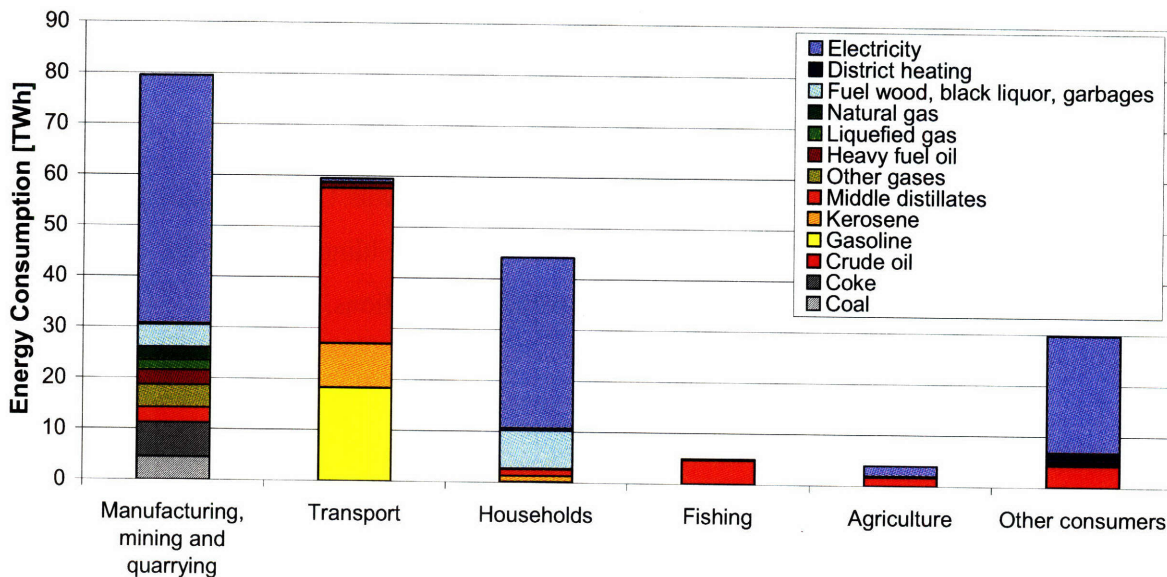


Figure 2-5: Domestic energy consumption in Norway by consumer type (TWh). “Other consumers” is comprised largely of commercial buildings [Statbank 2007].

The reduction of energy consumption in buildings (Households and Other Consumers categories in Figure 2-5), which accounts for more than 30% of the 222 TWh of domestic energy

consumption in Norway, is of particular interest to the goals of TRANSES [Statbank 2007], [Hestnes 2007a], [Wigenstad 2005]. Furthermore, more than 75% of the energy used in buildings can be attributed to electricity [Statbank 2007].

2.5 Norwegian Building Codes

In Norway, stringent codes exist to limit the energy consumption in new constructions. These codes include limitations to the window, wall, roof, and floor U-values, infiltration rates, heat recovery effectiveness, fan power, ventilation rates, temperature settings and internal gains. The Norwegian Office of Building Technology and Administration updates the Norwegian Building Codes (NBC) roughly every 10 years. The most recent update was released in 2007.

2.5.1 Envelope U-Values

Table 2-1 provides an overview of the maximum U-value and window area requirements in new, non-residential constructions, in the 2007 NBC.

Envelope Properties from 2007 NBC	Walls	Roof	Base	Doors	Windows
U-Value [W/m ² K]	0.18	0.13	0.15	1.2	1.2
Area [% of conditioned floor area]	---	---	---	---	20%

Table 2-1: Envelope U-value and window area requirements from the energy section of the 2007 Norwegian Building Codes (NBC) [BE 2008a].

2.5.2 Infiltration Rates

The maximum infiltration rate required in the 2007 NBC was 1.5 air changes per hour (ACH), measured under 50 Pa of pressure, in a non-residential building. To convert this measurement to the infiltration rate under typical operating conditions, Equation 2-1 is applied [NS3031 2007].

$$\eta_{infiltration} = \frac{\eta_{50Pa} * e}{1 + \frac{f}{e} * \left(\frac{V_{supply} - V_{return}}{V_{conditioned} * \eta_{50Pa}} \right)} \quad (2-1)$$

- $\eta_{infiltration}$ Infiltration rate in the building [ACH]
- η_{50Pa} Infiltration rate at 50 Pa of pressure [ACH]
- f, e Coefficients to account for terrain
- V_{supply} Ventilation supply air flow rate [m³/sec]
- V_{return} Ventilation return air flow rate [m³/sec]
- $V_{conditioned}$ Conditioned building volume [m³]

The wind exposure factors for the building are chosen from those presented in Table 2-2 on the basis of the building’s site conditions.

Wind Exposure Coefficients	Level of Protection from Wind		
	Unprotected	Moderately protected	Well-protected building
e	0.10	0.07	0.04
f	15	15	15

Table 2-2: Wind exposure coefficients for infiltration calculations [NS3031 2007].

In a balanced ventilation system V_{supply} equals V_{return} and the calculation of the operational infiltration rate simplifies to $\eta_{50Pa} * e$.

2.5.3 Heat Recovery Effectiveness, Fan Power, and Ventilation Rates

The 2007 NBC required a ventilation heat recovery effectiveness of 70% and a specific fan power (SFP) of 2/1 kW/m³/sec (occupied/unoccupied) in all non-residential buildings [BE 2008a].

The recommended outdoor air flow rates for assuring acceptable indoor air quality in Norwegian buildings are shown in Table 2-3. As a point of comparison, minimum outdoor air flow rates from European (EN) and American standards (ASHRAE) are given in Table 2-4 and Table 2-5.

Norwegian Standards for Outdoor Airflow in Buildings	Airflow per Person [L/s/person]	Airflow for building materials [L/s/m ²]		
		Very low polluting building	Low polluting building	Non low-polluting (“typical”) building
Category I (most occupants satisfied)	10	0.5	1	2.0
Category II	7	0.35	0.7	1.4
Category III (fewest occupants satisfied)	4	0.3	0.4	0.8

Table 2-3: Outdoor airflow requirements for acceptable indoor air quality in Norwegian buildings [Hanssen 2007].

The row highlighted in grey (Category II) in Table 2-3 provides outdoor air flow rates that are appropriate to satisfy the majority of occupants in a building and are also the recommended air flow rates for newly constructed Norwegian buildings [Hanssen 2007]. However, both Category I and III were also acceptable for satisfying indoor air quality requirements. The “very low polluting”, “low polluting”, and “non-low polluting” building conditions refer to the level of air-borne contaminants that were released by the building’s materials. Non-low polluting materials may be regarded as typical for Norwegian buildings.

Table 2-4 presents the air flow rates recommended in the European Standards, specifically EN 13779 [EN13779 2004].

European Standards for Outdoor Air Flow in Buildings	Level of Indoor Air Quality	Rate of outdoor air per person Non-smoking area [L/s/person]
IDA 1	High (<400 ppm CO ₂)	>15
IDA 2	Medium (400-600 ppm CO ₂)	10-15
IDA 3	Acceptable (600-1000 ppm CO ₂)	6-10
IDA 4	Low (> 1000 ppm CO ₂)	<6

Table 2-4: Minimum outdoor air flow rates from European standards, EN 13779 [EN13779 2004].

The air flow rates recommended in Table 2-4 are dependent on the total acceptable amount of CO₂ in the building. “High” air quality requires lower CO₂ concentrations in the building, demanding that more outdoor air be provided to decrease the amount of CO₂ in the building space.

Table 2-5 provides an excerpt from the American standards for outdoor air flow rates and was taken from the *American Society of Heating, Refrigerating, and Air-Conditioning Engineers (ASHRAE) Standard 62: Ventilation for Acceptable Indoor Air Quality* [ASHRAE 62 2004].

American Standard for Outdoor Airflow in Buildings	Outdoor Air Flow Rate			
	Expected # of People/m ²	Required outdoor air flow [L/s/person]	Required outdoor air flow [L/m ² s]	Combined air flow rate [L/s/person]
Classroom	0.35	5	0.6	6.7
Laboratory	0.25	5	0.9	8.6
Training Shop	0.20	5	0.9	9.5
Music Rooms	0.35	5	0.3	5.9
Libraries	0.1	2.5	0.6	8.5
Office Space	0.05	2.5	0.3	8.5
Gymnasium	0.3	-----	1.5	-----
Corridors	-----	-----	0.3	-----
Auditoriums	1.5	2.5	0.3	2.7

Table 2-5: Minimum outdoor air flow rates from ASHRAE Standard 62-2004 [ASHRAE 62 2004]. The number of expected people per m² should only be used when the actual occupancy is unknown.

The outdoor air flow required by ASHRAE Standard 62 was between 6-10 L/s/person, which coincided well with the 6-10 L/s/person recommended at level IDA 3 in EN 13779 (Table 2-4), and was 2-4 L/s/person less than the 8-14 L/s/person recommended for a Norwegian building in which the majority of occupants were satisfied (Category II in Table 2-3 with an occupant density of ~ 0.2 people/m² and non low-polluting materials).

2.5.4 Temperature Settings and Temperature Independent Loads

Typical values for indoor temperature setpoints, temperature independent load capacities, and internal gains were defined in the 2007 release of *NS 3031: Calculation of energy performance of buildings, Method and Data* [NS3031 2007], and are given in Table 2-6 (temperature setpoints) and Table 2-7 (temperature independent loads and internal gains). The schedules of operation for lighting, plug loads, domestic hot water (DHW), people, and ventilation were the same as those for heating in all of the building types shown in Table 2-6 and Table 2-7.

Temperature Settings and Schedules	Schedule [hrs/days/weeks]	Occupied/Unoccupied Heating Setpoint [°C]	Cooling Setpoint [°C]
House	16/7/52 (24/7/52)	21/19	-----
Building Block	16/7/52 (24/7/52)	21/19	-----
Kindergarten	10/5/52	21/19	-----
Office	12/5/52	21/19	22
School	10/5/44	21/19	22
University	12/5/52	21/19	22

Table 2-6: Temperature setpoints and schedules for typical houses, building blocks, kindergartens, offices, schools, and university buildings in Norway [Gustavsen 2007],[NS3031 2007].

The 2007 release of NS3031 [NS3031 2007] indicated that lighting, plug loads, and people contributed 100% heat gain to the building, while domestic hot water (DHW) contributed no heat gain to the building. Plug loads included all equipment that was plugged into wall sockets (i.e. refrigerators, computers, printers, electric cooking stoves, and all other electric appliances).

Temperature Independent Loads & Internal Gains	Lighting		Plug Loads		Domestic Hot Water		People	
	W/m ²	kWh/m ² /year	W/m ²	kWh/m ² /year	W/m ²	kWh/m ² /year	W/m ²	kWh/m ² -year
House	2.9	17	4	23	5.1	30	1.5	13
Building Block	2.9	17	4	23	5.1	30	1.5	13
Kindergarten	8	21	2	5	3.8	10	6	16
Office	8	25	11	34	1.6	5	4	13
School	10	22	6	13	4.5	10	12	26
University	8	25	11	34	1.6	5	6	19

Table 2-7: Recommended values for temperature independent loads and internal gains in houses, building blocks, kindergartens, offices, schools, and university buildings in Norway [NS3031 2007].

2.5.5 Typical Annual Energy Consumption in Norwegian Buildings

Finally, work performed as a part of the 2007 NBC provided minimum values for the energy consumption in various building types (Figure 2-6).

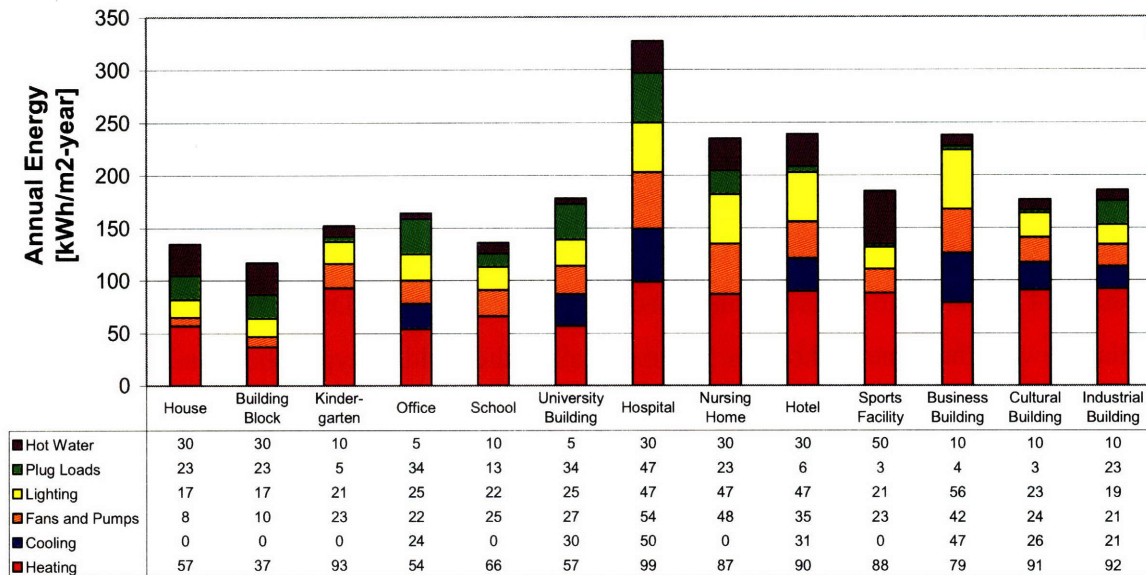


Figure 2-6: Minimum energy consumption requirements for new constructions and major renovations in houses, building blocks, kindergartens, offices, schools, university buildings, hospitals, nursing homes, hotels, sports facilities, business buildings, cultural buildings, and industrial buildings in Norway [Gustavsen 2007]. All values are given in energy consumption per unit of conditioned floor area (kWh/m²-year).

2.6 Energy Performance in Buildings Directive (EPBD)

The recently instituted European Building Performance Directive, adopted by many European countries including Norway, seeks to establish a system for rating the energy consumption in both new constructions and major renovations of existing buildings.

“The objective of this Directive is to promote the improvement of the energy performance of buildings within the Community, taking into account outdoor climatic and local conditions, as well as indoor climate requirement and cost-effectiveness” [EPBD 2002].

The EPBD was introduced in November of 2002 and required that all participating countries implement (1) a method for calculating the energy performance of buildings, (2) minimum energy performance requirements for new buildings with a useful floor area greater than 1,000 m², (3) minimum energy performance requirements for large renovation projects (renovation costs amount to more than 25% of the building’s value) with a useful floor area greater than 1,000 m², (4) a certification procedure for rented, sold, or public buildings, and (5) regular inspection of boilers and air-conditioning systems. It is the responsibility of the participating countries to establish a committee to implement these requirements and develop standards for their execution [EPBD 2002].

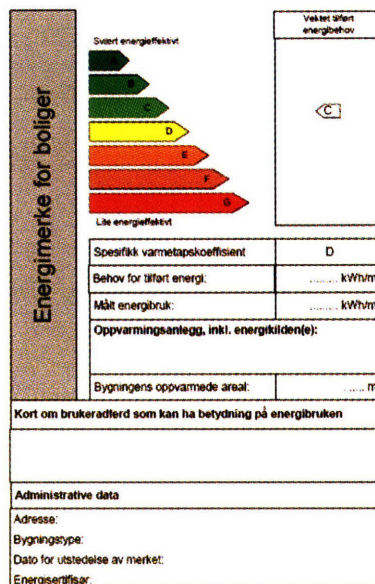


Figure 2-7: Example EPBD certificate for Norwegian buildings [Wigenstad 2005].

According to the EPBD standards, buildings are classified by their energy consumption on a scale from A to G. Class A buildings consume the least amount of energy and class G buildings consume the most energy. In Norway, the minimum energy rating for newly

constructed or renovated buildings is level C. Work by Wigenstad et al. [Wigenstad 2005] proposed preliminary energy consumption values for classifying, or rating, Norwegian buildings. These ratings differed by building type and are shown in Table 2-8 for offices, kindergartens, and schools. A chart with all Norwegian building types is located in Appendix B.

		A	B	C	D	E	F	G
Offices	Energy [kWh/m ²]	≤ 80	81-120	121-160	161-190	191-225	226-335	> 335
Kindergartens	Energy [kWh/m ²]	≤ 80	81-120	121-160	161-190	191-225	226-335	> 335
Schools	Energy [kWh/m ²]	≤ 65	66-100	101-130	131-160	161-190	191-290	> 290

Table 2-8: Energy consumption requirements for obtaining various EPBD ratings in Norway [Wigenstad 2005].

The energy consumption values that are required to reach level “C” in Table 2-8 correspond with the total annual energy consumption that was shown in Figure 2-6. This is consistent with the observation that all new constructions should achieve a level “C” EPBD rating.

The energy consumption values presented in Table 2-8 are not equal to the building’s site energy. Rather, they are a weighted sum of the energy consumed by each energy carrier in the building (i.e. oil, gas, electricity, etc.), and are calculated according to Equation 2-2.

$$EPBD \text{ Energy Consumption} = \sum_{i=1}^N \frac{Energy_i}{\eta_{production,i} * \eta_{regulation,i} * \eta_{distribution,i}} * IF_i \quad (2-2)$$

- $Energy_i$ Energy consumption by each energy carrier in the building [kWh/m²]
- IF_i Influence factor for that energy carrier
- $\eta_{production,i}$ Efficiency of the energy produced at the building site for energy carrier i
- $\eta_{regulation,i}$ Efficiency of the building’s control system for energy carrier i
- $\eta_{distribution,i}$ Efficiency of distribution of energy carrier i
- N Number of energy carriers in the building

Each potential energy carrier (i.e. oil, natural gas, etc.) is assigned an influence coefficient (IF) on the basis of the political, social, environmental, and future energy interests of the country designating the EPBD ratings, in this case Norway. The efficiencies (η) represent the losses in the production of energy (i.e. boiler efficiency), in the control of energy supplied to the building (i.e. inefficiencies in the response to heating thermostats), and the distribution of energy within the building (i.e. efficiency of pumps and heat loss in hydronic heating systems). The total efficiency of the energy supplier is equal to the product of these three efficiencies.

Wigenstad et al. [Wigenstad 2005] recommended preliminary efficiencies and influence coefficients for various energy carriers. Values for district heating, electric resistance heating, and oil boiler heating systems are given in Table 2-9.

Heat Source	Production Efficiency $\eta_{\text{production}}$	Regulation Efficiency $\eta_{\text{regulation}}$	Distribution Efficiency $\eta_{\text{distribution}}$	Total Efficiency $\eta_{\text{total}} = \eta_{\text{production}} * \eta_{\text{regulation}} * \eta_{\text{distribution}}$	Influence Factor, IF	Total Modifier (IF/η_{total})
Electricity	1.00	1.00	1.00	1.00	1.00	1.00
District Heat	0.98	0.95	0.95	0.88	0.55	0.625
Oil Boiler	0.85	0.95	0.95	0.77	1.00	1.30

Table 2-9: Modification factors to account for various primary energy sources when calculating the EPBD rating for Norwegian buildings [Wigenstad 2005].

Given this information a simple example can be performed to demonstrate the calculation of the EPBD rating for a generic building. First, assume that office building “X” consumes 180 kWh/year of energy for heating, fans and pumps, lighting, plug loads, and domestic hot water. Of this 180 kWh/year of energy demand, 100 kWh/year is required to meet heating demands. Applying the efficiencies and influence factors from Table 2-9 to the calculation of the energy consumption described in Equation 2-2, this results in an EPBD energy consumption of 210 kWh/year with an the oil boiler, 143 kWh/year with district heating, and 180 kWh/year with the electric resistance heating. This would result in a level “E” rating with the oil boiler system, a level “C” rating with the district heating system, and a level “D” rating with the electric resistance heating system. Thus, district heating enables the building to obtain the lowest EPBD rating of the three potential heating systems. This is important to recognize, as the choice of heating system for a new construction or major renovation might be influenced by its potential EPBD rating.

3 Procedures for Evaluating Energy and Demand Savings

A review of previous work was performed to identify the most applicable methods of estimating retrofit energy savings in Norwegian buildings. First, procedures for estimating retrofit energy savings (section 3.1) were investigated. From this investigation, calibrated computer simulations were selected as the most appropriate method of retrofit evaluation in this work. Finally, methods of calibrating building energy simulations for retrofit evaluation were assessed (section 3.2). Issues related to calibrated simulations that were also considered were: data collection, metrics for calibration, retrofit selection, cost estimation, and energy savings prediction uncertainty (sections 3.2.1 through 3.2.5).

3.1 General Energy Savings Evaluation Procedures

The International Performance Measurement and Verification Protocol (IPMVP) [IPMVP 2002] and ASHRAE Guideline 14-2002: Measurement of Energy and Demand Savings (ASHRAE Guideline 14) [ASHRAE 14 2002] were developed to guide engineers, building managers, and energy service companies (ESCOs) in performing retrofit installations of energy conservation measures (ECMs). Both of these guidelines recommend three methods (step 1, 3, 4, and 5 in Figure 3-1) for assessing ECM energy savings in buildings.

- The *whole building approach* uses the building's main meter (often the utility meter) to compare the building's energy consumption before and after the installed ECM.
- The *retrofit isolation approach* uses sub-meters to measure the energy consumption for the system to which the ECM is applied.
- The *whole building calibrated simulation approach* applies computer simulations to first calibrate models against pre-retrofit building conditions, and then to estimate the potential for energy savings from ECMs.

Figure 3-1 provides a synopsis of the ECM analysis procedure recommended by the IPMVP and ASHRAE Guideline 14. This is a general procedure and does not discriminate between the three methods for assessing ECM energy savings listed above.

- (1) Select the **method for retrofit evaluation** – either retrofit isolation, whole-building utility metering, or calibrated simulations.
- (2) Create a **measurement and verification (M & V) plan** that includes the steps to be taken and the incident costs of calculating the ECM savings.
- (3) Design, test and install any necessary measurement equipment as per the M & V plan. Verify proper commissioning of measurement equipment.
- (4) Measure the “baseline”, or **pre-retrofit, energy consumption** in the building.
- (5) Install ECMs and measure the **post-retrofit energy use**.
- (6) **Neutralize independent variables**.
- (7) **Calculate savings** as: *pre-retrofit energy demand – post-retrofit energy demand*, with the necessary adjustments according to step #6.
- (8) **Report the calculated savings** and the associated uncertainty.

Figure 3-1: Summary of recommended procedures for evaluating ECM energy savings according to ASHRAE Guideline 14 [ASHRAE 14 2002] and the IPMVP [IPMVP 2002].

The measurement and verification (M & V) plan (step 2 in Figure 3-1) defines the scope of the project and the steps to be taken, including: the ECMs to be evaluated, the method of ECM evaluation (as per step 1 of Figure 3-1), all necessary measurements, and the associated time and costs for performing the savings evaluation [IPMVP 2002]. After these features of the project are documented measurements are made and data is collected. This includes the pre-retrofit energy consumption in the building (step 3 and 4 in Figure 3-1). Following the pre-retrofit measurements retrofits are installed and additional measurements are made (step 5 in Figure 3-1). The independent variables are then neutralized and the difference between the pre-retrofit and post-retrofit energy consumption is calculated (steps 6 and 7 in Figure 3-1).

Both ASHRAE Guideline 14 and the IPMVP emphasize the need to neutralize independent variables (step 6 in Figure 3-1), the most common of which are weather conditions. This is done to ensure that the calculated energy savings (step 7 in Figure 3-1) are due only to the installed ECM(s), not changes in independent variables. As such, the pre and post retrofit energy consumption (steps 4 and 5 in Figure 3-1) must be normalized against a common set of weather data, either pre retrofit, post retrofit, or for a typical weather.

Steps 2 through 7 of the procedure in Figure 3-1 are general considerations in any retrofit evaluation procedure, meaning that they exist independently from the method of ECM evaluation that is chosen in step 1. Thus, the more interesting decision is made during the first step when

the method of ECM evaluation is selected. Consequently, careful consideration is given to this step of the procedure in both the IPMVP and ASHRAE Guideline 14. Table 3-1 summarizes a number of issues for consideration when choosing the most appropriate ECM evaluation method for a given building analysis.

Consideration	ECM Evaluation Method		
	Whole Building	Retrofit Isolation	Whole Building Calibrated Simulation
Ability to determine savings of individual ECMs	No	Yes	Yes
Possible ECMs	Any building component	No envelope ECMs	Any building component
Understanding by non-technical personnel	Can be simple	Can be simple	Difficult
Special skills of personnel	Little to none	Installation of and data collection from metering systems	Experience with simulation tools
ECM's interaction with the rest of the building	Cannot be measured	To be ignored or measured	Can be evaluated with some difficulty
Savings evaluation before installing ECM?	No	No	Yes
Best length of post-retrofit period	At least one year	Representative periods	Maybe none
Best application [IPMVP]	<ul style="list-style-type: none"> energy consumption of whole facility is to be assessed many different types of ECMs in one building ECMs cannot easily be isolated ECM savings are large enough to be separated from noise in the base-year data 	<ul style="list-style-type: none"> no concern for interactive effects of ECM(s) sub-meters already exist to isolate ECM measurement of individual ECMs is less costly than option whole-building evaluation 	<ul style="list-style-type: none"> base-year or post-retrofit data are unavailable too many ECMs to use the retrofit isolation approach <ul style="list-style-type: none"> multiple, interactive, ECMs require understanding of interactive effects major changes to be made experienced energy simulation professional is available and can be funded building and ECMs can be modeled by an acceptable simulation software and calibration can be achieved

Table 3-1: Summary of methods for estimating retrofit energy savings. All data was taken from ASHRAE Guideline 14 [ASHRAE 14 2002], except where indicated (IPMVP) [IPMVP 2002].

The whole-building and retrofit isolation approaches are only appropriate when energy consumption information is available both before and after ECM(s) are installed. Thus, they are useful when the retrofits to be installed are already known. In contrast, whole building calibrated simulation is capable of evaluating ECMs before their installation. Additionally, whole building calibrated simulations are capable of assessing a diverse range of potential ECMs, making it possible to identify optimal or near optimal retrofit options prior to their installation. Recall that the purpose of this work was to identify retrofits for installation from amongst a list of candidates. Consequently, in this work, whole building calibrated simulations were the most

applicable of the three methods presented. Therefore, the remainder of the literature review focuses on methods of performing ECM evaluation with calibrated simulations.

3.2 Calibrated Simulations and Energy Conservation Measure (ECM) Savings Estimation

Table 3-2 presents the methodology for performing ECM savings assessments with whole building calibrated simulations that was recommended by ASHRAE Guideline 14 [ASHRAE 14 2002].

- | |
|---|
| <ol style="list-style-type: none">(1) Produce a calibrated simulation plan(2) Collect data(3) Input data into simulation software and run model(4) Compare simulation model output to measured data; refine model until an acceptable level of calibration is achieved(5) Simulate retrofits(6) Compare resulting baseline and post-retrofit models to estimate energy savings(7) Report observations and savings |
|---|

Table 3-2: Procedure for calibrating whole building simulations, as recommended by ASHRAE Guideline 14 [ASHRAE 14 2002].

Each of the steps in the calibration procedure in Table 3-2 will be more fully defined in sections 3.2.1 through 3.2.5 with the aid of the articles summarized in Table 3-3.

Author	Building Type & Location	Data Collection	Simulation Program	Type of Calibration	Frequency of Measured Data	Metric for Calibration	ECMs
Norford et al.	Office in New Jersey	As-built & Design Docs. Site Visit Meas.	DOE-2.1C	Manual	Monthly/ Hourly	Annual & Monthly % Diff.	No
Pan et al.	High Rise in China	Design Docs. Site Visit Meas.	DOE-2	Manual	Monthly	Monthly RMSE & CVRMSE	Yes
Pedrini et al.	Various Offices in Brazil	Design Docs. Site Visit Meas.	DOE-2.1E	Manual	Monthly/ Hourly	Annual & Monthly % Diff.	No
Westphal and Lamberts	Office in Brazil	Design Docs. Site Visit Meas.	EnergyPlus	Sensitivity Analysis	Monthly/ Hourly	Hourly Profiles, Annual & Monthly % Diff.	No
Yoon et al.	High Rise in South Korea	As-built Docs. Site Visits Meas.	DOE-2.1E	Manual	Monthly	RMSE & CVRMSE	No
Zhu	High Rise in Florida	As-built Docs. Site Visits Meas.	eQuest	Manual	Monthly	t-statistic	Yes
Tamburrini et al.	Factory in Scotland	As-built & Design Docs. Site Visit	ESP-r	Manual	Monthly	Graphical	Yes
Soebarto	Academic & Municipal Buildings in Texas	As-built Docs. Site Visit Meas.	ENER-Win	Manual	Monthly/ Hourly	CVRMSE/ NMBE & Graphical	No
ASHRAE RP-1051	Office in Pennsylvania	As-built Docs. Site Visit	DOE-2	Sensitivity Analysis	Monthly	CVRMSE/ NMBE	Yes

Table 3-3: Summary of building energy simulation articles [Norford 1994],[Pan 2006],[Pedrini 2002],[Westphal 2005],[Yoon 2003],[Zhu 2006], [Tamburrini 2003], [Soebarto 1997],[Reddy 2006].

3.2.1 Calibrated Simulation Plan

The calibrated simulation plan is similar to the M & V plan in Figure 3-1 and enables the modeler to be organized and efficient in performing whole building calibrated simulations.

ASHRAE Guideline 14 [ASHRAE 14 2002] recommends that all information pertinent to the success of the calibration be documented in this plan, including, but not limited to:

- (1) identifying and describing any ECMs that are to be installed in the building
- (2) documenting the building's base-year data and any non-ECM related changes to the base-year
- (3) identifying conditions for neutralizing independent variables (i.e. weather)
- (4) specifying the software for modeling the building
- (5) deciding the scale for savings measurements (i.e. whole-building, sub-system, or unitary equipment)
- (6) defining the time scale for calibration (i.e. hourly, daily, weekly, or monthly)
- (7) defining the acceptable limits for statistical calibration measures
- (8) specifying metering points for data collection – these are used in making spot measurements in the building
- (9) describing any expected inaccuracies

3.2.2 Data Collection for Defining Building Energy Models

A review of the literature summarized in Table 3-3 indicated that the most common means of collecting building data were as-built documents, site visits, conversations with building managers, hourly utility data, measurements, and typical values.

3.2.2.1 As-built Documents

As-built documents consist of architectural drawings, mechanical drawings, electrical drawings, and manufacturer data sheets that describe the conditions in the building after its construction. These documents provide information on the building orientation, dimensions, envelope, heating system, ventilation system, cooling system, and lighting and are obtained from building managers, manufacturers, contractors, and architects [Pedrini 2002],[Pan 2006],[Soebarto 1997].

The importance of using as-built building data was emphasized in work by Norford et al. [Norford 1994] in which a more than 200% discrepancy was found (and resolved) between the simulated energy consumption based on design documents and the actual energy consumption in an office building in New Jersey.

3.2.2.2 Site Visits

Site visits consist of observations, conversations with building managers, and spot measurements. The site visit is useful in defining internal gains, occupancy and operation schedules, operation setpoints, and controls strategies [Pedrini 2002],[Pan 2006]. Yoon et al. [Yoon 2003] emphasized the use of site visits as a tool for verifying data from design documents, while Tamburrini et al. [Tamburrini 2003] highlighted the importance of site visits in their study of a Scottish factory building in which, contrary to initial assumptions that the ventilation system was well maintained, the site visit revealed that only five of a possible 125 system fans were functioning properly.

3.2.2.3 Utility Data

The IPMVP recommends that utility data for the building be collected on a monthly basis for at least a full year prior to evaluating retrofits. This data should be inspected for inconsistencies or errors prior to accepting it as an accurate benchmark against which to calibrate simulations.

Utility data is most commonly available on a monthly basis; however, hourly utility data may also be available. Such is the case in Norwegian buildings that consume more than 100,000 kWh of electricity per year, for which electricity use is reported on an hourly basis [Målfrid 2007],[Arentz 2007].

3.2.2.4 Hourly Measurements

Hourly whole-building measurements are an additional tool for defining the energy consumption in a building. These measurements are useful for defining hourly utility data or for extracting information about building loads.

Soebarto [Soebarto 1997] used “on-off” tests to find the installed lighting and plug load capacities in a building in Texas. This test was performed by monitoring the whole-building electricity meter while turning the lighting and plug loads on and off in a controlled manner (at parity of all other building conditions).

Work by Yoon et al. [Yoon 2003] went a step further. They used data loggers to take hourly measurements of the lighting and plug loads and their schedules of operation in a high rise building in South Korea. Additionally, ASHRAE Guideline 14 [ASHRAE 14 2002] suggests

that such measurements may be made by isolating lighting and plug load circuits in the building's electrical panel.

3.2.2.5 Measurements

The measurement techniques presented in Table 3-4 were taken from ASHRAE Guideline 14, and range from spot measurements (several hours) to long-term measurements (several months to several years), and from zero to thousands of dollars (USD) in capital costs.

		Energy and Power	Temperature	Velocity and Flow Rates	Other
Ventilation & Heating	<i>HRU & Heating</i>	<ul style="list-style-type: none"> • Watt meter • Btu Meter 	<ul style="list-style-type: none"> • Temp probe • Surface temp sensor 	-----	<ul style="list-style-type: none"> • RH probe
	<i>Fans</i>	<ul style="list-style-type: none"> • Watt meter 	-----	<ul style="list-style-type: none"> • Velocity probe • Anemometer 	<ul style="list-style-type: none"> • Pressure transmitter • Portable tachometer
	<i>Pump</i>	<ul style="list-style-type: none"> • Watt meter 	-----	<ul style="list-style-type: none"> • Flow meter 	<ul style="list-style-type: none"> • Pressure transmitter
	<i>Vent. Dist. Sys.</i>	-----	<ul style="list-style-type: none"> • Temp. probe • Temp. sensor 	<ul style="list-style-type: none"> • Flow hood • Velocity Probe 	<ul style="list-style-type: none"> • Press./Depres. (losses)
	<i>Electric Resistance</i>	<ul style="list-style-type: none"> • Watt meter 	-----	-----	-----
	<i>Boiler</i>	<ul style="list-style-type: none"> • Watt meter • Btu meter 	<ul style="list-style-type: none"> • Surface temp. sensor 	<ul style="list-style-type: none"> • Flow meter 	-----
	<i>Pump</i>	<ul style="list-style-type: none"> • Watt meter 	-----	-----	-----
	<i>Distrib. System</i>	<ul style="list-style-type: none"> • Btu meter 	<ul style="list-style-type: none"> • Surface temp. sensor 	<ul style="list-style-type: none"> • Flow meter • Ultrasonic flow meter 	<ul style="list-style-type: none"> • Surface temp. sensor
	<i>Other</i>	-----	-----	-----	<ul style="list-style-type: none"> • Status sensor
Envelope	<i>U-Values</i>	-----	<ul style="list-style-type: none"> • Surface temp. sensor 	-----	<ul style="list-style-type: none"> • Pyranometer • Pyrheliometer
	<i>Windows</i>	-----	<ul style="list-style-type: none"> • Surface temp. sensor 	-----	<ul style="list-style-type: none"> • Tape measure
	<i>Infiltration</i>	-----	-----	<ul style="list-style-type: none"> • PFT test • SF6 tracer gas • Blower door 	<ul style="list-style-type: none"> • Anemometer (wind speed)
Internal Gains	<i>Lighting</i>	<ul style="list-style-type: none"> • Watt meter 	-----	-----	-----
	<i>Equipment</i>	<ul style="list-style-type: none"> • Watt meter 	-----	-----	-----
	<i>DHW</i>	<ul style="list-style-type: none"> • Watt meter 	<ul style="list-style-type: none"> • Electric thermometer 	-----	-----

Table 3-4: Measurement techniques for defining building energy consumption in buildings [ASHRAE 14 2002].

Spot measurements (several seconds to hours) with hand-held watt meters, thermometers, anemometers, and tape measures can be a cost effective means of data collection during site visits. Equipment for these measurements range from up to 11,000 USD (~ 66,000 NOK) for high-end, portable, watt meters to as little as 150 USD (~ 900 NOK) for portable digital thermometers. These meters do not require specialized training or technicians to operate, and when available are useful for defining and verifying input values during the site visit [ASHRAE 14 2002].

Detailed measurements are those that cannot easily be performed by the modeler or that are taken over periods longer than a few days (long-term). Examples of detailed measurement techniques include tracer gas and blower door tests for measuring infiltration rates at the building site, and weekly or monthly electrical metering (with a watt meter or a data logger) to determine load profiles. These techniques require specialized equipment and trained personnel to ensure accurate measurements and can be both time intensive and monetarily expensive [ASHRAE 14 2002]. Additionally, all measurements must be made at the building and often require multiple site visits.

More detailed information on measurement techniques for defining building energy consumption characteristics can be found in both ASHRAE Guideline 14 [ASHRAE 14 2002] and the IPMVP [IPMVP 2002].

3.2.2.6 Typical Practice

Typical practice values are equivalent to the most common value for an input in buildings with similar climates, cultures, and uses. This data is recommended for defining inputs that are hard to obtain without detailed measurement techniques (infiltration rates) or that are expected to have only a minor influence on the overall energy consumption in the building. Unknown schedules may also be developed according to this standard. The use of typical practice should be done with care as these values are averages taken over a portion of the building stock and might not necessarily represent the actual input value for the building of interest. As a result, they should not be used for inputs that are expected to have a strong influence over the quality of calibration of the model (see section 3.2.4.2.2 for information about strong parameters and influential inputs).

3.2.2.7 Uncertainty and Data Collection

The IPMVP [IPMVP 2002] highlights the need to recognize the inaccuracies that arise during data collection, and recommends that all uncertain inputs be documented along with their expected range of values.

RP-1051 [Reddy 2006] defines the common causes of uncertain model inputs as “lack of experience (or even negligence), and improper specification of material properties or system parameters”. Additionally, RP-1051 defines six data quality levels for performing calibrated simulations and suggests that the potential for input uncertainties decreases at higher levels of data quality.

Level 1	As-built drawings and utility data for 1 year are available and may be used to calibrate the model
Level 2	Walk through in addition to utility bills and as-builts
Level 3	Name plate information and on-site measurements in addition to as-builts, utility bills, and a site visit
Level 4	Short term equipment monitoring (hourly monitoring for days to weeks)
Level 5	Hourly whole-building electricity data available
Level 6	Hourly end-use data in addition to whole-building electrical data

Table 3-5: Six levels of simulation input data quality from RP-1051[REDDY 2006].

Level 1 includes the data that is most commonly available in buildings, and so also has the lowest associated cost. However, because of the low data quality at this level the potential for input inaccuracies tends to be high. Conversely, level 6 typically implies higher costs because of the low availability of such detailed data in buildings, but also corresponds to increased certainty in the accuracy of the inputs [Reddy 2006].

3.2.3 Simulation Tools and Input Data

Both ASHRAE and the International Organization for Standardization (ISO) have developed methodologies for calculating building energy performance in the absence of detailed simulation software. These methods may or may not include both steady-state and transient building energy calculations, and provide a reasonable level of accuracy in predicting ECM energy savings [Jokisalo 2007],[Waltz 2000]. Such tools are commonly used because they are easy to implement and do not require extensive modeler experience. However, many of these

tools oversimplify the calculation of building energy, especially with respect to transient and solar effects, which can be particularly important in accurately modeling buildings with thermally massive constructions (see Appendix A).

Consequently, it is necessary to have a well-calibrated and highly detailed building model to ensure accurate savings predictions [Waltz 2000]. The IMPVP [IPMVP 2002] requires that well-tested and accepted simulation software be used in ECM evaluations. This software must perform hourly energy calculations and be capable of modeling all required building inputs [ASHRAE 14 2002].

Table 3-6 gives an overview of the capabilities, interface, target audience, available support, and associated costs for several of the most commonly used and well accepted building energy simulation programs.

	Capabilities	Interface	Intended for use by	Available Support	Cost
DOE-2	energy performance, design, retrofit, research, residential, and commercial buildings.	graphical interfaces available -not included w/program	architects, engineers, and academics	web resources	\$0-\$2000
Ecotect	environmental design & analysis, conceptual design & validation, solar control, thermal design and analysis, prevailing winds, natural and artificial lighting, life cycle assessment & costing, scheduling, and acoustic analysis.	graphical interface	architects	web resources	Student = \$75
IES-VE	energy simulation, environmental performance, commercial buildings, residential buildings, visualization, complex buildings, and systems	graphical interface	architects and engineers	web resources and phone	\$2000-\$5000 (student = \$100)
TRNSYS	energy simulation, load calculation, building performance, research, energy performance, renewable energy, and emerging technology.	object oriented graphical interface	engineers, architects, academics, and energy consultants	web resources	\$2100-\$4200
EnergyPlus	energy simulation, load calculation, building performance, simulation, energy performance, heat balance, and mass balance.	object oriented interface	engineers, architects, and academics	web resources	\$0
ESP-r	energy simulation, environmental performance, commercial buildings, residential buildings, visualization, and complex buildings and systems	graphical interface	engineers, architects, academics, energy consultants	web resources and email	\$0
TAS	building simulation, comfort, CFD, thermal analysis, and energy simulation.	graphical interface	engineers and architects	web resources	\$1600

Table 3-6: Summary of commonly used building energy simulation software [EERE 2008A].

The availability of an intuitive graphical interface makes tools like Ecotect popular among architects. However, when performing calibrations against existing building data it is often the case that such user friendly interfaces come at the expense of algorithm accuracy. IES-VE and TAS are both exceptions to this; they offer intuitive interfaces and strong modeling

capabilities. However, much like TRNSYS, these programs come at a significant cost. The low cost and extensive capabilities of programs like EnergyPlus, ESP-r, and DOE-2 make them some of the most commonly used tools for whole building calibrated simulations, regardless of their lack of an intuitive user interface. DOE-2 is especially popular because of the availability of interfaces with which to develop simple models, and is one of the most well established building energy simulation tools. However, DOE-2 is only able to model predefined heating, ventilation and air conditioning (HVAC) system configurations, while its successor, EnergyPlus, has a much wider range of HVAC input capabilities.

The use of text-based files for input to programs like DOE-2 and EnergyPlus enables the modeler to automate the process of running parametric analyses. This saves the modeler from having to go through the process of manually changing and rerunning simulations during parametric and sensitivity analyses [EPlus 2007a].

Each of the programs presented in Table 3-6 is capable of running hourly annual simulations using formatted weather files. The EnergyPlus website has an extensive database of International Weather for Energy Calculations (IWEC) and Typical Meteorological Year (TMY) weather files, all formatted for EnergyPlus simulations. In addition, these weather files may be edited to accommodate real-time weather data [EPlus 2007b]. This is important in performing calibrated simulations where weather data for the building site and utility billing period are necessary to ensure accurate calibration of building models [ASHRAE 14 2002].

3.2.3.1 Data Input

Pan et al. [Pan 2006] suggested the following order of input when creating simulated models of a high rise building in China: (1) geometry and orientation, (2) heating, ventilation and air conditioning (HVAC) zoning, (3) external surface characteristics, (4) temperature independent loads, (5) HVAC schedules, and (6) plant equipment characteristics. Zhu [Zhu 2006] used a similar order of data entry in his case study of an office in Florida: (1) geometry, (2) internal loads, and (3) HVAC.

Inevitably, the order of model input will depend on the intended calibration methodology and the choice of modeling software. Software is able to dictate data entry by requiring a “hierarchy” of inputs (i.e. surfaces are used to define thermal zones, thermal zones contain equipment, equipment calls controls schedules, etc.). Additionally, some simulation calibration

methods, discussed in section 3.2.4.2, determine the order of data entry by breaking the calibration processes into steps based on load types (i.e. first calibrating lighting, equipment, and fan loads then heating and cooling loads).

3.2.3.2 Model Input Uncertainty

When entering input data it is in the best interest of the modeler to make simplifications to decrease computation time and ease the input of data. Some user manuals, like that available with the EnergyPlus program [EPlus 2007a], provide guidance regarding the type of modeling simplifications and assumptions that can be made without compromising the accuracy of the model (i.e. geometry simplifications, window simplifications, guidelines for thermal zoning, etc.). However, it is widely accepted that experience is the best means of ensuring accurate assumptions and simplifications [Lomas 1992].

RP-1051 [Reddy 2006] underscores the potential for uncertainties arising from modeler error and assumptions, reinforcing the need for an experienced building modeler when entering data into simulations. Also emphasized is the need for an accurate modeling tool, like the simulation programs listed in Table 3-3, to avoid uncertainties.

3.2.4 Calibration Methods for Building Energy Simulations

Calibration is the process through which building simulations are adjusted to obtain an acceptable fit with measured energy consumption data from the building of interest. Calibration is commonly performed either through a manual “tuning” of model inputs or using sensitivity analysis techniques. Metrics for quantifying the fit with measured data, or the quality of the calibration, include statistical and graphical analysis on an hourly, daily, weekly, monthly, or annual basis. This section investigates a number of techniques for calibrating building energy simulations, requiring varying levels of modeler expertise.

3.2.4.1 Metrics for Calibration

3.2.4.1.1 Graphical Calibration

Graphs of building energy consumption and power demand depicting monthly, weekly, daily or even hourly utility billing over the course of a year are commonly used to visualize the differences between simulated and measured energy consumption. Work by Westphal and

Lamberts [Westphal 2005], Pedrini et al. [Pedrini 2002], and Norford et al. [Norford 1994] all utilized monthly energy graphs and hourly measurements to calibrate building models.

Additionally, daily profiles may be used for calibrating against end-use loads. These daily profiles are either measured or generated using day-typing methods [Soebarto 1997],[ASHRAE 14 2002],[Bou Saada 1995]. Work by Bou-Saada and Haberl [Bou Saada 1995] advocated the use of “representative days” to calibrate building models against end-use energy consumptions. These representative days were developed through a binning process in which the hourly profiles for each day in the calibration year were categorized according to (1) average outdoor temperature ($< 7^{\circ}\text{C}$, $7^{\circ}\text{C} < T < 24^{\circ}\text{C}$, $> 24^{\circ}\text{C}$) and (2) weekdays and weekends. Box-whisker plots were then used to graph the minimum, mean, maximum, 25th, and 75th percentile ranges of the hourly energy consumption of each binned day-type. Bou-Saada and Haberl then utilized the resulting hourly energy consumption profiles to calibrate simulations.

Soebarto [Soebarto 1997] used a procedure similar to that developed by Bou Saada and Haberl [Bou Saada 1995], differing in that all data were collected over a 2-4 week period and were graphed using box-whisker plots for the minimum, mean, maximum, 10th, 25th, 75th, and 90th percentile ranges of the hourly energy consumption. Subsequently, a simulation of a building in Texas was calibrated against this short-term data. Soebarto showed that a model that was calibrated against these short-term daily profiles showed a good match when compared to a full year of monthly utility data [Soebarto 1997].

3.2.4.1.2 Statistical Calibration

ASHRAE Guideline 14 [ASHRAE 14 2002] recommends the use of the normal mean bias error (NMBE) (Equation 3-1) and the coefficient of variation of the root mean square error (CVRMSE) (Equation 3-2) to quantify the fit between simulated and measured energy consumption on either a monthly or hourly basis. These two statistics compliment each other; the NMBE quantifies the difference in the mean of the two data sets, while the CVRMSE quantifies the variation between individual data points.

$$NMBE = \frac{\sum_{i=1}^n y_i - \hat{y}_i}{(n-p) \times \bar{y}} \times 100 \quad (3-1)$$

$$CVRMSE = \frac{\sqrt{\frac{\sum_{i=1}^n (y_i - \hat{y}_i)^2}{n-p}}}{\bar{y}} \times 100 \quad (3-2)$$

y_i The measured data point

\hat{y}_i The simulated data point

\bar{y} The average of the measured data points

n The number of data points in the series

p The number of independent variables, equal to 1 for calibrated simulations

ASHRAE Guideline 14 also recommends minimum values for the NMBE and CVRMSE on a monthly and hourly basis for considering a model to be calibrated (Table 3-7).

	Monthly	Hourly
NMBE	5%	10%
CVRMSE	15%	30%

Table 3-7: Threshold values of the NMBE and CVRMSE statistics required to accept simulations to be calibrated on a monthly basis [ASHRAE 14 2002].

RP-1051 [Reddy 2006] used sensitivity analysis in conjunction with the recommended NMBE and CVRMSE values in Table 3-7 to identify multiple calibrated simulations of an office building in Pennsylvania. The calibrated simulations resulting from sensitivity analysis were ranked according to the goodness of fit (GOF) statistic in Equation 3-3 to select a set of Top 20 solutions with which to evaluate ECMs.

$$GOF = \sqrt{\frac{w_{CVRMSE}^2 CVRMSE^2 + w_{NMBE}^2 NMBE^2}{w_{CVRMSE}^2 + w_{NMBE}^2}} \quad (3-3)$$

w_{CVRMSE} & w_{NMBE} Weights assigned to the CVRMSE and NMBE; must sum to one.

RP-1051 [Reddy 2006] suggested that those simulations with a GOF value less than 6% (with w_{CVRMSE} and w_{NMBE} both equal to 0.5) be deemed well-calibrated. This is discussed in more detail in section 3.2.5.3.

Yoon et al. [Yoon 2003] and Soebarto [Soebarto 1997][Soebarto 1997] also recommended the NMBE and CVRMSE for calibrating models – Yoon et al. with annual utility bills and Soebarto with daily load profiles. Yoon et al. recommended NMBE and CVRMSE

values between 5%-15% to consider a model calibrated, while Soebarto [Soebarto 1997] found that a 20% CVRMSE for the daily energy and 15% CVRMSE for the daily peak power were adequate for considering models to be calibrated.

Work by Westphal and Lamberts [Westphal 2005], Pedrini et al. [Pedrini 2002], and Norford et al. [Norford 1994] calculated the percent difference (% Diff) on a monthly and annual basis to compare the simulated and measured energy consumption in office buildings in Brazil (Westphal and Lamberts and Pedrini et al.) and in New Jersey (Norford et al.). Pedrini et al. recommended a percent difference in whole building energy use < 5% on an annual basis and < 10-15% on a monthly basis. The values used by Westphal and Lamberts were similar to those used by Pedrini et al., requiring a percent difference < 5% on an annual basis and < 20% on a monthly basis. Norford et al. required a whole building seasonal percent difference < 10% and a seasonal end-use percent difference < 20%. In addition, Norford et al. required a whole building monthly percent difference less than 15% and a monthly end-use percent difference of 25%.

Zhu [Zhu 2006] used a statistical software tool and paired sample t-tests to quantify the level of calibration between simulations and utility data in a high rise in Florida. According to this work, a probability value of 0.652 at a significance level of 0.05 results in an acceptable calibration.

Work by Reddy and Claridge [Reddy 2000] proposed that the expected uncertainty in retrofit energy savings predictions be the criteria for identifying calibrated models. They suggested that the desired level of energy savings (F), the energy savings uncertainty (U), and the level of confidence in the energy savings prediction (t) all be defined by the project decision makers (investors, building managers, etc.) prior to model calibration. After these uncertainty criteria are defined, the required CVRMSE for identifying calibrated models can be calculated from Equation 3-4. Reddy and Claridge argued that the interests of the project decision makers (investors, building managers, etc.) are better incorporated into both calibration and retrofit energy savings when uncertainty is the metric for calibration.

$$CVRMSE = \frac{U * F}{1.26 * t * \left[\left(1 + \frac{2}{n} \right) \frac{1}{m} \right]^{\frac{1}{2}}} \quad (3-4)$$

<i>CVRMSE</i>	The coefficient of variation of the root mean square error between the measured and calibrated data
<i>n</i>	The number of time-steps in the calibration period
<i>m</i>	The number of time-steps retrofit period
<i>F</i>	The ratio of energy savings to pre-retrofit energy use: (Pre-retrofit energy-Post-retrofit energy)/(Pre-retrofit energy)
<i>1.26</i>	This is an empirical coefficient
<i>t</i>	This is the t-statistic which incorporates the confidence level for the predicted savings
<i>E_{save,m}</i>	The predicted energy savings over the m periods
<i>ΔE_{save,m}</i>	The variation in the predicted energy savings over m periods
<i>U=ΔE_{save,m}/E_{save,m}</i>	The uncertainty, or interval of variation, for the predicted savings fraction, F.

The topic of uncertainty in retrofit energy savings predictions, including a detailed description of each variable in Equation 3-4, is discussed in greater detail in section 3.2.5 on ECM energy savings.

3.2.4.2 Calibration Methods

Simulations may be calibrated by manually adjusting inputs or by applying automated sensitivity analysis techniques. Manual tuning consists of using available graphical and statistical metrics to adjust simulation inputs until an acceptable fit with measured data is achieved. Sensitivity analysis aids in tuning models by isolating inputs that have the greatest influence on the output of the simulation [Reddy 2000].

3.2.4.2.1 Manual Calibration

Work performed by Pedrini et al. [Pedrini 2002] on Brazilian office buildings separated the manual tuning processing into three stages: (1) simulation from design documents, (2) site visits and building audits, and (3) end-use measurements. Monthly energy consumption was examined in stages 1 and 2, while daily load profiles were examined in stage 3. Hourly utility billing was used to generate the representative day profiles used for calibration in stage 3.

Yoon et al. [Yoon 2003] calibrated a model of a high rise building in South Korea according to a six-step procedure: (1) base case modeling, (2) base load consumption analysis, (3) swing-season calibration, (4) site interview and measurements, (5) heating and cooling season calibration, (6) validation of calibrated base case model. Short term measurements were made in steps 3 and 5 and site visits were advocated to verify any uncertain or unknown inputs at each stage in the procedure.

Work by Norford et al. [Norford 1994] and Soebarto [Soebarto 1997] used two-stage procedures to calibrate building energy models against measured data. First, temperature independent loads (lighting, plug loads, hot water, fans) were calibrated, followed by temperature dependent loads (heating, cooling). Measured hourly data and representative day profiles were used to tune the simulation at each stage.

3.2.4.2.2 Sensitivity Analysis

Sensitivity analysis is used to identify influential inputs in calibrated simulations. These are either local sensitivity analyses - concerned with individual inputs, or global sensitivity analyses – concerned with the cumulative effect of changing many inputs simultaneously.

Influential inputs are useful in identifying (1) where further data should be collected, (2) candidate ECMs, and (3) inputs where uncertainties would have the greatest effect on the accuracy of the simulation [Lomas 1992].

Commonly used sensitivity analysis techniques include differential sensitivity analysis (DSA) (local), factorial and fractional factorial design (FD) (global), monte carlo analysis (MCA) (global), and parametric analysis (PA) (global).

A good overview of available sensitivity analysis techniques is provided by Saltelli et al. [Saltelli 2004].

3.2.4.2.2.1 Differential Sensitivity Analysis

Differential sensitivity analysis (DSA) is a local sensitivity analysis technique in which individual inputs are examined for their effect on the results of the simulation. First, a number of inputs for analysis are identified. Each of these inputs is then assigned a range of possible values. Simulations are run, incrementing one input at a time. The result is $(p \cdot n)$ simulations, where p is the number of parameters and n is the number of states that each parameter can take.

The influence of each input is then quantified using a sensitivity or influence coefficient, as in Table 3-8.

Form	Formula	Dimension	Common Name(s)
1	$\Delta OP/\Delta IP$	OP dim/IP dim	Sensitivity coefficient, influence coefficient
2a	$(\Delta OP/OP_{bc})/(\Delta IP/IP_{bc})$	No dim	Influence coefficient, point elasticity
2b	$(\Delta OP/OP_{bc})/(\Delta IP)$	%/IP dim	Influence coefficient
3a	$[\Delta OP/((OP_1+OP_2)/2)]/[\Delta IP/((IP_1+IP_2)/2)]$	No dim	Arc mid-point elasticity
3b	$[\Delta OP/\Delta IP]/[OP_{mean}/IP_{mean}]$	No dim	Sensitivity coefficient

Table 3-8: Influence and sensitivity coefficients for quantifying the impact of a parameter on a building energy model [Lam 1996]. ΔOP is the change in the output of interest, OP_{bc} is the base case value of the output, ΔIP is the change in the input, and IP_{bc} is the base case value of the input.

The parameters are then ranked according to their sensitivity coefficient and the most influential parameters are either confirmed with further measurements or manually tuned by the modeler to reach calibration [Lam 1996].

Lomas and Eppel [Lomas 1992] showed that the local sensitivity results from DSA can be summed to find global sensitivities when two conditions hold true: (1) the individual input changes are very small and (2) the interactions between parameters can be taken to be linear. However, they do not provide guidelines for recognizing when an input change is “small enough” to analyze global sensitivities.

3.2.4.2.2 Factorial Design

Factorial design is a method for assigning coefficients to a linear model that considers the interactions of a selected number of inputs. Common linear models include polynomial and Taylor series approximations, as shown in Equation 3-5.

$$\begin{aligned}
 Y = & \alpha_0 + \sum_{i=1,N} \alpha_i X_i + \sum_{i \neq j} \alpha_{ij} X_i X_j + \sum_{i \neq j \neq k} \alpha_{ijk} X_i X_j X_k \\
 & + \dots + \alpha_{ijk \dots N} X_i X_j X_k \dots X_N
 \end{aligned}
 \tag{3-5}$$

α The coefficients indicating levels of sensitivity

X The model parameters

This process is able to assess the influence of individual parameters and parameter interactions. However, factorial design can be time consuming and require a large number of simulations – up to 2^p for p parameters. The number of simulations can be reduced by using fractional factorial design in which the interactions between inputs are simplified to include only first order effects, thus reducing the number of coefficients that need to be assigned [Fürbringer 1995],[Saltelli 2004].

3.2.4.2.2.3 Parametric Analysis

Parametric analyses investigate all possible combinations of input parameters over a range of values, and in doing so are able to identify the combination(s) of inputs that result in optimal and near optimal solutions (in the case of calibration this would be the simulation with the best fit with the measured data). The number of simulations required during parametric analysis is equal to n^p where n is the number of states that each parameter, p , can take. This can make parametric analyses time consuming and inefficient when a large number of parameters is to be investigated.

3.2.4.2.2.4 Monte Carlo Analysis

MCA evaluates the global sensitivities of model parameters while also identifying parameter combinations that lead to calibrated simulations. MCA assigns a range of values to unknown or uncertain parameters. This assigned range corresponds to some probability density function, most often based on a normal, triangular, or uniform distribution [Reddy 2006],[Harhoff 2006],[Saltelli 2004]. Random vectors of possible input combinations are then generated and simulations are run. MCA may result in many calibrated solutions (depending on the assigned parameter ranges), from which the distribution of states for each input can be extrapolated. The number of simulations run during MCA is at the discretion of the modeler, although previous work has shown that the number of simulations is independent of the number of uncertain parameters, and is commonly on the order of 60-100 simulations [Lomas 1992],[Fürbringer 1995].

Strong parameters are identified by using statistical tests like the χ^2 test. This test calculates how closely the distribution of the parameter values in the calibrated simulations matches with the probability density function (PDF) used to describe the input parameter values

(see Equation 3-12 in section 3.3) [Reddy 2006], [Lomas 1992], [Fürbringer 1995],[Saltelli 2004].

3.2.4.2.2.5 Other Sensitivity Analysis Techniques

Lomas and Eppel investigated the use of a stochastic sensitivity analysis (SSA) in which sensitivity analysis is performed for a number of parameters at each simulation time step. However, they found that SSA was restricted in its applicability and complicated in its implementation [Lomas 1992].

Fürbringer and Roulet [Fürbringer 1995] suggest the Plackett and Burman design as an alternative sensitivity analysis technique to factorial design and monte carlo analysis. The Plackett and Burman design is similar to factorial design and is able to screen influential parameters. The Plackett and Burman design requires N simulations, where N is the number of factors under investigation [Box 2005]. However, this technique is only applicable when the interactions between parameters are negligible.

3.2.5 Retrofit Selection Methods for Building Energy Models

3.2.5.1 Methods and Metrics for Selecting Retrofits

In cases where the intended ECMs for a building are unknown, candidate can be identified according to the intentions of building managers, from typical practice, from a generic list of possible retrofits, with parametric analysis techniques [Engblom 2006], or with optimization techniques [Christensen 2003],[Griffith 2007].

Considerations in selecting retrofits for installation include the potential for energy savings, capital and amortized costs, occupant comfort, environmental impact, and component lifetimes [ASHRAE 14 2002],[Petersdorff 2005],[De Wit 2002].

Work by de Wilde and der Voorden [De Wilde 2004] recommended a five-step procedure for assessing ECMs: (1) define retrofit options, (2) identify the outputs of concern (i.e. comfort, energy efficiency, etc.), (3) assign “performance indicators” to identify acceptable outputs, (4) assess the performance of retrofit options, (5) weight retrofit options according to their performance for different outputs. Recommended outputs included energy savings, cost, environmental impact, and occupant comfort.

Engblom et al. [Engblom 2006] investigated retrofits to Norwegian office buildings that were chosen from a list of common retrofits for such buildings. A parametric analysis was then run to identify the most cost effective energy conservations measures (ECMs) for installation in the building. Analyzed conservation measures included single building component retrofits and whole building system upgrades.

Optimization algorithms are available to identify optimal retrofit scenarios with calibrated building simulations. The GenOpt [GenOpt 2004] software was developed at Lawrence Berkley National Laboratory (LBNL) for use in optimizing both retrofit to existing buildings and new construction designs. This tool provides a number of optimization algorithms than can be run on models from any text-based simulation program - including EnergyPlus and DOE-2. The BeOpt [Christensen 2003] optimization software that was developed at the National Renewable Energy Laboratory (NREL) is an easy to use tool with an intuitive graphical interface that calls on the DOE-2 simulation program. However, this program is designed for analysis of Zero Net Energy Homes, and is not easily modified for other building types. Both of these tools are capable of reaching optimal building designs for a chosen output given a number of candidate inputs provided by the modeler.

3.2.5.2 Cost Estimates During ECM Analysis

The National Renewable Energy Laboratory (NREL) [NREL 1995] has developed a guide for performing economic analyses of renewable energy projects. This guide provides an extensive description of the most common economic markers used in evaluating building energy project costs, including Net Present Value (NPV), Life Cycle Cost Analysis (LCCA), Payback Period (PP), Savings to Investment Ratio (SIR), Internal Rate of Return (IRR), and Annualized Cost (AC). The NPV is emphasized as one of the most common measures of economic evaluation. Additionally, the guide points out that the use of different economic markers to evaluate the same project may provide dissimilar results, likely because inputs are not accounted for in the same way [NREL 1995].

Work by Gorgolewski recommended the use of the savings to investment ratio (SIR) to identify optimal ECM options for housing in Great Britain. This is the ratio of the savings resulting from the investment to the cost of the investment. An SIR less than one indicates that the cost of the investment is greater than its return, while an SIR greater than one indicates a

profitable investment. This is a useful indicator for comparing the economic viability of candidate retrofits [Gorgolewski 1995].

Work by Gustafsson in assessing building energy retrofits using sensitivity analysis applied life cycle cost analysis (LCCA) to indicate what type of heating system – district heat, oil boiler, or heat pump – would be the most cost effective retrofit for a generic Swedish building. The optimal heating system design was chosen based on the system with the lowest TLCC [Gustafsson 2001].

Work performed by Petersdorff et al. in the context of evaluating cost effective climate protection in the European Union recommended the use of the total annual cost (TC_{annual}) as the metric for assessing the economic impact of a retrofit project. Where, the total annual cost was equal to the difference between the annual investment cost and the annual utility bill savings. Retrofits with a total annual cost < 0 were considered to be cost effective, while retrofits with a total annual cost > 0 were not considered cost effective.

$$TC_{annual} = IC_{annual} - \Delta EC \quad (3-6)$$

$$IC_{annual} = IC_{total} * a \quad (3-7)$$

$$a = \frac{(1+i)^n + i}{(1+i)^n - 1} \quad (3-8)$$

TC_{annual}	The annual cost of the retrofit [Cost/year]
ΔEC	The difference in annual energy costs before and after retrofit [Cost/year]
IC_{annual}	The annual investment cost [Cost/year]
IC_{total}	The total investment cost for a retrofit [Cost/year]
a	The annuity factor for annualizing retrofit costs
i	The interest rate
n	The lifetime of the retrofit [years]

Petersdorff et al. [Petersdorff 2005] recommended $i = 4\%$ and $n = 30$ years ($a = 0.0578$) for building envelope components and $i = 4\%$ and $n = 20$ years ($a = 0.0736$) for technical equipment components. A case study done by [Statbank 2007] suggested an interest rate of 7% for amortizing heat pump installations in Norway. The minimum interest rate in such calculations is typically taken as the bank interest rate, which was equal to 4% in Norway in 2007 [Statbank 2007].

Engblom [Engblom 2006] recommended the use of the simple payback period in assessing retrofits to the Norwegian office building stock, where the payback period is equal to

the capital cost of the investment divided by the annual savings due to the installed ECM. This simple payback period is just that – simple. Work by NREL [NREL 1995] suggested that the simple payback period not be used when ranking a number of options because it does not account for savings after the payback period has terminated. Additionally, the simple payback period does not account for the future value of money.

The calculation of utility costs in Norwegian buildings varies according to the building type, and as such will be discussed with respect to the case study building in Chapter 8.

3.2.5.3 Uncertainty in ECM Energy Savings Predictions

Uncertainties arise when an input value is not known, or is only known over a range of possible values [ASHRAE 14 2002]. These input uncertainties then propagate into calibration uncertainties and subsequently into retrofit prediction uncertainties.

3.2.5.3.1 Quantifying ECM Energy Savings Uncertainty

ASHRAE Guideline 14 suggests that uncertainties be accounted for by presenting the simulated ECM energy savings with an interval of expected savings at a known confidence level. For example, a retrofit might be expected to have a 10% variation in savings at 90% confidence; 90% of the time the predicted value of energy savings would be expected to fall within 10% of the real value. Further, ASHRAE Guideline 14 recommends that the expected uncertainty, or variation in energy savings, be quantified according to Equation 3-9.

$$U = \frac{\Delta E_{save,m}}{E_{save,m}} = t \cdot \frac{1.26 \cdot CVRMSE [(1 + \frac{2}{n}) \frac{1}{m}]^{1/2}}{F} \quad (3-9)$$

<i>CVRMSE</i>	The coefficient of variation of the root mean square error between the measured and calibrated data
<i>n</i>	The number of time-steps in the calibration period
<i>m</i>	The number of time-steps retrofit period
<i>F</i>	The ratio of energy savings to pre-retrofit energy use: (Pre-retrofit energy-Post-retrofit energy)/(Pre-retrofit energy)
1.26	This is an empirical coefficient
<i>t</i>	This is the t-statistic which incorporates the confidence level for the predicted savings
<i>E_{save,m}</i>	The predicted energy savings over the m periods
<i>ΔE_{save,m}</i>	The variation in the predicted energy over m periods
<i>U=ΔE_{save,m}/E_{save,m}</i>	The uncertainty, or interval of variation, for the predicted savings fraction, F.

The simulated energy savings, expressed as a percentage of the base-year energy consumption, is equal to F, and the uncertainty in this value is equal to F*U. The empirical factor of 1.26 arose when the uncertainty relationships that were developed by Thiel [Thiel 1971] were converted in work by Reddy and Claridge [Reddy 2000] to the simple solution seen in Equation 3-9. A more detailed derivation of these equations is found in Reddy and Claridge [Reddy 2000] and ASHRAE Guideline 14 [ASHRAE 14 2002].

Reddy and Claridge [Reddy 2000] developed Equation 3-9 as a metric for calibration (see section 3.2.4.1 of this chapter). However, ASHRAE Guideline 14 adopted it as a means of quantifying the level of uncertainty in ECM energy savings evaluations. When using Equation 3-9 ASHRAE Guideline 14 [ASHRAE 14 2002] suggests that the level of uncertainty in retrofit predictions be less than 50% of the annual reported savings at a 68% confidence level (t = 1) for retrofits to be considered as plausible installations.

Table 3-9 presents the value of the t-statistic for varying degrees of freedom, keeping in mind that the number of independent variables, p, in calibrated simulations is equal to one, and n is the number of time-steps in the calibration period.

n-p	68% confidence	80% confidence	90% confidence	95% confidence
5	1	1.48	2.02	2.57
10	1	1.37	1.81	2.23
15	1	1.34	1.75	2.13
20	1	1.33	1.73	2.09
25	1	1.32	1.71	2.06
Infinite	1	1.28	1.65	1.96

Table 3-9: Values of the t-statistic for quantifying confidence in retrofit energy savings predictions during uncertainty analysis. Where, $p = 1$ for calibrated simulations and n is the number of time steps in the simulation period [ASHRAE 14 2002].

Figure 3-3 through Figure 3-5 applied Equation 3-9 to graph the uncertainty (U) associated with retrofit energy savings predictions that are made on a monthly basis. CVRSME values of 15%, 10%, and 5% are plotted at predicted energy savings (F) from 0% to 100%. The four figures present the relationship between uncertainty and energy savings at different levels of confidence.

Uncertainty vs. Savings at 95% Confidence

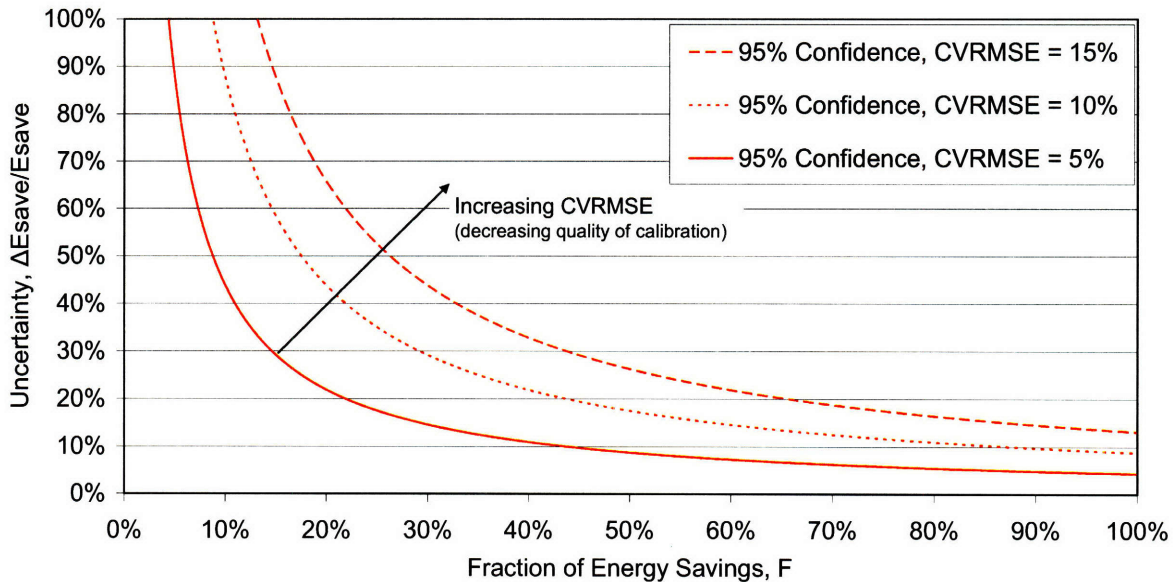


Figure 3-2: Energy savings uncertainty at 95% confidence and 5% (solid), 10% (short dash), and 15% (long dash) CVRMSE [ASHRAE 14 2002].

Uncertainty vs. Savings at 90% Confidence

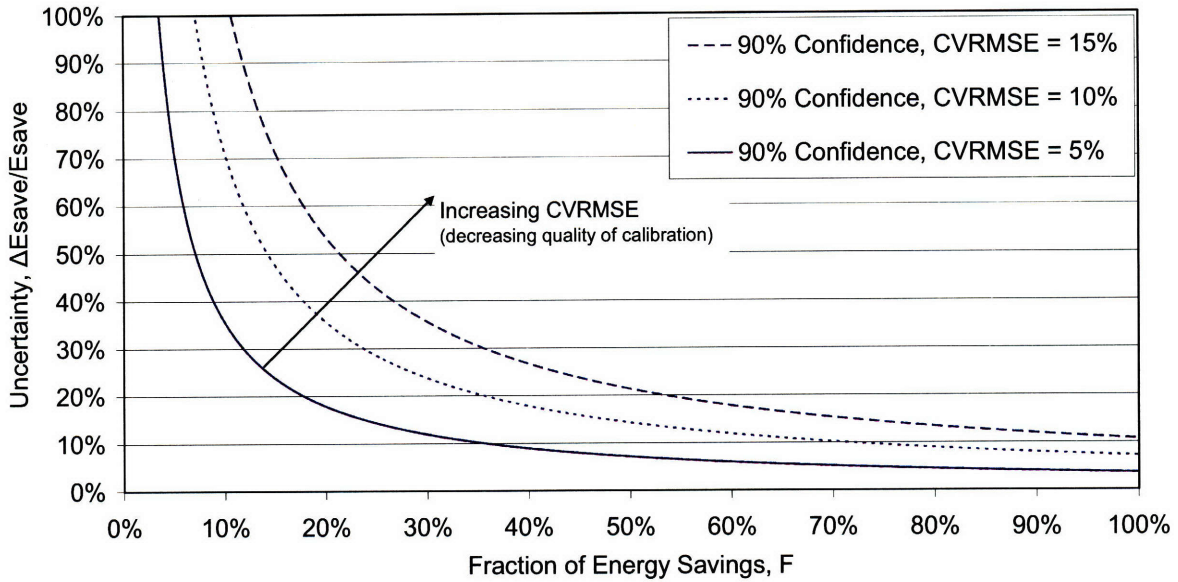


Figure 3-3: Energy savings uncertainty at 90% confidence and 5% (solid), 10% (short dash), and 15% (long dash) CVRMSE [ASHRAE 14 2002].

Uncertainty vs. Savings at 80% Confidence

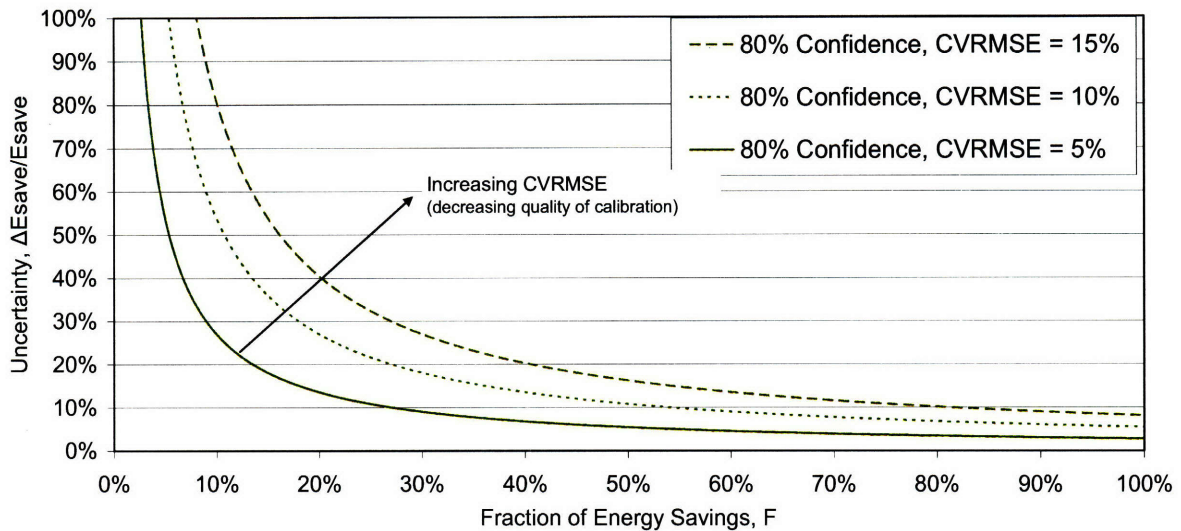


Figure 3-4: Energy savings uncertainty at 80% confidence and 5% (solid), 10% (short dash), and 15% (long dash) CVRMSE [ASHRAE 14 2002].

Uncertainty vs. Savings at 68% Confidence

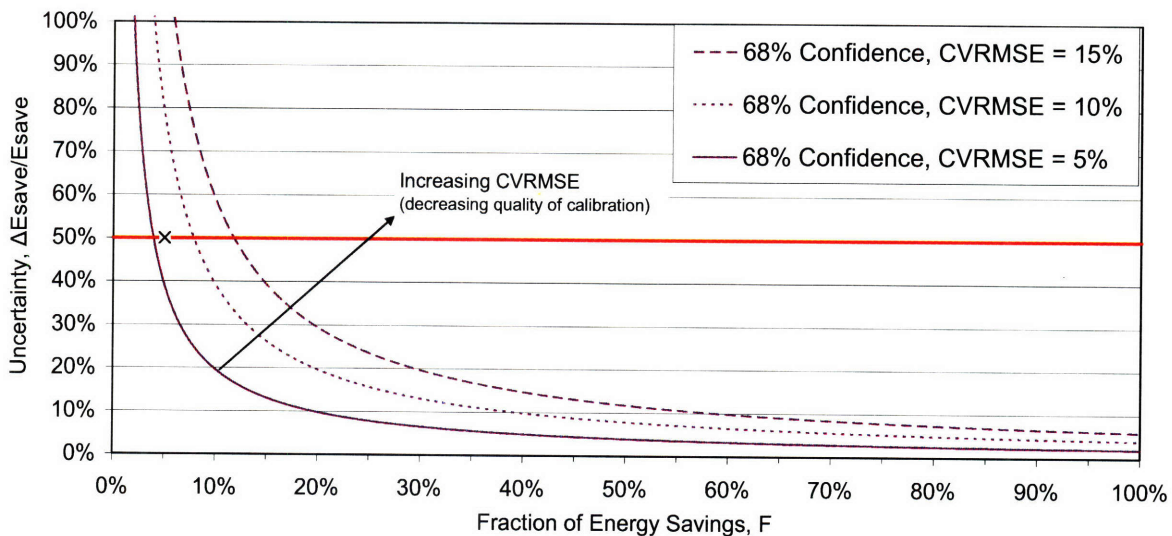


Figure 3-5: Energy savings uncertainty at 68% confidence and 5% (solid), 10% (short dash), and 15% (long dash) CVRMSE [ASHRAE 14 2002]. The red line indicates the maximum uncertainty for accepting energy savings prediction to be accurate. The “x” indicates the uncertainty criteria required in RP-1051 [REDDY 2006].

Note how the uncertainty (y-axis) increases dramatically as the fraction of energy savings (x-axis) goes to zero. Additionally, note how the savings uncertainty increases for calibrations with higher CVRMSE values. Intuitively, this makes sense – poorly calibrated solutions should have a greater degree of uncertainty in their predicted ECM energy savings.

Work by de Wit and Augenbroe [De Wit 2002] emphasized the potential impact that uncertainties in collected data and calibrated models can have on the ECM decision making processes. In order to incorporate uncertainty in their prediction of occupant comfort, they advocated the use of probability density functions. They argued that presenting a range of feasible simulation results allows better informed ECM selections to be made.

3.2.5.3.1.1 Uncertainty and Calibration Criteria from RP-1051

RP-1051 [Reddy 2006] suggests that performing ECM evaluations with multiple calibrated solutions reduces savings uncertainties by providing an interval of predicted energy savings. Additionally, RP-1051 suggests that any retrofit with predicted annual energy savings less than 5% be rejected as too uncertain. This is a minimum criterion. RP-1051 goes on to suggest that only energy savings predictions greater than, or equal to, 10% be considered accurate. The basis for these uncertainty criteria may be observed in Figure 3-3 through Figure

3-5, where savings of less than 5% to 10% (x-axis) show an exponential increase in the uncertainty of the retrofit energy savings prediction. Figure 3-5 was also examined to find the CVRMSE value at which the 5% energy savings threshold recommended by RP-1051 and the 50% uncertainty at 68% confidence criteria that was recommended in ASHRAE Guideline 14 [ASHRAE 14 2002] intersected; this point is indicated by the black “X” in Figure 3-5. This point was of interest because it combined the uncertainty criteria recommended in RP-1051 and ASHRAE Guideline 14 to identify the CVRMSE value for considering calibrated simulations to be certain. This occurred just above the 5% CVRMSE in Figure 3-5, at CVRMSE ~ 7%. Recalling that RP-1051 identified well-calibrated models as those with a monthly NMBE $\leq 5\%$ for both power and energy (Table 3-7), and a GOF $\leq 6\%$, a quick calculation was performed to compare the 7% threshold value of CVRMSE that was calculated from the uncertainty criteria and the CVRMSE required to meet the NMBE and GOF requirements from RP-1051. The result was a required CVRMSE $\leq 7\%$ for models to meet the calibration criteria suggested in RP-1051 – the same CVRMSE required for considering models to be both calibrated and certain in ASHRAE Guideline 14. Consequently, it was shown that the 6% GOF and 5% minimum energy savings values from RP-1051 coincided well with the calibration and uncertainty criteria from ASHRAE Guideline 14 [ASHRAE 14 2002]. No clear basis for the 10% energy savings uncertainty threshold recommended in RP-1051 was identified. This is discussed further in the work performed in Chapter 8.

3.2.5.3.1.2 Autocorrelation and ECM Energy Savings Uncertainty

One important point about the application of Equation 3-9 is that it is intended only when analyzing the uncertainty in data sets with uncorrelated residuals. For residuals to be uncorrelated, all data points in the set must be independent from each other. Monthly and weekly energy consumption data are often uncorrelated, meaning that the data are independent from month to month or week to week. However, when working with daily or hourly data, correlation often occurs, especially in building energy data that is highly dependent on weather conditions. Since hourly or daily temperature values are often determined by the temperature in the hour or day immediately preceding it these data are commonly considered to be correlated. And, since building energy models are often strongly dependent on temperature, it is often the case that hourly or daily building energy models also have correlated residuals. The level of

correlation in the residuals of a data set is easily calculated by entering the data set into a spreadsheet, copying it, and pasting it in the adjacent column with a 1 row (time-step) offset. The R^2 value of these two columns of data can then be calculated, and the correlation coefficient ρ , equal to R , can be determined. Reddy and Claridge [Reddy 2000] recommend that data sets with $\rho > 0.5$ be considered correlated. Additionally, Reddy and Claridge modified Equation 3-9 to account for cases where correlation occurs in the data (Equation 3-10). This modification normalized the uncertainty equation over the calculated number of independent observations, n' , in the correlated data set (Equation 3-11).

$$U = \frac{\Delta E_{save,m}}{E_{save,m}} = t \cdot \frac{1.26 \cdot CV \left[\frac{n}{n'} \left(1 + \frac{2}{n'} \right) \frac{1}{m} \right]^{1/2}}{F} \quad (3-10)$$

$$n' = n \cdot \frac{1 - \rho}{1 + \rho} \quad (3-11)$$

3.2.6 Lessons Learned

A review of previous work on energy conservation measure (ECM) evaluation indicated that whole building calibrated simulation was the most appropriate method for estimating the potential energy savings of candidate retrofits. Furthermore, previous work emphasized the importance of documenting the intended procedure before proceeding with any type of calibration. This calibration plan should include information regarding the data that needs to be collection, what measurements need to be taken, what simulation software is to be used, what retrofits are to be examined, and what metrics are to be used for calibration and retrofit evaluation.

The need for as-built building information and thorough site visits were also emphasized. Site visits should include short term monitoring with hand held meters. Hourly energy consumption information can also be a useful tool during both data collection and calibration. Additionally, more detailed measurements may be taken.

Two methods of calibrating building models were identified: manual tuning and sensitivity analysis. Metrics for calibration included the statistical normal mean bias error (NMBE) and coefficient of variation of the root mean square error (CVRMSE). These calibration metrics enable calibrated models to be identified and should be complimented by

graphical metrics for visual inspection of the calibration quality. Monte Carlo sensitivity analysis techniques were emphasized as an easy to implement method of identifying influential inputs during calibration.

It is inevitable that inaccuracies and uncertainties are generated during input and calibration – both of which propagate into retrofit energy savings predictions. This uncertainty cannot be ignored as it is an important part of the retrofit selection process. Equations for quantifying ECM savings uncertainty were presented in ASHRAE Guideline 14 [ASHRAE 14 2002], and RP-1051 [Reddy 2006] advocated the use of multiple calibrated simulations to decrease uncertainty during retrofits assessments. Additionally, modeler experience, detailed building information, and the use of a well-test computer software were all emphasized as means of improving retrofit energy savings prediction accuracy.

Sensitivity analysis and optimization techniques are useful in identifying optimal retrofits, but they can be computationally expensive. This makes the use of a generic list of retrofits that can be ranked according to cost and energy savings metrics reasonable for selecting retrofits for installation.

3.3 ASHRAE RP-1051 [Reddy 2006]

After reviewing the available methods of calibration the procedure proposed in ASHRAE RP-1051 [Reddy 2006] was taken as the base for further calibration procedure development in this work. As such, a summary of the procedure is provided here, as are a list of issues and concerns that will be addressed in subsequent chapters. Figure 3-6 shows the procedure for performing ECM evaluations proposed by ASHRAE RP-1051.

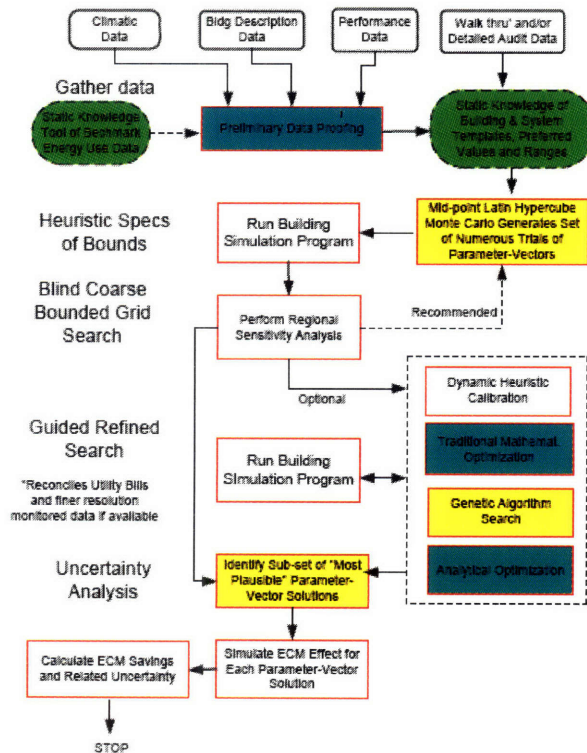


Figure 3-6: Procedure for calibrating building energy simulations recommended in ASHRAE RP-1051 [Reddy 2006].

3.3.1 Data Collection

First, data is collected according to level 3 in Table 3-5 of section 3.2.2. This data is then input into a simulation model and uncertain inputs are identified. A Latin Hypercube Monte Carlo (LHMC) analysis is then run to identify calibrated solutions and the input parameters that are most influential in reaching calibration.

3.3.2 Latin Hypercube Monte Carlo (LHMC) Analysis

The first step in the LHMC analysis is to assign a range of expected values to each uncertain input, or parameter. The input values in this range are at the discretion of the modeler, but should define the interval of feasible parameter values. After defining each parameter range RP-1051 advocates the use of probability density functions (PDFs), namely the normal, triangular, and uniform distributions, to discretize each parameter range into three states: low, middle, and high. Random vectors of parameters with varying input states are then generated and a number of simulations are run (between 100 and 10,000 simulations were run in RP-1051).

Those simulations with monthly energy and power demand predictions satisfying the NMBE (Equation 3-1 in Chapter 3) and CVRMSE (Equation 3-2 in Chapter 3) threshold values from ASHRAE Guideline 14 (Table 3-7 in Chapter 3) are accepted as calibrated and are called “candidates”. The candidate solutions are then ranked according to their goodness of fit (GOF) (Equation 3-3 in Chapter 3) values and those with the 20 lowest GOF values are termed the “Top 20 solutions” and are used to evaluate ECM energy savings.

3.3.2.1 Strong Parameters

An important step in the LHMC procedure is the identification of “Strong” parameters. The parameter strength is a measure of its influence on the ability of a model to reach calibration. As stated in RP-1051: “the objective of a sensitivity analysis in our context is to identify the parameters that are strong (i.e. those that influence the statistical goodness-of-fit criteria)” [Reddy 2006]. Because the input to the LHMC analysis is random, when a parameter is strong it will tend to appear amongst the candidate solutions (those with satisfactory NMBE and CVRMSE values) with a preferred value, or with a non-random distribution of values. The Strong parameters identified during LHMC are only influential in reaching calibrated solutions, and do not necessarily indicate areas where ECMs might be most beneficial. Additionally, the strong parameters are only known to be strong over the range of values assigned to them during the LHMC; changes in the range of input values may yield different strong parameters. Therefore, assigning reasonable input ranges is important to identifying strong parameters.

The strength of a parameter is quantified using the χ^2 test. The χ^2 test is a well-known statistical method to test the randomness of a distribution: the higher the value, the less random the distribution. According to RP-1051 when only three values are possible (degree of freedom = 2), it can be said within a 99% interval of confidence that a parameter is Strong, meaning not randomly distributed, when its χ^2 value is above the threshold of 9.21. The formula for calculating the χ^2 is shown in Equation 3-12, where: p_{exp} is the expected occurrence (equal to the number of candidates divided by the number of parameter states), and p_{obs} is the observed occurrence.

$$\chi^2 = \sum_{s=1}^3 \frac{(p_{obs,s} - p_{exp,s})^2}{p_{exp,s}} \geq 9.21 \quad (3-12)$$

d.f.	99.9%	99.5%	99%	95%	80%	70%	50%	10%
2	13.815	10.597	9.210	5.991	3.219	2.408	1.386	0.211

Table 3-10: Values of the χ^2 statistic, organized according to confidence interval. D.f. stands for the number of degrees of freedom, equal to the number of parameter states (n), less 1 (n-1).

The input vectors to the LHMC (100 to 10,000 input vectors were investigated in RP-1051) have random parameter distributions, meaning that the χ^2 value of the LHMC input vectors is very close to zero. RP-1051 recommends checking the randomness of the LHMC inputs prior to running building energy simulations. If the parameter distribution is not random a new set of random parameter combinations should be generated. Consequently, when examining the results of the LHMC for calibrated building models, non-influential, or weak parameters are expected to retain their random distributions; strong parameters are expected to show up with highly non-random distributions.

3.3.2.2 Fine Grid Search

The strong parameters describe those areas where uncertainty in the inputs is most critical to the results of the calibration. This means that strong parameters are important in recognizing where further information may need to be gathered, or where a fine grid search could be performed. The fine grid search is performed on the Top 20 parameter vectors (20 lowest GOF values) with the goal of further improving their GOF values. The fine grid search subdivides each of the three states of the strong parameters into three sub-ranges (for a total of nine discrete values) and simulations are run for all possible combinations (parametric analysis) of values for each of the Top 20 solutions. The total number of simulations for the fine grid search amounts to $m \cdot 3^n$, where n is the number of strong parameters and m is the number of Top solutions, i.e. 20. In models with a large number of strong parameters the number of simulations to run a fine grid search can increase quickly.

As an example, assume that parameter p1 and p2 were both identified as strong parameters after an LHMC analysis. Looking at only one of the Top 20 solutions, for which p1 was strong at state 2 and p2 was strong at state 3, the fine grid search would require $1 \cdot 3^2$

simulations to investigate all possible combinations of p1 and p2 for this single solution. The combinations of p1 and p2 needed to perform the fine grid search are shown in Table 3-11.

	Run 1	Run 2	Run 3	Run 4	Run 5	Run 6	Run 7	Run 8	Run 9
p1	2L	2	2H	2L	2	2H	2L	2	2H
p2	3L	3L	3L	3	3	3	3H	3H	3H

Table 3-11: Example input vectors for running a fine grid search during LHMC calibration.

“L” and “H” denote the low and high values that were assigned to subdivide the three parameter ranges that initially defined the LHMC parameter input.

3.3.2.3 Number of LHMC Simulations

RP-1051 recommends running iteratively higher numbers of LHMC simulations to identify all strong parameters. If the same strong parameters are identified in successive LHMC runs, then RP-1051 suggests that the method could be considered to have “converged”, meaning no further simulations need to be run.

Alternatively, RP-1051 suggests that the strong parameters may be “frozen” at their most probable value and the LHMC analysis may be re-run on only the remaining parameters (thus searching in a reduced solution space) to identify new strong parameters.

3.3.3 Retrofit Selection

The choice of which energy conservation measures (ECMs) to evaluate is at the discretion of the modeller – no procedure for doing so is presented in RP-1051. However, for those retrofits that are analyzed, RP-1051 recommends presenting the energy savings graphically. In these graphs the median values of predicted ECM savings from the Top 20 LHMC solutions should be bounded by twice the standard deviation of the predicted energy savings among the Top 20 solutions. In this way, a range of predicted energy savings are given for each retrofit under consideration. The median is plotted rather than the mean to reduce the influence of outliers. Further, retrofits with predicted energy savings less than or equal to 5% were rejected as absolutely too uncertain, while 10% energy savings was recommended as the minimum for accepting predictions as “accurate”.

3.3.4 Concerns and Recommendations for Future Work

RP-1051 applied the LHMC calibration procedure to two synthetic buildings and two real case study buildings with mixed results. Based on the results of these case studies and known issues with the procedure, RP-1051 highlights several areas of concern:

- The choice of the Top 20 set of solutions is somewhat arbitrary. Why not 5, 10, or 30 solutions?
- The need for a fine grid search and the usefulness of freezing strong parameters remains in question.
- There is no magic number of LHMC simulations to ensure that the appropriate strong parameters are identified. Between 5,000 and 10,000 runs are recommended, but this is somewhat arbitrary and is loosely based on the two case study buildings that were examined.
- A GOF value $\leq 6\%$ should be taken as the standard for accepting calibrations for the Top 20 solutions. Are there alternative metrics for ranking calibrated solutions?
- ECM savings predictions of less than 5% should be rejected as being unreliable due to the potential effects of uncertainties in the model. ECMs with savings predictions $\geq 10\%$ are recommended as acceptable given the uncertainty that is inherently contained in models that are calibrated against monthly utility data.
- It is recommended that a methodology be developed for identifying which measurements would be necessary to improve the accuracy of the simulation.

Several of these concerns will be addressed in the work performed in subsequent chapters; specifically, the number of Top solutions for performing retrofit evaluation, the number of LHMC simulations required, and the usefulness of freezing strong parameters and running a fine grid search. Uncertainty in retrofit predictions will also be examined. RP-1051 made no observations about the effect of installing ECMs that change strong parameter values; this will be investigated in subsequent chapters.

4 Retrofit Analysis: Case Study

Two calibrated simulation procedures were assessed as potential tools for evaluating energy saving retrofits in Norwegian buildings. These were the Latin Hypercube Monte Carlo (LHMC) analysis procedure that was proposed in RP-1051 and the manual model calibration proposed by Norford et al. [Norford 1994] and Soebarto [Soebarto 1997]. Both of these procedures were appropriate for generating calibrated building simulations to assess a variety of retrofit options. These two procedures were applied to a case study of a Norwegian building to:

- Identify resources and methods of collecting building energy use information (Chapter 5).
- Evaluate the most appropriate applications for the LHMC and manual calibration methods (Chapters 7 and 8).
- Assess techniques for isolating important model inputs (Chapter 7).
- Assess the influence of unknown or uncertain inputs on retrofit energy savings predictions (Chapters 5, 6, 7, and 8).
- Recommend retrofits for installation in the case study building (Chapter 8).
- Establishment a procedure, or guide, for assessing building energy performance and identifying energy saving retrofits (Chapter 10).

The steps taken in performing this case study were as in Figure 4-1. Each of these steps is discussed in detail in Chapters 5 through 8.

- (1) A **building was selected** from the Norwegian building stock (Chapter 4).
- (2) Building **data was collected** from as-built documents, site visits, utility data and measurements (Chapter 5).
- (3) Collected data was **input** into a simple energy calculation model and into a computer simulated building energy model (Chapters 6 and 7).
- (4) A **calibration** was performed manually and with LHMC sensitivity analysis (Chapter 7).
- (5) Finally, the calibrated building model was used to evaluate potential energy saving **retrofits** in the case study building (Chapter 8).

Figure 4-1: Steps that were taken in performing the case study.

The desire for an accurate and easy to implement procedure for estimating energy savings required that errors and uncertainties in building selection, data collection, input, calibration, and retrofit energy savings prediction be investigated during the case study. The goal was not to eliminate uncertainties, but to analyze means of (1) identifying uncertain inputs, (2) finding their most likely values, and (3) quantifying these uncertainties during energy savings prediction.

4.1 Selection of a Case Study Building

The case study building was chosen on the basis of the five criteria listed in Table 4-1. These criteria are listed in the order in which they were prioritized when soliciting candidate case study buildings from national and local building owners.

<i>Features of a desirable case study building:</i>
<ul style="list-style-type: none"> ○ Potential to influence energy savings on a national level ○ Accessibility (proximity to Trondheim, Norway) ○ Cooperative building managers ○ Availability of building drawings and documentation ○ Potential for application of case study results

Table 4-1: Desirable features of a case study building.

The potential to influence energy savings on a national level refers to the choice of building type for case study. This includes houses, offices, schools, shops, hotels, etc. Ideally, the building type chosen for study would constitute a large enough portion of the energy demand in national building stock to have a significant influence on reducing the stock level energy demand.

The proximity of the building to Trondheim, Norway was important for enabling site visits by the modelers, who were studying at the Norwegian University of Science and Technology (NTNU), located in Trondheim, during the time of the case study.

The cooperation of the building managers was important to establishing a quality relationship for the acquisition and exchange of building data. This relationship was very highly valued as it ensured the greatest access to the building and building documents.

The availability of building drawings and documentation was important to ensure that a representative building model could be created. This meant that high quality data describing the

building geometry, materials, heating systems, ventilation systems, lighting, equipment, and utility billing were desirable.

The potential applicability of the case study results refers to the possibility that the recommended retrofits resulting from this work might actually be installed in the case study building. This means that an ideal candidate would already be under consideration for retrofit and that the building owners would be interested in the possibility of applying the results of the case study to the building's renovation.

4.1.1 Sources of Candidate Buildings

Several Norwegian building management organizations were contacted to select a building for study.

4.1.1.1 National Organizations

Entra Eiendom is a real estate company of more than 140 employees that controls over 980,000 m² of properties (mainly offices) throughout Norway. The company is owned by the Kingdom of Norway and is headquartered in Oslo, where over 70% of its properties are located. Offices are also located throughout Norway, including Trondheim, where Entra manages nearly 90,000 m² (10% of total holdings) of property [Entra 2007].

Statsbygg is a property and construction management administrator under the control of the Norwegian Ministry of Renewal and Administration. Statsbygg is responsible for managing more than 2.3 million m² of state owned properties consisting of cultural buildings, colleges, royal properties, administration buildings, embassies, and diplomatic residences in Norway and abroad. In addition, Statsbygg is responsible for managing the construction and development of new and existing government properties. Nearly half of the 670 employees of Statsbygg work at the organization's headquarters in Oslo, while the remaining employees work in Northern, Central, Western, and Eastern regional offices (including Trondheim) [Statsbygg 2007].

ENOVA is an organization under the control of the Royal Norwegian Ministry of Petroleum and Energy that is concerned with the supply and demand of energy in Norway. Although not directly involved in research activities, ENOVA manages the money in the Norwegian Energy Fund to "limit energy use considerably more than if developments were allowed to continue unchecked; to increase annual use of water-based central heating based on

new renewable energy sources, heat pumps and waste heat of 4 TWh by the year 2010; to install wind power capacity of 3 TWh by the year 2010 and increase environmentally friendly land-based use of natural gas” [ENOVA 2007],[ENOVA 2005]. As a part of the effort to achieve these goals ENOVA funds energy monitoring initiatives in Norwegian buildings [ENOVA 2007],[ENOVA 2005].

4.1.1.2 Local Organizations

Trondheim Eiendom (Municipality) is run by the city of Trondheim and oversees the maintenance and construction of all buildings owned by the city. This includes schools, offices, and administrative buildings [TEV 2007a],[Arentz 2007].

E.C. Dahls Eiendom is a real estate company located in Trondheim that controls the rental and sale of offices, shops, hotels, and other properties [EC Dahls 2007].

4.1.2 Candidate Identification and Selection

4.1.2.1 Building Type

It is hoped that the results of this case study can be expanded to other buildings of similar type, making it important that the chosen building type be capable of affecting a high level of change in the energy consumption of the Norwegian building stock. In order to select a building type stock level energy consumption data were collected and are shown in Figure 4-2.

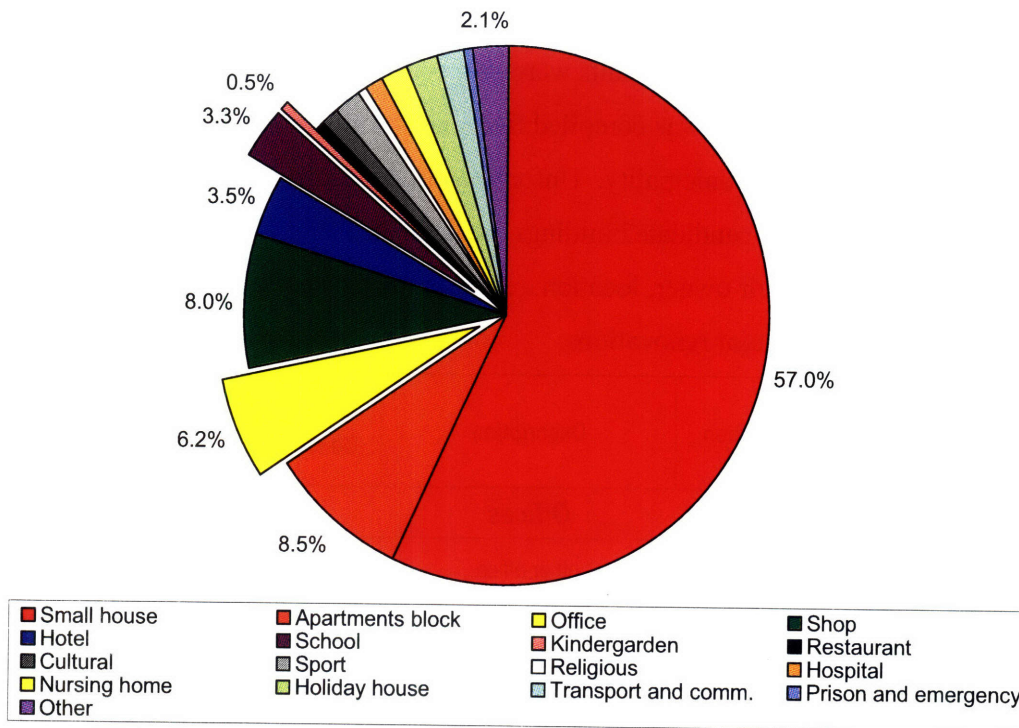


Figure 4-2: Energy consumption in the Norwegian building stock by building type [Sartori 2008a]. Schools and Offices are the slices that are removed from the pie. Holiday houses are vacation homes that are occupied intermittently.

The energy percentage presented in Figure 4-2 is an indicator of the contribution of a single building category to the total building stock energy consumption, and highlights housing (small houses and apartments – 65.5%), shops (8%), hotels (3.5%), schools (schools and kindergartens – 3.8%), and offices (6.2%) as the five greatest energy consumers in the Norwegian building stock. Of these five building types offices and schools were the favored buildings for this case study analysis. Offices were preferred because of their continuity with previous work performed by Engblom et al. [Engblom 2006] while schools were chosen because of the readily available data and high level of cooperation from the Trondheim Municipality. Residential buildings were not chosen because there is already a substantial body of work being performed on these building types [Myhre 2000],[Engblom 2006].

4.1.2.2 Candidate Building Identification

Inquiries were made to Entra Eiendom, Statsbygg, ENOVA, Trondheim Eiendom (Municipality), and EC Dahls Eiendom in search of candidate buildings. In soliciting candidate buildings from these organizations the need for a school or office close to Trondheim was given

precedence, although the cooperation of building managers, availability of documentation, and potential application of the case study results were also considered.

A list of candidate buildings was compiled from data provided by ENOVA, EC Dahls Eiendom, and the Trondheim Municipality. Unfortunately, candidates were not offered by Entra Eiendom or Statsbygg. These candidate buildings are listed in Table 4-3 and Table 4-3 with a brief description including their owner, location, usage, year of construction, floor area, specific energy, and the date of any major renovations.

ID #	Owner/ Manager	Location	Description	Year Const.	Floor Area [m ²]	Specific Energy [kWh/m ²]	Renov. Year
Offices							
T-1984	Transittgata 1, Trondheim Havn	Trondheim	other office	1984	3,317	230	----
T-1985a	E C Dahls Eiendom	Trondheim	office and administration, townhall	1985	3,150	157	2000
T-1958	E C Dahls Eiendom	Trondheim	office and administration, townhall	1958	2,300	124	1985
T-1975	E C Dahls Eiendom	Trondheim	bank, post office	1975	13,500	320	----
T-1978	E C Dahls Eiendom	Trondheim	bank, post office	1978	9,080	318	----
T-1956	E C Dahls Eiendom	Trondheim	office and administration, townhall	1956	2,800	257	----
T-1962	E C Dahls Eiendom	Trondheim	office and administration	1962	2,900	270	2003
T-1985b	Trondheim Eiendom	Trondheim	office and administration, townhall	1985	1,880	158	2000
S-1977	-----	Steinkjer	office and administration, townhall	1977	9,000	270	----
S-1989	-----	Steinkjer	office and administration, townhall	1989	9,000	175	----
N-1955	Havnegata 12, Gjensidige	Namsos	office and administration, townhall	1955	2,000	287	1995
L-1986	-----	Levanger	office and administration, townhall	1986	4,453	184	----

Table 4-2: Candidate office buildings for case study. Each building is labeled according to the first letter in the location and the year of construction [TEV 2007A],[EC Dahls 2007],[ENOVA 2007]. The specific energy is the energy consumed at the building site.

ID #	Owner/ Manager	Location	Description	Year Const.	Floor Area [m ²]	Specific Energy [kWh/m ²]	Renov. Year
Schools							
Steindal School	Trondheim Kommune	Trondheim	Secondary school building, two stories, rectangular layout	1978	4,400	173	1997
Lilleby School	Trondheim Kommune	Trondheim	Secondary school building	1920's	4,710	138	----
Lade School	Trondheim Kommune	Trondheim	Secondary school building	1960's- 1970's	6,121	204	2007- may be torn down
Huseby School	Trondheim Kommune	Trondheim	Secondary school building	1970's	10,676	324	----

Table 4-3: Candidate school buildings for case study [TEV 2007a],[Arentz 2007]. The specific energy is the energy consumed at the building site.

4.1.2.3 Case Study Building Selection

Conversations with building managers narrowed the list in Table 4-3 to buildings owned by EC Dahls Eiendom and the Trondheim Municipality. These two building owners were chosen because of their interest in collaborating on the case study. The importance of this interest cannot be emphasized enough, as a close collaboration is essential to gathering detailed building information.

Further conversations revealed that both the Steindal School and office building T-1962 were to be renovated in the coming years, making the case study potentially useful to reducing the building's energy consumption. Upon isolating these two candidates available utility data and building documentation were examined. Based on the quality and quantity of this data, in conjunction with the cooperation of building managers and the applicability of the work, the Steindal School was selected as the case study building.

4.2 Presentation of Case Study: Steindal School

4.2.1 General building description



Figure 4-3: Image of the Steindal School, looking at the North façade of the building.

The Steindal elementary school is located in Trondheim, Norway (Latitude: 63° 36'; Longitude 10°, 23') and serves some 300 students and 40 administrators. The building consists of two parts – the original, or main, building that was built 1978 and an addition, or annex that was built in 1997. The total conditioned floor area is 4,400m² and is divided between two floors (see section 5.1.3).

Outdoor air is supplied by two balanced ventilation systems with heat recovery, one in the Main building and one in the Annex, while heating is supplied locally in each room by electric resistance radiators; the building has no cooling system.

Electricity is then the only energy carrier in the school, and, at the time of the case study, hourly data on consumption were available from the local electricity company from 2004 through 2006.

A more detailed description of the Steindal School is provided in Chapter 5.

4.2.2 Municipality

The Trondheim Municipality is located in the city of Trondheim and oversees the operation and maintenance of all buildings owned by the city. This includes all primary and secondary schools.

The Municipality maintains a central control center in their downtown Trondheim office to control the temperature setpoints, schedules, and ventilation availability, in addition to monitoring the real-time temperature and ventilation setpoints, in each of their school buildings.

The Trondheim Municipality plans to renovate the Steindal School in the upcoming years, and is interested in the results of this study as a guide for selecting energy saving retrofits. The Municipality's intended retrofits include a water based heating system and an occupant controlled ventilation system [Arentz 2007].

5 Data Collection

Data was collected to describe the pre-retrofit energy use in the building prior to assessing retrofits for the Steindal School. Information was gathered on heating, cooling, ventilation, lighting, plug load, and domestic hot water use. Utility bills and weather data were also collected. The resources for collecting this information included as-built documents, site visits, hourly utility billing, and typical practice [Wigenstad 2005],[NS3031 1987]. In the interest of presenting a simple and cost effective procedure for data collection detailed measurements were not performed in this case study.

All collected information corresponded to the calibration year, in this case 2006. At the time of the case study, 2006 was the most recent full calendar year of available utility data for the school. Thus, all data that was collected to describe the energy consumption in the Steindal School was from 2006. Data for other years were examined briefly during calibration (Chapter 7) and prior to retrofit (Chapter 8), but *all data that is discussed in this chapter is from 2006.*

The energy consumption in the Steindal School was defined according to ten categories of collected data:

- Utility Data
- Weather Data
- Geometry and Envelope
- Occupancy
- Lighting
- Plug Loads
- Domestic Hot Water
- Cooling
- Heating
- Ventilation

Each of these categories included data on materials, equipment, setpoints, schedules, and controls schemes and collectively they described the building's energy consumption characteristics.

These data were input into the EnergyPlus computer software and a model was developed to describe the energy use in the Steindal School. The order of input to EnergyPlus

corresponded roughly with the organization of categories, beginning with weather and progressing through heating and ventilation inputs. From here forward the terms “collected data” and “input” will be used interchangeably to describe the information that was used to define the EnergyPlus building model.

Here it is necessary to recall the emphasis that was placed on identifying, quantifying, and understanding retrofit energy savings uncertainties in this work. These uncertainties were thought of in three parts: sources, resolutions, and implications. Each of these parts was then addressed during data collection (Chapter 5), calibration (Chapter 7), and retrofit (Chapter 8). In the data collection performed here the emphasis was placed on highlighting the sources of uncertainties. Identifying sources of uncertainty during data collection enabled a more efficient calibration to be performed (Chapter 7). Thus, following the definition of each set of inputs a brief discussion of the accuracy of the collected data is presented.

Ideally, with unlimited funds and access to detailed measurement techniques, all uncertainties in the collected data would be resolved prior to calibration. However, this is not an economically feasible or realistic means of addressing uncertainties. Thus, alternative techniques like calibration (Chapter 7) and simple estimates (Chapter 6) were applied to address input uncertainties in later chapters.

5.1 Collected Data

5.1.1 Utility Data

5.1.1.1 Hourly Utility Data

When performing calibrations (Chapter 8) it is necessary to have accurate utility data against which to benchmark the building model. During the case study of the Steindal School hourly utility billing was available from 2004 through 2006 [TEV 2007b],[Entra 2007]. All demands for heating, ventilation, lighting, plug loads, and domestic hot water in the building were met by electricity; this was the only energy carrier listed on the utility bill. Examination of the cumulative energy consumption (Figure 5-1) exhibited an energy consumption of 760,720 kWh in 2006, significantly lower than the 997,900 kWh consumed in 2004 and the 963,136 kWh consumed in 2005.

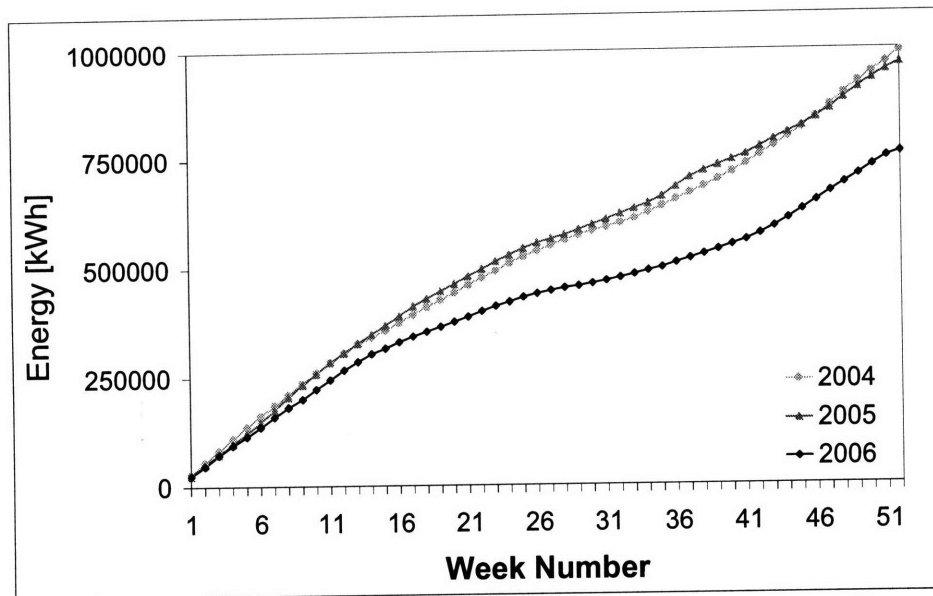


Figure 5-1: Cumulative weekly energy consumption in the Steindal School from 2004 through 2006 [TEV 2007b],[Entra 2007].

Conversations with teachers and members of the municipality indicated that this was the result of changes in schedules of operation and temperature settings. These changes were made by teachers and students in the context of a community program aimed to teach and promote energy savings [Hobber 2007],[Kringstad 2007]. In the interest of developing a model that accurately mimicked the existing building conditions, the EnergyPlus building model was calibrated against 2006 utility data (Chapter 7).

5.1.1.1.1 Uncertainty

Prior to accepting the hourly 2006 utility data as the benchmark for calibration the data was examined for outliers and inconsistencies. This examination revealed that all of the hourly energy consumption meter readings (for all 8760 hours in the year) had values that were multiples of 4. Observation of hourly utility data from other schools in Trondheim indicated that only a handful of schools were subject to the “multiple of 4” issue. The majority of schools in Trondheim had hourly energy readings that were multiples of 1 kWh, not 4 kWh. Because it occurred at other schools, it was suggested that the “multiple of 4” meter reading at the Steindal School was linked to the type of meter that was installed. However, attempts to obtain information about the utility meter from the Trondheim Municipality and the utility metering

company were unsuccessful, and without information about the energy meter, it was difficult to pinpoint the exact cause or calculation of the “multiple of 4” meter readings.

This was of concern because the EnergyPlus computer software was able to output hourly energy consumption data that was not subject to the “multiple of 4” rule that was observed in the collected utility data. Thus, for any hour x of some day y the EnergyPlus model might predict a value of 79 kWh of energy consumption, while the utility data might indicate a measured energy consumption of 80 kWh. The two might really be equal, but, because the measured utility data was always a multiple of 4 there was no way to verify this. Thus, uncertainties were expected to arise during hourly calibrations because of the behavior of the measured utility data. The implications of this uncertainty are discussed in Chapter 7.

5.1.2 Weather data

5.1.2.1 Collected Weather Data

The very cool Norwegian climate often leads to high heating demands in Norwegian school buildings [BE 2008a]. Thus, a large portion of the overall energy consumption in the Steindal School was expected to be heating energy, and the amount of heating energy demanded on an hourly, daily, or monthly basis was expected to be strongly tied to the outdoor weather conditions. Consequently, to obtain a calibrated model of the energy consumption in the Steindal School, accurate weather data was needed.

Under ideal conditions hourly weather data for all variables required by the EnergyPlus software would have been available from the building site for every hour of the calibration year. However, this was not the case at the Steindal School in 2006, and so best practice substitutions were made. Hourly temperature and wind speed data were available from the Trondheim and Kvithamar weather stations from 2006 (Figure 5-2) [MET 2007],[Bioforsk 2007]. In addition, global solar radiation data were available from Kvithamar from 2006 [Bioforsk 2007].

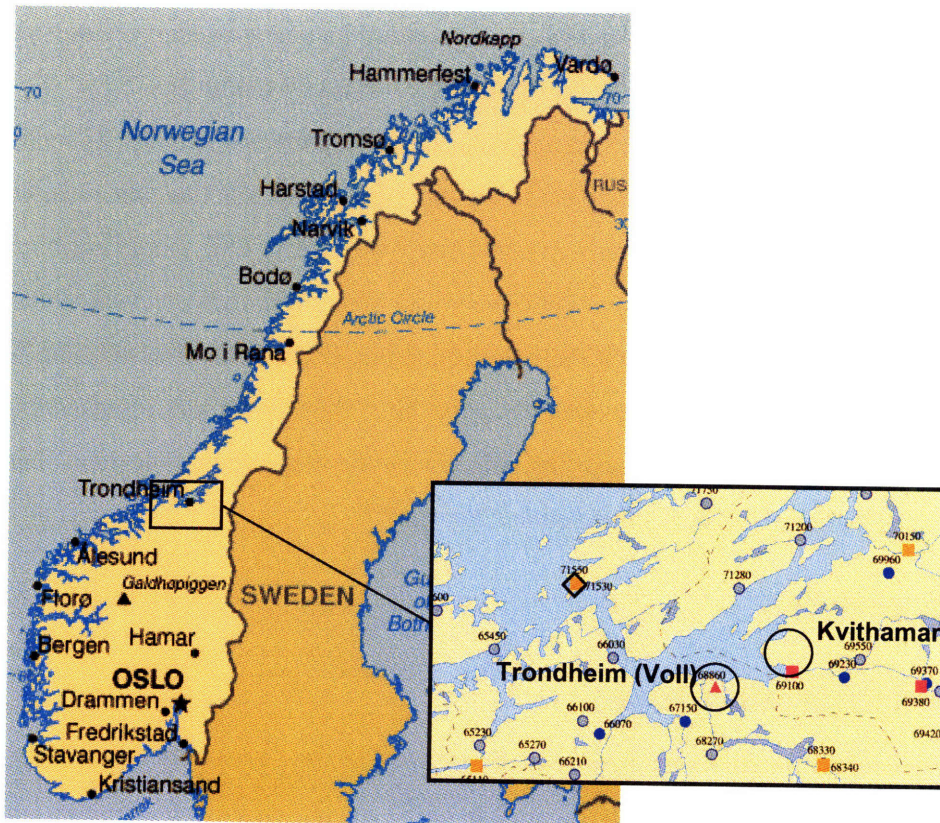


Figure 5-2: Location of weather stations for collecting data to describe the conditions at the Steindal School [MET 2007],[Bioforsk 2007],[Factbook 2008a].

However, the EnergyPlus computer program requires that the hourly solar radiation be provided in terms of global, direct, and diffuse quantities. Because only global radiation was available from the local meteorological stations in 2006 two methods were investigated for defining the weather data needed for the EnergyPlus simulation.

The first method applied algorithms developed by Liu and Jordan [Liu 1960] to break the global radiation down into direct and diffuse components based on a number of other variables including the clearness of the sky and the level of cloud cover in each hour in 2006. However, hourly cloud cover and sky clearness data were unavailable, making this method difficult, if not impossible, to implement.

The second method used the global, diffuse, and direct solar radiation data from the International Weather for Energy Calculations (IWEC) weather file from Oslo, Norway to describe the conditions at the Steindal School in 2006. The radiation data from the IWEC weather files for Osteraund, Sweden, and Bergen, Norway were also considered, but showed a

poorer match with the 2006 global radiation data from Kvithamar than did the Oslo weather file (Figure 5-3).

Location	Description	Average Hourly Global Radiation [W/m ²]	Peak Hourly Global Radiation [W/m ²]	Total Annual Global Radiation [kW/m ²]
Trondheim 2006	Data from Kvithamar (25 km Northeast of Trondheim)	95	809	836,900
Oslo IWEC	Typical weather year for Oslo (coastal climate, Southern fjord region, 390 km South of Trondheim)	100	785	878,600
Bergen IWEC	Typical weather year for Bergen (rainy climate, Western coastal region, 430 m Southwest of Trondheim)	85	774	746,700
Ostersund IWEC	Typical weather year for Ostersund (inland region, 214 km East of Trondheim)	102	750	889,200

Figure 5-3: Global radiation data from Trondheim, Oslo, and Bergen in Norway and Ostersund in Sweden [MET 2007],[Bioforsk 2007],[EPlus 2007b].

The direct and diffuse solar radiation data from the IWEC weather file for Oslo, Norway was used in this work. It was the belief of the modeler that it was best to use well developed data from an established weather file than to develop estimates using the algorithms prescribed by Liu and Jordan [Liu 1960] with highly uncertain cloudiness and sky clearness data. Additionally, Oslo weather data is commonly used to represent the weather conditions in Norway [Engblom 2006], and the global radiation data from the Oslo IWEC file showed a better match with global radiation data from Trondheim in 2006 than did Bergen or Ostersund.

Therefore, the weather file that was applied during the EnergyPlus simulations (Chapter 7) was the IWEC weather file corresponding to Oslo, Norway, with two modifications. These two modifications were the replacement of the typical hourly temperatures and wind speeds in the IWEC Oslo file with hourly temperature and wind data from Trondheim in 2006. All other weather data in the IWEC weather file was for a typical weather year in Oslo, including all radiation and precipitation data.

5.1.2.1.1 Uncertainty

Comparisons of the global radiation data from Kvithamar and the IWEC Oslo weather file indicated that the greatest differences in solar exposure occurred in the winter, when the Oslo radiation data overestimated the amount of solar radiation in Trondheim. This observation was offset by the fact that the building was exposed only to short periods of sunlight, mostly on its South façade, during the winter. Additionally, a relatively small percentage (~5% of the

conditioned floor area) of the South façade (section 5.1.3) was glazed, and the windows on this façade had a low-emissivity coating. This meant that the solar heat gained in the building during the winter was expected to be small, minimizing the influence of the discrepancies between the Kvithamar and IWEK Oslo radiation data. Thus, although the use of the solar radiation data for a typical year in Oslo generated some input uncertainty, it was accepted as the best available information for the building site. Therefore the weather data was not varied during calibration (Chapter 7).

5.1.3 Geometry and Envelope

The geometry and envelope inputs included the building location, dimensions, materials, and constructions. These inputs were defined during site visits and from as-built documents.

5.1.3.1 Building Surroundings, Site, and Ground Temperature

5.1.3.1.1 Site and Surroundings

Site visits indicated that the Steindal School was located on a hill to the South of the city of Trondheim with an East-West building orientation. Additionally, the South and East walls of the building's ground floor were below grade and not exposed to the outdoors (Figure 5-4).

The North windows were partially shaded from sun and wind by a sparse group of trees and the South windows were shaded from low East and West sun angles by the three entrance wardrobes to the building (Figure 5-4 and Figure 5-5). There were no other buildings near the school.

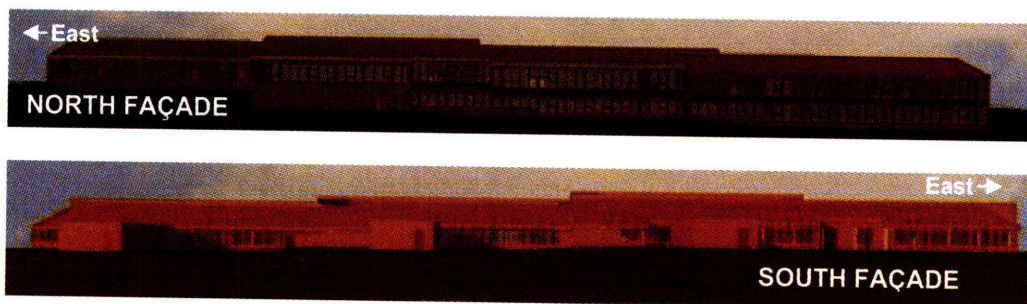


Figure 5-4: North and South façades of the Steindal School. Note the shading from the three entrance wardrobes on the South façade [Hestnes 2007b].

5.1.3.1.2 Ground Temperature

It was necessary to distinguish between the EnergyPlus definition of ground temperature and the more common ASHRAE definition. The ground temperature defined by EnergyPlus was the interface temperature between the ground and adjacent building surfaces. This was *not* the same as the undisturbed ground temperature of the soil prescribed in the ASHRAE Handbook of Fundamentals [ASHRAE 2005]. The ground temperature described by ASHRAE was the temperature at some distance from the building surface and was approximated by the average annual outdoor air temperature (6.5°C in Trondheim in 2006).

The EnergyPlus user's manual [EPlus 2007c] emphasized that the ASHRAE defined ground temperature was too low for the temperature of the interface between the conditioned building spaces and the ground. Instead, the EnergyPlus user's manual suggested that the interface temperature be approximately 2°C less than the average indoor temperature. The average indoor temperature in the Steindal School was between 18°C and 20°C; the suggested EnergyPlus "ground temperature" was between 16°C and 18°C (section 5.1.9). As a first approximation, the EnergyPlus default value of 18°C was input into the EnergyPlus model.

5.1.3.1.3 Uncertainty

All of the inputs concerning the building site and surroundings were accurate, except for the ground temperature values. The orientation of the building was taken directly from as-built documents and its accuracy was confirmed during site visits. However, the ground temperature was approximated from typical practice values and had a high degree of uncertainty in its value. As a result, a number of different ground temperatures were tested during calibration (Chapter 7). Additionally, simple calculations were made (Chapter 6) to obtain a better estimate of the interface temperature between the ground and adjacent building surfaces.

Modules for calculating the average monthly ground temperatures for floor slab and basement configurations [EPlus 2007c] were provided with the EnergyPlus software, but these were independent from the EnergyPlus simulator, more difficult to implement, and did not resolve the fact that the EnergyPlus simulation engine used a one-dimensional heat transfer calculation. Thus, the simple estimates and calibration in Chapters 6 and 7 were performed to identify the most appropriate ground temperatures at the Steindal School.

5.1.3.2 Building Geometry

The building footprint, number of floors, floor height, window area, and building zones were defined with data from as-built documents. These data were verified during the site visit with measurements and observations.

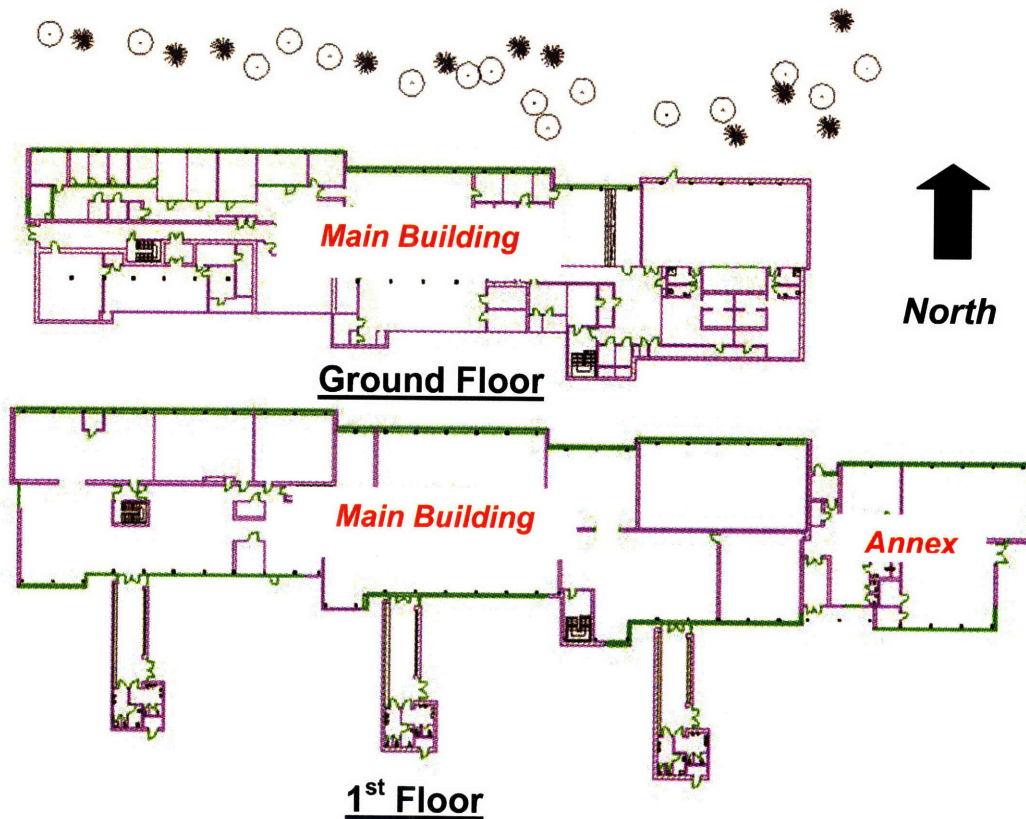


Figure 5-5: Building floor plan, taken from as-built documents [Hestnes 2007b],[Municipality 2007a].

5.1.3.2.1 Footprint and Floor Area

The building footprint is shown in Figure 5-5. This footprint was simplified to a rectangle with an aspect ratio of 6:1 (~118m East to West x ~20.5m North to South) with three protruding rectangles (Figure 5-6). This modification was made to ease the modeling of the geometry¹. No changes were made to the building's floor area, volume, or orientation.

¹ This is good modeling practice for both basic hand calculations and detailed models like those used in EnergyPlus. Over defining the building geometry makes the model computationally expensive (a heat balance must be done on each building surface) and time consuming.

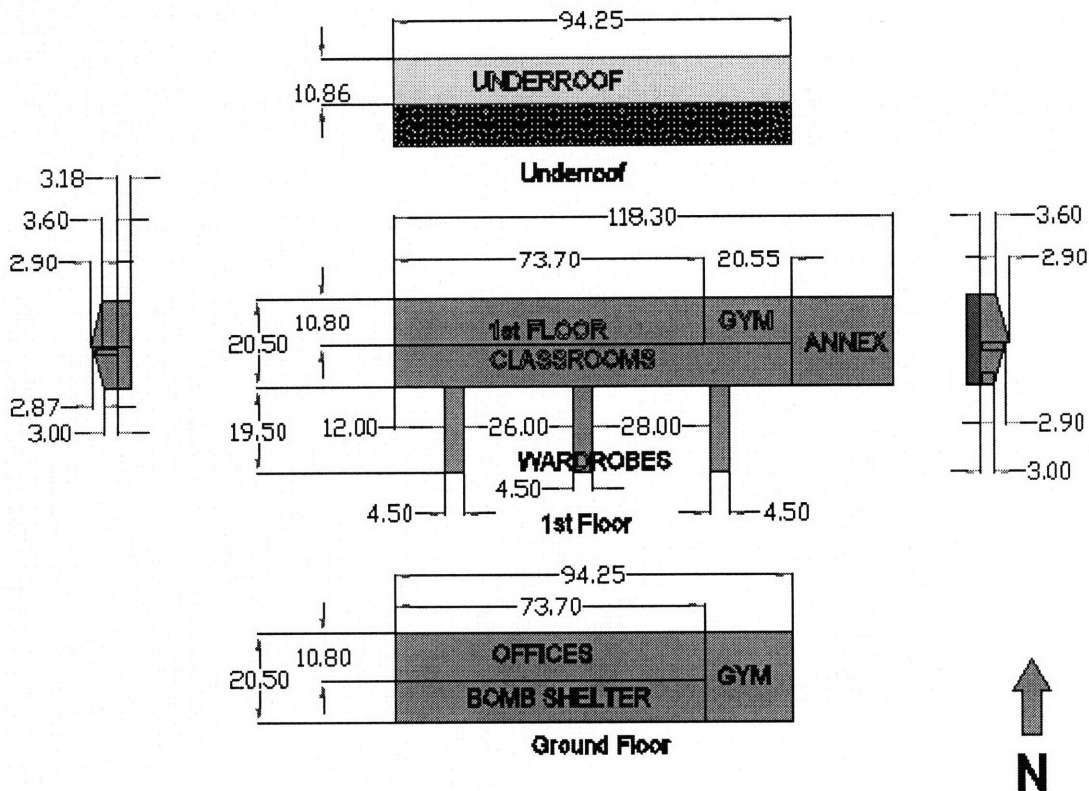


Figure 5-6: Simplified layout of the Steindal School's floor plan, including dimensions. All dimensions are in meters. The brown areas indicate ground and the black hatched area indicates the building roof.

5.1.3.2.2 Number of Floors and Floor Height

The school was two stories high with a ground and 1st floor. As-built documents indicated floor heights between 3 m and 6.5 m in the building (Figure 5-6). The roof was pitched at a 17° angle from the building's East-West ridge. The North half of the roof included an open space above the first floor classrooms and gymnasium (Underroof) with a volume of 1,500 m³. The total building volume was equal to 18,360 m³.

The *utility floor area* was the total floor area confined by the walls of the building and was equal to 5,409 m². The *conditioned floor area* was the total floor area that was heated and/or ventilated, and was equal to 4,400 m² (Table 5-2).

5.1.3.2.3 Window Area

As-built documents indicated that the density of windows was greatest on the North façade; 57% of the building's North façade was glazed. The remaining windows were

distributed between the South (32% of the South façade), East (4% of East façade), and West (4% of West façade) façades; 33% of the building's total wall area was glazed (Table 5-1).

All windows were double glazed and between 2.2 m-2.6 m high by 1 m wide (areas of 2.2 m² – 2.6 m²) with wooden framing (Figure 5-7 and Table 5-1). Site visits indicated that a section of the windows was operable. The dimensions of the windows and window frames were verified using a tape measure during the site visit.

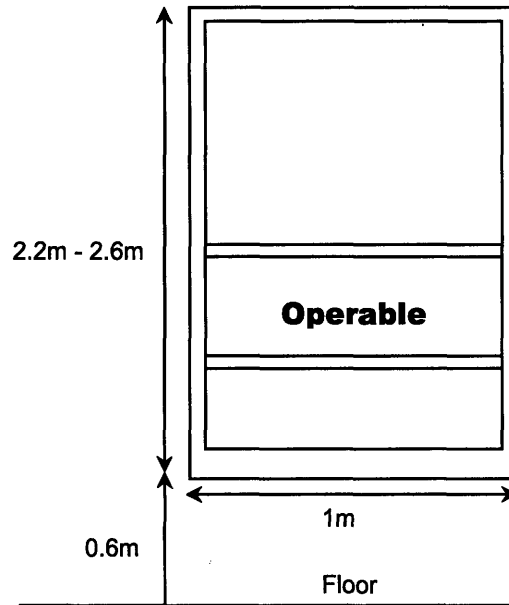


Figure 5-7: Window dimensions for those windows on the North and South façades of the Steindal School. Drawing not to scale.

Building Façade	Floor	Number of Windows per Floor	Area per Window [m ²]	Window Area per Façade [m ²]	Window-Wall Ratio [%]
North Wall	1 st Floor	98	2.6	416	57%
	Ground Floor	62	2.6		
South Wall	1 st Floor	89	2.6	232	32%
East Wall	1 st Floor	5	2.6	13	4%
West Wall	1 st floor	2	2.6	12	4%
	Ground Floor	3	2.2		
Total Glazed Area		259	2.2-2.6	673	33%

Table 5-1: Window distribution between North, East, South, and West facades on the ground and 1st floors. The percent of the wall area is the fraction of the wall area that is glazed. The parent surface for each set of windows is given in the left hand column of the table.

5.1.3.2.4 Building Zoning

The interior of the building was partitioned into zones on the basis of room use, occupancy patterns, and heating and ventilation system layouts. This resulted in seven building zones: teacher and administrator offices (Offices), storage (Bomb shelter), entryways (Wardrobes), gymnasium (Gym), 1st floor classrooms (1st Floor), addition (Annex), and attic (Underroof), shown in Figure 5-8.

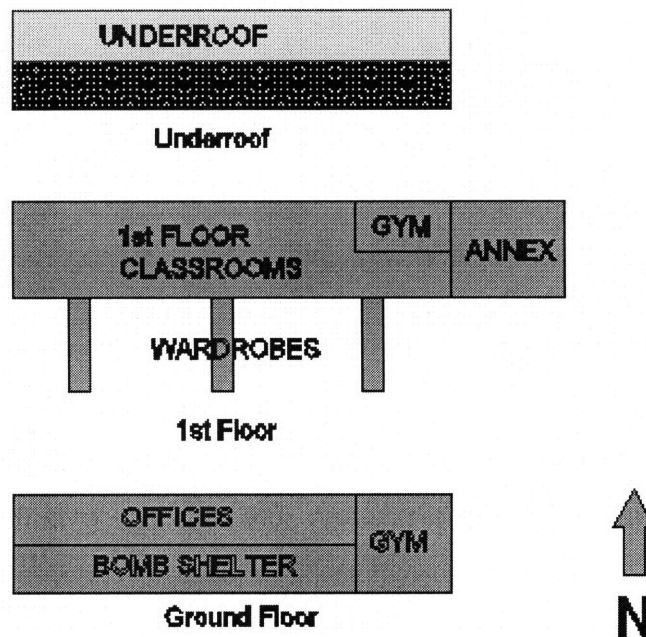


Figure 5-8: Layout of building zones based on building usage. The Underroof is directly above the North half of the 1st Floor (classrooms) and Gym. The hatched black area indicates the roof of the building.

The “Main” building was made up of the 1st Floor, Gym, Offices, and Bomb Shelter zones. The “Annex” was made up of only the Annex zone.

The total conditioned floor area of the building included all zones except the Underroof zone, which was neither heated nor ventilated. A brief description of each zone is provided in Table 5-2.

Building Zone	Description and Use	Utility Floor Area [m ²]	Conditioned Floor Area [m ²]	Zone Volume [m ³]
Bomb Shelter	Storage and computer game room – used infrequently. Heated and ventilated.	715	715	2,273
Offices	Teacher and administrator offices – occupied into the evening. Heated and ventilated.	796	796	2,531
1 st Floor	Classrooms for upper grades. Open layout with a partition running East to West. Heated and ventilated.	1,710	1,710	6,934
Gym	Gymnasium – used by classes throughout the day. Heated and ventilated.	421	421	2,139
Wardrobes	Primary entrances to the building. Heated.	263	263	632
Annex	Play area and classrooms for lower grades – occupied before, during, and after school. Heated and ventilated.	493	493	2,350
Underroof	Not occupied, no heating or ventilation.	1,011	-----	1,500
Total		5,409	4,400	18,360

Table 5-2: Utility floor area, conditioned floor area, and volume of each building zone in the Steindal School. Conditioned spaces are those with ventilation and/or heating.

5.1.3.2.5 Uncertainty

The simplifications to the building geometry were made according to best practice assumptions and were considered to be accurate. The building zoning was characterized by observed occupancy, ventilation, and heating patterns in the school, and were as accurate as possible with the available information. None of the building geometry characteristics were evaluated during calibration (Chapter 7).

5.1.3.3 Building Envelope

5.1.3.3.1 Materials

The structural materials in the Steindal School were brick, concrete, and wood. The insulation materials were mineral wool and extruded polystyrene. Additional materials were used in wall, roof, base, and window constructions. The properties of these materials were taken from the EnergyPlus computer program materials database [EPlus 2007e] and the 1987 of Norwegian Standard 3031 (NS3031) [NS3031 1987]. A summary of the materials and properties used in the walls, roof, and floors in the Steindal School is given in Table 5-3. The properties given are those required to fully define each material in the EnergyPlus computer program.

		Conductivity (k) [W/mK]	Density (ρ) [kg/m ³]	Specific Heat (C _p) [kJ/kgK]	Absorptance			
					Thermal	Solar	Visible	
Insulation	Mineral Wool	0.043	10	837	0.9	0.75	0.75	
	Expanded Polystyrene (EPS)	0.035	29	1,213	0.9	0.5	0.5	
Structural	Brick	1.31	2,083	920	0.9	0.6	0.6	
	Heavyweight (HW) Concrete	1.73	2,243	837	0.9	0.65	0.65	
	Lightweight (LW) Concrete	0.173	641	837	0.9	0.65	0.65	
Other	Gypsum Plaster	0.16	801	837	0.9	0.75	0.75	
	False Ceiling Board	0.04	240	710	0.9	0.5	0.5	
	Steel Siding	44.97	7,689	418	0.9	0.7	0.7	
	Roof Gravel	1.44	881	1,674	0.9	0.65	0.65	
	Wood	0.12	593	2,510	0.9	0.78	0.78	
	Resistance, R [m ² K/W]					Thermal	Solar	Visible
		Linoleum Tile	0.009			0.9	0.7	0.7
		Ceiling Air Space	0.176			----	----	----
		Wall Air Space	0.157			----	----	----

Table 5-3: Summary of materials, with properties, that were present in the walls, roof, and floors of the Steindal School [EPLUS 2007E],[NS3031 1987].

Window materials were taken from the EnergyPlus materials database [EPlus 2007e] and are shown in Table 5-4 and Table 5-5. These materials were chosen to match the manufacturer's specifications [Pilkington 2007] as closely as possible.

Window Glazing Properties	Clear Glazing	Low-E Glazing	Grey Glazing	Low-E Spectrally Selective Glazing
Thickness [cm]	0.4	0.4	0.6	0.6
Conductivity [W/mK]	0.9	0.9	0.9	0.9
Solar Transmittance [%]	0.837	0.630	0.455	0.430
Solar Reflectance: Front Side of Glazing [%]	0.075	0.220	0.053	0.300
Solar Reflectance: Back Side of Glazing [%]	0.075	0.190	0.053	0.420
Visible Transmittance [%]	0.898	0.850	0.431	0.770
Visible Reflectance: Front Side of Glazing [%]	0.081	0.079	0.052	0/070
Visible Reflectance: Back Side of Glazing [%]	0.081	0.056	0.052	0.060
Infrared Transmittance [%]	0	0	0	0
Infrared Emissivity: Front Side of Glazing [%]	0.84	0.1	0.84	0.84
Infrared Emissivity: Back Side of Glazing [%]	0.84	0.84	0.84	0.03

Table 5-4: Summary of glazing material, and properties, that were present windows of the Steindal School [EPlus 2007e].

Window Gap Properties	Air	Argon
Thickness [cm]	1.27	1.27
Conductivity [W/mK]	0.027	0.018

Table 5-5: Summary of gases that were present between the two panes of glass in the windows of the Steindal School [EPlus 2007e].

The distribution of these materials in the Steindal School is discussed in the following section on building constructions.

5.1.3.3.1.1 Uncertainty

The majority of the materials in the Steindal School were installed during the original building construction in 1978. Over time, and with prolonged exposure to moisture, these materials were expected to degrade, especially the mineral wool insulation. In order to account

for this degradation and the unknown initial conditions of the mineral wool, the insulation conductivity was varied between 0.036 W/mK and 0.050 W/mK during calibration (Chapter 7).

Additionally, the thermal conductivity of the windows was expected to increase over time as a result of gas leakage and deterioration of the window materials, making the use of the manufacturer’s specified materials inappropriate. Consequently, the conductivity of windows was also varied during calibration (Chapter 7).

The remaining material properties also had some degree of uncertainty associated with their values. However, these were not addressed during calibration because they were expected to result in only minor changes to the building model.

5.1.3.3.2 Constructions

Combinations of the materials listed in Table 5-3 were used to define wall, roof, and floor constructions in the Steindal School. EnergyPlus constructions were generated by creating “Construction” objects that called on the “Material” objects that were defined in Table 5-3. For example, the East wall in the Annex was composed of the following combination of materials: (exterior) brick - air gap - mineral wool – gypsum (interior). These materials were assigned to a “Construction” object that was then used to define the East wall of the Annex in the EnergyPlus building description.

5.1.3.3.2.1 Thermal Conductance, or “U-Value”

Before running the EnergyPlus simulations the steady-state “U-Value”, or thermal conductance, was calculated for each wall, roof, floor, and window construction in the building. This U-value characterized each construction’s resistance to the transfer of heat, where the amount of heat transferred was equal to the U-value multiplied by the surface area and the temperature difference across the construction (Equation 5-1).

$$Q = UA(T_{inside} - T_{outside}) \tag{5-1}$$

Q	Steady-state heat transfer [W]
U	U-value [W/ m ² K]
A	Area [m ²]
$T_{inside} - T_{outside}$	Temperature difference [K]

Constructions with low U-values are highly resistant to heat transfer and those with high U-Values are not very resistant to heat transfer; the U-value is the inverse of thermal resistance.

Therefore, the U-value of each construction was calculated as the inverse of the total resistance to conductive, convective, and radiative heat transfer of each building surface; the 1987 release of NS3031 [NS3031 1987] provided an equation for calculating this U-value (Equation 5-2). Additionally, NS3031 provided equivalent resistances ($R_{\text{convection,radiation}}$) to account for the convective and radiative heat transfer on the interior and exterior of each building surface. The recommended resistance on the interior of the surface was equal to $0.13 \text{ m}^2\text{K/W}$; the recommended resistance on the exterior surface was $0.04 \text{ m}^2\text{K/W}$. The total U-value for each building surface in the Steindal School was calculated according to Equation 5-2.

$$U - \text{Value} = \frac{1}{R_{\text{convection,radiation,inside}} + \sum_{\substack{\text{outsidematerial} \\ \text{insidematerial}}} \frac{t_{\text{material}}}{k_{\text{material}}} + R_{\text{convection,radiation,outside}}} \quad (5-2)$$

U	U-value [$\text{W}/\text{m}^2\text{K}$]
$R_{\text{convection,radiation,inside}}$	Interior convection and radiation resistance [$\text{m}^2\text{K}/\text{W}$]
$R_{\text{convection,radiation,outside}}$	Interior convection and radiation resistance [$\text{m}^2\text{K}/\text{W}$]
t_{material}	Thickness of construction material from as-built documents [m]
k_{material}	Conductivity of construction material [W/mK]

The overriding assumption in the calculation of the U-value in Equation 5-2 was that a steady-state energy balance was being performed. This meant that the heat transferred across the construction did not include transient, or time dependent, effects. Thus, the U-values calculated according to Equation 5-2 were valid only for simple annual energy calculations, like those performed in Chapter 6, and not to the detailed EnergyPlus analyses performed in Chapter 7.

The U-values shown in the following sections on wall, roof, and ground constructions were calculated according to Equation 5-2 with the values for the interior and exterior convective/radiative ($R_{\text{convection,radiation}}$) resistances provided in [NS3031 1987]. The exception to this was the windows, for which center-of-glass U-values were provided by the manufacturer [Pilkington 2007].

5.1.3.3.2.2 Wall Constructions

The basic design was the same for nearly all exterior wall constructions: brick exterior with mineral wool insulation, an air gap, and gypsum interior. However, the thickness of the mineral wool varied for the North, South, East, and West walls in the Main building and the Annex. Additionally, the South wall in the Bomb Shelter and the East wall on the ground floor

of the Gymnasium abutted the ground, not the exterior environment, and were composed of concrete with no insulation.

All of the wall constructions used in the Steindal School are described in Figure 5-9 through Figure 5-12 and Table 5-6. Included are the materials, U-value, and location of each construction. Constructions are defined from the interior building surface to exterior building surface. All constructions that were located in the Main building are highlighted in red; all constructions in the Annex are highlighted in magenta.

Exterior Wall Constructions	North and South Walls	
	Main Building	Annex
Interior Surface Layer	11 cm Brick	1.7 cm Gypsum
Layer#2	13 cm Mineral Wool	15 cm Mineral Wool
Layer #3		2 cm Air Space
Exterior Surface Layer	11 cm Brick	11 cm Brick
U-Value [W/m²K]	0.30	0.25

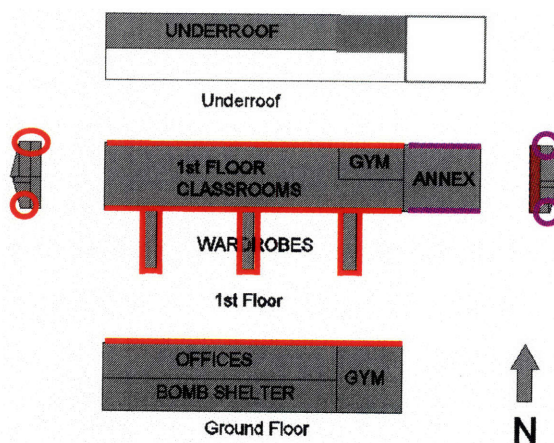


Figure 5-9: North and South wall constructions in the Main building and Annex of the Steindal School. Applicable Main building walls are highlighted in red, while the Annex walls are highlighted in magenta.

The West exterior wall construction was slightly different from the North, South, and East walls of the building. Rather than using a gypsum and brick construction, a heavyweight concrete was used for this wall, likely because it was one of the walls of the Bomb Shelter. This did not have a significant influence on the *steady-state* U-value shown in Figure 5-10, but was important in incorporating the wall's thermal mass into the EnergyPlus simulation. The constructions and locations for both the West and East walls are shown in Figure 5-10.

Exterior Wall Constructions	West Wall	East Wall
	<i>Main Building</i>	<i>Annex</i>
Interior Surface Layer	15 cm HW Concrete	1.7 cm Gypsum
Layer #2	13 cm Mineral Wool	15 cm Mineral Wool
Layer#2		2 cm Air Space
Exterior Surface Layer	11 cm Brick	11 cm Brick
U-Value [W/m²K]	0.30	0.25

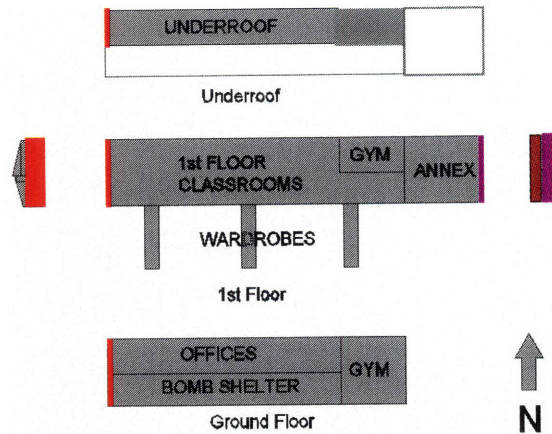


Figure 5-10: East and West wall constructions in the Main building and Annex. Applicable Main building walls are highlighted in red, while the Annex walls are highlighted in magenta.

The wall along the roof ridge separated the Underroof, 1st Floor, Gym, and Annex zones from the exterior environment. This wall was short, but extended the entire length of the building and was composed of concrete and brick.

Exterior Wall Constructions	South Wall Along Roof Ridge	
	<i>Main Building</i>	<i>Annex</i>
Interior Surface Layer	15 cm HW Concrete	20 cm HW Concrete
Layer#2	2 cm Air Space	
Exterior Surface Layer	11 cm Brick	11 cm Brick
U-Value [W/m²K]	1.9	2.8

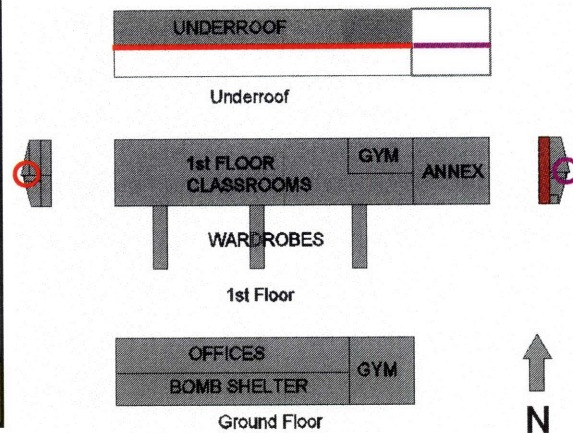


Figure 5-11: South roof ridge wall construction. Applicable Main building walls are highlighted in red, while the Annex walls are highlighted in magenta.

The South wall in the Bomb Shelter and the East wall in the Gym both abutted the ground and had a concrete construction with no insulation.

Ground Wall	Bomb Shelter and Gym: South and East Walls
	<i>Main Building</i>
Interior Surface Layer	10 cm LW Concrete
Exterior Surface Layer	20 cm HW Concrete
U-Value [W/m²K]	1.14

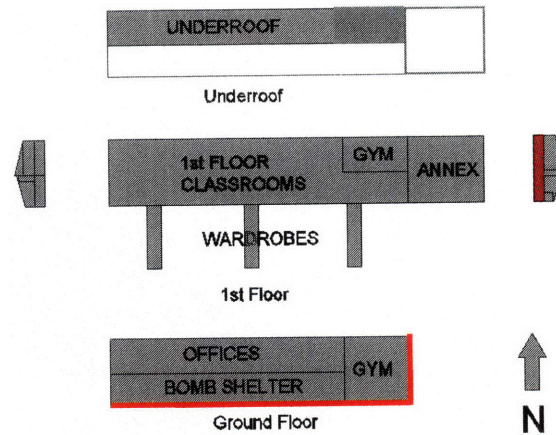


Figure 5-12: Ground wall construction. Applicable Main building walls are highlighted in red, while the Annex walls are highlighted in magenta.

5.1.3.3.2.3 Roof Construction

The roof constructions in the Annex and the South half of the Main building were similar; both were composed of a roofing metal – mineral wool – air gap – ceiling tile construction. The Wardrobe roofs had a gravel – mineral wool – ceiling tile construction. The North roof over the Underroof space in the Main building was a steel roofing – concrete – open air space construction.

The roof constructions are summarized in Figure 5-13 and Figure 5-14. The South roof of the Main building is highlighted in red, the North roof in the Main building is highlighted in blue, the North and South roofs in the Annex are highlighted in magenta, and the wardrobe roof is highlighted in orange.

Roof Constructions	South Roof	North Roof	North and South Roof	Wardrobe Roof
	<i>Main Building</i>	<i>Main Building</i>	<i>Annex</i>	<i>Wardrobes</i>
Interior Surface Layer	0.2 cm Ceiling Tiles	Open Air Space	0.2 cm Ceiling Tiles	0.2 cm Ceiling Tiles
Layer#2	Air Gap	15 cm HW Concrete	Air Gap	15 cm Mineral Wool
Layer #3	20 cm Mineral Wool	-----	20 cm Mineral Wool	-----
Exterior Surface Layer	0.015 cm Steel Roofing	0.015 cm Steel Roofing	0.015 cm Steel Roofing	5 cm Roof Gravel
U-Value [W/m²K]	0.18	3.94	0.18	0.24

Figure 5-13: Roof constructions in the Main building and Annex. Main building roofs are highlighted in red (South) and blue (North), Annex roofs are highlighted in magenta, and Wardrobe roofs are highlighted in orange.

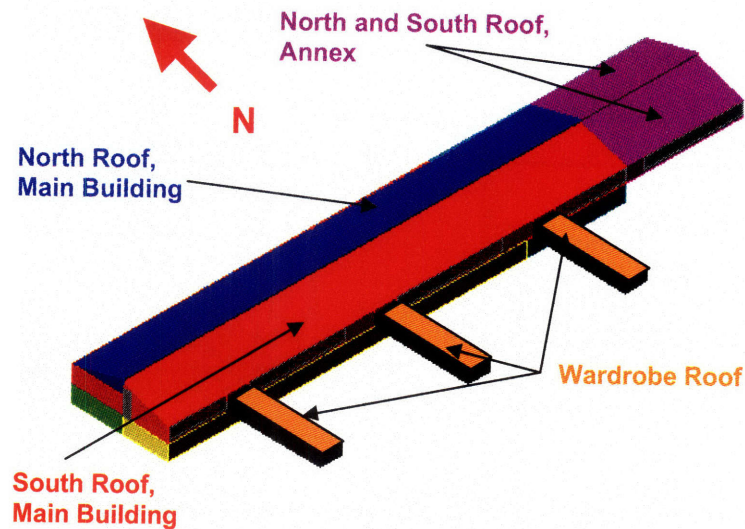


Figure 5-14: Location of roof constructions in the Steindal School. Main building roofs are highlighted in red (South) and blue (North), Annex roofs are highlighted in magenta, and Wardrobe roofs are orange.

Note the very poor insulating properties of the North roof in the Main building. The calculated U-value was equal to $3.94 \text{ W/m}^2\text{K}$ - significantly higher than any of the other roof, wall, or floor constructions. This was particularly alarming given the large area of the North roof above the Main building ($\sim 1,000 \text{ m}^2$). This was better understood when the surface between the unheated Underroof and the abutting heated spaces below it was examined.

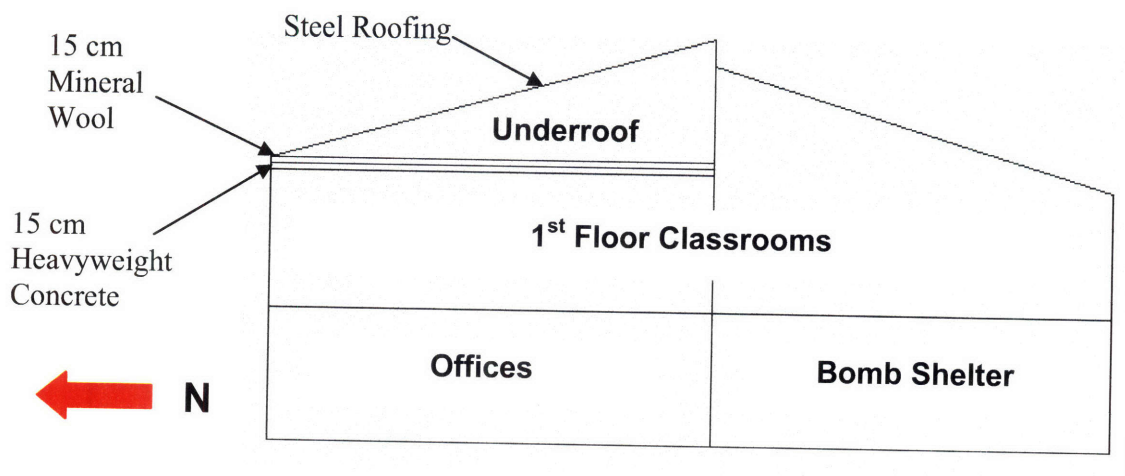


Figure 5-15: Vertical cross-section of Steindal School showing the Offices, Bomb Shelter, 1st Floor, and Underroof. The location of the mineral wool in the North roof over the 1st Floor classrooms is indicated.

This review indicated that 15 cm of mineral wool was used to separate the unheated Underroof space from the abutting 1st Floor and Gymnasium zones of the building. This is shown in the building cross-section in Figure 5-15, where the steel roofing is labeled, as are the 15 cm of mineral wool and concrete that separated the Underroof space from the heated 1st Floor classrooms and the Gym in the Steindal School. Thus, the majority of the insulation in the North roof was provided by the ceiling above the 1st Floor and Gym. However, the U-value of the North roof construction shown in Figure 5-13 only accounted for the steel roofing and concrete in the roof above the Underroof space, not for the materials in the ceiling of the 1st Floor and Gymnasium. The EnergyPlus computer simulation (Chapter 6) and the simple estimates (Chapter 7) both included the influence of the 15 cm of mineral wool between the Underroof and the heated building.

5.1.3.3.2.4 Ground Floor Construction

The ground floor construction was the same in the Main building and the Annex. The construction and materials for the ground floor are shown in Table 5-6.

Ground Floor Construction	Ground Floor
	<i>Main Building & Annex</i>
Interior Surface Layer	Linoleum Tile
Layer #2	10 cm HW Concrete
Exterior Surface Layer	5 cm Expanded Polystyrene (EPS)
U-Value [W/m²K]	0.6

Table 5-6: Ground floor construction.

5.1.3.3.2.5 Window Construction

Three different window constructions were installed in the building, all of which were double-paned. The windows on the North façade of the Main building were from the original construction in 1978, while those on the South façade and in the Annex were installed in 1997. The U-values and solar properties for these windows were provided by the manufacturer [Pilkington 2007] and are shown in Table 5-7. The given U-value is the center-of-glass U-Value and does not include edge-effects or the window frames. However, these components were included in the EnergyPlus window definition, and the window U-value was calculated within the simulation engine accordingly.

The windows in the Main building are indicated in red and those in the Annex are indicated in magenta. The South windows in the Main building are shown with a dotted red line; the North windows are shown with a solid red line.

Window Configurations	North Windows	South Windows	All Annex Windows
	<i>Main Building</i>	<i>Main Building</i>	<i>Annex</i>
Thermal Properties			
Interior Glazing	0.4 cm Clear Glazing	0.4 cm Clear Glazing	0.4 cm Low-E Glazing
Gas Between Glazings	1.2 cm Air	1.5 cm Argon	1.5 cm Argon
Exterior Glazing	0.4 cm Clear Glazing	0.6 cm Low-E Spectrally Selective Glazing	0.6 cm Grey Glazing
U-Value [W/m²K]	2.9	1.1	1.1
Radiation Properties			
% Solar Gained	74	31	35
% Light Transmitted	80	34	65
% Light Reflected	14	6	10

Table 5-7: Thermal and radiation properties of the windows in the Steindal School, as per data provided by the manufacturer [PILKINGTON 2007].

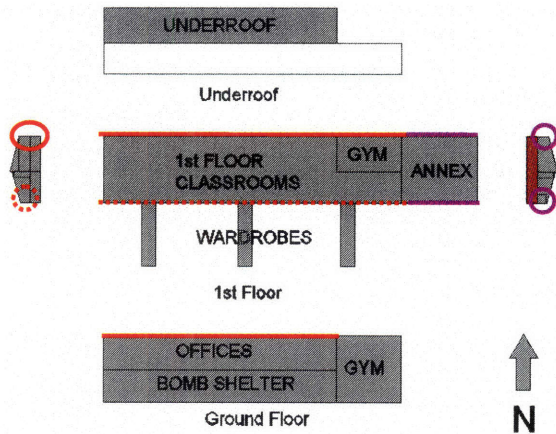


Figure 5-16: Window locations in the Steindal School. Solid red circles and lines indicate the location of the North windows, dashed red lines and circles indicate the location of the South windows, and magenta lines and circles indicate the location of the Annex windows.

All window frames were made of wood, and were laid out as in Figure 5-7.

5.1.3.3.2.6 Interior Partitions

The interior partitions separated the building spaces and included walls, ceilings, and floors. These partitions were broken down into three types: ceilings and floors between zones, walls between zones, and walls internal to zones. Site visits and as-built drawings indicated that all of the building's partitions were made of brick or concrete. These interior partitions, along with wooden furniture, contributed to the volume of thermal mass in the building. The constructions of the interior partitions and other forms of internal mass in the Steindal School are given in Table 5-8.

		Interior Partitions									
		Ceilings & Floors Between Zones		Walls Between Zones				Walls Internal to Zones		Internal Mass	
		Offices and Bomb Shelter to 1 st Floor	1 st floor to Under-roof (Ceiling)	Bomb Shelter to Offices	1 st Floor to Under-roof (Wall)	Gym to 1 st Floor	Main Building to Annex	Gymnasium to Locker-rooms	Dividing wall in 1 st Floor Class-rooms and Annex	Internal Mass – wooden chairs, desks, etc.	
Construction Materials	Surface #1	False Ceiling Board	False Ceiling Board	50 cm HW Concrete	15 cm HW Concrete	20 cm HW Concrete	15 cm HW Concrete	20 cm HW Concrete	11cm Brick	2.54 cm Wood	
		Ceiling Air Space	Ceiling Air Space		5 cm Mineral Wool		13 cm Mineral Wool		3 cm Air Gap		
		15 cm HW Concrete	15cm HW concrete		11 cm Brick		11 cm Brick				11 cm Brick
		Linoleum Floor Tile	15 cm Mineral Wool								
Surface #2											
U-Value [W/m²K]		0.97	0.22	1.9	0.63	2.2	0.29	2.7	3.1	2.13	

Table 5-8: Summary of constructions used in the interior ceilings, floors, walls, and other internal mass in the Steindal School.

These partitions provided resistance against the transfer of heat between zones with significantly different temperature setpoints, as with the heated Offices and unheated Bomb Shelter and the heated 1st Floor and the unheated Underroof. Additionally, they increased the interior thermal mass of the building. This thermal mass was important in estimating the heat storage capacity in the school. During the day the thermal mass was heated to the indoor temperature setpoint. Then, when the temperature was decreased during nights and weekends, the thermal mass released this heat back into the building. Work performed in Appendix A indicated that thermal mass was able to reduce the annual energy consumption in a generic Norwegian building. However, this work also indicated that thermal mass played a large role in

increasing the peak annual power demand when temperature setback was permitted, as was the case in the Steindal School. Consequently, it was important to ensure that the thermal mass in the Steindal School was accounted for correctly in this case study.

5.1.3.3.2.7 Uncertainty

The location and construction of each of the interior partitions was taken from as-built documents. This data was as accurate as possible. As a result, the location and composition of the interior partitions was not addressed during calibration (Chapter 7).

5.1.3.4 Infiltration Rate

Typical values from the 1987 release of NS3031 [NS3031 1987] were used to define the infiltration rates in the Steindal School. The recommended infiltration rates from NS3031 are given in Table 5-9. Table 5-9 specifies infiltration rates on the basis of two factors: the degree of protection from wind at the building site and the geographic location within the country. No considerations are made for the age, window area, or other features of the building being analyzed.

Location	Degree of protection	Air Change
		[1/h]
Inland region and interior fjord region, wind speeds = 0-2 m/s	Well-protected	0.1
	Free-mild protection	0.15
	Vulnerable	0.2
Exposed inland region, coastal regions in the south, middle-west, and north, wind speeds = 2-5 m/s	Well-protected	0.2
	Free-mild protection	0.3
	Vulnerable	0.4
Outer coastal regions in western Norway and in northern Norway. High mountain regions, wind speeds > 5 m/s	Well-protected	0.3
	Free-mild protection	0.4
	Vulnerable	0.5

Table 5-9: Recommended infiltration rates for Norwegian buildings from the 1987 release of NS3031 [NS3031 1987].

The Steindal School was located in a middle-west coastal region of Norway and was free-mildly protected from wind exposure, making the appropriate level of infiltration, according to typical values, equal to 0.3 air changes per hour (ACH).

The infiltration rate for each zone of the Steindal School was varied slightly from the 0.3 ACH prescribed in Table 5-9. These changes were made on the basis of observations that the Annex had tighter window seals than the Main building, the Bomb Shelter had a small external wall area, and the Gym had fewer windows than the rest of the Main building. The Underroof

had no openings and was an unheated space; the infiltration in this space was neglected. Table 5-10 summarizes the estimated infiltration rates for each building zone in the Steindal School.

Zone	Infiltration Rate [ACH]
Bomb Shelter	0.1
Offices	0.3
1 st Floor	0.3
Gym	0.2
Wardrobes	0.3
Annex	0.2

Table 5-10: Estimated infiltration rates for each zone in the Steindal School.

5.1.3.4.1 Uncertainty

There was a high degree of uncertainty associated with the typical values that were used to define the infiltration rates in the Steindal School. Because the typical values were *very* general and did not incorporate important factors like the age, type, or quality of construction in the building the true infiltration rate in the Steindal School was expected to deviate from the values that were used. This uncertainty was addressed with simple estimates in Chapter 6 and again during calibration in Chapter 7. No detailed measurements were used to verify the infiltration rates in the Steindal School, however, the simple estimates that were made in Chapter 6 attempted to qualitatively evaluate the level of infiltration in the school by correlating changes in energy consumption with changes in wind speed.

5.1.4 Occupancy

Data collected from building managers [Skjennald 2007] indicated that approximately 300 students in kindergarten through seventh grade and 40 administrators and teachers occupied the Steindal School on a typical day. The maximum number of occupants in each zone was assigned according to the observed use of each building space. For example, the maximum occupancy in the 1st Floor was based on conversations with teachers that indicated that between 10 a.m. and 1 p.m. all students in grades one through seven were in the classrooms on the 1st Floor. This meant that a maximum of 265 students were expected in the 1st Floor during these periods. The maximum occupancy of the Annex occurred immediate before and after school and was equal to 60 students. The maximum gym occupancy corresponded with one class of 20 students; the maximum Office occupancy was the total number of teachers and administrators,

and was equal to 40 people. Table 5-11 summarizes the maximum number of occupants in each building space.

	Zone			
	Offices	1 st Floor	Gym	Annex
Maximum Number of Occupants	40	265	20	60

Table 5-11: Maximum number of occupants per zone. Fractional schedules were used to modify the number of occupants in each zone throughout the day [Kringstad 2007].

The Bomb Shelter and Wardrobes were occupied only intermittently; the occupants in these spaces were not included in the EnergyPlus model. Note that the sum of the occupancies listed in Table 5-11 exceeds the 340 students, teachers, and administrators that were expected to occupy the building on school days. This is because the values in Table 5-11 were the maximum occupancies for each building space; the actual occupancy in each space was equal to some fraction of this maximum.

The heat gain from the occupants was the amount of heat (in watts) released by a typical person in the school. Observations that the majority of occupants were children who were either reading or writing resulted in an estimate of 100 W/person. This was slightly less than 110W - 120W of energy released by a typical adult performing these tasks as specified in the ASHRAE Handbook of Fundamentals [ASHRAE 2005]. This heat was released into the building in the form of sensible, latent, and radiant heat. The fraction of the 100 W/person that was latent heat was calculated within the EnergyPlus simulation engine as a function of indoor temperature. At an indoor temperature equal to 18°C to 20°C, between 25% and 30% of the 100 W/person was added to the building's interior as latent heat [EPlus 2007d]; the remaining 70%-75% of the 100 W/person was sensible heat gain. The amount of radiant heat was taken at the EnergyPlus default value of 30% of the sensible heat gain. In all cases the occupants contributed 100% heat gain to the building.

Furthermore, the 100 W/person of heat gain used to model the occupants in the Steindal School was consistent with work performed by Wigenstad et al. [Wigenstad 2005], which recommended that a heat gain density of 12 W/m² and 6 W/m² be used to estimate the amount of heating energy contributed to a typical Norwegian school or kindergarten, respectively, by its occupants. Converting to W/person by multiplying these occupant heat gain densities by the ratio of the conditioned floor area to the number of occupants in the Steindal School, an

estimated heat gain of 155 W/person (schools) and 78 W/person (kindergartens) was found². In this estimate schools encompass all grades from first through high school, meaning that the heat gain in the Steindal School, which was only grades one through seven, was likely to be lower than the 155 W/person for schools. This further supported the use of 100 W/person as a reasonable occupant heat gain in the Steindal School.

Conversations with teachers in the school indicated that the occupancy schedules varied by grade level, with a typical start time of 8:30 and end time between 12:30 and 14:30. This did not influence the occupancy schedules in the Offices, Gym, or Annex, but did mean that the number of occupants in the 1st Floor classrooms was equal to some fraction of the maximum throughout the day. In order to apply a single schedule to the 1st Floor classroom zone the occupancy schedules for all of the grade levels was averaged to find a single start and stop time. The daily schedules for each occupied zone in the Steindal School are summarized in Table 5-12. Start and stop times are indicated for each occupied zone. Unoccupied periods are shaded with grey; occupied periods are shaded in white. M (Monday), T (Tuesday), W (Wednesday), R (Thursday), F (Friday) indicate the day of the week; M-F indicates all days, Monday through Friday.

² Heat gain per person = Heat Gain Density* Conditioned Floor Area/# Occupant
155 W/person = 12*4,400/340
78 W/person = 6*4,400/340

Daily Occupancy Schedules				
Time of Day	Classrooms	Offices	Gym	Annex
Weekdays				
0-1				
1-2				
2-3				
3-4				
4-5				
5-6				
6-7				
7-8	Start: M-F: 8:30 End: M 14:00, T-F 13:30	Start: M-F: 7:30 End: M-F 17:00	Start: M-F: 8:30 End: M 14:00, T-F 13:30 Start: M-F 19:00 End: M-F 21:00	Start: M-F: 8:00 End: M-F 16:00
8-9				
9-10				
10-11				
11-12				
12-13				
13-14				
14-15				
15-16				
16-17				
17-18				
18-19				
19-20				
20-21				
21-22				
22-23				
23-24				
Weekend				
1-24				

Table 5-12: Daily occupancy schedules for the Classrooms, Offices, Annex, and Gym in the Steindal School [Kringstad 2007],[Skjennald 2007].

The annual occupancy patterns for the school were taken from the school's 2006 calendar. Students were absent from the school for all five of the vacation periods; teachers were absent during all vacations, but had a shorter vacation during the summer. Table 5-13 shows the days during which vacations were taken as well as the total number of occupied weeks in 2006. All weeks not indicated in Table 5-13 followed the weekday occupancy schedule in Table 5-12.

Annual Vacation Schedule (2006)						# Occupied Weeks in 2006
Vacation:	Vinterferie (Winter)	Paskeferie (Easter)	Summer	Hostferie (Fall)	December Break	
Dates	Feb 25 th – March 5 th	Apr 8 th – Apr 17 th	Jun 24 th – Aug 20 th	Oct 7 th – Oct 15 th	Dec 20 th – Jan 2 nd	
Vacation Length, Students (Classrooms & Annex)	1 week	1 week	8 weeks	1 week	1.5 weeks	39.5
Vacation Length, Teachers (Offices)	1 week	1 week	1 week**	1 week	1.5 weeks	46.5

**During the summer vacation the offices are unoccupied during week 29.

Table 5-13: Scheduled vacations for students and teachers in the Steindal School. Specific dates correspond to the 2006 schedules from the Steindal School [Skjennald 2007].

During week 28, 30, 31, and 32 (summer vacation) the Offices were occupied from 8 a.m. to the stops times indicated in Table 5-23 (typically around 12 pm). The occupancy in these weeks coincided with the ventilation schedule. No other building zones were occupied during these weeks.

5.1.4.1 Uncertainty

The 100 W/person of heat gain was taken from ASHRAE documentation and verified against values that were specific to Norwegian schools and kindergartens. As a result, this value was accepted as having only a small amount of uncertainty arising from variations in activities (i.e. children playing in the gym) and was not varied during calibration (Chapter 7).

The fraction of radiant, latent, and sensible heat gain was taken to be acceptable. No matter how the 100 W/person was divided it was still added to the building as 100% heat gain. Additionally, the latent energy was expected to influence the building's cooling demand, and, in the absence of a cooling system in the Steindal School, this was negligible.

The occupancy schedules and the number of occupants were verified during site visits and conversations with teachers and occupants. As a result, the occupancy schedules were expected to be accurate and were not varied during calibration (Chapter 7).

5.1.5 Lighting

5.1.5.1 Interior Lighting

Site visits indicated that installed lighting fixtures in the 1st Floor classrooms, Offices, Annex, Gymnasium, Bomb Shelter, and Wardrobes were 120 cm (~48") fluorescent tube fixtures with two bulbs per fixture. As-built documents indicated a lighting fixture density of one fixture per every 6.1 m² of conditioned floor area. The specifications for the bulbs and ballasts in the lighting system were not known, but were taken to be T-12 bulbs with magnetic ballasts and a total bulb and ballast power demand of 82 W per fixture [EERE 2008B]. This resulted in an installed lighting density that was equivalent to the 13 W/m² (82 W per fixture/6.1 m² per fixture) that was typical for Norwegian school buildings [Wigenstad 2005]. The installed lighting capacity in each zone was then calculated as the product of the zone's floor area and the building's lighting density and is shown in Table 5-14.

Lighting Distribution [W/zone]	Typical Norwegian School	T-12 Bulbs and Fixtures
Bomb Shelter [W]	9,000	9,500
Offices [W]	10,500	11,000
1 st Floor [W]	22,000	23,000
Gym [W]	5,000	8,000
Wardrobes [W]	1,000	1,000
Annex [W]	6,500	7,000
Whole Building [W]	54,000	59,500
Lighting Density [W/m²]	13	13.4

Table 5-14: Interior lighting distribution in the Steindal School [EERE 2008B],[Steindal 2007],[WIGENSTAD 2005]

The daily and annual interior lighting schedules coincided with the building's occupancy schedules, which were shown in Table 5-12 and Table 5-13 [Kringstad 2007].

The electricity demanded by the lighting fixtures was released into the building as 100% heat gain.

5.1.5.1.1 Uncertainty

The choice of 82W fixtures with T-12 bulbs and magnetic ballasts was made on the basis of the observed density of fixtures in the building and the expected lighting density for typical Norwegian school buildings. The use of typical values resulted in a high degree of uncertainty in the lighting density. For example, the use of T-8 rather than T-12 lighting fixtures reduced the lighting density from 13.4 W/m² to 10.1 W/m². Thus, if the ballasts in the building were electronic with T-8 bulbs rather than magnetic with T-12 bulbs a significant reduction in the building's lighting capacity would have been observed. In the absence of further data, this uncertainty was investigated during calibration (Chapter 7).

5.1.5.2 Exterior Lighting

Observations made during the site visit indicated that several small outdoor lights were located on the exterior of the building near the entrances, and were turned on and off in response to the level of available sunlight. These lights were most often on during the dark winter months when the exterior lighting capacity (~1 kW) was negligible compared to the heating loads in the building. Consequently, the exterior lighting was omitted in all analyses.

5.1.6 Plug Loads

The plug loads in the school were attributed to computers, copiers, prints, and other appliances. The installed zone plug load capacities were initially estimated from zone floor areas and the plug load density for typical Norwegian schools. However, site visits indicated that the majority of the plug loads were concentrated in the Offices and 1st Floor. Consequently, the plug load capacities were reassigned according to the observations made in the school and were roughly based on the typical values for Norwegian schools. Table 5-15 shows the calculated zone plug load capacities from the typical values for Norwegian school buildings and the values assigned by the modeler. Additionally, plug load density values are shown for both the whole building and individual zones.

Plug Load Distribution [W/zone]	Description	Typical Norwegian School	Values Used
Office [W]	Computers, copiers, printers, electric range and oven	6,000	15,000
1 st Floor [W]	Computers and misc. equipment	12,000	15,000
Annex [W]	Computers, electric range and oven, misc. equipment	2,000	5,000
Whole Building [W]	Computers, electric ranges and ovens, refrigerators, office equipment, misc. other equipment	20,000	35,000
Plug Load Density [W/m ²]		4.5	8

Table 5-15: Installed plug load capacity and distribution in the Steindal School [Steindal 2007],[Wigenstad 2005].

The schedules of plug load operation varied according to the equipment type and location. Computers and office equipment schedules coincided with user occupancy (Table 5-12 and Table 5-13); refrigerators and freezers were run constantly.

The electricity demanded by the plug loads was released into the building as 100% heat gain.

5.1.6.1.1 Uncertainty

The plug loads were assigned based on the best estimate of the modeler and were highly uncertain. As a result, the installed plug load capacity was investigated during calibration (Chapter 7).

5.1.7 Domestic Hot Water

The domestic hot water (DHW) consumption was the energy necessary to supply hot water to showers, sinks, and bathrooms in the Steindal School. The installed DHW capacity in the school was estimated from the modeler's observation of DHW use in the school and was significantly lower than the typical values found in Norwegian schools (Table 5-15).

Domestic Hot Water Distribution [W/zone]	Description	Typical Norwegian School	Values Used
Office [W]	Bathrooms, kitchens	5,000	-----
1 st Floor [W]	Bathrooms	9,000	-----
Gym [W]	Showers and bathrooms	2,000	5,000
Wardrobes [W]	Bathrooms	2,000	-----
Annex [W]	Bathroom, kitchens	2,000	-----
Whole Building [W]	Bathrooms, kitchens, showers	20,000	5,000
DHW Density [W/m²]		4.5	1.1

Table 5-16: Estimated domestic hot water capacity in the Steindal School [Steindal 2007],[Wigenstad 2005].

Additionally, all of the domestic hot water consumption in the Steindal School was attributed to the locker rooms in the gymnasium, and so all 5 kW of installed DHW capacity was allocated to the Gym zone. Consequently, the hot water schedule coincided with the occupancy schedule for the gym; when the gym was occupied the domestic hot water was on.

The DHW contributed no heat to the building. All heat from DHW was removed from the building when the water was drained.

5.1.7.1 Uncertainty

There was a high degree of uncertainty associated with the 5 kW of DHW capacity that was assigned to the Steindal School. This value was well below the total installed capacity of 20 kW for typical Norwegian Schools. However, the uncertainty in this value was initially neglected because it was assumed to have a small influence on the overall energy consumption in the Steindal School. This was a poor assumption on the part of the modelers, and was resolved during calibration (Chapter 7). Additionally, the assumption that the domestic hot water was only demanded when the Gymnasium was occupied meant that all domestic hot water demands were attributed to the gymnasium locker rooms. It was much more likely that domestic hot water was demanded throughout the building over the course of the day. However, because the domestic hot water load was expected to be small, and because it contributed no heat gain the building, the decision to model it as a single load in the Gymnasium was reasonable. The validity of this schedule was tested with simple estimates in Chapter 6.

5.1.8 Cooling

Site visits and as-built documents indicated that there was no cooling system installed in the Steindal School [Simmons 2007],[Steindal 2007],[NVP 1997]. However, the building's operable windows (section 5.1.3) provided natural ventilation to cool the building during the warm summer months of June, July, and August. It was assumed that these operable windows were only opened when the outdoor temperature was greater than the indoor temperature (section 5.1.9), minimizing their impact on the annual energy consumption in the school. Consequently, the operable windows were not included in the EnergyPlus building model.

5.1.9 Heating

5.1.9.1 Heating Capacity

The space heating in the Steindal School was 100% electric resistance heat. The heat in the 1st Floor, Offices, Gym, and Annex was supplied by electric resistance wall panels. Additionally, heat was supplied to sections of the Gym, Wardrobes, Bomb Shelter, and Offices by electric resistance heating cables. The installed heating capacity in each building zone was taken from contractor documentation and as-built drawings and is shown in Table 5-17.

Heating Distribution [W/zone]	Electric Resistance Wall Panels
Bomb Shelter [W]	-----
Offices [W]	36,000
1 st Floor [W]	56,000
Gym [W]	15,000
Entrance Wardrobes [W]	-----
Annex [W]	19,000
Whole Building [W]	126,000
Heating Density [W/m²]	29

Table 5-17: Installed heating capacity in the Steindal School [Steindal 2007].

The system was 100% efficient; all of the electricity supplied to the heaters was converted to heat. The supply of heat to the school was controlled by thermostats; heating was available for the entire year.

5.1.9.2 Temperature Setpoints

The temperature setpoints were programmed into the zone thermostats and were maintained by the electric resistance heating system. The setpoints and schedules for the thermostat settings were taken from the Trondheim Municipality's control center. The occupied (white) and unoccupied (gray) temperature schedules and setpoints (°C) are shown in Table 5-18. The times for each temperature change are also given. M-F indicate the days of the week, Monday through Friday.

Daily Schedules					
Time of Day	Classrooms	Offices	Gym	Annex	Wardrobes
<i>Weekdays</i>					
0-1	18°C	19°C	18°C	18°C	18°C
1-2					
2-3					
3-4					
4-5					
5-6					
6-7					
7-8	20°C	21°C	20°C	20°C	
8-9					
9-10					
10-11					
11-12					
12-13					
13-14					
14-15	18°C	19°C	18°C	18°C	
15-16					
16-17					
17-18					
18-19					
19-20					
20-21					
21-22	18°C	19°C	18°C	18°C	
22-23					
23-24					
<i>Weekend</i>					
1-24	18°C	19°C	18°C	18°C	18°C

Table 5-18: Daily schedule of temperature setpoints in the Steindal School, divided by building zone [Municipality 2007b].

Collected data indicated that the temperatures were changed directly from the unoccupied (setback) to occupied temperatures in the mornings; no ramping was used to minimize the influence of thermal mass. However, a temperature deadband of 1°C was permitted by the thermostats. This meant that the room temperature was permitted to fluctuate above and below the setpoint temperature by 1°C before the heating system responded.

On an annual basis the temperature setpoint schedules coincided with the occupancy schedules in Table 5-12. Data collected from the control center indicated a vacation temperature setpoint for all spaces in the building of 14°C. This setpoint was assigned during the December vacation. The temperature setpoint for all other vacation periods, including the summer, winter, Easter, and fall vacations was equal to the setback temperature in each zone: 18°C in the 1st Floor, Gym, Wardrobes, and Annex and 19°C in the Offices.

5.1.9.3 Uncertainty

The heating capacity and temperature schedules were defined from as-built documents and data provided by the Municipality. The installed heating capacity was confirmed in contractor's data sheets and the temperature settings were verified during conversations with building occupants and managers. The confirmation of these inputs increased the certainty that they were accurate. However, because of the cool climate in Trondheim the amount of heating energy in the building was expected to be significant, and thus the temperature setpoints were expected to have a strong influence on the accuracy of the EnergyPlus model of the school. As a result, the influence of higher and lower temperature setpoints was investigated during calibration (Chapter 7), but only within a limited range of variation (+/- 2°C) above and below the specified setpoints. Daily temperature schedule length changes were also investigated, but only for one of the models that was calibrated (Chapter 7).

5.1.10 Ventilation

5.1.10.1 Ventilation System Type

The ventilation system in the Steindal School was a constant volume mechanical ventilation system. One hundred percent outdoor air was supplied to the building by two balanced air handler units: one in the Main building and one in the Annex. Both ventilation systems included heat recovery; neither had a cooling system. Supply and exhaust fans drove the flow of air between the building's exterior and interior.

5.1.10.2 Ventilation Flow Rates

The ventilation flow rate was the volume of air flowing through the ventilation system and into the building. Design documents specified an air flow rate equal to 46,800 m³/hr in the

Steindal School; 40,000 m³/hr of air flow in the Main ventilation system and 6,800 m³/hr of air flow in the Annex ventilation system. Measurements made by ventilation contractor during the school's 1997 renovation specified a supply air flow rate equal to 39,500 m³/hr and a return air flow rate equal to 37,250 m³/hr [NVP 1997] in the Main ventilation system. Similarly, measurements by the ventilation contractor during the 1997 installation specified equal return and supply air flow rates of 6,700 m³/hr [AS MOE 1997] in the Annex ventilation system.

Velocity measurements were made during the site visit to the Steindal School with a hand held anemometer to confirm the ventilation flow rates. Where possible, these measurements were taken in ducts that were far from bends or junctions and at points that were located in the middle of the duct air stream. These velocities were then multiplied by the area of the ducts in which the measurements were taken to find the volumetric flow rate of air at each location. These measurements were then compared to the expected flow rates from design documents and the percent difference was calculated as the design flow rate less the measured flow rate divided by the design flow rate. Three measurements were taken at each duct location. The measured flow rates, design flow rates, and % difference are shown in Table 5-19.

	Duct Dimensions		Measured Velocities	Mean Vel.	Design Vel.	Mean Flow Rate	Design Flow Rate	% Diff.
	Diam. [mm]	Area [m ²]	U1/U2/U3 [m/s]	Um [m/s]	Ud [m/s]	Vm [m ³ /hr]	Vd [m ³ /hr]	% diff. [%]
SUPPLY								
Reading S-1	200	0.031	4.45/4.50/4.43	4.46	4.42	504	500	1%
Reading S-2	200	0.031	4.50/4.30/4.30	4.37	4.42	494	500	-1%
Reading S-3	200	0.031	3.78/3.86/4.00	3.88	4.42	439	500	-12%
Reading S-4	200	0.031	4.89/4.92/4.95	4.92	4.42	556	500	11%

Table 5-19: Measurements of the supply ventilation flow rates in the Steindal School, made with a hand-held anemometer during site visits in May, 2007.

EXHAUST	Duct Dimensions		Measured Velocities	Mean Vel.	Design Vel.	Mean Flow Rate	Design Flow Rate	% Diff.
	Diam. [mm]	Area [m ²]	U1/U2/U3 [m/s]	Um [m/s]	Ud [m/s]	Vm [m ³ /hr]	Vd [m ³ /hr]	% diff. [%]
Reading E-1	200	0.031	3.39/3.52/3.63	3.51	4.42	397	500	-21%
Reading E-2	200	0.031	4.13/4.31/4.40	4.28	4.42	484	500	-3%
Reading E-3	200	0.031	3.30/3.43/3.49	3.41	4.42	385	500	-23%
Reading E-4	800	0.503	9.45/9.60/9.30	9.45	9.12	17100	16500	-4%
Reading E-5	200	0.031	1.70/1.80/1.80	1.77	1.77	200	200	0%

Table 5-20: Measurements of the exhaust ventilation flow rates in the Steindal School, made with a hand-held anemometer during site visits in May, 2007.

With the exception of Reading E-1 and Reading E-3, all of the measured ventilation rates were within 11-12% of the design values. Additionally, ventilation Reading E-4, which was made in the large return air duct where friction losses and turbulence were expected to be at a minimum, was within 5% of the design flow rates. On the basis of these observations the air flow rate in the Steindal School was taken to be equal to 46,800 m³/hr, as per design documents.

Air flows were distributed to each of the building zones on the basis of information collected from as-built drawings. The resulting rate of air supplied to the Bomb Shelter, Offices, 1st Floor, Gym, and Annex are shown in Table 5-21. There was no ventilation in the Underroof or the Wardrobes.

Ventilation Flow Rate: Zone Level	Ventilation Flow Rate [m ³ /hr/zone]
Bomb Shelter [m ³ /hr]	5,400
Offices [m ³ /hr]	6,500
1 st Floor Classrooms [m ³ /hr]	22,700
Gymnasium [m ³ /hr]	5,000
Annex [m ³ /hr]	6,800
Whole Building [m³/hr]	46,800

Table 5-21: Ventilation flow rates in each zone of the Steindal School in 2006 [Steindal 2007].

All ventilation duct work was located in the heated portion of the building, except for those portions entering and leaving the heat recovery units, which were located in the unheated Underroof space and were insulated.

5.1.10.2.1 Uncertainty

The ventilation flow rates specified in design documents matched the measured flow rates to within 11%-12% in most cases. However, because both the fan and ventilation heating energies in the Steindal School were strongly tied to the ventilation flow rates, even this 11-12% error could have a strong influence on the ability of the EnergyPlus model to mimic the building's energy consumption. As a result, the ventilation flow rates were varied by approximately +/- 10% during model calibration. The implications of this variation are discussed further in Chapter 7.

5.1.10.3 Ventilation Fan Power

Centrifugal fans were used to drive the supply and exhaust air flows in the Main ventilation system. These fans were installed in the summer of 2006 as replacements for the system's original fans, which were installed in 1978 [Simmons 2007]. Data sheets that were collected from the fan manufacturer specified a pressure drop of 1200 Pa and an efficiency of 70% for each of these fans [Zhiel-Abegg 2008]. The power demand for each fan was then calculated as in Equation 5-3. At a ventilation flow rate of 11 m³/sec (40,000 m³/hr) the resulting power demand was equal to 19 kW per fan for a total of 38 kW for both system fans.

A similar calculation was performed to find the power demanded by the centrifugal supply and exhaust fans in the Annex ventilation system. Data collected from the fan manufacturer specified a pressure drop of 600 Pa and a fan efficiency of 75% for both the supply and exhaust fans [AS MOE 1997]. The power demand for each fan was then calculated as in Equation 5-3. At a ventilation flow rate of 1.9 m³/sec (6,800 m³/hr) the resulting power demand was equal to 1.5 kW per fan for a total of 3 kW for both system fans.

$$Power = \frac{\Delta P \dot{V}}{\eta} \quad (5-3)$$

<i>Power</i>	Power demanded by the fan [W]
<i>V</i>	Ventilation flow rate [m ³ /sec]
<i>ΔP</i>	Pressure drop across the fan [Pa]
<i>η</i>	Efficiency of the fan expressed as a decimal between 0 and 1.

The total ventilation fan power in the Steindal School was equal to 41 kW.

5.1.10.3.1 Uncertainty

The specifications for the fan pressure in the Main building ventilation system were taken from the manufacturer's documents and were expected to be reasonably accurate. However, detailed fan curves were not available for input into the EnergyPlus model, and so some uncertainty was expected in these values. As a result, the fan pressure was permitted to vary during calibration (Chapter 7), but only by +/- 15% of the 1,200 Pa specified.

5.1.10.4 Ventilation Heat Recovery Type

The ventilation heat recovery system in the Steindal School enabled heat to be exchanged between the warm return air from the building and the cool outdoor air entering the building. The use of a heat recovery unit was especially important in the Steindal School because all of the building's supply air was outdoor air; no direct mixing between outdoor and return air occurred. Thus, to maximize the amount of heat transfer from the return air to the incoming outdoor air stream, a mechanical heat recovery unit was needed. A schematic of a counterflow rotary wheel heat recovery unit is shown in Figure 5-17.

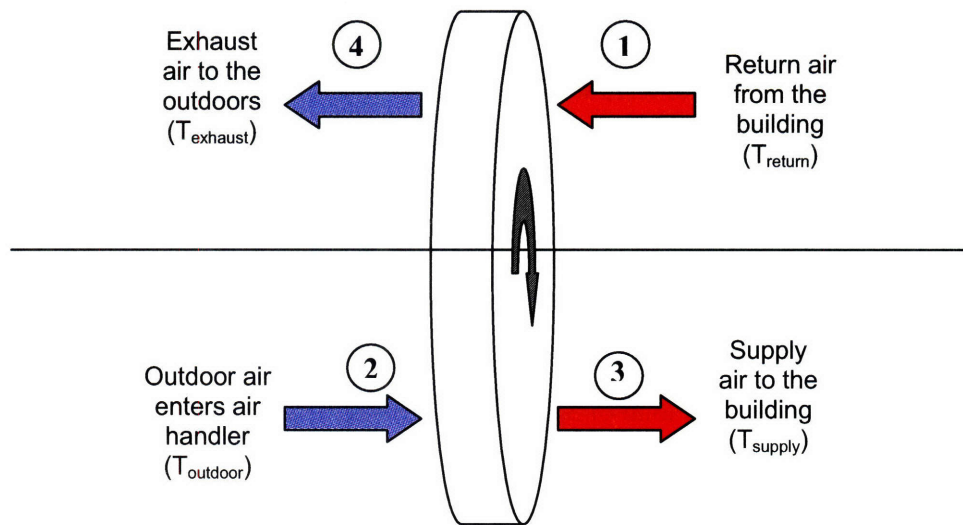


Figure 5-17: Schematic layout for a generic rotary wheel heat recovery unit.

In Figure 5-17 the warm return air enters the heat recovery unit at point 1 and the cool outdoor air enters the unit at point 2. The two air streams are separated, as indicated by the horizontal line in Figure 5-17, and exchange heat as they pass through the rotating heat recovery wheel. The cooled return air stream is exhausted from the building at point 4 and the warmed outdoor air is

sent to a heater at point 3 where its temperature is raised to the ventilation supply temperature and the air enters the building.

Two types of heat recovery units were installed in the Steindal School: rotary wheel and plate. The rotary wheel heat recovery unit was located in the Main ventilation system of the school and consisted of two rotating wheels, each 1.8 m in diameter, placed side by side. These two wheels exchanged sensible (dry) heat without mixing the return and outdoor air streams. The heat recovery unit in the Annex ventilation system was a cross flow plate heat recovery unit. This unit transferred energy via conduction through a metal plate that was placed between the return and outdoor air streams. This cross flow heat recovery unit was only able to exchange dry (sensible) heat between the two air streams. Both heat recovery units enabled 100% outdoor air to be supplied to the building. Typical efficiencies for rotary heat recovery units range from 70% to 80%; those for cross flow plate heat recovery units range from 60% to 70%.

The effectiveness, or efficiency, of each heat recovery unit was equal to the fraction of the heat in the return air stream that was transferred to the incoming outdoor air stream. This percentage is most accurately calculated as the ratio of the total enthalpy, including both latent and sensible energies, at the supply and exhaust of the heat recovery unit. However, because the latent energy content is difficult to analyze, the temperature effectiveness, calculated as in Equation 5-4, is often used to estimate the heat recovery effectiveness in ventilation systems.

$$\eta = \frac{T_{supply} - T_{outdoor}}{T_{return} - T_{outdoor}} * 100 \quad (5-4)$$

η	Temperature effectiveness [%]
T_{supply}	Temperature of the supply air leaving the heat recovery unit [°C]
T_{return}	Temperature of the return air from the building [°C]
$T_{outdoor}$	Temperature of the outdoor air entering the heat recovery unit [°C]

The temperature effectiveness of the Main and Annex heat recovery units were calculated at the Trondheim municipality's control center with data that was collected from temperature sensors in both heat recovery units.

5.1.10.5 Ventilation Heat Recovery Effectiveness

Measurements made by ventilation contractors specified a heat recovery effectiveness of 74% at an air flow rate of 20,000 m³/hr in the Main ventilation system. However, this was not an

accurate estimate of the operational effectiveness of the heat recovery unit, which ran at an air flow rate of 40,000 m³/hr, twice the 20,000 m³/hr in the contractor's measurements. The operational heat recovery effectiveness was subsequently taken from the heat recovery effectiveness curves that were provided by the ventilation contractor. This resulted in an effectiveness of 60%-65% at the 40,000 m³/hr operational air flow rate [NVP 1997].

At the request of the modelers the operational heat recovery effectiveness was recorded by the Trondheim Municipality's control center for both the Main and Annex heat recovery units for periods in February, March, and September of 2007 (Figure 5-18 and Figure 5-19). These heat recovery effectiveness values were calculated internally in the Municipality's monitoring software, but were based on temperature measurements at the zone return, outdoor air inlet, system exhaust, and system supply of the heat recovery unit (indicated by points 1-4 in Figure 5-17). Each data point shown in Figure 5-18 and Figure 5-19 represents a single measurement, taken at each hour of the day over a week long period. Filled data points represent measurements that were made in February and March of 2007; unfilled data points represent measurements that were made in September of 2007. Data logging was performed when the ventilation was both on and off; the data points falling at zero heat recovery effectiveness were logged when the system was off.

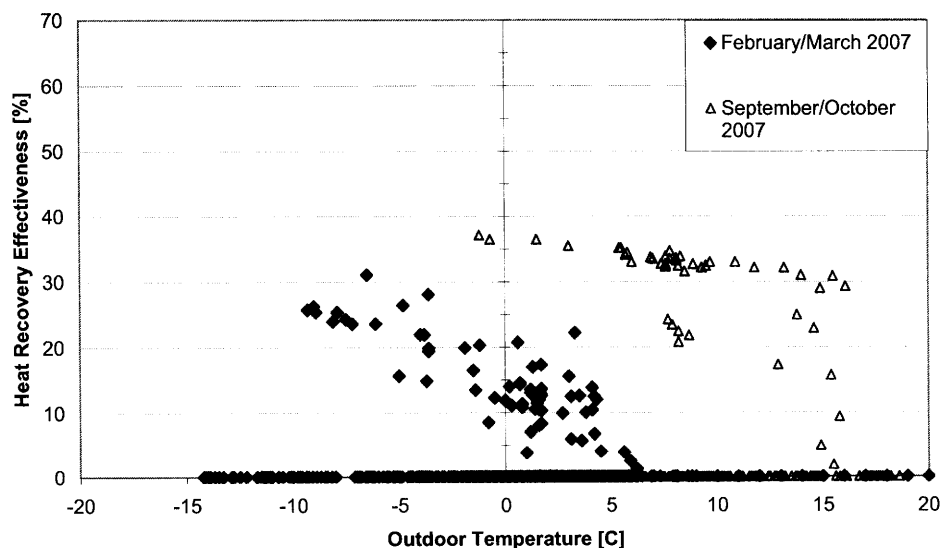


Figure 5-18: Main ventilation system heat recovery effectiveness measurements from Municipality data. The data are split into measurements taken in the Spring (filled diamonds) and Fall (unfilled triangles) [Municipality 2007b].

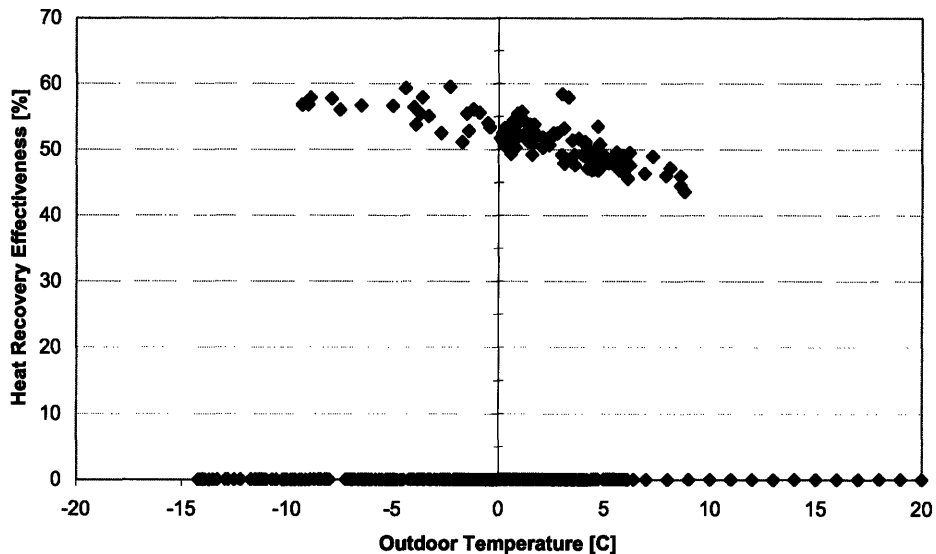


Figure 5-19: Annex ventilation system heat recovery effectiveness measurements from Municipality data. All measurements were made between February and March in 2007 [Municipality 2007b].

Data from the Municipality’s control center indicated a heat recovery effectiveness of ~35% in the Main ventilation system (Figure 5-18). This was significantly smaller than the 65% that was extrapolated from design documents. As a first approximation, the heat recovery effectiveness in the Main ventilation system was taken to be between the 35% recorded by the Municipality and the 65% from contractor’s specifications; a heat recovery effectiveness of 50% was approximated for the Main ventilation system.

Data from the Municipality’s control center estimated the temperature effectiveness of the cross flow heat recovery unit in the Annex to be between 45%-60% (Figure 5-19). This was lower than the 66% effectiveness that was measured by the ventilation contractor when the system was installed in 1997 [AS MOE 1997]. A closer inspection of the data presented in Figure 5-19 indicated that 50% was a reasonable estimate for the heat recovery effectiveness in the Annex ventilation system.

5.1.10.5.1 Uncertainty

There was a large amount of uncertainty associated with the heat recovery effectiveness values from the Steindal School. The available data from the Municipality (Figure 5-18) from the Main ventilation system was inconsistent and inaccurate, and that from the Annex ventilation system (Figure 5-19) showed a variation of between 5%-10% effectiveness – a significant amount when the efficiency is between 45% and 55%. Additionally, there appeared to be a

correlation between outdoor temperature and heat recovery effectiveness in Figure 5-18 and Figure 5-19, the cause of which was not apparent.

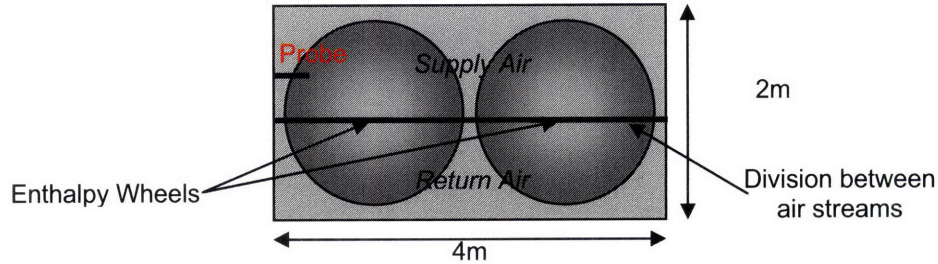


Figure 5-20: Cross-section of the Main ventilation system heat recovery layout. Note the placement of the temperature probe. Drawing not to scale.

Conversations with building managers indicated that the temperature probe that was used to calculate the effectiveness of the heat recovery unit in the Main ventilation system (according to Equation 5-4) was located 10-15 cm into a duct that was approximately 4 m wide by 2 m high (8 m²). The unique arrangement of the heat recovery system, with two 1.8 m diameter heat recovery wheels placed side by side (Figure 5-20), caused a high degree of temperature stratification within the air duct. The greatest mixing, and thus the most accurate temperature measurements, occurred in the middle of the outlet duct, and the poorest mixing occurred near the walls of the duct, where the temperature probe was located. This led to measured temperatures that were lower than the actual temperature of the mixed air stream and resulted in a lower temperature difference between the incoming outdoor air (point 2 in Figure 5-17) and the supply air (point 3 in Figure 5-17) leaving the heat recovery unit, which, when applied to the calculation of efficiency in Equation 5-4, led to an underestimate of the heat recovery effectiveness.

Additionally, conversations with members of the municipality indicated that the Main ventilation system controls in the Steindal School were not functioning properly from February through March in 2007 – the period during which the first sequence of heat recovery effectiveness measurements were made by the municipality. The measurements that were made during this period were indicated by the blue diamonds in Figure 5-18. These data points were highly erratic and did not show the consistency that was expected for the heat recovery effectiveness. This system malfunction made the data collected from the municipality unreliable and highly uncertain.

The Annex ventilation system heat recovery effectiveness data that were recorded by the Municipality were more consistent and accurate than the Main ventilation system heat recovery data that were collected. This was because the dimensions of the ducts in the Annex heat recovery unit were significantly smaller, limiting the influence of temperature stratification on the measured effectiveness and leading to more accurate measurements.

Both Figure 5-18 and Figure 5-19 indicated a correlation between the outdoor temperature and the heat recovery effectiveness in the Steindal School's ventilation systems. This was unexpected, as the design of the heat recovery system dictated that the effectiveness be independent of the temperature differences across the unit. Consequently, the cause of the correlation between temperature and heat recovery effectiveness was not obvious. However, it was suggested that this temperature correlation was associated with the measurement devices that were utilized by the municipality. These devices may not have been properly calibrated, well placed, or well-maintained; any of these concerns could have led to inaccurate measurements from one of the three temperature probes that were required to calculate the temperature effectiveness of the heat recovery units. Additionally, measurements with a hand-held probe were difficult to make because the access to the interior of the heat recovery unit was limited.

Analysis of the heat recovery effectiveness of both the Main ventilation system and the Annex ventilation system showed a high degree of uncertainty in their expected values. As a result, the heat recovery effectiveness of both of these systems was varied during calibration (Chapter 7). The Main ventilation system effectiveness was varied between 40%-65%, while the Annex ventilation system was varied between 40%-60%. These were intended to encompass the range of possible values that were identified during data collection.

5.1.10.6 Ventilation Heating

Data collected from the Municipality's control center indicated a minimum temperature of 18°C for the supply air stream. The maximum supply air temperature was 25°C. These temperatures were measured by probes in the supply ducts, and were located immediately downstream from the heating elements in the Main and Annex ventilation systems.

The heating element in the Main ventilation system was a hydronic heating coil placed at the outlet of the enthalpy wheel heat recovery unit, at point 3 in Figure 5-17. The heating

capacity of this coil was limited by the 185 kW electric boiler in the Bomb Shelter of the building.

EnergyPlus required that a UA-value be defined for the ventilation heating coil in the Main building. This UA-value determined the amount of heat that was transferred from the coil per degree Kelvin and was measured in W/K. However, specifications for the UA-value of the coil were not available from the Steindal School, making it necessary to perform a calculation to estimate the UA-value [Incropera 2001]. This calculation was performed according to the best practice assumptions for a cross flow heat exchanger with unmixed heat transfer fluids and is discussed in Appendix C. The result of this calculation was an approximate UA-value equal to 3,750 W/K for the hydronic heating coil in the Main building's ventilation system. However, in terms of the energy required in the Steindal School this calculation was unnecessary; any heating demand that was not met by the ventilation heating coil was compensated for by the space heating. Recalling that both the ventilation and space heating systems were electric and 100% efficient, even if the space heating needed to compensate for the ventilation heating, all ventilation heating was still met by electricity. This made the specification of an appropriate UA-value less consequential than if the ventilation and space heating were supplied by different energy sources, in which cases the two would need to be distinct.

The heat source in the annex ventilation system was an electric resistance coil heater, also placed at point 3 in the generic heat recovery unit in Figure 5-17. The capacity of this heating coil was equal to 24 kW.

5.1.10.6.1 Uncertainty

The simple estimate of the UA-value of the heating coil in the Main ventilation system provided a first estimate of the heat transfer properties of the unit. However, this estimate was based on the best approximation available to the modeler and had a high degree of uncertainty in its value. Thus, the UA-value of the hydronic heating coil was varied during calibration (Chapter 7).

The heating capacity of the electric resistance coil in the Annex ventilation system was taken from nameplate data and was considered to be accurate. The heating capacity of the electric resistance heating coil in the Annex was not varied during calibration (Chapter 7).

5.1.10.7 Ventilation Schedule

Ventilation schedules were provided by the Municipality's control center and are shown in Table 5-22 and Table 5-23. Grey areas indicate periods when the ventilation was off; white areas indicate times when the ventilation was on. The ventilation flow rate during operation is also shown with the on and off times for each ventilation system.

Daily Schedules			
Time of Day	Main Ventilation System	Annex Ventilation System	
Weekdays			
0-1			
1-2			
2-3			
3-4			
4-5			
5-6			
6-7	<i>Start: M-F: 6am</i> 40,000 m³/hr <i>End: M-F: 4pm</i>	<i>Start: M-F: 6am</i> 6,800 m³/hr <i>End: M-F: 5pm</i>	
7-8			
8-9			
9-10			
10-11			
11-12			
12-13			
13-14			
14-15			
15-16			
16-17			
17-18			
18-19			
19-20			<i>Start: W: 7pm</i> 40,000 m³/hr <i>End: W: 9pm</i>
20-21			
21-22			
22-23			
23-24			
Weekend			
1-24			

Table 5-22: Daily ventilation schedules in the Main and Annex ventilation systems in 2006 [Municipality 2007b].

The Main and Annex ventilation systems operated on slightly different daily schedules, but operated on the same annual schedules. Annually, the ventilation was off during the December vacation (Dec 20th – Dec 31st) and week 29 (summer vacation); the ventilation operated on shorter daily schedules during weeks 28, 30, 31, and 32 (summer vacation). The schedules of operation for weeks 28 through 32 are shown in Table 5-23. The ventilation was turned on at 6 a.m. on all days during weeks 28, 30, 31, and 32.

	Week 28 July 10 th – July 16 th	Week 29 July 17 th – July 23 rd	Week 30 July 24 th – July 30 th	Week 31 July 31 st – August 6 th	Week 32 August 7 th – August 13 th
Main Ventilation System	On until 12:00	OFF	On until 12:00	On until 12:00	On until 15:30
Annex Ventilation System	On until 12:00	OFF	On until 12:00	On until 12:00	On until 16:00

Table 5-23: Daily schedule of ventilation air supply during weeks 28-32 (summer vacation) in 2006 [Municipality 2007b].

5.1.10.7.1 Uncertainty

The ventilation schedules and temperature setpoints were specified at the Trondheim Municipality’s control center and were automated to match predetermined schedules. As a result, the ventilation schedules were expected to be accurate and were not varied during calibration (Chapter 7).

5.2 Summary of Collected Data

5.2.1 Data Collection Resources

Data collection resources included as-built documents, site visits, conversations with building managers, simple measurements, and typical values. These resources were used to define the ventilation, heating, geometry, envelope, and internal gains in the Steindal School for the 2006 calendar year. Data that was unavailable from as-built documents and site visits were defined according to typical values for Norwegian school buildings. A summary of the resources that were used to collect data on the Steindal School is shown in Table 5-24. Listed alongside each resource are the inputs that it was used to define.

Data Collection Resource	Geometry and Envelope	Internal Gains	Heating	Ventilation
As-Built Documents	<ul style="list-style-type: none"> • Footprint • Orientation • Dimensions • Floor Plan • Materials 	<ul style="list-style-type: none"> • Lighting type • Lighting capacity • Lighting arrangement 	<ul style="list-style-type: none"> • System type • Distribution system (zoning) • Equipment type and capacity 	<ul style="list-style-type: none"> • System type • Distribution system (zoning) • Heating capacity • Cooling capacity • Heat recovery effectiveness • Equipment type and capacity • Fan specifications
Site Visits and Conversations with Building Managers (including spot measurements)	<ul style="list-style-type: none"> • Infiltration – “draftiness” • Floor plan • Room use • Materials check 	<ul style="list-style-type: none"> • Lighting capacity • Equipment capacity • External lighting • Occupancy • Domestic Hot Water (DHW) capacity • Schedules 	<ul style="list-style-type: none"> • System type • Distribution system (zoning) • T° setpoints and tstat locations • Equipment nameplate data • Schedules 	<ul style="list-style-type: none"> • System type • Distribution system (zoning) • Flow rates • Heat recovery effectiveness • Equipment nameplate data • Schedules
Typical Practice	<ul style="list-style-type: none"> • Infiltration levels 	<ul style="list-style-type: none"> • Lighting capacity • Equipment capacity • DHW capacity • Schedules 	<ul style="list-style-type: none"> • T° setpoints • T° schedules 	<ul style="list-style-type: none"> • Schedules

Table 5-24: Summary of data collection resources that were used to define the energy consumption characteristics of the Steindal School.

The majority of inputs were defined during data collection and verified through site visits and conversations with building managers. Only after these resources had been exhausted were typical values used to define lighting, plug load, and hot water capacities. Thus, the preferred resources for data collection were as-built documents, site visits, and conversations with building managers.

Chapter 6 discusses ways in which simple energy estimates were applied to verify the accuracy of the data collected from as-built documents, site visits, conversations with building managers, and typical values. This verification was intended to present simple ways in which input data could be validated before performing energy simulations.

5.2.2 Summary of Inputs

The data collected in sections 5.1.1 through 5.1.10 were input into EnergyPlus models in Chapter 7 to define the EnergyPlus model of the Steindal School. These inputs are summarized

in Table 5-25 and Table 5-26. The order in which the data are presented in Table 5-25 and Table 5-26, and throughout Chapter 5, was the order in which these inputs were entered into the EnergyPlus model. This order was developed based in previous work (Chapter 3) and was conducive to the hierarchy of inputs needed to accurately define the EnergyPlus model. An example of this hierarchy was discussed in reference to the materials and construction objects in section 5.1.3.

Utility Data (5.1.1)	
<i>Utility Billing</i>	Electricity billing available hourly from January 2004-November 2007
Weather (5.1.2)	
<i>Weather Data Availability</i>	2006 temperatures from Trondheim (Voll), wind from Kvithamar, radiation data from Oslo IWEK file
Geometry and Envelope (5.1.3)	
<i>Building Site & Surroundings</i>	Located on a hill South of Trondheim, light shading from trees on the North façade.
<i>Ground Temperature</i>	18°C
<i>Building Geometry</i>	18,300 m ³ volume with 5,409m ² /4,400m ² of utility/conditioned floor area.
<i>Envelope U-Values</i>	Exterior Walls ~ 0.25-0.30 W/m ² K; Ground Wall ~ 1.14 W/m ² K; Roof ~ 0.18-0.24 W/m ² K; Ground Floor ~ 0.6 W/m ² K; Windows ~ 1.1-2.9 W/m ² K
<i>Window Solar Heat Gain Properties</i>	74%/31% solar heat gain through North/South Main building façade windows, 34% solar heat gain through Annex windows
<i>Window-Wall Area</i>	33% of building wall area
<i>Infiltration Rate</i>	0.3 ACH
Occupancy (5.1.4)	
<i>Occupant Density</i>	0.08 people/m ² @ 100W/person
<i>Maximum # Occupants per Zone</i>	Offices: 40 people; 1 st Floor: 265 people; Gym: 20 people; Annex: 60
<i>Occupancy Schedules</i>	Offices: 7:30-17:00; 1 st Floor: 8:30-13:30/14:00; Gym: 8:30 -13:30/14:00; Annex: 8:00-16:00
Lighting (5.1.5)	
<i>Lighting Density</i>	13.4 W/m ²
<i>Lighting Installed Capacities</i>	Bomb Shelter: 9,500 W; Offices: 11,100 W; 1 st Floor: 23,000 W; Wardrobes: 1,000 W; Gym: 8,000 W; Annex: 7,000 W
<i>Lighting Schedules</i>	See Occupancy Schedules
Plug Loads (5.1.6)	
<i>Plug Load Density</i>	8 W/m ²
<i>Plug Load Installed Capacities</i>	Offices: 15 kW; 1 st Floor: 15 kW; Annex: 5 kW
<i>Plug Load Schedules</i>	See Occupancy Schedules
Domestic Hot Water (DHW) (5.1.7)	
<i>DHW Density</i>	1.1 W/m ²
<i>DHW Installed Capacity</i>	5 kW in Gymnasium
<i>DHW Schedule</i>	See Gymnasium Occupancy Schedule

Table 5-25: Summary of weather, envelope, occupancy, lighting, plug load, and domestic hot water energy consumption characteristics from the Steindal School in 2006.

Heating (5.1.9)	
<i>Heating System Type and Capacity</i>	126 kW of electric resistance heating
<i>Temperature Setpoints (Occupied/Unoccupied)</i>	21°C/19°C offices, 20°C/18°C in all other spaces
<i>Installed Heating Capacities per Zone</i>	Offices: 36 kW ; 1 st Floor: 56 kW; Gym: 15 kW; Annex: 19 kW
<i>Heating Schedules</i>	Offices: 7:00-17:00; 1 st Floor: 7:00-14:00; Gym: 7:00-14:00; Wardrobes: On at all times; Annex: 7:00-16:00
<i>Heating Efficiency</i>	100%
Ventilation (5.1.10)	
<i>Ventilation System Type</i>	Main: Balanced w/rotary wheel HX; Annex: Balanced w/cross flow HX
<i>Ventilation Installed Fan Capacity</i>	Main: 2 x Fans @ 19 kW each; Annex: 2 x Fans @ 1.5 kW each
<i>Ventilation Installed Heating Capacity</i>	Main: 185 kW w/ UA _{coil} = 3,750 W/K ; Annex: 24 kW
<i>Ventilation Heat Recovery Effectiveness</i>	Main: 50%; Annex: 50%
<i>Ventilation Flow Rates</i>	Main: 40,000 m ³ /hr; Annex: 6,800 m ³ /hr
<i>Ventilation schedules (Occupied/Unoccupied)</i>	Main: 6:00-16:00/Off; Annex: 6:00-17:00/Off on weekdays/weekends
<i>Ventilation Flow Rate per Zone</i>	Bomb Shelter: 5,400 m ³ /hr; Offices: 6,500 m ³ /hr; 1 st Floor: 22,700 m ³ /hr; Gym: 5,000 m ³ /hr; Annex: 6,800 m ³ /hr

Table 5-26: Summary of heating and ventilation energy consumption characteristics from the Steindal School in 2006.

5.3 Sources of Uncertainty

Those inputs identified as having a high degree of uncertainty associated with their values were highlighted during data collection and are shown in Table 5-27. Methods of resolving the uncertainty in these inputs were investigated and are discussed in Chapters 6 and 7 of this work. These methods included simple energy balances and calibration. Table 5-27 organizes the uncertain inputs from those that were expected to be most influential during model calibration to those that were expected to be least influential in during calibration (Chapter 7). Because the building was located in a cool climate the envelope, heating, and ventilation inputs were expected to have a significant influence on the amount of energy consumed in the school, and were subsequently emphasized during calibration. Additionally, because there was a very high uncertainty associated with the heat recovery effectiveness of the ventilation system, this was expected to be one of, if not the, most influential input during calibration. These expectations were based on the modeler's observations and knowledge of the building system.

Ventilation (5.1.10)	
<i>Ventilation Heat Recovery Effectiveness</i>	Main: 50%; Annex: 50%
<i>Ventilation Flow Rates</i>	Main: 40,000 m ³ /hr; Annex: 6,800 m ³ /hr
<i>Ventilation Flow Rate per Zone</i>	Bomb Shelter: 5400 m ³ /hr; Offices: 6500 m ³ /hr; 1 st Floor: 22700 m ³ /hr; Gym: 5000 m ³ /hr; Annex: 6800 m ³ /hr
<i>Ventilation schedules (Occupied/Unoccupied)</i>	Main: 6:00-16:00/Off; Annex: 6:00-17:00/Off on weekdays/weekends
<i>Ventilation Installed Fan Capacity</i>	Main: 2 x Fans @ 19 kW each; Annex: 2 x Fans @ 1.5 kW each
<i>Ventilation Installed Heating Capacity</i>	Main: 185 kW w/ UA _{coil} = 3,750 W/K ; Annex: 24 kW
Geometry and Envelope (5.1.3)	
<i>Infiltration Rate</i>	0.3 ACH
<i>Envelope U-Values</i>	Exterior Walls: 0.25-0.30 W/m ² K; Base Wall: 1.14 W/m ² K; Roof: 0.18-0.24 W/m ² K; Base: 0.6 W/m ² K; Windows: 1.1-2.9 W/m ² K
<i>Ground Temperature</i>	18°C
Heating (5.1.9)	
<i>Temperature Setpoints (Occupied/Unoccupied)</i>	21°C/19°C offices, 20°C/18°C in all other spaces
<i>Heating Schedules</i>	Offices: 7:00-17:00; 1 st Floor: 7:00-14:00; Gym: 7:00-14:00; Wardrobes: On at all times; Annex: 7:00-16:00
Lighting (5.1.5)	
<i>Lighting Density</i>	13.4 W/m ²
<i>Lighting Installed Capacities</i>	Bomb Shelter: 9,500 W; Offices: 11,100 W; 1 st Floor: 23,000 W; Wardrobes: 1,000 W; Gym: 8,000 W; Annex: 7,000 W
<i>Lighting Schedules</i>	Offices: 7:30-17:00; 1 st Floor: 8:30-13:30/14:00; Gym: 8:30 -13:30/14:00; Annex: 8:00-16:00
Plug Loads (5.1.6)	
<i>Plug Load Density</i>	8 W/m ²
<i>Plug Load Installed Capacities</i>	Offices: 15 kW; 1 st Floor: 15 kW; Annex: 5 kW
<i>Plug Load Schedules</i>	Offices: 7:30-17:00; 1 st Floor: 8:30-13:30/14:00; Gym: 8:30 -13:30/14:00; Annex: 8:00-16:00
Domestic Hot Water (DHW) (5.1.7)	
<i>DHW Density</i>	1.1 W/m ²
<i>DHW Installed Capacity</i>	5 kW in Gymnasium
<i>DHW Schedule</i>	See Gymnasium Occupancy Schedule

Table 5-27: Summary of uncertain data from collected information on the energy consumption in the Steindal School in 2006.

Not all of the uncertainties that were identified in sections 5.1.1 through 5.1.10 were analyzed during calibration (Chapter 7) or with simple estimates (Chapter 6). It would have been both time consuming and expensive to address all of the uncertain model inputs. Instead, the modeler applied her observations of the degree of uncertainty associated with each input and the input's anticipated influence on the EnergyPlus model calibration to determine the inputs to be investigated in Chapters 6 and 7.

No detailed measurements were used in this investigation. Rather, uncertain inputs were identified during data collection and investigated with both simple estimates and during calibration.

Several important points must be emphasized to conclude this chapter on data collection:

- **Uncertainties exist.** Because buildings never quite match the as-built specifications or expected operating conditions, and are subject to degradation over time, even inputs collected from the most reliable of resources may have uncertainties associated with their values. What is most important is that the modeler identifies that these uncertainties exist and address them as necessary.
- **Modeler bias exists.** Although a number of inputs were identified as having uncertain values, the modeler chose only to investigate between 10 and 20 of them with simple estimates and during calibration. The choice of which inputs to investigate was made by the modeler and consequently, was bias by the modeler's knowledge and experience.

Both of these issues were focal points of subsequent work on simple estimates, calibration, and building retrofitting (Chapters 6-8).

At this point all of the collected data was entered into the EnergyPlus simulation software. The order of inputs was the same as the order in which the collected data was presented in this chapter: geometry, materials, internal gains, and heating and ventilation.

6 Simple Estimates and Input Verification

Several simple analyses were performed to estimate the values of uncertain inputs before moving forward with the calibration of the EnergyPlus model. The first of these analyses applied a steady-state energy balance to estimate the heating, fan, lighting, plug load, and domestic hot water consumptions in the building. The second analysis utilized the available hourly data to qualitatively estimate the level of infiltration in the Steindal School. The annual energy balance did not include the influence of thermal mass.

All references to energy consumption in this chapter refer to the site energy consumed at the Steindal School in 2006; all energy consumed in 2006 was electricity.

6.1 Annual Steady-State Energy Consumption

The annual steady-state energy balance was intended as a “back of the envelope” calculation of the annual energy consumption in the Steindal School. This calculation required that the energies into and out of the school be balanced. These energies were attributed to solar radiation, occupants, lighting, plug loads, domestic hot water, fans, envelope transmission losses, ventilation heating, and space heating. The absence of a cooling system meant that only a heat energy balance was performed on the building. Additionally, because of the cool climate in Trondheim (the average outdoor temperature in 2006 was approximately 6.5°C), heating was required on all but a few of the 365 days in the year. Figure 6-1 depicts the balance of heat gains (orange and red arrows) and losses (blue arrow) to and from the building (grey box). All data were taken from Chapter 5, unless otherwise noted.

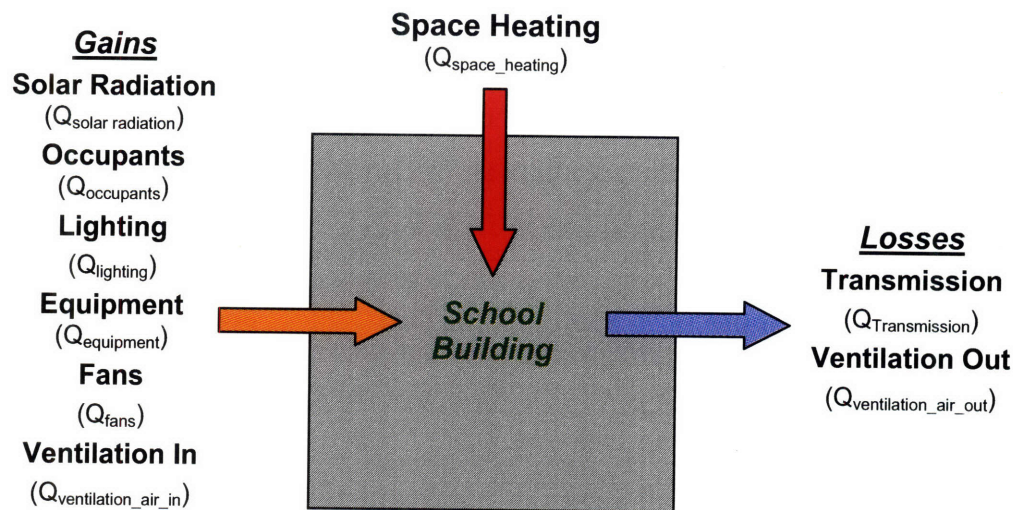


Figure 6-1: Energy balance in the Steindal School. This balance accounts for all heat flows into and out of the interior of the building.

The heat gains from domestic hot water (DHW) were omitted from this heat balance because all potential heating from the DHW was removed from the building via drains. However, the electric energy required to heat the DHW was included in the calculation of the total annual electricity consumption in the building.

6.1.1 Temperature Independent Loads

The heat gains from solar radiation, occupants, lighting, equipment, and ventilation fans were all included in the annual heat balance. All of these loads were calculated according to the load densities and schedules of operation from Chapter 5, except the solar heat gains, which were approximated with the solar heat gain factor (SHGF) method. The domestic hot water electricity consumption was also calculated according to the load densities and schedules of operation from Chapter 5.

6.1.1.1 Solar Gains

The annual solar gains were approximated with the solar heat gain factor (SHGF) method. This method provided values for the heat gained through windows at various latitudes and orientations for a number of hours throughout the 21st day of each month. The annual heat gain was estimated by multiplying the amount of heat gained on the 21st day of each month by

the number of days in that month, and summing the solar heat gain from each of the twelve calendar months to get the yearly total.

Daily SHGF data for the 21st day of each month in buildings at a latitude of 64°N (Trondheim is located at 63.5°N) were taken from the 1997 ASHRAE Handbook of Fundamentals [ASHRAE 1997] and are shown in Table 6-1.

Total solar heat gain through windows on the 21 st day of each month	# Days per Month	North [Wh/m ² /day]	East [Wh/m ² /day]	South [Wh/m ² /day]	West [Wh/m ² /day]
January	31	32	79	890	3
February	28	183	789	3533	177
March	31	429	1981	4915	943
April	30	827	3202	4814	2107
May	31	1558	4126	4467	3417
June	30	2057	4521	4284	4275
July	31	1628	4275	6089	4521
August	31	896	3417	6291	4126
September	30	448	2107	4612	3202
October	31	196	943	3325	1981
November	30	32	177	883	789
December	31	0	3	69	79

Table 6-1: Solar heat gained through a clear, single paned, windows on the 21st day of each month at 64°N latitude (Wh/m²/day) [ASHRAE 1997].

The SHGF data provided by the ASHRAE Handbook of Fundamentals were typical values and did not account for variations in the conditions at the particular building site, i.e. cloud cover. Additionally, these values were for single paned windows with a solar heat gain coefficient (SHGC) of 0.87. Thus, the solar heat gains through the windows on each façade were calculated by multiplying the values in Table 6-1 by the appropriate solar coefficient (SC) and window area (A_{window}) (Table 6-2). The SC is equal to the SHGC of the window of interest ($\text{SHGC}_{\text{window}, i}$) divided by the 0.87 SHGC of the single paned reference window ($\text{SHGC}_{\text{reference}}$).

Window conditions on each facade	Facade			
	North	East	South	West
SC	0.74	0.31	0.31	0.74
Window Area [m ²]	391.4	12.5	232	11.6

Table 6-2: Properties for calculating the solar heat gain through the windows in the Steindal school. The solar coefficient and window area for all four building facades were taken from Chapter 5.

The total annual heat gain through the windows on each façade was calculated by multiplying the solar heat gain on the 21st day of each month (given in Table 6-1) by the number of days in each month, summing these products to get the total annual solar heat gain, and multiplying by the SC and window area. The resulting annual heat gains through the windows on each façade in the Steindal School are shown in Table 6-3.

Annual solar heat gain through windows	North [kWh/year]	East [kWh/year]	South [kWh/year]	West [kWh/year]	Whole Building [kWh/year]
Solar Heat Gain	73,250	3,000	96,700	6,700	179,700

Table 6-3: Annual solar heat gain per façade in the Steindal School. Calculated according to the solar heat gain factor (SHGF) method.

The total annual solar heat gain was equal to 179,700 kWh/year.

6.1.1.2 Occupants

The occupants in the Steindal School contributed 100% heat to the building at a rate of 100 W/hr/person. In the absence of a mechanical cooling system in the Steindal School, no distinction was made between the latent and sensible heat gain from people.

Collected data indicated a typical occupancy of 340 people; 300 students and 40 teachers and administrators. The school was occupied by the students for 39.5 weeks per year, 5 days per week, and 6 hours per day, for a total of 1,185 hours per year. The teachers and administrators occupied the school for 46.5 weeks per year, 5 days per week, and 8 hours per day, for a total of 1,860 hours per year. The average number of occupied hours per year was the weighted average of the number of occupied hours for students and teachers and was equal to:

$(300 \cdot 1,185 + 40 \cdot 1,860) / 340 \sim 1,260$ hours. The heat gain from occupants was then calculated as in Equation 6-1.

$$Q_{occupants} = t * \frac{N_{people} * Q_{person}}{1,000} = 1,260 * \frac{340 * 100}{1,000} = 42,800 \frac{kWh}{year} \quad (6-1)$$

$Q_{occupants}$ Annual heat gain from occupants [kWh/year]; 1,000 converts from Wh to kWh

t Number of occupied hours per year [hr]

N_{people} Number of occupants [people]

Q_{person} Heat gain per occupant [W/person]

The total annual heat gain from occupants was equal to 42,800 kWh/year.

6.1.1.3 Lighting

The lighting density in the Steindal School was equal to 13.4 W/m² and was scheduled to operate for 1,260 hours per year as per occupancy schedules. The lighting contributed 100% heat gain to the building, meaning that all electricity consumed by the lights entered the building as heat. The conditioned floor area of the building was equal to 4,400m². The total annual lighting load was then calculated in Equation 6-2.

$$E_{lights} = Q_{lights} = t * \frac{\rho_{lights} * A_{conditioned}}{1,000} = 1,260 * \frac{13.4 * 4,400}{1,000} = 74,300 \frac{kWh}{year} \quad (6-2)$$

E_{lights} Annual electricity consumed by lighting [kWh/year]; 1,000 converts from Wh to kWh

Q_{lights} Annual heat gain from lights [kWh/year]

t Number of operating hours per year [hr]

ρ_{lights} Installed lighting density [W/m²]

$A_{conditioned}$ Conditioned floor area [m²]

The total annual heat gain from lighting was equal to the total annual electricity consumed by lighting, and was equal to 74,300 kWh/year.

6.1.1.4 Plug Loads

The installed plug load density in the Steindal School was equal to 8 W/m². The number of operating hours in 2006 was equal to 1,260 hours, as per occupancy schedules. The plug loads contributed 100% heat gain to the building. The conditioned floor area of the building was equal to 4,400 m² as per collected data. The total annual plug load energy consumption was subsequently calculated as in Equation 6-3.

$$E_{plugloads} = Q_{plugloads} = t * \frac{\rho_{plugloads} * A_{conditioned}}{1,000} = 1,260 * \frac{8 * 4,400}{1,000} = 44,400 \frac{kWh}{year} \quad (6-3)$$

$E_{plugloads}$ Annual electricity consumed by plug loads [kWh/year]; 1,000 converts from Wh to kWh

$Q_{plugloads}$ Annual heat gain from plug loads [kWh/year]

t Number of operating hours per year [hr]

$\rho_{plugloads}$ Installed plug load density [W/m²]

$A_{conditioned}$ Conditioned floor area [m²]

The total annual heat gain from plug loads was equal to the total annual electricity consumed by the plug loads, and was equal to 44,400 kWh/year.

6.1.1.5 Domestic Hot Water (DHW) Loads

The majority of the annual DHW energy was consumed during showers in the gymnasium locker rooms. The total DHW load in the Steindal School was equal to 1.1 W/m² and was run for 1,185 hours in 2006, as per occupancy schedules in the Gym. The domestic hot water contributed no heat gain to the building; all heating energy from domestic hot water was removed from the building when the water drained from showers and sinks. The conditioned floor area was equal to 4,400 m². The energy for DHW was then calculated as in Equation 6-4.

$$E_{DHW} = t * \frac{\rho_{DHW} * A_{conditioned}}{1,000} = 1,185 * \frac{1.1 * 4,400}{1,000} = 5,700 \frac{kWh}{year} \quad (6-4)$$

E_{DHW} Annual electricity consumed by DHW [kWh/year]; 1,000 converts from Wh to kWh

t Number of operating hours per year [hr]

ρ_{DHW} Installed DHW density [W/m²]

A_{DHW} Conditioned floor area [m²]

The total annual electricity consumed by domestic hot water was equal to 5,700 kWh/year.

6.1.1.6 Ventilation Fan Loads

The fan energy required in the Steindal School was equal to the sum of the fan energies consumed in the Main and Annex ventilation systems. In the interest of simplicity, this was calculated as the total installed fan capacity of 41 kW (38 kW in the Main building and 3 kW in the Annex) multiplied by the annual number of operating hours in the Main ventilation system; the Main ventilation fans operated for 2,330 hours per year.

The supply and exhaust fans were located in the ventilation air stream, meaning that all electrical energy that was consumed by the fans was transferred to the ventilation air as heat. In the case of the supply fan, this heat was then added to the building, as indicated in the heat balance in Figure 6-1. However, the heat contributed by the exhaust fans was removed from the building and did not contribute any heat gain to the interior of the space. Therefore, because only the supply fans contributed heating energy to the building, only half of the total annual electricity consumed by the ventilation fans was added to the building as heat, as per Equation 6-6. The calculation of the total annual fan energy was performed as in Equation 6-5.

$$E_{fans} = P_{fans} * t = 41 * 2,330 = 95,500 \frac{kWh}{year} \quad (6-5)$$

$$Q_{fans} = \frac{E_{fans}}{2} = \frac{95,500}{2} = 47,750 \frac{kWh}{year} \quad (6-6)$$

E_{fans} Annual energy consumed by ventilation fans [kWh/year]

Q_{fans} Annual heat gain from ventilation fans [kWh/year]

t Number of operating hours per year [hr]

P_{fans} Installed fan power [kW]

The total annual heat gain from the ventilation fans was equal 47,750 kWh/year. This was half of the 95,500 kWh/year of electricity consumed by the fans annually.

6.1.1.7 Total Heat Gains

The total heat gain from temperature independent loads was equal to the sum of the heat gains from solar radiation, occupants, lights, plug loads, and ventilation fans. The DHW contributed no heat gain to the building.

$$Q_{gains} = Q_{solar} + Q_{occupants} + Q_{lights} + Q_{plugloads} + Q_{fans} =$$

$$179,700 + 42,800 + 74,300 + 44,400 + 47,750 = 388,950 \frac{kWh}{year} \quad (6-7)$$

The total annual heat gain in the Steindal School was equal to 388,950 kWh/year.

6.1.2 Transmission and Envelope Losses

Transmission and envelope losses included all energy that flowed from the interior of the building to the outdoors or ground via conduction, convection, radiation, or infiltration.

Conductive, convective, and radiative heat transfer occurred across the walls, roof, floor, and windows of the building; infiltration occurred around windows, doors, and other exterior openings.

As mentioned previously, all of the energy transferred via transmission was assumed to flow from the building's interior to exterior. This assumption was based on the observation that the average daily outdoor temperature was less than the building's heating setpoint for all but a handful of the 365 days in 2006. Subsequently, the annual transmission heat loss from each building surface was calculated as $Q = UA\Delta T$, where U was the U-value of the building surface, A was the area of the building surface, and ΔT was the average annual temperature difference

between the indoor temperature setpoint and the average annual outdoor temperature at the Steindal School.

The average outdoor temperature ($T_{out,ave}$) at the Steindal School was taken from the 2006 Trondheim weather data and was equal to 6.5°C.

The average indoor temperature ($T_{in,ave}$) was calculated (Equation 6-8) from the setpoints and schedules set forth during data collection in Chapter 6, and was equal to the weighted sum of the occupied and unoccupied temperature setpoints (Table 6-4).

Building Temperature Setpoint	Temperature Setpoint [°C]	# Hours at Setpoint per Year [hr]
Occupied Temperature	20	2,600
Setback Temperature	18	6,160

Table 6-4: Occupied and unoccupied temperature setpoints and hours of operation in the Steindal School in 2006.

$$T_{in,ave} = \left(\frac{T_{occupied} * t_{occupied}}{8,760} + \frac{T_{unoccupied} * t_{unoccupied}}{8,760} \right) = \left(\frac{20 * 2,600}{8,760} + \frac{18 * 6,160}{8,760} \right) = 18.6^{\circ}C \quad (6-8)$$

$T_{in,ave}$ Average annual indoor temperature [°C]

$T_{occupied}$ Occupied temperature setpoint [°C]

$T_{unoccupied}$ Unoccupied temperature setpoint [°C]

$t_{occupied}$ Number of occupied hours per year [hr]

$t_{unoccupied}$ Number of unoccupied hours per year [hr]

The exterior temperature was at or below this value for more than 8,000 of the 8,760 hours in 2006 and, when the outdoor temperature exceeded 18.6°C, it was only 1-2°C higher. Thus, it was considered reasonable to estimate the total number of hours in which heat was leaving the building as all 8,760 hours in the year. Additionally, this allowed for the ΔT for calculating the transmission losses to be approximated as the difference between the average indoor and outdoor temperature, as shown in Equation 6-9.

$$\Delta T_{ave} = T_{in,ave} - T_{out,ave} = 18.6 - 6.5 = 12.1^{\circ}C \quad (6-9)$$

ΔT_{ave} Average annual indoor-outdoor temperature difference [°C]

$T_{out,ave}$ Average annual outdoor temperature [°C]

The ground floor and ground walls of the building abutted the ground rather than the outdoor air, and were subject to different exterior conditions than the walls and roofs that were exposed to the outdoor air. The ground heat transfer calculation is discussed in section 6.1.2.2.

6.1.2.1 Exterior Walls, Roofs, and Windows

The transmission through the exterior walls, roofs, and windows was calculated according to the steady-state $Q = UA\Delta T$ relationship. The U-values and area for the walls, roof, and windows were taken from collected data (Chapter 6); ΔT was equal to 12.1°C, as calculated in Equation 6-9.

In the interest of simplicity, the following assumptions were made:

- The U-value of the Annex and South roof of the Main building was equal to 0.18 W/m²K and was representative of the entire roof of the building.
- The U-value of the windows was weighted according to the window area and U-value corresponding to each of the three window types in the building.
- The U-value of the North and South exterior walls in the Main building was equal to 0.30 W/m²K and was representative of all exterior walls in the building.

The U-values and areas of the walls, roof, and windows that were used in the simple annual calculation are summarized in Table 6-5.

	U-Value [W/m ² K]	Area (A) [m ²]
Walls	0.30	1,695
Roof	0.18	2,784
Windows	2.20	689

Table 6-5: Properties for calculating the steady-state heat loss via transmission through exterior walls, roofs, and windows. The U-value for the windows was the area-weighted average of the three difference window types in the building.

The annual heat loss from each of the exterior building surfaces was calculated in Equation 6-10 through Equation 6-12, where 8,760 was the number of hours that heat loss occurred through the exterior walls, roof, and windows during 2006.

$$Q_{wall} = t * \frac{U_{wall} * A_{wall} * \Delta T_{ave}}{1,000} = 8,760 * \frac{0.30 * 1,695 * 12.1}{1,000} = 53,900 \frac{kWh}{year} \quad (6-10)$$

Q_{wall}	Annual heat loss from exterior walls [kWh/year]; 1,000 converts from Wh to kWh
t	Number of active hours per year [hr]
U_{wall}	U-value of exterior walls [W/m ² °C]
A_{wall}	Total exterior wall area [m ²]
ΔT_{ave}	Average annual indoor-outdoor temperature difference [°C]

$$Q_{roof} = t * \frac{U_{roof} * A_{roof} * \Delta T_{ave}}{1,000} = 8,760 * \frac{0.18 * 2,784 * 12.1}{1,000} = 53,100 \frac{kWh}{year} \quad (6-11)$$

Q_{roof}	Annual heat loss from roof [kWh/year]; 1,000 converts from Wh to kWh
t	Number of active hours per year [hr]
U_{roof}	U-value of roof [W/m ² °C]
A_{roof}	Total roof area [m ²]
ΔT_{ave}	Average annual indoor-outdoor temperature difference [°C]

$$Q_{window} = t * \frac{U_{window} * A_{window} * \Delta T_{ave}}{1,000} = 8,760 * \frac{2.20 * 689 * 12.1}{1,000} = 160,700 \frac{kWh}{year} \quad (6-12)$$

Q_{wall}	Annual heat loss from windows [kWh/year]; 1,000 converts from Wh to kWh
t	Number of active hours per year [hr]
U_{window}	U-value of windows [W/m ² °C]
A_{window}	Total window area [m ²]
ΔT_{ave}	Average annual indoor-outdoor temperature difference [°C]

6.1.2.2 Ground Walls and Floor

The heat transfer between the ground and the building was two-dimensional, making the one-dimensional $Q = UA\Delta T$ approximation inaccurate. The heat transfer was two-dimensional rather than three-dimensional because the ground slab and walls were both much longer than they were wide or tall. Therefore, edge-effects were neglected. Consequently, it was not adequate to simply take the difference between the average annual ground temperature and the indoor temperature and multiply by the U-value and area of the ground walls and floors; this would have resulted in a severe over-estimate of the heat lost via conduction to the ground [EPlus 2007c]. Instead, Chapter 32 of the 2005 ASHRAE Handbook of Fundamentals [ASHRAE 2005] was consulted to identify a procedure for calculating the ground heat loss from slab floors and basements that accounted for the soil type, average ground temperature, and orientation of the ground walls and floors in the building. This calculation was involved and consisted of a number of equations. Thus, in the interest of keeping the explanation of the annual energy calculation concise, the calculation of heat loss from the ground that was made according to the 2005 ASHRAE Handbook of Fundamentals was moved to Appendix C. However, the calculated value of the ground heat loss from the Steindal School is shown in Equation 6-13.

$$Q_{ground} = 68,100 \frac{kWh}{year} \quad (6-13)$$

According to this approximation the transmission losses through the ground were greater than the walls or roof of the building. The very low U-value of the roof and the fact that the ground floor and wall area was almost twice the exterior wall area made the observed relationship between the ground, wall, and roof heat loss believable.

Recall that the EnergyPlus simulation software calculates ground heat transfer as a one-dimensional problem – all two and three dimensional heat transfer effects are neglected. Additionally, recall that EnergyPlus defines the ground temperature as the temperature at the interface between the building and the ground. This meant that under steady-state heat transfer conditions, the ground heat transfer in EnergyPlus is a simple $Q = UA\Delta T$ calculation.

During data collection (Chapter 5) the interface temperature was taken to be equal to the EnergyPlus default value of 18°C. However, this value appeared much too high for the conditions at the Steindal School, and so, a simple estimate was performed to better approximate the ground interface temperature of the EnergyPlus building model in Chapter 7. In this estimate the $Q = 68,100$ kWh/year of heat loss that was calculated according to the ASHRAE Handbook of Fundamentals was equated to a simple $Q = UA\Delta T$ relationship for the ground walls and floors. This resulted in an approximate ΔT from the interior of the building to the exterior surface of the ground walls and floor, the calculation of which is shown in Equation 6-14. The U-values and areas (A) that were used in this calculation are shown in Table 6-6.

	U-Value [W/m ² K]	Area (A) [m ²]
Floor	0.60	1,932
Ground Wall	1.14	365
Floor	0.60	493

Table 6-6: Material properties for calculating the heat loss via transmission through ground walls and floors.

$$\Delta T_{ground} = \frac{Q_{ground} \cdot \text{heat loss, ASHRAE}}{8,760 * \sum_{i=1}^{\#surfaces} U_i A_i} 1,000 = \frac{68,100}{8,760 * (0.60 * 1,932 + 1.14 * 365 + 0.60 * 493)} * 1,000 = 4.2^\circ C \quad (6-14)$$

- Q_{ground} Annual heat loss from ground floor and walls [kWh/year]; 1,000 converts from Wh to kWh
 t Number of active hours per year [hr]
 U_i U-value of surface i, in contact with the ground [W/m²°C]
 A_i Area of surface I, in contact with the ground [m²]

Thus, under steady-state conditions, and at an average annual indoor temperature of 18.6°C, the exterior surface temperature of the ground wall and ground floor was estimated to be 18.6°C - 4.2°C = 14.4°C. This approximate interface temperature was considered during calibration in Chapter 7.

6.1.2.3 Infiltration

The cool climate in Trondheim created a demand for heating energy to warm the incoming infiltration air to the indoor temperature setpoint. The amount of heating required depended on the rate of infiltration entering the building, the density of the outdoor air, the specific heat of the outdoor air, and the temperature differential between the indoor and outdoor air. The rate of infiltration in the Steindal School was approximately 0.3 air changes per hour (ACH), or 1.53 m³/sec, and was defined according to typical infiltration rates from the 1987 release of NS3031 [NS3031 1987] (section 5.1.3.3 of Chapter 5). The density of air was taken to be 1.2 kg/m³, the specific heat of air was taken to be 1,000 J/kgK, and the annual average temperature difference was equal to 12.1°C (see Equation 6-9). The heating loss via infiltration was then calculated as in Equation 6-15, where 8,760 was the number of hours per year that infiltration occurred.

$$Q_{infiltration} = \frac{t * (\rho_{air} C_{p_{air}} \dot{V}_{infiltration}) (\Delta T_{ave})}{1000} = \frac{8,760 * 1.2 * 1,000 * 1.53 * 12.1}{1000} = 194,600 \frac{kWh}{year} \quad (6-15)$$

$Q_{infiltration}$	Annual heat loss due to infiltration [kWh/year]; 1,000 converts from Wh to kWh
t	Number of active hours per year [hr]
ρ_{air}	Density of air [kg/m ³]
$C_{p_{air}}$	Specific heat of air [J/kgK]
$\dot{V}_{infiltration}$	Volumetric Air Flow Rate [m ³ /sec]
ΔT_{ave}	Average annual indoor-outdoor temperature difference [°C]

6.1.2.4 Total Transmission Heat Loss

The total transmission heat loss was equal to the sum of the heat loss from walls, roofs, windows, floors, and infiltration in the Steindal School.

$$\begin{aligned}
Q_{\text{transmission}} &= Q_{\text{walls}} + Q_{\text{roof}} + Q_{\text{windows}} + Q_{\text{floor}} + Q_{\text{infiltration}} = \\
53,900 + 53,100 + 160,700 + 68,100 + 194,600 &= 530,400 \frac{\text{kWh}}{\text{year}}
\end{aligned}
\tag{6-16}$$

$Q_{\text{transmission}}$ = Total heat loss due to transmission from the building [kWh/year]

According to this simple estimate, more than 60% of the total transmission losses that occurred in the Steindal School were via infiltration and windows. These two means of heat loss far outweighed the transmission from walls, roofs, and floors in the building. The high heat loss via windows was attributed to the large area of poorly insulating windows that were present on the North façade. The apparent influence of infiltration on the overall heat balance in the building brought into question the 0.3 ACH that were assigned in the Steindal School according to the 1987 release of NS3031 [NS3031 1987] (Chapter 5). Therefore, a simple analysis was performed in section 6.2 to qualitatively verify that this air change rate was reasonable for the school.

The total transmission heat loss was equal to 530,400 kWh/year.

6.1.3 Ventilation Heating Energy

The ventilation heating energy was the energy required to heat the ventilation air to the supply setpoint of 18°C. In this calculation the ventilation supply temperature of 18°C was taken to be equivalent to the indoor temperature setpoint of 18.6°C; the 0.6°C difference was neglected. The ventilation system in the Steindal School was balanced and included heat recovery. No distinction was made between the Main and Annex ventilation systems in this simple estimate, the two were treated as a single system.

Data collected in Chapter 6 indicated that the heat recovery effectiveness in the Steindal School was approximately 50%. The ventilation system ran at a flow rate of 13 m³/sec for 2,330 hours each year and the average outdoor temperature in Trondheim in 2006 was equal to 6.5°C. The annual heating energy required to bring the incoming ventilation air up to the 18.6°C supply temperature was then calculated as in Equation 6-17.

$$E_{ventilation} = Q_{ventilation} = t * \frac{\rho_{air} C_{p air} V_{ventilation} (T_{vent} - T_{out,ave}) * (1 - \eta_{HRU})}{1,000} =$$

$$2,330 * \frac{1.2 * 1,000 * 13 * (18.6 - 6.5) * (1 - 0.5)}{1,000} = 219,900 \frac{kWh}{year} \quad (6-17)$$

$E_{ventilation}$	Annual electricity consumed by ventilation heating [kWh/year]
$Q_{ventilation}$	Annual heating for ventilation [kWh/year]; 1,000 converts from Wh to kWh
t	Number of operating hours per year [hr]
ρ_{air}	Density of air, taken to be 1.2 [kg/m ³]
$C_{p air}$	Specific heat of air, taken to be 1000 [J/kgK]
$V_{ventilation}$	Ventilation volumetric air flow rate [m ³ /sec]
T_{vent}	Supply air temperature [°C]
T_{out}	Average annual outdoor air temperature [°C]
η_{HRU}	Effectiveness of heat recovery system

All of the ventilation heating energy was supplied by electricity; the total ventilation heating energy was equal to 219,900 kWh/year.

6.1.4 Annual Space Heating and Total Annual Heating Energy

The annual space heating energy was equal to the difference between the heat losses and gains as presented in Figure 6-1. This calculation is shown in Equation 6-18.

$$Q_{space_heating} = (Q_{transmission}) - (Q_{gains}) = 530,400 - 388,950 = 141,450 \frac{kWh}{year} \quad (6-18)$$

The total annual heating energy in the building was the sum of the space heating energy ($Q_{space_heating}$) and the ventilation heating energy ($Q_{ventilation_heating}$), calculated in Equation 6-19.

$$Q_{heating} = Q_{space_heating} + Q_{ventilation_heating} = 141,450 + 219,900 = 361,350 \frac{kWh}{year} \quad (6-19)$$

The total annual space heating energy was equal to 141,450 kWh/year; the total annual heating energy was equal to 361,350 kWh/year.

6.1.5 Annual Electricity Demand and Load Profiles

The total annual electricity consumption was equal to the sum of the annual heating, fan, lighting, plug load, and domestic hot water electricity consumptions.

$$E_{Electricity} = E_{heating} + E_{fans} + E_{lighting} + E_{plugloads} + E_{DHW} = 361,350 + 95,500 + 74,300 + 44,400 + 5,700 = 581,250 \frac{kWh}{year} \quad (6-20)$$

The calculated annual electricity consumption in the Steindal School was equal to 581,250 kWh/year; approximately 25% less than the 760,720 kWh/year of measured electricity consumption in the Steindal School in 2006. The magnitude of this difference was likely caused by the oversimplification of the building model; the inclusion of thermal mass and a more accurate portrayal of the seasonal, daily, and hourly variations in energy consumption would be expected to result in a better fit with the measured utility data.

The load distribution from the simple annual estimate was compared to the values for typical Norwegian schools to get a sense of how reasonable the calculated loads were. The annual energy consumption presented in Figure 6-2 was converted from kWh/year to kWh/m²/year by dividing the annual energy consumption by the 4,400 m² of conditioned floor area in the Steindal School.

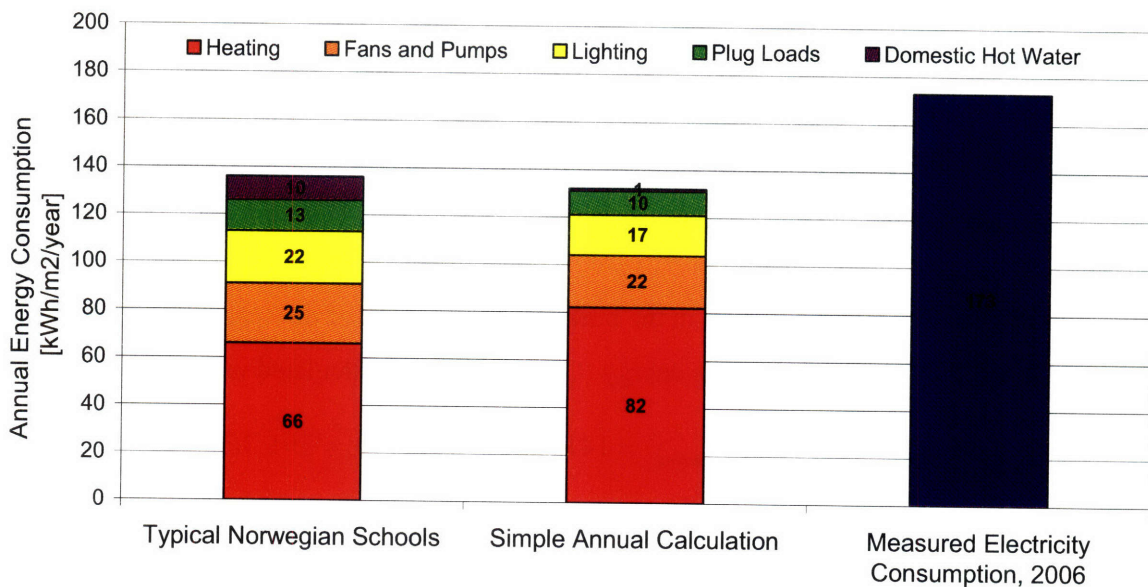


Figure 6-2: Annual energy consumption in typical Norwegian schools and the Steindal School. The results of the annual steady-state calculation and the 2006 measured electricity consumption in the Steindal School are both shown.

The large divergence from the typical domestic hot water (DHW) consumption values in Figure 6-2 suggested that the assumptions about DHW demand that were made in Chapter 5 were incorrect and that this input needed to be revisited. This was done, but only after the initial EnergyPlus model calibration had been performed. The fan, lighting, and plug load energy

consumptions were all within 3-5 kWh/m²/year of the typical values (Figure 6-2). The under approximation of the lighting and plug loads was somewhat surprising given that the installed densities of these loads were loosely based on typical values (Chapter 5). Consequently, the observed under approximation was attributed to the shorter than typical schedules of operation that were enacted by the teachers and students in the Steindal School in 2006. In addition, the fan and pump load was not established from typical values (Chapter 5), making the small (3 kWh/year) difference between the calculated and typical fan and pump energies was somewhat unexpected.

The heating energy consumption was not necessarily expected to match the typical heating values for Norwegian schools (1) because the 173 kWh/m²/year of total electricity consumption in the Steindal School in 2006 demanded that one or more of the building loads be in excess of the typical values and (2) because the envelope and heating system characteristics were highly dependent on the building's year of construction, materials, and quality of construction, all characteristics that varied significantly from school to school. The annual steady-state calculation's divergence from the measured electricity consumption in the Steindal School was expected to improve with more accurate means of accounting for solar and heating energies, like those present in the EnergyPlus models that were developed during calibration (Chapter 7).

6.2 Infiltration Rates: Qualitative Assessment

During data collection (Chapter 5) the infiltration rate in the Steindal School was assigned according to typical values from the 1987 release of Norwegian Standard 3031 [NS3031 1987] (Table 5-9 in Chapter 5), and was equal to 0.3 air changes per hour (ACH).

Site visits verified that the building did not feel particularly “drafty”, but, this was not enough to accept the typical values from NS3031 as being representative of the real conditions in the Steindal School. Thus, a qualitative assessment was made with hourly temperature, wind, and energy consumption data from the school. The goal of this qualitative estimate was to identify any correlation between infiltration levels and changes in heating energy in the Steindal School.

At the Steindal School, the low outdoor temperatures demanded that heating energy be supplied to compensate for envelope transmission losses via the walls, roof, floors, and

infiltration. Therefore, if the infiltration rates in the Steindal School were high, a large amount of heating energy was likely to be demanded, while the opposite was expected at low infiltration rates. Additionally, it was known that wind was the primary driver in causing hour-to-hour variations in the building's infiltration rate. Thus, in order to establish a qualitative estimate of the level of infiltration in the Steindal School an attempt was made to correlate the amount of heating energy demanded in the school with the wind speed at the site; a strong correlation between heating energy and wind speed would suggest a high infiltration rate; a weak correlation would suggest a low infiltration rate. In buildings with high nominal infiltration rates (i.e. 0.5-1.5 ACH) the heat demand's sensitivity to changes in wind speed was expected to be greater; the opposite was expected in buildings with low nominal infiltration rates (<0.5 ACH).

Understanding these principles, an attempt was made to isolate the heating energy for infiltration from the lighting, plug load, domestic hot water, and ventilation loads in the Steindal School. By isolating the heating energy needed to raise the temperature of the infiltration air, changes in heating energy at varying wind speeds could be inspected and the dependence between wind speed and infiltration could be assessed. Fortunately, schedules of operation, detailed in Chapter 5, indicated that the only building load that was available on weekends in the Steindal School was heating. Thus, it was anticipated that the relationship between heating demand and infiltration rate could be assessed with the hourly energy consumption and wind data from weekends when heating was required. However, the heating energy for infiltration first had to be isolated from the envelope transmission losses from walls, roofs, floors, and windows in the Steindal School. Additionally, the building needed to be undergoing steady-state heat transfer, meaning that the building's thermal mass needed to be inactive. Consequently, an estimate was made of the magnitude and rate of decay of the heating contribution from thermal mass in the Steindal School.

6.2.1 Thermal Mass

Thermal mass was present on both the interior and exterior of the Steindal School and was composed of brick and concrete. The internal mass was also comprised of wooden chairs, tables, and desks (Table 5-8 in section 5.1.3.3.2). The thermal mass stored heating energy when the building was at its occupied temperature setpoint of 20°C on weekdays and released heating energy when the temperature was setback to 18°C on nights and weekends. The building was

undergoing steady-state heat transfer only when the heating contribution of the thermal mass approached zero. Consequently, a calculation was performed to estimate the rate of decay of the heating contribution from the building's thermal mass. This calculation applied the 1st term approximation of the series solution for estimating the heat storage in plane walls [Incropera 2001]. This method was chosen over the much simpler thermal capacitance method because the dimensionless Biot number (Bi) was > 0.1 for all walls, ceilings, and floors in the Steindal School (see Table C-3 in Appendix C), making the lumped capacitance method invalid for these building surfaces, and requiring that a more accurate modeling method be used. The calculation of the heating contribution of the thermal mass in the Steindal School is shown in Appendix C. This calculation was conservative; the chosen boundary conditions were expected to cause an overestimate of the stored energy and a slower rate of decay of the energy released from the building's thermal mass. Additionally, the 2°C temperature setback was relatively low compared to the 4°C that is often applied in Norwegian university buildings [Hansen 2007], and consequently, the amount of time required for the thermal mass to reach steady-state was expected to be small.

The result of this calculation was the time variant heating contribution from thermal mass shown in Figure 6-3. The heating energy (y-axis) from the interior thermal mass is given by the yellow triangles, the contribution from external walls, roofs, and floors is given by the aqua circles, and the total heating energy from the interior and exterior thermal mass is given by the pink squares. The dark blue diamonds indicate the hourly electricity consumption in the Steindal School in 2006 for hours on Fridays, Saturdays, and Sundays during which the outdoor temperature was constant (0°C +/-2°C) and the wind speeds were low (< 2 m/s). Assuming that all other variables were fixed - the indoor temperature setpoints were the same for all data points, no mechanical equipment or lighting was turned on, and solar radiation was negligible - differences in the energy demanded from hour to hour were expected to correspond with changes in the heating contribution from the building's thermal mass.

The thermal mass began to release its heating energy when the zone temperatures in the school were setback from 20°C to 18°C at 5 p.m. on Friday afternoon. This is indicated by the "zero" hour on the x-axis in Figure 6-3. Midnight on Friday ("Start of Weekend") and Saturday ("Start of Sunday") are also indicated. The number of hours from the start of temperature setback is indicated along the x-axis. Three heating contributions from thermal mass are shown.

“Internal” refers only to those building surfaces that are located inside of the building and that separate building zones. “External” refers to all walls, roofs, and floors that are located on the exterior surfaces of the building, but that face the interior space. “Total” refers to all walls, ceilings, and floors that are made of thermal massive materials and are located on the inside of the building - this is the total heating contribution from the “Internal” and “External” thermal mass. These surfaces are discussed in detail in section C.2 of Appendix C.

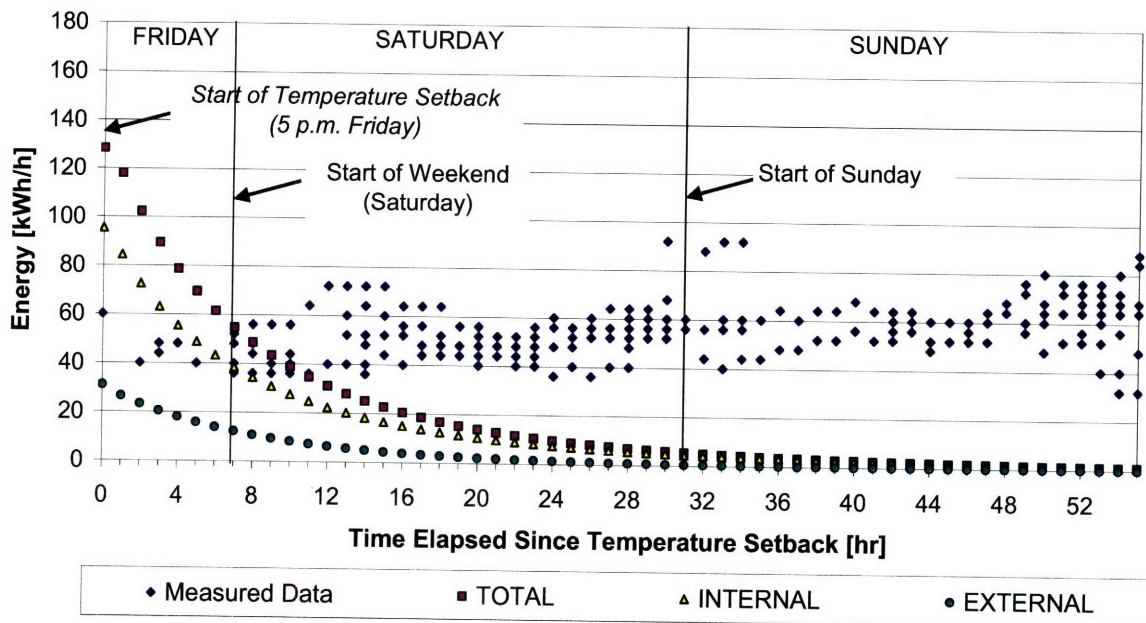


Figure 6-3: Heating contribution from thermal mass on weekends in the Steindal School. The calculated heating contribution from the interior thermal mass in the Steindal School is shown. Also shown is the measured hourly energy consumption for all data points occurring from 5 p.m. (0th hour, x-axis) on Friday through midnight (55th hour, x-axis) on Sunday when $T_{\text{outdoor}} = 0 \pm 2^{\circ}\text{C}$ and windspeed < 2 m/s at the Steindal School in 2006. “Total” refers to all walls, ceilings, and floors that are made of thermal massive materials and are located on the inside of the building. “Internal” refers only to those building surfaces that separate building zones. “External” refers to all walls, roofs, and floors that are located on the exterior surfaces of the building, but that face the interior space. These surfaces are discussed in detail in section C.2 of Chapter Appendix C.

Figure 6-3 shows that the thermal mass contributes a significant amount of heating energy to the building in the first 15-25 hours after the temperature is setback. However, by midnight on Saturday (hour 19 on the x-axis), the heating contribution from the thermal mass is almost negligible. There is no apparent correlation between reduced heating from thermal mass and increased electricity demand (blue diamonds); the band of measured electricity data points is almost linear (with some spread). This is likely due to the fact that the calculated heating contribution from thermal mass was an overestimate; the building probably reaches steady-state

conditions late of Friday night or early on Saturday morning, not during the afternoon on Saturday as is indicated in Figure 6-3. On the basis of this observation, the building was assumed to be undergoing steady-state heat transfer starting on Saturday and lasting through Sunday. Therefore, when making the qualitative estimate of the level of infiltration in the Steindal School, data points from both Saturday and Sunday were examined.

6.2.2 Infiltration Rate

The qualitative estimate of the level of infiltration in the Steindal School attempted to correlate changes in the building's energy demand with variations in the local wind speed. As previously mentioned, this was done on Saturdays and Sundays when heating was expected to be the only active load and the building was undergoing steady-state heat transfer with its environment. Thus, envelope transmission heat losses, including infiltration, were expected to be the only factors influencing the energy consumption in the Steindal School on these days. The transmission heat losses from walls, roofs, floors, and windows were expected to be strongly influenced by the exterior temperature and, to a lesser degree by solar radiation and wind speeds at the site. Thus, in order to isolate the transmission heat losses via walls, roofs, floors, and windows from infiltration the influence of solar radiation and temperature were neutralized in this analysis. Consequently, in selecting the hours to be examined for correlations between heating energy and infiltration, the following constraints were applied:

- The hours from 8 a.m. through 5 p.m. were omitted from this analysis. This was done to eliminate heat gains from solar radiation. The remaining hours were 1 a.m. through 7 a.m. and 6 p.m. through 12 a.m.
- Hours with constant outdoor temperatures (T_{outside}) were examined. Three data sets were examined: one in which $T_{\text{outside}} = 0^{\circ}\text{C} + 1^{\circ}\text{C}$, one in which $T_{\text{outside}} = 5^{\circ}\text{C} + 1^{\circ}\text{C}$, and one in which $T_{\text{outside}} = -5^{\circ}\text{C} + 1^{\circ}\text{C}$.

This left wind speed as the only variable influencing the infiltration rate in the Steindal School, and so, plots of energy consumption vs. wind speed were generated to assess the relationship between the heating energy and infiltration rate. Three plots were generated: one of temperature vs. wind speed for those hours with $T_{\text{outside}} = 0^{\circ}\text{C} + 1^{\circ}\text{C}$ (Figure 6-4), another of temperature vs. wind speed for those hours with $T_{\text{outside}} = 5^{\circ}\text{C} + 1^{\circ}\text{C}$ (Figure 6-5), and a third of temperature vs. wind speed for those hours with $T_{\text{outside}} = -5^{\circ}\text{C} + 1^{\circ}\text{C}$ (Figure 6-6). Figure 6-4,

Figure 6-5, and Figure 6-6 present the energy (y-axis) vs. wind speed (x-axis) values for the night and early morning hours on Saturdays and Sundays at the Steindal School in 2006. The data are divided between the months of January-March (blue diamonds), April-September (orange circles), and October-December (blue triangles). The data points were separated according to the months of the year to distinguish between spring, when the temperatures were expected to be highly variable, and winter, when the temperatures were expected to be consistently low. During the spring the building was expected to be more susceptible to the influence of temperature changes in the hours immediately preceding the data point of interest. Therefore, the spring data points were isolated from the winter ones to emphasize the spring data points in which temperature histories might be expected to influence the building's energy consumption.

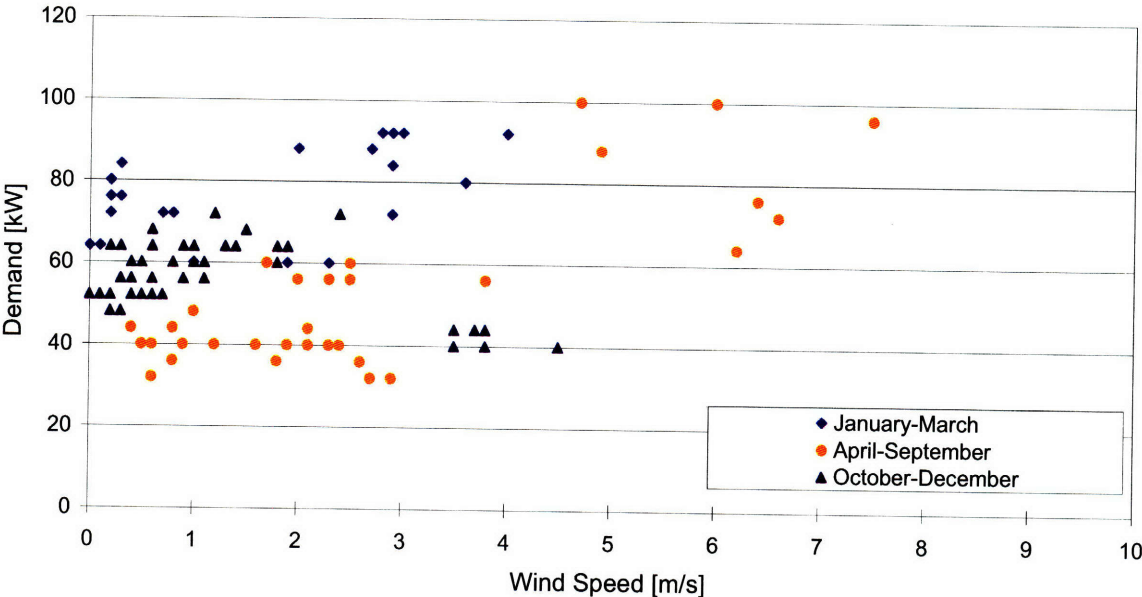


Figure 6-4: Energy demand (kW) versus wind speed (m/s) at outdoor temperatures of 0°C/+1°C during the night time hours on Saturdays and Sundays in the Steindal School in 2006. Wind data was from Kvithamar, Norway.

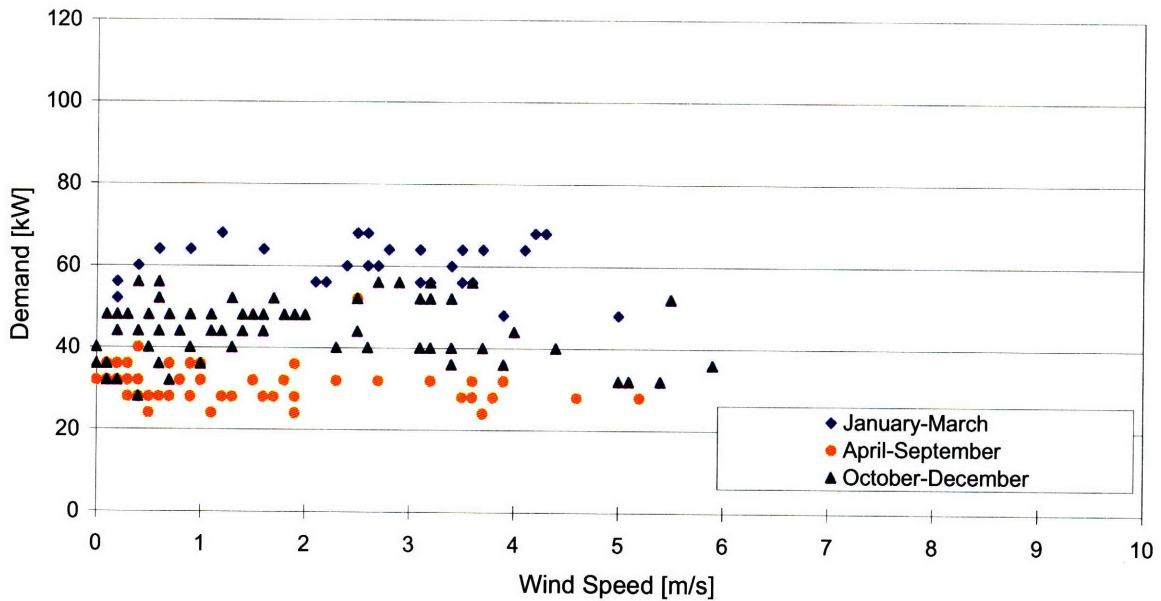


Figure 6-5: Energy demand (kW) versus wind speed (m/s) at outdoor temperatures of 5°C+1°C during the night time hours on Saturdays and Sundays in the Steindal School in 2006. Wind data was from Kvithamar, Norway.

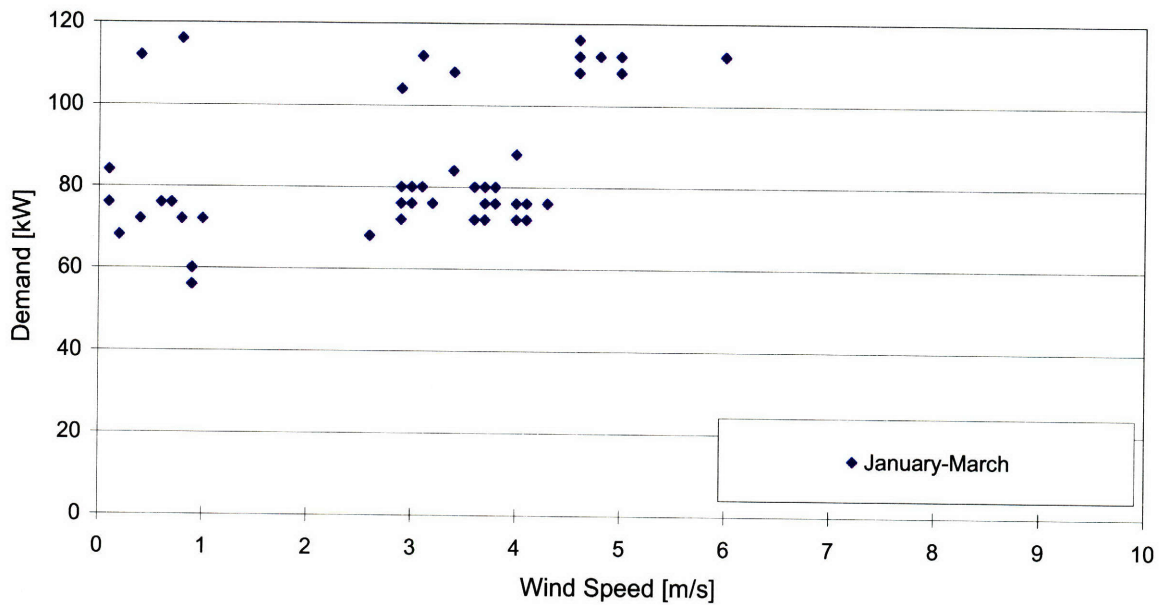


Figure 6-6: Energy demand (kW) versus wind speed (m/s) at outdoor temperatures of -5°C+1°C during the night time hours on Saturdays and Sundays in the Steindal School in 2006. Wind data was from Kvithamar, Norway.

Figure 6-4 indicated a slight rise in energy consumption with increasing wind speed during the mild spring and summer months from April through September (orange circles). However, there was a high degree of variation among the data points at high wind speeds, making it difficult to

detect whether or not any correlation existed. The energy vs. wind speed plots at outdoor temperatures of $5^{\circ}\text{C}/1^{\circ}\text{C}$ (Figure 6-5) showed no relationship between energy consumption and wind speed, while the $-5^{\circ}\text{C}/1^{\circ}\text{C}$ (Figure 6-6) data set contained very few data points and showed a high degree of variation. On the basis of these observations the influence of infiltration in the Steindal School was expected to be small. This analysis used wind data from the Kvithamar weather station. This was the same wind data from data collection (see section 5.1.2 in Chapter 5) that was applied during calibration (Chapter 7), and was used in the absence of measured wind speed data at the building site.

The use of weather station data rather than site data was of consequence because, in areas with highly varied topographies, like those commonly found in Norway, highly localized wind patterns tend to be generated. Thus, the use of weather station data rather than site data created some uncertainty as to the validity of the qualitative infiltration estimate. However, the area around the Steindal School was relatively open, and the only wind block was a sparse group of trees on the North side of the building (see section 5.1.3 of Chapter 5). Thus, the wind conditions at the site were not expected to be strongly influenced by the immediate surroundings. However, in an attempt to increase the confidence in the relevance of the assessment performed above, wind data was taken from several other weather stations near Trondheim and the qualitative infiltration rate estimate was repeated. The locations of these weather stations, with respect to the Steindal School, are shown in Figure 6-7.



Figure 6-7: Map of weather stations near the Steindal School where wind data was collected [Bioforsk 2007],[GoogleMaps 2007].

On the basis of proximity and similar geographies the wind data from Kvithamar, Skjetlein, and Frosta were expected to be the most representative of the conditions at the Steindal School. All of the measurement equipment at these stations was located in open settings with no wind blocks nearby. Figure 6-8 shows the average daily wind speed at each site for the 365 days in 2006. The average daily wind speed (y-axis) is plotted against the day of the year (x-axis) for all five weather stations.

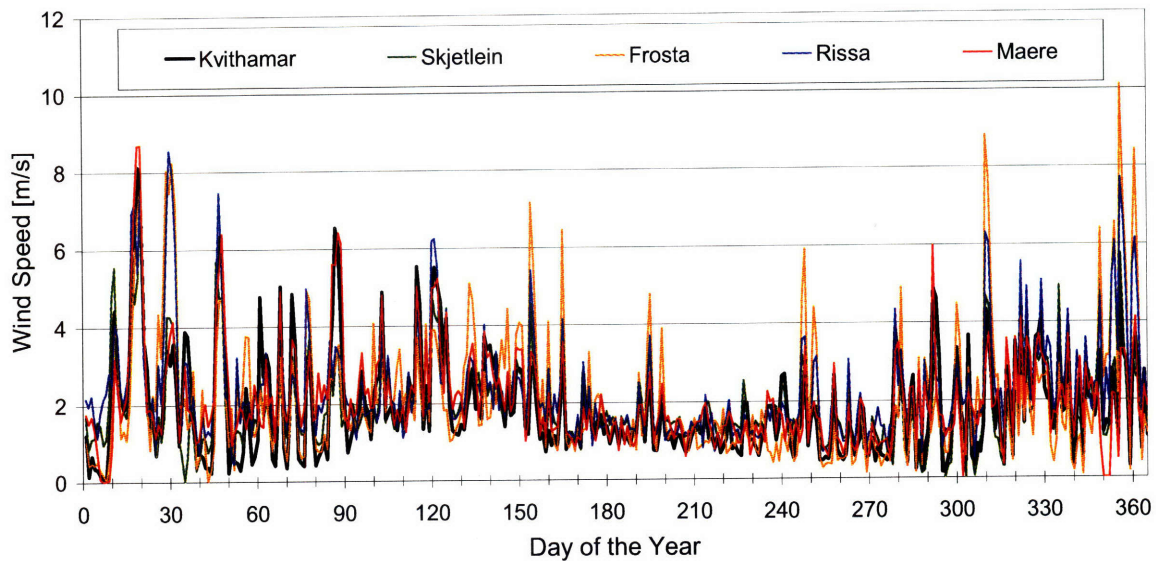


Figure 6-8: Average daily wind speed in 2006 at Kvithamar, Skjetlein, Frosta, Rissa, and Mære weather stations (m/s).

Although the amplitude of the daily wind speed values varies between the five weather stations in Figure 6-8, the general pattern of variation is similar for all five of the sites. This is especially apparent from day 10 through day 25, where there is a close match between both the amplitude and period of the spike in wind speed. The consistency in the pattern of variation between the five locations suggests that similar wind patterns might be expected at the Steindal School. However, in order to compensate for the variations in wind speed amplitude between the five locations graphs of energy consumption vs. wind speed were generated with wind data from Frosta, Rissa, Mære, and Skjetlein rather than Kvithamar (Figure 6-5). However, only data with outdoor temperatures of $0^{\circ}\text{C} \pm 1^{\circ}\text{C}$ were examined; plots with outdoor temperatures of $5^{\circ}\text{C} \pm 1^{\circ}\text{C}$ and $-5^{\circ}\text{C} \pm 1^{\circ}\text{C}$ were not generated. Figure 6-9 shows the temperature vs. wind speed at the Steindal School with weather data from Skjetlein (a), Frosta (b), Mære (c), and Rissa (d).

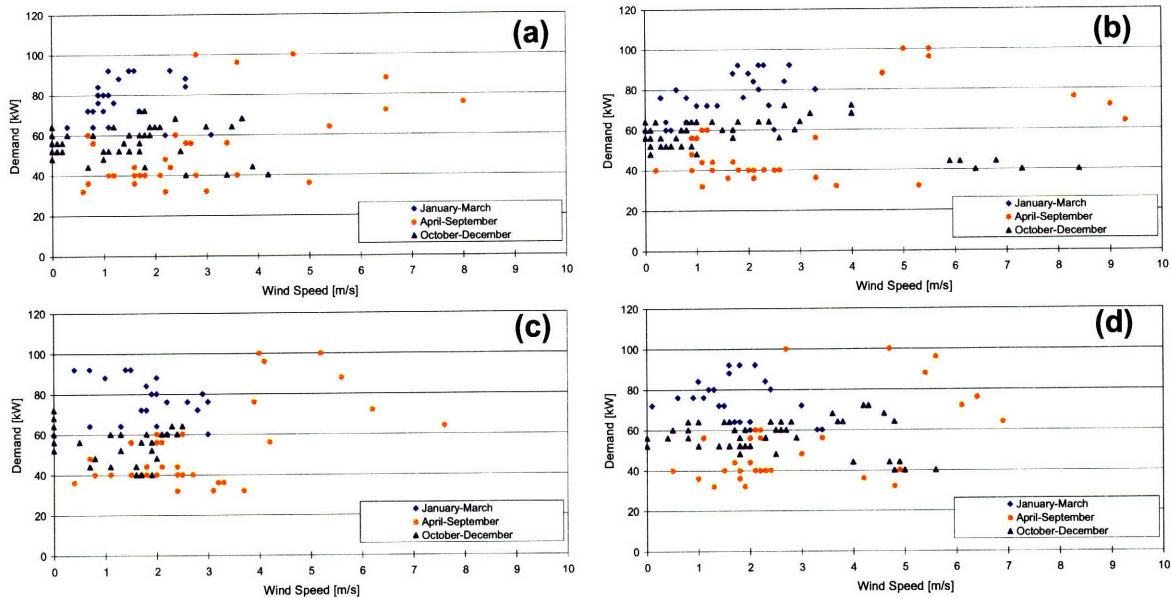


Figure 6-9: Energy demand (kW) versus wind speed (m/s) with 2006 wind data from various weather stations near the Steindal School. All data shown had an outdoor temperature of $0^{\circ}\text{C}+1^{\circ}\text{C}$ and occurred during the night time hours on Saturdays and Sundays in the Steindal School in 2006. (a) Skjetlein; (b) Frosta; (c) Mære; (d) Rissa.

All four of the charts in Figure 6-9 showed a large variation in energy consumption values at high wind speeds. This high degree of variation suggested that no correlation existed between energy consumption and wind speed, and supported the observations that were made with the Kvithamar wind data. Thus, it was suggested that the level of infiltration in the Steindal School was likely to be moderate to low. On the basis of these observations the 0.3 ACH infiltration rate that was applied to the Steindal School in Chapter 5 was considered to be reasonable.

6.2.3 Other Considerations

Several other methods of utilizing the available hourly data were proposed for estimating the heat recovery effectiveness of the Main ventilation system, the UA-value of the building envelope, and the magnitude of the lighting, equipment, domestic hot water, and fan loads. However, there was a high degree of variation amongst the candidate data points that were needed to perform such analyses, which would have made the estimates of these inputs highly uncertain. Thus, no real improvement in the certainty of the input data would have been achieved, and so, in the interest of simplicity and time, these analyses were omitted.

6.3 Lessons Learned

The simple annual estimate allowed the modeler to assess the “believability” of the inputs that were defined in Chapter 5. All of these estimates were simple to make and did not require any complicated computer software to perform. The simple estimate also provided valuable information about ground temperatures, lighting, plug loads, fan energy, and domestic hot water consumption. The 14.4°C estimate of the interface temperature between the ground and the building appeared to be more reasonable than the 18°C default value suggested in EnergyPlus. In addition, the lighting, plug load, and fan energies were within 3-5 kWh/year of the typical values, increasing the confidence in their accuracy. However, the domestic hot water energy consumption was only one tenth of the typical value, making it more uncertain. The large (25%) deviation between the calculated annual electricity consumption and the measured electricity consumption from 2006 highlighted the need for more detailed building energy models to perform further analyses.

The qualitative infiltration rate assessment was useful in verifying the “believability” of the typical infiltration rates that were used in the EnergyPlus model of the Steindal School. The simple annual estimate indicated that more than 40% of the building’s annual transmission losses were via infiltration, making this input important to generating an accurate building model. Thus, the qualitative estimate was performed in an attempt to increase the certainty in the infiltration value. Because wind data was not available from the site itself, data from a number of sites close to the school were examined and consistently showed that the infiltration rates in the school were expected to be moderate to low in 2006. However, these observations are highly dependent on the assumption that the wind conditions at the Steindal School were not strongly influenced by the local topography. Thus, this qualitative estimate provided some assurance in the accuracy of the infiltration rates, but would not be suggested for performing quantitative evaluations of the infiltration rates in the Steindal School.

7 Calibration

Calibration is used to tune building energy models to emulate the actual energy consumption in a building. This is most commonly done by tuning models that have been developed from collected building data (Chapter 5) against measured utility data on a monthly, weekly, daily, or hourly time scale. In the case study performed here, the emphasis was placed on identifying the most reasonable method of calibration in the absence of detailed measurements.

Two methods of performing calibration were investigated here: a manual calibration and a calibration with sensitivity analysis. The manual tuning procedure calibrated in two steps, first accounting for temperature independent loads, and second, for temperature dependent loads. The sensitivity analysis calibration was adapted from work done in RP-1051 [Reddy 2006] and used Latin Hypercube Monte Carlo analysis (LHMC) to aid in reaching calibrated models. In performing these two calibrations the following concerns were addressed:

Manual Calibration

- Ability of a manually tuned model to match measured utility data
- Usefulness of the two-stage manual calibration procedure
- Calibration using hourly energy data

Latin Hypercube Monte Carlo Calibration

- Improvements in the manual calibration using LHMC analysis
- Ability of LHMC to reach calibrated solutions in “semi” or “un” calibrated models
- Validity of using the goodness of fit (GOF) as a criterion for ranking candidate solutions
- Usefulness of freezing strong parameters and performing a fine grid search during LHMC

7.1 Metrics for Calibration

The simple example of two steady-state models (see Chapter 6) developed with data collected from the Steindal School (see Chapter 5) provided a rough estimate of the distribution of annual end-use energy consumption. However, the simple steady-state models failed to

include the influence of thermal mass in the building, which is especially important given the heavy concrete and brick construction used in the Steindal School. A transient model was developed with the EnergyPlus computer software to incorporate these effects. EnergyPlus was chosen on the basis of modeler familiarity and the strength of the simulation engine. This model was significantly more difficult and time consuming to use than the steady-state model, because it required a detailed understanding of the computer software and a much more meticulous definition of inputs.

The transient models developed with the EnergyPlus computer program were simulated on an hourly time scale. The software permits simulation on a more refined scale – down to 10 minute intervals. However, in anticipation of the need for thousands of simulations during LHMC, hourly simulations were run.

A variety of outputs were available for every hour of the simulation including end-use energies, plant and system flow rates, and temperature data.

7.1.1 Graphs

The Microsoft Excel computer software was used to graph the measured utility data and EnergyPlus model outputs on a monthly, weekly, daily, and hourly scale. These graphs included the whole building electricity loads, and in the case of the EnergyPlus output, the end-use loads: heating, cooling, fans and pumps, lighting, plug loads, and hot water. Visualization of the end-use loads allowed the modeler to judge the “believability” of the simulation output, while comparison between the simulated and measured energy consumptions allowed for visual inspection of the fit between the two data sets.

7.1.2 Statistics

Scripts were written with the Matlab software to calculate the statistical fit between measured and simulated electricity data. The statistics applied were the coefficient of variation of the root mean square error (CVRMSE) and the normal mean bias error (NMBE). These were calculated on a monthly, weekly, daily, and hourly basis. Equations for these statistics were given in section 3.2.4 of Chapter 3, but are worth repeating here.

$$NMBE = \frac{\sum y_i - \hat{y}_i}{n \times \bar{y}} \leq 5\% \text{ (monthly) \& } 10\% \text{ (hourly)} \quad (7-1)$$

$$CVRMSE = \sqrt{\frac{\sum (y_i - \hat{y}_i)^2}{n-1}} \times \frac{1}{\bar{y}} \leq 15\% \text{ (monthly) \& } 30\% \text{ (hourly)} \quad (7-2)$$

y_i Measured value at time, i

\hat{y}_i Simulated value at time, i

\bar{y}_i Average of measured values over all i from 0 to n.

n Length of data series: 8760 hours, 365 days, 52 weeks, or 12 months

Equation 7-1 and Equation 7-2 also present the threshold values for considering a simulation to be calibrated. A $NMBE \leq 5\%$ and a $CVRMSE \leq 15\%$ were required on a monthly basis, and a $NMBE \leq 10\%$ and $CVRMSE \leq 30\%$ were required on an hourly basis, as per ASHRAE Guideline 14 [ASHRAE 14 2002] (section 3.2.4 of Chapter 3); weekly and daily threshold values were not provided.

Ideally, it would be advantageous to calibrate the models of the Steindal School against hourly energy consumption data. However, recall from section 5.1.1 in Chapter 5 the “multiple of 4” rule that was observed in the hourly utility data measurements. The energy demand that was reported at each hour of the year was a multiple of 4 kWh. Consequently, differences between the measured and reported energy consumption for a give hour could be up to 2 kWh different due to round-off errors in the reported data. This error was attributed to the type of utility meter that was used in the school.

To understand the influence of the “multiple of 4” rule on the statistical calibration, let us assume the worst case scenario: all of the 8,760 data points in the 2006 utility data were off by 2 kWh. This would result in an error of nearly 2.5 % in the annual energy consumption³, the monthly CVRMSE and NMBE, and the hourly NMBE and CVRMSE. This is particularly significant when trying to reach the monthly threshold calibration values of $CVRMSE = 15\%$ and $NMBE = 5\%$; a 2.5% error would mean a $CVRMSE = 15\% \pm 2.5\%$ and a $NMBE$ of $5\% \pm$

³ $Annual_Error = \frac{\sum_{i=1}^{8760} (Value_expected_i - Value_observed_i)}{Total_Annual_Energy_Consumption} * 100 = \frac{2 * 8760}{760,720} * 100 = 2.5\%$

2.5%. This is less significant when attempting to reach the hourly CVRMSE = 30% and NMBE = 10%. However, these calculations represent the upper limit of expected error, which was extremely unlikely to occur. Thus, the “multiple of 4” rule was neglected during calibration.

In order to rank the numerous candidates resulting from Latin Hypercube Monte Carlo analysis (LHMC) a secondary criterion was used, called the goodness of fit (GOF), defined in Equation 7-3.

$$GOF = \sqrt{\frac{NMBE_{kWh}^2 + NMBE_{kW}^2 + CV_{kWh}^2 + CV_{kW}^2}{4}} \quad (7-3)$$

When the criteria in Equation 7-1 and Equation 7-2 for the CVRMSE and NMBE are satisfied on a monthly basis for both energy consumption (kWh) and peak power demand (kW), the resulting GOF is about 11%. Nevertheless, results from RP-1051 [Reddy 2006] suggest that satisfactory accuracy in the future prediction of energy saving measures is achieved by those candidates that have a GOF of about 6% (the lower the better). As discussed in Chapter 3, with the monthly calibration criteria defined in RP-1051, a $GOF \leq 6\%$ ensured that models were able to accurately predict retrofit energy savings. This is discussed further in Chapter 8.

7.2 Manual Calibration

The manual calibration examined the monthly and weekly CVRMSE and NMBE statistics, in combination with monthly, weekly, and hourly energy and power profiles to compare and tune the simulated building electricity against the available utility data from 2006. The weather file that was used in this calibration was the International Weather for Energy Calculations (IWEC) weather file from Oslo, Norway with temperature and wind data from Trondheim in 2006. The definition of this weather file was discussed in Chapter 5.

Calibration against 2004 and 2005 utility data is discussed in Section 7.3. For these years, less input data was available, and so a simpler model was calibrated through Latin Hypercube Monte Carlo analysis.

7.2.1 Model Description and Manual Calibration Procedure

The model developed in the manual calibration was for the 2006 utility data and was based on the data collected in Chapter 5. The manual calibration looked at two periods of the year: temperature independent and heating. In the absence of a cooling system in the Steindal

School, no cooling ($T_{\text{outdoor}} > T_{\text{indoor}}$) period was analyzed. However, the lack of a cooling system allowed the temperature independent period to be expanded from days where $T_{\text{outdoor}} \sim T_{\text{indoor}}$ to days where $T_{\text{outdoor}} \geq T_{\text{indoor}}$.

First, the temperature independent period ($T_{\text{outdoor}} \geq T_{\text{indoor}}$) was examined. Second, the heating ($T_{\text{outdoor}} < T_{\text{indoor}}$) period was examined. By splitting the years into “bins” based on outdoor temperatures and schedules of operation, building loads were able to be isolated during the manual calibration.

Inputs that were not be considered during this calibration included the building dimensions, thermal zoning, occupancy, temperature setpoints, ventilation flow rate, installed space heating, and schedules of operation. These were not included because there was a high level of certainty in their input values.

Throughout sections 7.2.2 through 7.2.4 the manually calibrated model is referred to as the “Original” model. This was done to distinguish between the first calibrated building model, which included modeler errors (see section 7.2.4), and the adjusted building model (see section 7.2.5), in which these errors were resolved. The first calibrated model, with errors, was referred to as the “Original” model, while the adjusted building model was referred to as the “Corrected” model.

7.2.2 Temperature Independent Period Calibration

The temperature independent loads were the first to be calibrated. These included occupancy, lighting, equipment, domestic hot water, and ventilation fan loads. Temperature independent days were defined as those with average daily outdoor temperatures equal to or greater than 18°C (the unoccupied temperature setpoint in the school). The first periods of the year that were examined were weekends and unoccupied weekdays without ventilation (as in week 29 in the Steindal School, see section 5.1.10 in Chapter 5) from April through August. This period encompassed all temperature independent days.

The steps in performing the temperature independent calibration were as follows:

- First, temperature independent weekends were examined. These were Saturdays and Sundays during April, May, June, July, and August.
- Second, temperature independent weekdays were examined. These were Mondays, Tuesdays, Wednesdays, Thursdays, and Fridays in which the average

daily temperature was greater than the indoor temperature setpoint. However, because many of these days occurred during the school's summer vacation, days with outdoor temperatures 1°C -3°C lower than the 18°C indoor temperature setpoint were also examined.

7.2.2.1 Temperature Independent Weekend Calibration

Data from Chapter 5 indicated that the only building load that was active on weekends was space heating. In addition, the space heating was expected to be inactive on temperature independent weekends. Consequently, the energy consumption in the building was expected to be very close to zero. However, inspection of the measured hourly energy consumption profiles from this period indicated a previously unrecognized constant load that fluctuated between 16 kWh and 20 kWh. Unfortunately, rather than performing additional site visits to identify the source of this load the modelers simply termed it a “baseload” and added it to the EnergyPlus model as electrical equipment contributing 100% heat gain to the 1st Floor classrooms. It is important to recognize that the assignment of this as a generic electrical load was a poor assumption on the part of the modeler. However, this error was not recognized until the conclusion of the LHMC calibration, and so its consequences will be discussed then (section 7.4).

7.2.2.2 Temperature Independent Weekday Calibration

Observation of the hourly electricity profiles on weekdays in April, May, June, July, and August indicated a significant reduction in the temperature independent loads from June through August. This reduction was greater than the scheduled decrease in ventilation fan, plug load, and hot water loads during the summer vacation, making an erroneous input or a change in lighting schedules the likely cause. This discrepancy was resolved by halving the lighting loads in the Annex, 1st Floor, and Offices during the summer vacation (June 4th, 2006 – August 26th, 2006) to correspond with the expected decrease in occupancy and increase in available sunlight. This change improved the visual fit with the measured electricity consumption on temperature independent days (Figure 7-1).

Figure 7-1 shows the measured (Measured) and simulated (Original) hourly electricity consumption (y-axis) as a function of time (x-axis) during a week in June.

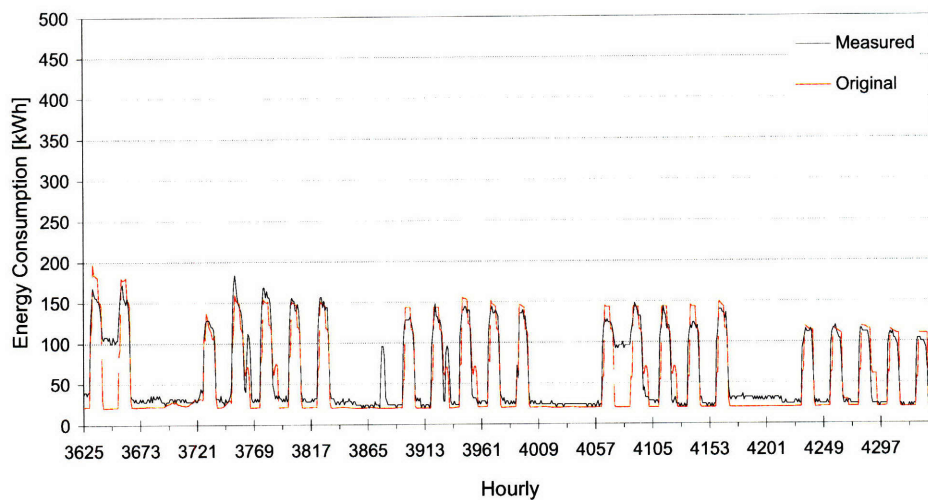


Figure 7-1: Fit between simulated and measured energy consumption for June (hours 3625–4344 in 2006). The Original calibrated model is shown by the dashed red line and the measured hourly utility data is shown by the solid black line. The hour of the year is along the x-axis (h), while the hourly energy consumption (kWh/h) is along the y-axis.

Figure 7-1 indicates a good visual fit between the measured and simulated hourly energy consumption during temperature independent weekends and weekdays. At this point the temperature independent building loads were taken to be calibrated.

No statistical comparisons were made in calibrating the temperature independent loads in the Steindal School. This was because there were very few temperature independent days against which to compare the simulated data, and because the threshold values for calibration (Equation 7-1 and Equation 7-2) only applied to whole-year simulations.

7.2.3 Heating Period Calibration

The heating loads were attributed to space heating and ventilation heating in the Steindal School. Heating was required to compensate for transmission losses from the building envelope. In addition, ventilation heating was needed to raise the temperature of the ventilation supply air to meet comfort conditions.

Several uncertain building envelope and ventilation inputs were identified during data collection (Chapter 5). These included ground temperatures, infiltration rates, and the heat recovery effectiveness in the Main ventilation system. Although other envelope and ventilation inputs (i.e. envelope U-values) also had uncertain values, simple estimates performed in Chapter 6 indicated that the ventilation heat recovery effectiveness, ground temperature, and infiltration

rate were expected to have the strongest influence on the energy consumption in the school. Therefore, these three inputs were analyzed at different values and in various combinations to reach the recommended monthly NMBE and CVRMSE (Equation 7-1 and Equation 7-2).

The steps that were taken in performing the heating period calibration were as follows:

- First, uncertain heating and ventilation inputs were identified.
- Second, heating weekends were examined. These were Saturdays and Sundays that occurred during January through March and September through December.
- Third, heating weekdays were examined. These were Mondays-Fridays that occurred during January through March and September through December.

7.2.3.1 Inputs for Variation

7.2.3.1.1 Ground Temperature

As pointed out in Chapter 6, heat transfer between the building and the ground was two-dimensional, making it difficult to account for in one-dimensional heat transfer models, like the one used in EnergyPlus. As such, the EnergyPlus input file required that the temperature of the interface between the ground and the building surface (wall or floor) be defined, rather than using the undisturbed ground temperature. This was discussed in some detail in Chapter 5, section 5.1.3 and Chapter 6, section 6.1.2. It is important to recognize that the ground temperatures that were assigned in the EnergyPlus model were located at the interface between the walls and floors of the school and the ground, not at some depth into the soil.

The EnergyPlus model required that monthly interface temperatures be assigned to the building model. The default value for these temperatures was 18°C, while calculations in Chapter 6 indicated that 14°C was a more reasonable value for the Steindal School. Thus, during the manual calibration the ground temperature was varied from 12°C up to 18°C to encompass these values.

7.2.3.1.2 Infiltration

Data collected in Chapter 5, and estimates made in Chapter 6, indicated that moderate to low infiltration rates, from 0.2 to 0.4 ACH, were appropriate for the Steindal School. Therefore, the nominal infiltration rate was varied between 0.2-0.4 ACH during the manual calibration. This nominal infiltration rate was the level of infiltration under average temperature and wind

conditions at the building site. In the EnergyPlus model, the infiltration rate was permitted to vary depending on the hourly wind and temperature conditions that were specified in the weather file. The equation for this variation is shown in Equation 7-4 [EPlus 2007a].

$$Infiltration = I_{design} F_{schedule} [A + B | T_{zone} - T_{ODB} | + C(Windspeed) + D(Windspeed)^2] \quad (7-4)$$

I_{design}	The nominal infiltration rate [m ³ /sec]
$F_{schedule}$	The availability factor; 1 if infiltration is available, 0 if infiltration is unavailable
T_{zone}	The temperature of the thermal zone [°C]
T_{ODB}	The outdoor dry bulb temperature [°C]
$Windspeed$	The hourly wind speed at the site [m/s]
$A-D$	Constant coefficients

Coefficients A-D were adapted from the recommended values from the BLAST computer software (taken as A = 0.5, B = 0.02, C = 0.13, and D = 0) to achieve a nominal infiltration rate (I_{design}) of 0.2, 0.3, or 0.4 ACH under typical temperature and wind conditions. In 2006, the infiltration was assumed to be “available” all year ($F_{schedule} = 1$). Checking that these inputs resulted in the appropriate nominal infiltration rates under typical building conditions: with an average indoor temperature of 18.6°C (T_{zone}), average outdoor temperature of 6.5°C (T_{ODB}), and average annual wind speed of 2 m/s ($Windspeed$) at the Steindal School in 2006, the nominal infiltration rate is equal to I_{design} , or 0.2, 0.3, or 0.4 ACH.

7.2.3.1.3 Ventilation Rates and Heat Recovery Effectiveness

In Chapter 5 the heat recovery effectiveness in the Main ventilation system was taken to be 50%. However, this value was highly uncertain. Design documents indicated a heat recovery effectiveness of 65%, while measured data from the Municipality indicated values between 35%-45% (Chapter 5). Therefore, in the manual calibration the value of the heat recovery effectiveness was varied between 40% and 65%.

Additionally, conversations with members of the Municipality indicated that the ventilation fans included a control that reduced the flow rate of air by half when the outdoor temperature was less than -6°C (Main system) and -10°C (Annex system). However, this control proved difficult to implement in EnergyPlus, requiring that the ventilation schedules be manually altered to reduce the ventilation rates during periods when the outdoor temperature was below these values.

7.2.3.2 Heating Weekend Calibration

Data from section 7.2.2.1 and Chapter 5 indicated that the only building loads that were active on weekends were the “baseload” and space heating. Therefore, of the uncertain inputs discussed above, only the infiltration rates and ground temperatures were active on weekends. Thus, these two inputs were varied to obtain a good visual fit with measured utility data on weekends in January through March and September through December. The ground temperature and infiltration values that resulted in the best visual fit with measured data are shown in Table 7-1 and Table 7-2.

Month	Monthly Ground Temperature [°C]
January	14
February	14
March	14
April	16
May	16
June	16
July	16
August	16
September	16
October	16
November	14
December	14

Table 7-1: Monthly ground temperatures resulting from the calibration of the Original building model of the Steindal School.

Zone	Nominal Infiltration Rate [ACH]
Offices	0.3
Bomb Shelter	0.1
1 st Floor	0.3
Annex	0.2
Wardrobes	0.3
Gym	0.2

Table 7-2: Average annual infiltration rates resulting from the calibration of the calibration of the Original building model of the Steindal School.

7.2.3.3 Heating Weekday Calibration

Weekdays from January through March and October through December were then examined to calibrate the heat recovery effectiveness in the building. The result was an efficiency of 50% in the Main building. Additionally, the Main ventilation system air flow rates were halved for the periods from February 25th through March 7th in response to outdoor

temperatures that were less than -6°C . Figure 7-2 and Figure 7-3 present hourly profiles for heating weekends and weekdays in February and November, respectively.

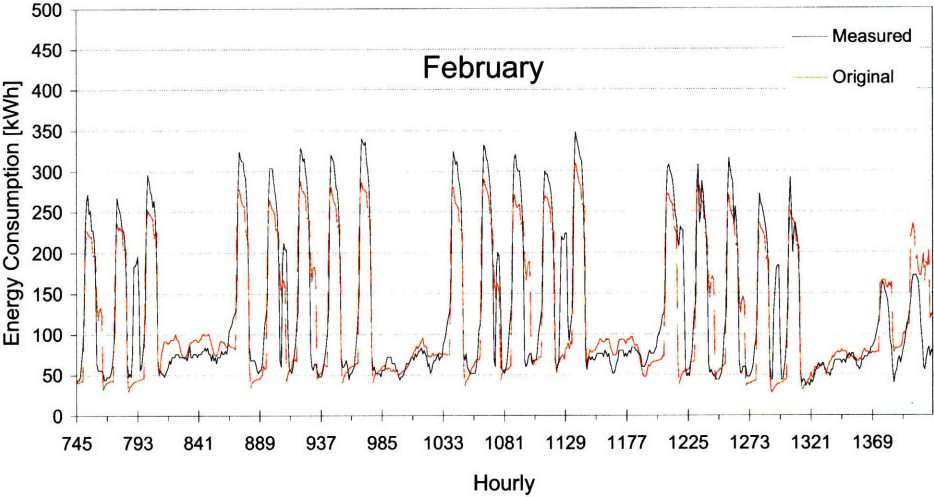


Figure 7-2: Fit between simulated and measured energy consumption for February (hours 745-1417 in 2006). The Original calibrated model is shown by the dashed red line and the measured hourly utility data is shown by the solid black line. The hour of the year is along the x-axis (h), while the hourly energy consumption (kWh/h) is along the y-axis.

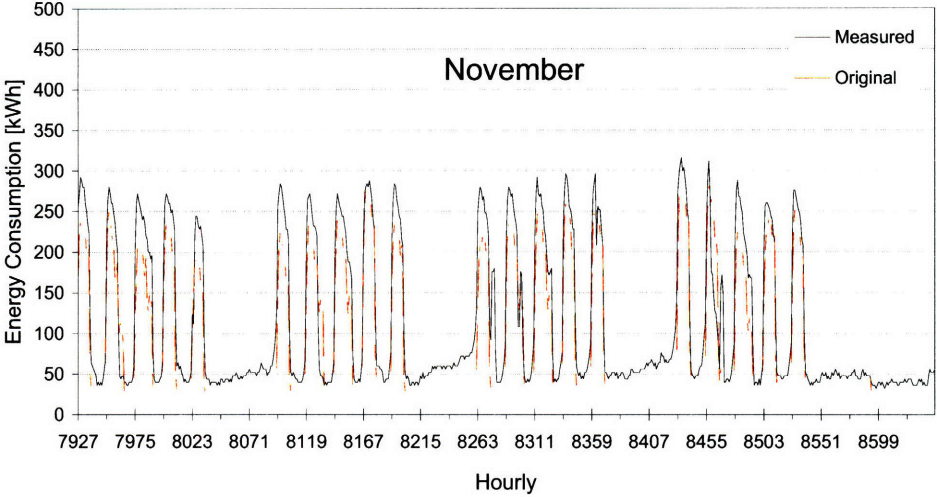


Figure 7-3: Fit between simulated and measured energy consumption for November (hours 7927-8647 in 2006). The Original calibrated model is shown by the dashed red line and the measured hourly utility data is shown by the solid black line. The hour of the year is along the x-axis (h), while the hourly energy consumption (kWh/h) is along the y-axis.

Schedules of operation in Chapter 5 indicated that all building loads were turned off by 5 p.m. on weekdays. However, observations of the measured hourly utility data indicated increased energy consumption through 9:00 p.m. (21:00) on Wednesday evenings during the school year. Conversations with building managers indicated that this additional load was due to activities taking place in the gymnasium of the building. This load was not observed during the temperature independent period (summer vacation) because the building was generally unoccupied during that time.

In response to this observation, the gymnasium lighting schedule was adapted to run until 9:00 p.m. on occupied Wednesdays. However, this load alone did not result in a good fit with measured data, and so the ventilation in the Main building was also turned on, greatly improving the fit.

7.2.4 Preliminary Results

At this point, according to the monthly $NMBE \leq 5\%$ and $CVRMSE \leq 15\%$ indices, the model was considered calibrated. Additionally, the model was within the range of the suggested $GOF \leq 6\%$ for application in ECM savings evaluations [Reddy 2006].

	Energy		Power		GOF
	NMBE	CVRMSE	NMBE	CVRMSE	
Monthly	0%	7%	-3%	8%	6%
Weekly	1%	8%	1%	9%	6%

Table 7-3: Monthly and weekly NMBE and CVRMSE values resulting from the manual calibration of the Original building simulation.

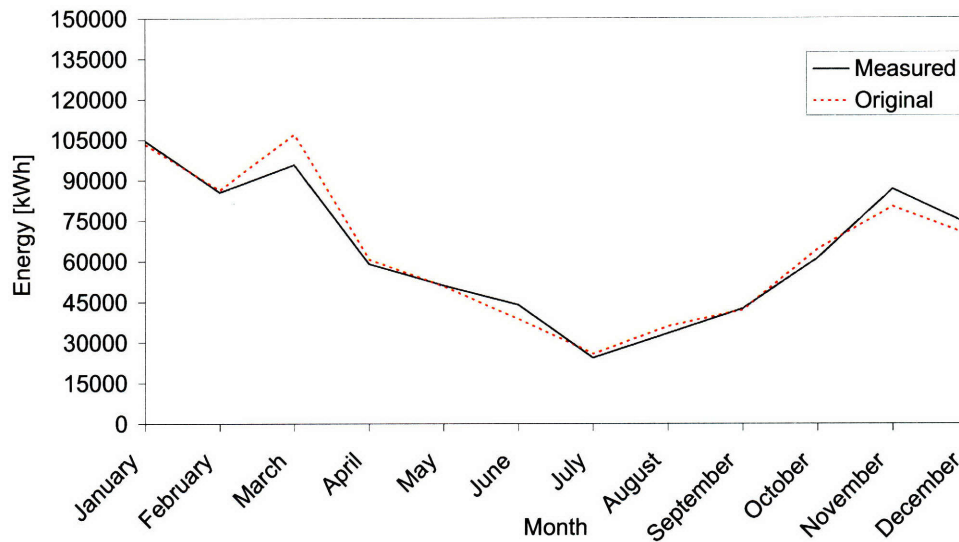


Figure 7-4: Monthly fit between simulated and measured energy consumption in 2006. The Original calibrated model is shown by the dashed red line and the measured utility data is shown by the solid black line. The month is along the x-axis, while the monthly energy consumption (kWh) is along the y-axis.

This model was then taken to have an acceptable level of calibration, and a Latin Hypercube Monte Carlo Analysis (LHMC) was performed (section 7.3).

However, during the investigation of retrofits following LHMC it became apparent that several modeling assumptions had been made that could compromise the accuracy of the predicted retrofit energy savings. These assumptions regarded (1) the handling of the 20kW baseload and (2) the lighting, equipment, hot water, and fan capacities. Thus, further data needed to be collected and a second calibration needed to be performed to resolve these errors. By failing to verify the sources of all building loads and input data prior to calibration, time was wasted and further effort had to be put forth to collect data and manually calibrate an additional model.

7.2.5 Round Two: Adjusted Calibration

From here forward, the original manually calibrated model, with errors, is referred to as the “Original” model, while the model resulting from the corrections made during the adjusted calibration is referred to as the “Corrected” model.

7.2.5.1 Temperature Independent Period Calibration

The first step in the adjusted calibration was the temperature independent period calibration. This step included the definition of the source of the 20 kW baseload and the confirmation of the lighting, equipment, hot water, and fan capacities.

Conversations with building managers and further observations of as-built documents indicated that the baseload was the result of electric resistance heating cables, refrigerators, and freezers that were left on throughout the year and distributed in the building as in Table 7-4.

Additionally, observation of the lighting arrangement in the school required that the lighting capacities be adjusted. The resulting lighting capacity was very similar to the estimate made with the typical values for Norwegian school buildings, and is shown in Table 7-4.

Similarly, the domestic hot water (DHW) consumption (defined on the basis of modeler conjecture) was previously underestimated and was corrected by calculating the expected hot water heating demand and justifying it against typical DHW consumptions for schools in Norway. Performing a simple estimate, as per Equation 6-4 in Chapter 6, with the DHW capacity updated from 5 kW to 25 kW, the annual electric energy demanded by the DHW was equal to 29.6 kWh (6.7 kWh/m²). This was still below the typical value of 10 kWh/m² for Norwegian schools [Wigenstad 2005], but was an improvement over the 1.1 kWh/m² that was calculated with the conditions in the Original model. Additionally, since the DHW contributed no heat gain to the building, the assumption that it ran for a total of just over 1,000 hours per year (approximately 5 hours per day) and was placed in the Gym was considered reasonable.

The changes to the specific fan power in the Main building ventilation system were made on the basis of closer inspection of the fan curves provided by the manufacturer. These changes reduced the fan pressure from 1,200 Pa to 1,000 Pa, resulting in a 2 kW decrease in the power demanded by each fan. Under these conditions, the total fan power in the Steindal School was reduced from 41 kW to 37 kW.

Table 7-4 summarizes the changes that were made to the temperature independent loads in the Steindal School. The left hand column under each header indicates the conditions in the Original calibrated model while the right hand column indicates the conditions in the Corrected model. If no changes were made both columns were filled with “----”.

	Baseload [kW]		Lighting [kW]		Domestic Hot Water [kW]		Fan Pressure [Pa/fan]	
	Original	Corrected	Original	Corrected	Original	Corrected	Original	Corrected
Bomb Shelter	0	3 (2/1*)	-----	-----	-----	-----	1,200 (Main)	1,000 (Main)
Gym	0	5	8	5.5	5	25		
Offices	0	6	11	10.5	-----	-----		
1 st Floor	20	0	-----	-----	-----	-----		
Wardrobes	0	6	1	1.5	-----	-----	-----	-----
Annex	-----	-----	7	6.5	-----	-----	-----	-----

*The 2kW are for electric resistance floor heating in the bomb shelter, and the 1kW is added as an equipment load to account for freezers and refrigerators.

Table 7-4: List of temperature independent load adjustments from the Original to Corrected model. These included properly defining the “baseload”, and improving the lighting, domestic hot water, and fan pressure (Main ventilation system) inputs.

7.2.5.2 Heating Period Calibration

Subsequently, the heating period calibration was rerun. This led to several additional changes to temperature setpoints and schedules, natural ventilation settings, and the heat recovery effectiveness in the Main ventilation system.

Observations of the hourly load profiles from January through March indicated that the simulation severely over-predicted the energy consumption during the week of February vacation from February 27th through March 5th in 2006 (Figure 7-6). In response, the indoor temperature during this period was set to 14°C, equal to the vacation temperature setting in the school. Additionally, Sunday the 5th had not originally been included in the vacation period, and was added to the vacation schedule. This change was applied to the temperature setpoints and schedules in the Office, 1st Floor, Gym, and Annex of the building.

After redistributing the baseload, it was observed that the temperatures in the Wardrobes and Gymnasium were extremely high, especially during summer periods. In response, natural ventilation was added to both of these zones during occupied periods (6 a.m. to 6 pm). This was equal to 1 ACH (0.3 m³/sec) in the Gymnasium and 3.5 ACH (0.7m³/sec) in the Wardrobes. These objects modeled the opening and closing of exterior doors and windows.

Finally, inspection of hourly profiles during occupied heating periods (heating weekdays) indicated that the predicted energy was too high. This discrepancy was resolved by revisiting the value of the heat recovery effectiveness. At a heat recovery effectiveness of 55% in both the Main and Annex ventilation systems, the monthly NMBE and CVRMSE for achieving calibration were satisfied.

7.2.6 Manual Calibration: Results

The resulting weekly and hourly energy consumption and peak power demand for the Original model and the Corrected model are shown in Figure 7-6 through Figure 7-10. The measured utility data from the Steindal School in 2006 are also shown.

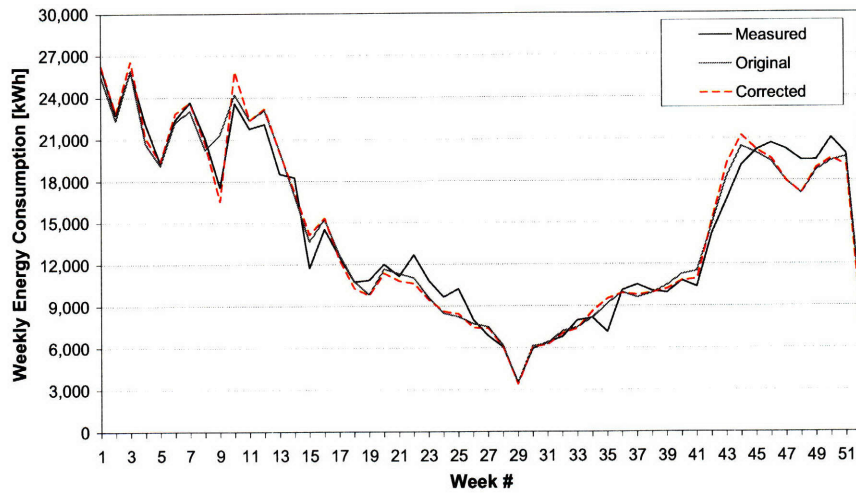


Figure 7-5: Weekly fit between simulated and measured energy consumption in 2006. The Original calibrated model is shown by the solid grey line, the Corrected model is shown by the dashed red line, and the measured utility data is shown by the solid black line. The week is numbered along the x-axis, while the weekly energy consumption (kWh) is along the y-axis.

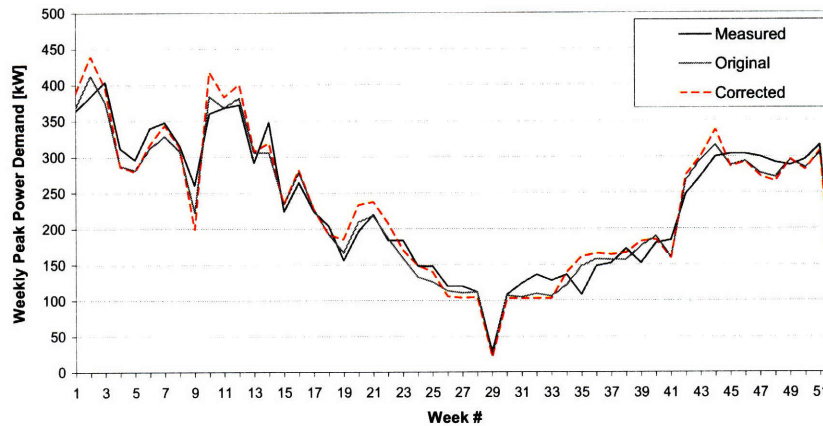


Figure 7-6: Weekly fit between simulated and measured peak power demand in 2006. The Original calibrated model is shown by the solid grey line, the Corrected model is shown by the dashed red line, and the measured utility data is shown by the solid black line. The week is numbered along the x-axis, while the peak power consumption (kW) is along the y-axis.

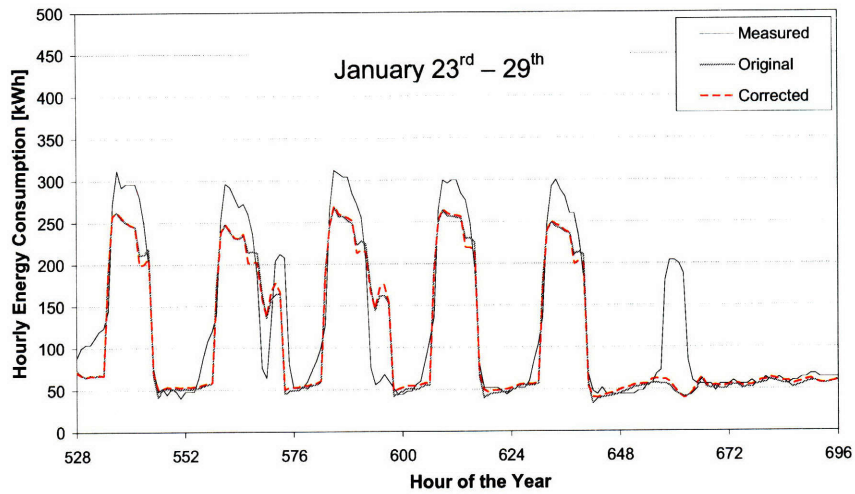


Figure 7-7: Hourly profiles for Original and Corrected manually calibrated models for January 23rd through January 27th, 2006. The Original calibrated model is shown by the solid grey line, the Corrected model is shown by the dashed red line, and the measured utility data is shown by the solid black line. The hour of the year is numbered along the x-axis, while the hourly energy consumption (kWh) is along the y-axis.

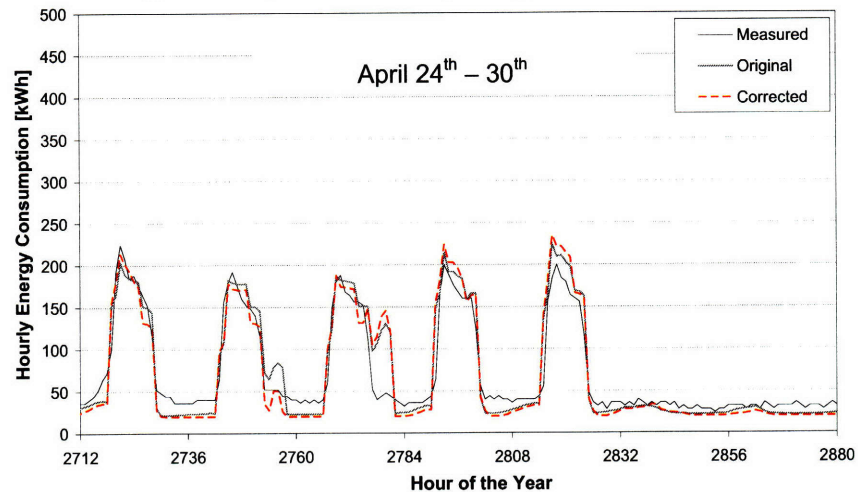


Figure 7-8: Hourly energy consumption profiles from the Original and Corrected manually calibrated models for April 24th through April 30th, 2006. The Original calibrated model is shown by the solid grey line, the Corrected model is shown by the dashed red line, and the measured utility data is shown by the solid black line. The hour of the year is numbered along the x-axis, while the hourly energy consumption (kWh) is along the y-axis.

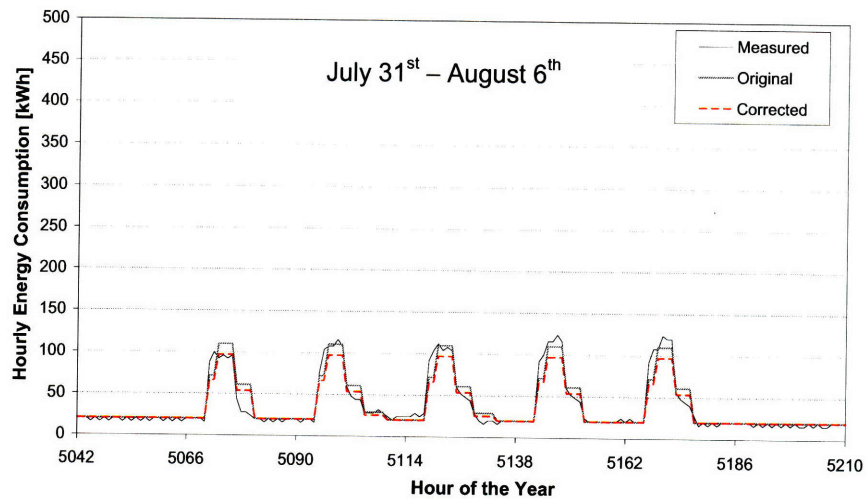


Figure 7-9: Hourly profiles for Original and Corrected manually calibrated models for July 31st through August 6th, 2006. The Original calibrated model is shown by the solid grey line, the Corrected model is shown by the dashed red line, and the measured utility data is shown by the solid black line. The hour of the year is numbered along the x-axis, while the hourly energy consumption (kWh) is along the y-axis.

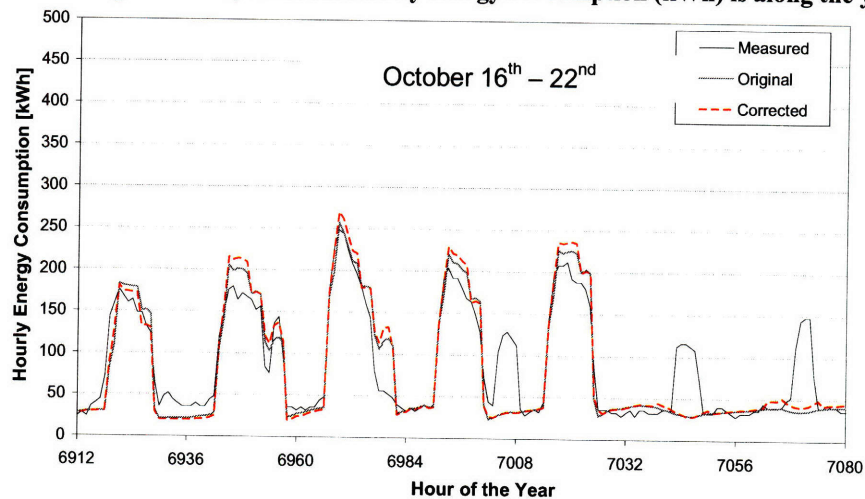


Figure 7-10: Hourly profiles for Original and Corrected manually calibrated models for October 16th through October 22nd, 2006. The Original calibrated model is shown by the solid grey line, the Corrected model is shown by the dashed red line, and the measured utility data is shown by the solid black line. The hour of the year is numbered along the x-axis, while the hourly energy consumption (kWh) is along the y-axis.

In Figure 7-7 through Figure 7-10 the Original and Corrected models show a similar fit with measured data. Looking at the weekly data, the adjustments in the Corrected model show the greatest improvement in week 9 (February Vacation), where the Corrected model matches the weekly energy consumption much more closely than the Original model. However, calculation of the CVRMSE, NMBE, and GOF values in Table 7-4 shows a poorer statistical calibration with the Corrected model than the Original model.

Time Period	Model	Energy		Peak Power		GOF
		NMBE	CVRMSE	NMBE	CVRMSE	
Annual	<i>Original</i>	3%		3%		3%
	<i>Corrected</i>	5%		5%		5%
Monthly	<i>Original</i>	0%	7%	-3%	8%	6%
	<i>Corrected</i>	0%	7%	-4%	11%	7%
Weekly	<i>Original</i>	1%	8%	1%	9%	6%
	<i>Corrected</i>	1%	8%	0%	11%	7%
Daily	<i>Original</i>	0%	17%	4%	16%	12%
	<i>Corrected</i>	0%	17%	2%	17%	12%
Hourly	<i>Original</i>	3%	37%	3%	37%	26%
	<i>Corrected</i>	5%	37%	5%	37%	26%

Table 7-5: Annual, monthly, weekly, daily, and hourly CVRMSE and NMBE resulting from the calibration of the Original and Corrected models.

According to the standards proposed by ASHRAE Guideline 14 [ASHRAE 14 2002] both the Original and Corrected models were considered to be calibrated on a monthly basis. However, neither model was able to meet the requirement for the hourly CVRMSE < 30%. Additionally, only the Original model, with a GOF ≤ 6%, would be considered adequately calibrated for performing retrofit evaluations according to RP-1051 [Reddy 2006].

The difficulty that was encountered in meeting the hourly CVRMSE was attributed to the slight under and over estimates of the hourly energy consumption during the first and last quarters of the year (see Figure 7-7 and Figure 7-10, respectively), and the lack of “fine tuning” to capture discrepancies between the annual schedules that were defined and changes in energy consumption that were observed in the hourly data (see hours 7,008, 7,050, and 7,070 during October in Figure 7-10). However, the model was not tuned to eliminate these because it would have been time consuming and extremely difficult to do so. Therefore, at this juncture, both the Original and Corrected models were considered to be calibrated.

Inspection of the annual end-use load profiles in Figure 7-11 and Figure 7-12 show a reduction in the fan load and an increase in the hot water load resulting from the adjustments made to the Corrected model.

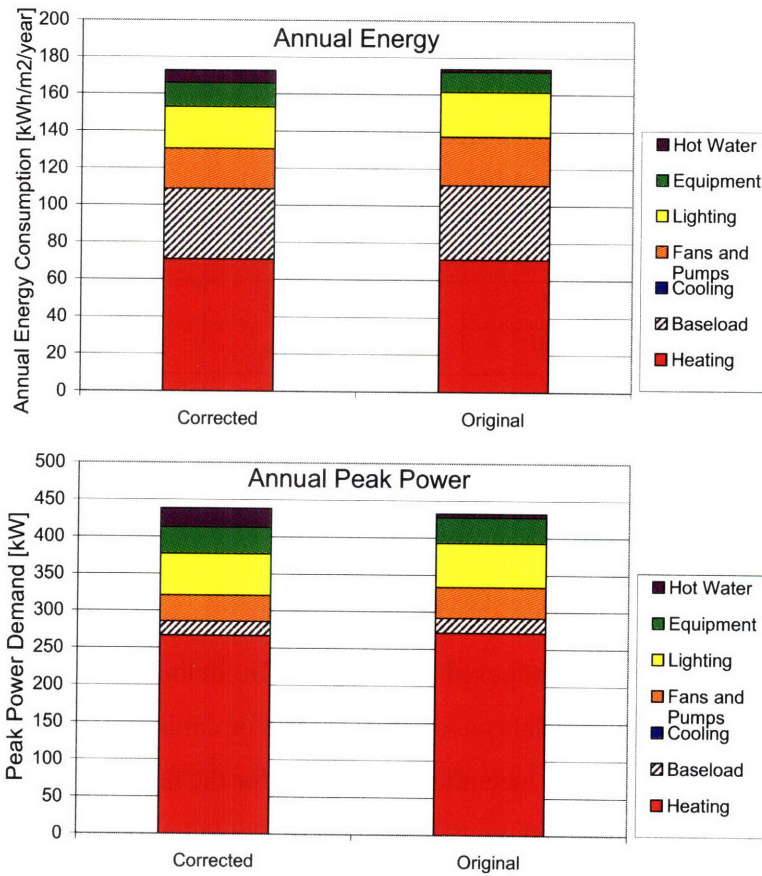


Figure 7-11: Annual end-use specific energy and peak power distribution resulting from manual calibration of the Original and Corrected models. The specific energy consumption and peak annual power demand are shown along the x-axis for each model (y-axis). The specific energy consumption was calculated as the total annual energy consumption, divided by the 4,400 m² of conditioned floor area.

Additionally, Figure 7-12 depicts the annual end-use energy consumption as compared to typical Norwegian school buildings and the total energy consumed in the Steindal School.

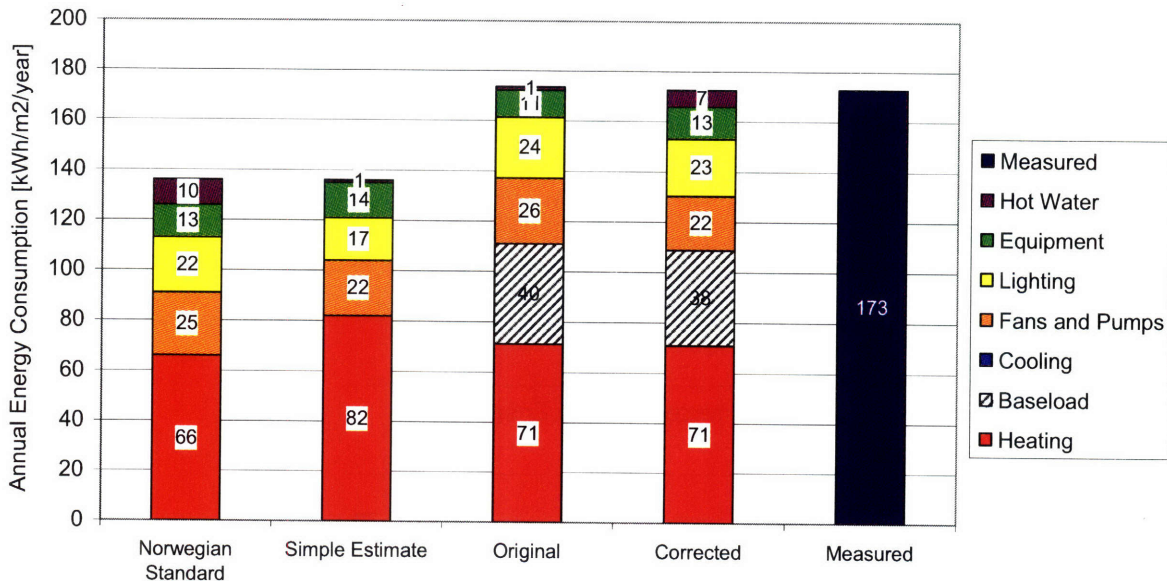


Figure 7-12: Comparison of the annual specific energy consumption in the Original model, Corrected model, Simple model, typical Norwegian schools, and the 2006 measured utility data in the Steindal School. The specific energy consumption is shown along the x-axis for each model (y-axis). The specific energy consumption was calculated as the total annual energy consumption, divided by the 4,400 m² of conditioned floor area.

The Corrected model showed better agreement with typical equipment, fans and pumps, lighting, and domestic hot water energies than the Original model. However, both models output annual energy consumptions that were very close to that in the Steindal School in 2006. The total annual energy consumptions in the Original and Corrected models were almost identical, with 759,400 kWh/year (173 kWh/m²/year) and 764,000 kWh/year (174 kWh/m²/year) of energy consumption resulting from the Original and Corrected models, respectively. These were both within 1% of the 760,720 kWh/year (173 kWh/m²/year) of electricity that was consumed in the Steindal School in 2006.

Figure 7-13 depicts the monthly end-use energy consumption in both the Original and Corrected model.

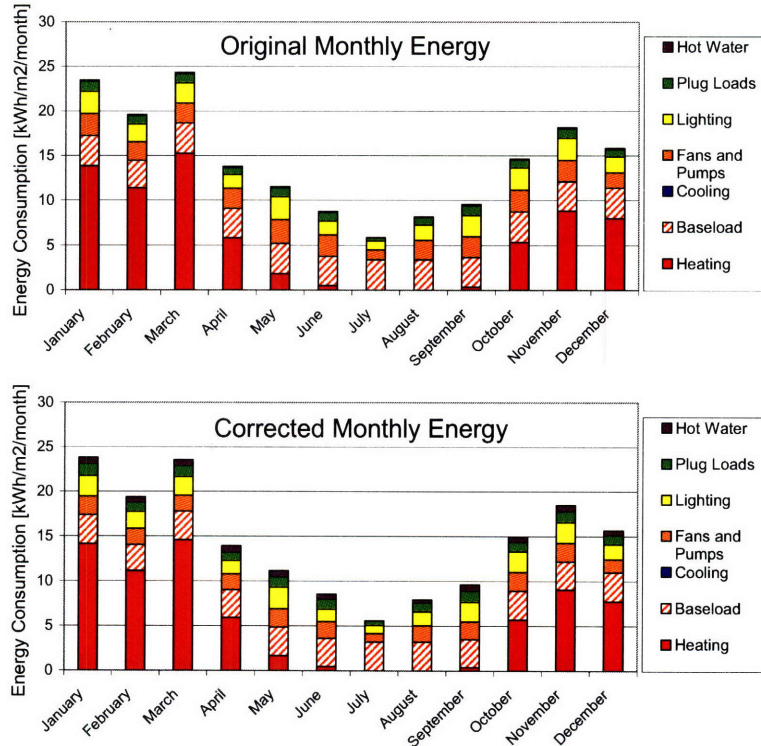


Figure 7-13: Monthly end-use load distributions resulting from the manually calibrated Original and Corrected building models. The specific energy consumption is shown along the x-axis for each model (y-axis). The specific energy consumption was calculated as the total annual energy consumption, divided by the 4,400 m² of conditioned floor area.

Note that the heating load and the baseload show little to no change on an annual or monthly basis, while the lighting, fans and pumps, and plug loads, and domestic hot water (DHW) all show a change from the Original to Corrected model; the lighting, fan and pumps, and plug loads were all decreased in the Corrected model, while the DHW was increased. These observations corresponded with the adjustments that were made during the second round of calibration.

7.2.7 Lessons Learned: Manual Calibration

The manual calibration resulted in two models that were considered to be calibrated according to the monthly statistical criteria set forth in ASHRAE Guideline 14 [ASHRAE 14 2002]: the Original and Corrected models. However, the Original model was subject to poor modeler assumptions, and was corrected with a second round of calibration. This resulted in the Corrected model, which showed only minor changes in the fit with measured data – not necessarily improvements – when compared to the Original model. However, by revisiting the input values to eliminate modeler errors the certainty in the values of the lighting, hot water,

baseload, and fan loads were greatly increased. The implications of this improved certainty will be investigated during retrofit in section Chapter 8. Additionally, the influence of the known errors in the Original model are investigated during sensitivity analysis in section 7.3.

Examination of hourly data enabled the identification of the baseload and permitted calibration against seasonal (temperature independent and dependent) loads. This hourly data, coupled with the certainty in schedules of operation (outlined during data collection in Chapter 5), enabled the building's end use loads to be isolated during calibration.

7.3 Latin Hypercube Monte Carlo Analysis

The level of modeler involvement in the manual calibration often results in simulations that are strongly biased by the experience and knowledge of the modeler. This can be advantageous if the modeler's experience leads to a well calibrated model that has a high degree of certainty in all input values. However, it can also be a disadvantage if the modeler's bias leads to input errors or poor input assumptions. RP-1051 [Reddy 2006] recommends the use of Latin Hypercube Monte Carlo (LHMC) analysis to reduce modeler bias during calibration.

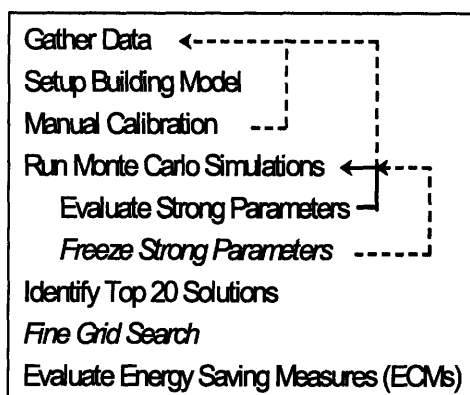


Figure 7-14: Procedure for calibration proposed in RP-1051 [Reddy 2006].

The LHMC analysis shown here was adopted from work performed in RP-1051 [Reddy 2006] and is intended to aid in reaching calibrated simulation while considering uncertainties in input values and their influence on the results of energy conservation measure (ECM) savings analysis. The first three steps of the procedure shown in Figure 7-3 have already been performed; data was collected in Chapter 5, and building model setup and manual calibration were performed in section 7.2. The Monte Carlo simulations are the focus of the work performed in this section.

During the Monte Carlo (LHMC) analysis influential parameters (Evaluate Strong Parameters) were identified, a number of calibrated models were found (Top 20 Solutions), and two optional calibration steps (indicated in italics in Figure 7-3) - freezing strong parameters and a fine grid search - were assessed. This process was discussed in detail in section 3.3 in Chapter 3, but will be reviewed briefly with respect to the Steindal School case study in the following sections. The focus of the LHMC was on:

- Assessing the ability of LHMC to aid in reaching calibrated solutions.
- Analyzing the consequences of the errors made in the manually calibrated (Original and Corrected) models when performing an LHMC analysis.
- Evaluating the number of LHMC runs that were needed to ensure that the calibration “converged”.
- Assessing the usefulness of freezing strong parameters and performing a fine grid search.
- Assessing the validity of using the goodness of fit (GOF) as a criterion for ranking candidate solutions.

7.3.1 LHMC Calibration: Input Models

Three models of the building were employed during the Latin Hypercube Monte Carlo analysis, here referred to as the Detailed-Original, Detailed-Corrected, and Simple models. These three models were each calibrated against 2006 utility data.

The Detailed-Original model and the Detailed-Corrected models were taken from the manual calibration, with seven zones and detailed schedules of building use. The Simple model had two zones (Main building and Annex) that were determined by the building’s two ventilation systems. The baseload corrections that were made in the Detailed-Corrected model had no influence on the Simple model; the baseload was simply assigned as 100% heat gain in the Main building.

It is important to note that the corrections made in the second round of manual calibration in section 7.2 were implemented *after* the initial LHMC was performed, and so certain aspects of the analysis such as the freezing of strong parameters, fine grid search, and running of iteratively higher numbers of simulations were performed only on the Detailed-Original model and were not repeated for the Detailed-Corrected model. However, the application of LHMC to the

Detailed-Corrected model was considered, although only for the 2000 LHMC simulations that were deemed acceptable during the investigation of the Detailed-Original model. It shall be noted that any differences arising between the results of the 2000 LHMC runs of the Detailed-Original and Detailed-Corrected models can be directly attributed to the changes made during the adjusted manual calibration (see section 7.2). This was because all other conditions were at parity during the LHMC, including the input combinations for each of the 2000 simulations.

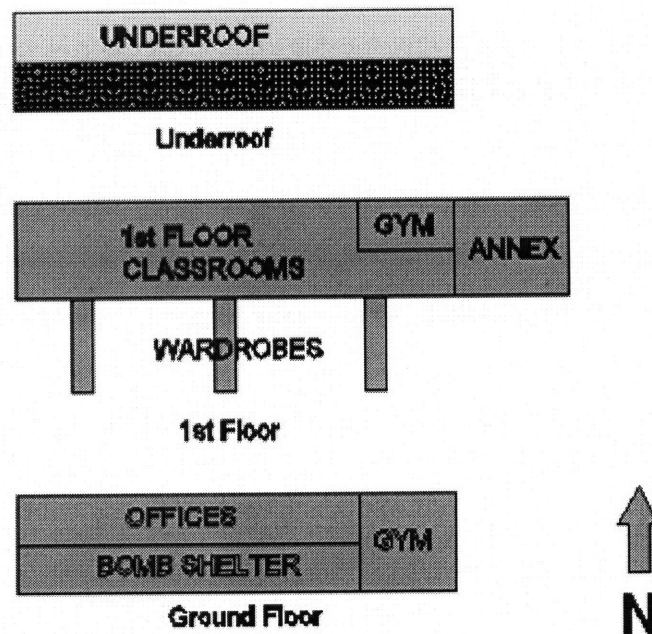


Figure 7-15: Floor plan of the Steindal School, including zone labels.

The Simple two-zone model employed more generalized schedules for the school and used a monthly time-scale for calibration, making it more representative of a typical case in energy simulation. Further, the Simple model took less time to simulate in EnergyPlus, roughly 25 seconds per simulation, while the Detailed-Original and Detailed-Corrected models took between 65-90 seconds on a typical PC. To test the robustness of the methodology the Simple model simulation was also run for 2005 (Simple 2005) and 2004 (Simple 2004) with no prior manual calibration. These years had higher temperature settings, less stringent schedules, and Main ventilation fans with a higher power demand, all of which were accounted for in the LHMC analysis.

Recall from Chapter 5 that in the absence of adequate weather data from the building site in 2006, weather data from a typical meteorological year in Oslo were used with modifications to include 2006 outdoor temperature and wind speeds from Trondheim. Similar weather files were generated to calibrate against the 2004 and 2005 utility data during the LHMC. The weather used in the LHMC for 2006 was the same one as in the manual calibration in section 7.2.

7.3.2 LHMC Calibration: Procedure

The next step of the procedure was the Latin Hypercube Monte Carlo analysis. As suggested in RP-1051 [Reddy 2006], a number between 10 and 20 parameters (15 in this case) were selected as being both influential (i.e. temperature settings and schedules) and known with some level of uncertainty (i.e. heat recovery effectiveness). These parameters were allowed to vary within a defined range, nominally selecting three possible values for each of them: low, middle and high, as shown in Table 7-6. For each parameter, the value resulting from the manual calibration of the Detailed-Original model was chosen as the middle value (or value 2); while the low and high values (or values 1 and 3 respectively) were defined to contain the best guess for that parameter – see the last two columns of Table 7-6. In general, the deviations from the middle values were around $\pm 15\%$, and were used to define a coarse grid of parameter values.

Param #	Group	Description	1 = low	2 = middle	3 = high	Unit	Manual calibration	Best guess
p1	Envelope	Mineral wool conductivity	0.036	0.043	0.05	W/mK	2	2
p2		U-value north windows	2.8	3.3	3.8	W/m ² K	2	1
p3		U-value new Windows	1.5	2	2.5	W/m ² K	2	1
p4		Ground temperature	12-14	14-16	16-18	°C	2	3
p5		Infiltration	0.2	0.3	0.4	ACH	2	2
p6	HVAC	Heating coil UA-value	3,500	3,750	4,000	W/K	2	2
p7		Heat recovery η , Main	45{40} (45)	55{50} (60)	65{60} (75)	%	2	3
p8		Heat recovery η , Annex	45	55	65	%	2	3
p9		SFP, Main	1,000 (1,200)	1,200 (1,500)	1,400 (1,800)	W/m ² /s	1{2}	1
p10		SFP, Annex	500 (600)	600 (700)	700 (800)	W/m ² /s	2	1
p11		Ventilation rate, Main	10	11	12	m ³ /s	2	2
p12		Ventilation rate, Annex	1.8	1.9	2	m ³ /s	2	2
p13	Int. Load	Internal Loads	83 {{(100)}}	100 {{(120)}}	117 {{(140)}}	kW	2	2
p14	Settings	Temperature Settings	18 (19), -2	20 (21.5), -2	21 (23), -2	°C	2	1
p15		Schedule	low	middle	high	-----	1	1

Table 7-6: List of values for the 15 parameters adopted in the Detailed-Corrected LHMC analysis. Values apply to all 2006 models except values in brackets - () and {} - which are used in the Simple and Detailed-Original models, respectively. HVAC and SFP are abbreviations for Heating, Ventilation and Air Conditioning and Specific Fan Power, respectively. The U-values shown result from calculations in EnergyPlus of windows with properties intended to match as closely as possible the configurations given in the manufacturer's specifications with frames and dividers included.

At this point, trying all the possible combinations would mean performing the unreasonable number of $3^{15} = 14,348,907$ simulations. The Latin Hypercube Monte Carlo method, instead, generated random combinations of the allowed parameter values (1, 2 or 3), resulting in multiple parameter vectors, on the order of hundreds or thousands. These vectors

were then passed to the simulation software, and the resulting energy consumption was evaluated against measured data. Additional information on LHMC and other Monte Carlo techniques can be found in Saltelli et al. [Saltelli 2004].

The fit between simulated results and measured utility data was then evaluated on a monthly basis for both power and energy, and was quantified using the normalized mean bias error (NMBE) and the coefficient of variation of the root mean square error (CVRMSE) (Equation 7-1 and Equation 7-2 in section 7.1). When a parameter vector produced results that satisfied the monthly $NMBE \leq 5\%$ and $CVRMSE \leq 15\%$ criteria, it was called a candidate. Candidates were then ranked based on their monthly goodness of fit (GOF) values (Equation 7-3).

An important step in the procedure was the identification of strong parameters. The parameter strength was a measure of its influence on the ability of a simulation to reach calibration; when a parameter was strong it tended to appear amongst the candidates with a preferred value, or with a non-random distribution of values (1, 2, or 3) (see section 3.3 in Chapter 3 for additional information about strong parameters). The strength of a parameter was quantified using the chi-square test, as suggested in RP-1051 [Reddy 2006]. The χ^2 test is a well-known statistical method to test the randomness of a distribution: the higher the value, the less random the distribution. When only three values are possible (degree of freedom = 2), as in our case, it can be said within a 99% interval of confidence that a parameter is strong, meaning not randomly distributed, when its χ^2 value is above the threshold of 9.21 (section 3.3 in Chapter 3). The formula for calculating the χ^2 is shown in Equation 7-5.

$$\chi^2 = \sum_{s=1}^3 \frac{(p_{obs,s} - p_{exp,s})^2}{p_{exp,s}} \geq 9.21 \quad (7-5)$$

p_{exp} **The expected probability**

p_{obs} **The observed occurrence**

Because the input to the LHMC analysis was randomly distributed, i.e. the distribution between states 1, 2, and 3 for any given parameter was approximately uniform, p_{exp} of the calibrated candidates was also expected to be uniform. Thus, the number of occurrences of each parameter state that was expected was equal to the total number of calibrated solutions divided by 3, with three being the number of possible states for each parameter. Parameters with high χ^2

values deviated greatly from p_{exp} , meaning that they showed a bias toward one or two of the parameter states. Such inputs were deemed “strong parameters”. However, because these strong parameters were dependent on the range of values assigned by the modeler, they could not be expected to be independent of modeler bias, and so, although the LHMC decreased the amount of control that the modeler had over the calibration, the presence of user bias was not eliminated.

Additionally, these parameters were only strong over the range of values assigned during the LHMC, and did not necessarily indicate areas where retrofits might have the greatest potential for energy savings. However, identifying strong parameters was important for recognizing where further information might be gathered to have the greatest impact on improving the quality of calibration.

RP-1051 recommended running iteratively higher numbers of simulations to identify strong parameters. Alternatively, it also suggested that the strong parameters be “frozen” at their most probable value and the LHMC analysis be re-run on only the remaining parameters (thus searching in a reduced solution space) to identify new strong parameters. It was proposed that the LHMC method was considered to have “converged” when no further strong parameters were identified by either running iteratively higher numbers of simulations or by freezing strong parameters. In this sense, convergence indicates the point at which no further LHMC runs are necessary and calibration is complete (see section 3.3 in Chapter 3 for additional information).

Finally, the Top 20 candidates, those with the lowest GOF values, were accepted for the evaluation of energy conservation measures (ECMs). A fine grid search was also performed on the Top 20 parameter vectors from the LHMC analysis with the goal of further improving their GOF values. The procedure for running this fine grid search was explained in section 3.3 in Chapter 3. The fine grid search subdivided the range of values for each of the strong parameters into three sub-ranges and simulations were run for all of the possible combinations for each of the Top 20 solutions. The total number of simulations for the fine grid search amounted to $m \cdot 3^n$, where n was the number of strong parameters and m was the number of Top solutions, i.e. 20.

7.3.3 LHMC Calibration: Results

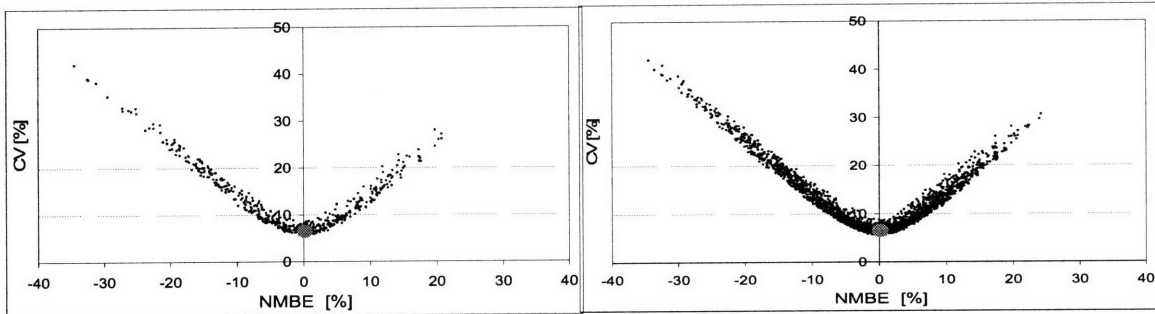
The Monte Carlo analysis began by running batches of simulations for the Detailed-Original model. Since the Detailed-Original model had been manually calibrated, the main purpose of running the Monte Carlo analysis was to test its validity as a tool for identifying

further candidate solutions. Simulations were run starting with a batch of 250 vectors of random input combinations and continuing with 500, 1000, 2000, 4000 and 8000 trials. In RP-1051 the authors suggested using the identification of strong parameters as a means to determine the convergence of the LHMC analysis (section 3.3 of chapter 3); this point proved to be controversial in the case study presented here. Some parameters were identified as strong in all of the batches, while others showed an “oscillating” strength, such that the same combination of strong parameters was never identified in successive batches. Despite this behavior the algorithm appeared stable with respect to the generation of candidates. Plotting on a scatter-chart the values of NMBE and CVRMSE for the Detailed-Original, Detailed-Corrected, and Simple models, as in Figure 7-16, it is apparent that the distribution of results intensifies with increasing simulations but does not change in pattern. Similarly, the improvements in the GOF of the Top 20 candidates did not show significant variation. So, although the definition of convergence as defined in RP-1051 [Reddy 2006] was not met, the authors decided to stop the analysis at 2000 trials since the best 20 GOF values had already stabilized at that point. It shall be noted that for the Simple case this equalled an overnight simulation time (ca. 16 hours) and for the Detailed-Original and Detailed-Corrected cases this equalled a weekend run time (ca. 36-50 hours).

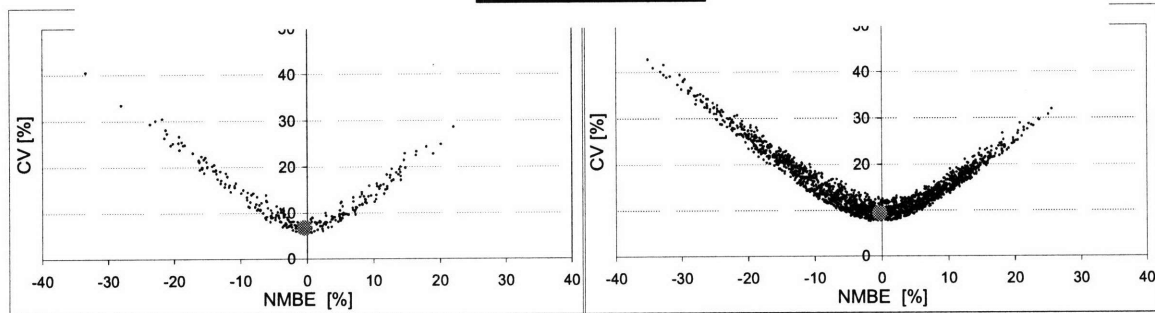
500 LHMC RUNS

Detailed-Corrected

2000 LHMC RUNS



Detailed-Original



Simple

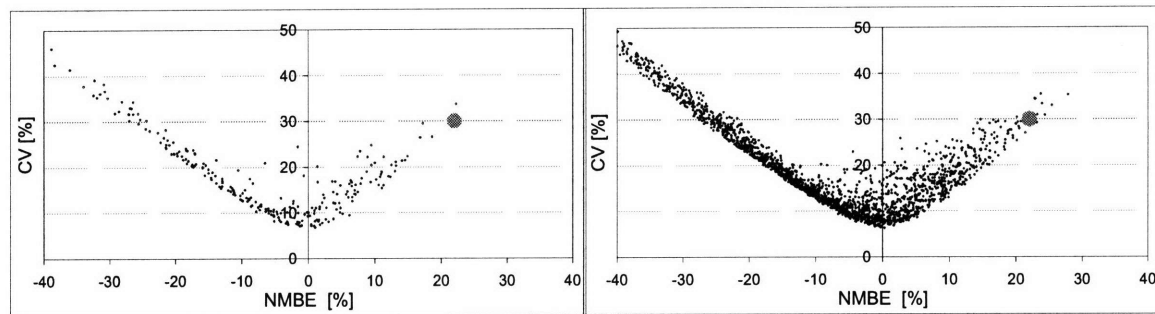


Figure 7-16: Goodness-of-fit (GOF) vs. Normal Mean Bias Error (NMBE) for the LHMC calibrated Detailed-Corrected, Detailed-Original, and Simple models run with 500 simulations (left) and 2000 simulations (right). The grey dot indicates the manually calibrated solution in the Detailed-Original and Detailed-Corrected models and the original “best guess” simulation in the Simple model. All results are for 2006.

It shall be noted that while the “best guess” combination of parameter values (grey dot in Figure 7-16) used for the Simple model generated a poor solution, this model could not be said to be entirely non-calibrated. Indeed, the values for the temperature independent loads (lighting, equipment and hot water), the choice of what parameters to include in the LHMC analysis, and the ranges of variability for their values, were determined during the process of calibrating the Detailed-Original model. Had other ranges of variability or parameters been considered the

results would likely have been much worse. Hence, the Simple model should be regarded as a semi-calibrated model rather than a completely uncalibrated one.

The comparison of measured utility data against simulated results after 2000 LHMC trials are shown in Figure 7-17; both energy and power are shown. The black line represents the measured data, the grey line the “best guess” solution, and the dashed line the candidate solution with the best GOF value.

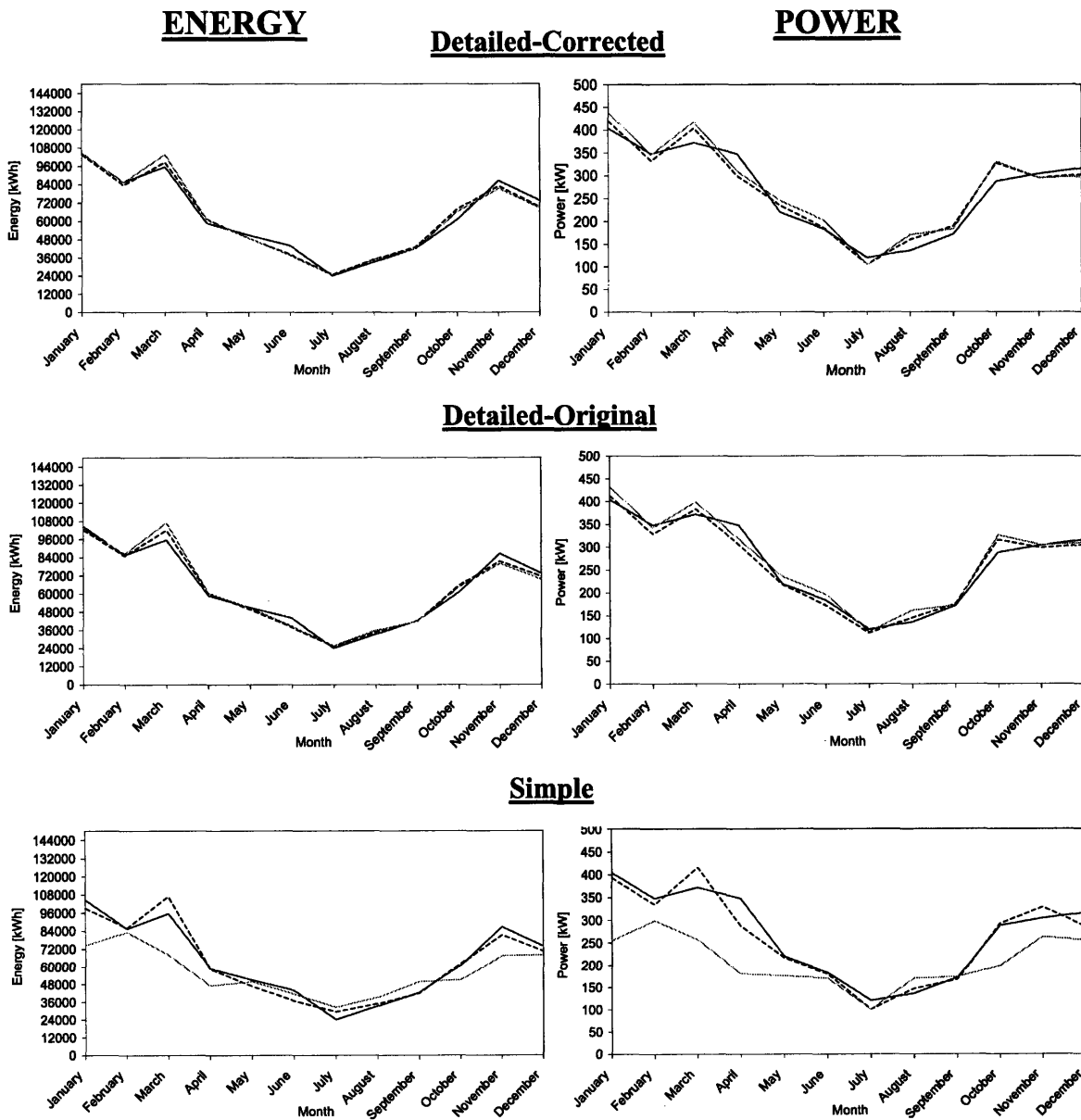


Figure 7-17: Energy (kWh, left) and Power (kW, right) vs. month of the year. The “best guess” is shown by the solid grey line, the best calibrated model (lowest GOF) is shown by the dashed black line, and the measured utility data is shown by the solid black line. All results are for the year 2006.

The monthly results for the Detailed-Corrected, Detailed-Original, and Simple models with 2000 trials are shown in Table 7-7; all were simulated for the reference year: 2006. Additional results are presented for the Simple model simulated for 2004 and 2005, as well as results for the optional steps of the fine grid search and parameter freezing, as applied to the Detailed-Original model.

Case	Best Guess					2000 Trials		2000 trials - Top 20 Solutions		
	NMBE [%]	CVRMSE [%]	NMBE [%]	CVRMSE [%]	GOF [%]	Candi. Found	Strong param.	Coarse grid GOF [%]	Fine grid GOF [%]	Freezing GOF [%]
Detailed-Original	0	7	-3	8	5.46	437	p7,p14	4.53-5.18	4.38-5.11	5.01-5.30
Detailed-Corrected	0	7	-4	11	6.74	362	p7,p8,p14	5.55-6.10	---	---
Simple	22	30	22	28	25.60	122	p5,p7,p14,p15	6.33-7.36	6.24-7.10	---
Simple 2005	40	44	34	39	39.22	7	p7,p15	8.56-9.28	8.54-9.24	---
Simple 2004	41	44	34	37	39.11	48	p7,p9,p11,p13,p15	8.47-9.23	7.99-8.79	---

Table 7-7: Summary of CVRMSE, NMBE, and GOF values resulting from the LHMC calibration. Results are shown for 2004, 2005, and 2006 data. Additionally, the resulting GOF values from the fine grid search and the “freezing” of strong parameters are shown.

The Simple model showed a significant improvement from the best guess solution, prior to LHMC analysis, to the best solution, as indicated in the graphs of power and energy in Figure 7-17. This is reflected by the fact that the GOF is significantly improved from the best guess value, from 25.60% down to 6.33%. A similar behaviour was noticed for 2004 and 2005, even though the model was not manually calibrated for these years. However, in these cases the best GOF values were around 8% or 9% rather than 6% or 7%, and in 2005 only seven candidates were found. Table 7-8 shows the NMBE, CVRMSE, and GOF for the best solution (lowest GOF) for each of the Detailed-Corrected, Detailed-Original, and Simple models on a monthly, weekly, daily, and hourly time scale.

LHMC Candidate	Model	Energy		Power		GOF [%]
		NMBE [%]	CVRMSE [%]	NMBE [%]	CVRMSE [%]	
Best-Monthly	Detailed-Corrected	0.38	5.6	-1.43	9.47	5.55
	Detailed-Original	0.41	5.56	1.19	6.77	4.46
	Simple	0.91	8.22	1.98	10.1	6.60
Best-Weekly	Detailed-Corrected	0.53	7.93	-0.43	10.83	6.72
	Detailed-Original	0.53	7.9	1.44	8.66	5.91
	Simple	0.09	13.14	1.37	13.85	9.57
Best-Daily	Detailed-Corrected	-0.11	17.46	2.04	17.14	12.27
	Detailed-Original	0.41	17.29	3.66	16.31	12.03
	Simple	-0.11	22.16	3.48	21.82	15.65
Best-Hourly	Detailed-Corrected	5.31	36.65	5.31	36.65	26.18
	Detailed-Original	2.94	37.17	2.94	37.17	26.37
	Simple	1.2	40.5	1.2	40.5	28.65

Table 7-8: Summary of monthly weekly, daily, and hourly NMBE, CVRMSE, and GOF of the “best” calibrations (those with the lowest GOF) from the Detailed-Corrected, Detailed-Original, and Simple models. All results are for the year 2006.

Note that, according to the threshold values in ASHRAE Guideline 14 [ASHRAE 14 2002] (Equation 7-1 and Equation 7-2 in section 7.1) no candidate solutions were found when calibrating on an hourly basis. Additionally, the Detailed-Original model showed a better statistical fit with measured data than the Detailed-Corrected model or the Simple model. Recall that during the manual calibration it was suggested that no hourly candidates were found because discrepancies existed in the hourly data that were not captured in the annual schedules of building operation. Because the inputs that were varied during the LHMC were broad (for example, *zone* level lighting capacities, *system* heat recovery effectiveness, and *overall* mineral wool conductivity) the LHMC was not expected to provide improvements at the level of detail necessary to meet the hourly calibration criteria.

The data in Table 7-7 and Figure 7-18 also indicate that the main heat recovery effectiveness (p7) and the schedules (p15) were the only two parameters identified as strong for all of the cases⁴. The temperature settings (p14) appeared as strong in multiple models, while the infiltration (p5), Annex heat recovery effectiveness (p8), specific fan power (p9), Main ventilation flow rate (p11), and internal gains (p13) all appeared as strong in one of the five cases.

⁴ p15 is excluded from the Monte Carlo analysis of the Detailed-Original and Detailed-Corrected model because its value is known with precision in 2006.

The distribution of parameter states for the “all candidates” (all candidate solutions for a given model) solution set and the Top 20 solution set are shown in Figure 7-18 for the Detailed-Corrected, Detailed-Original, and Simple models. Strong parameters, identified according to the χ^2 statistic, are indicated with red circles. Note that the expected output for parameters that are not considered to be strong is a uniform distribution (33%) between states 1, 2, and 3.

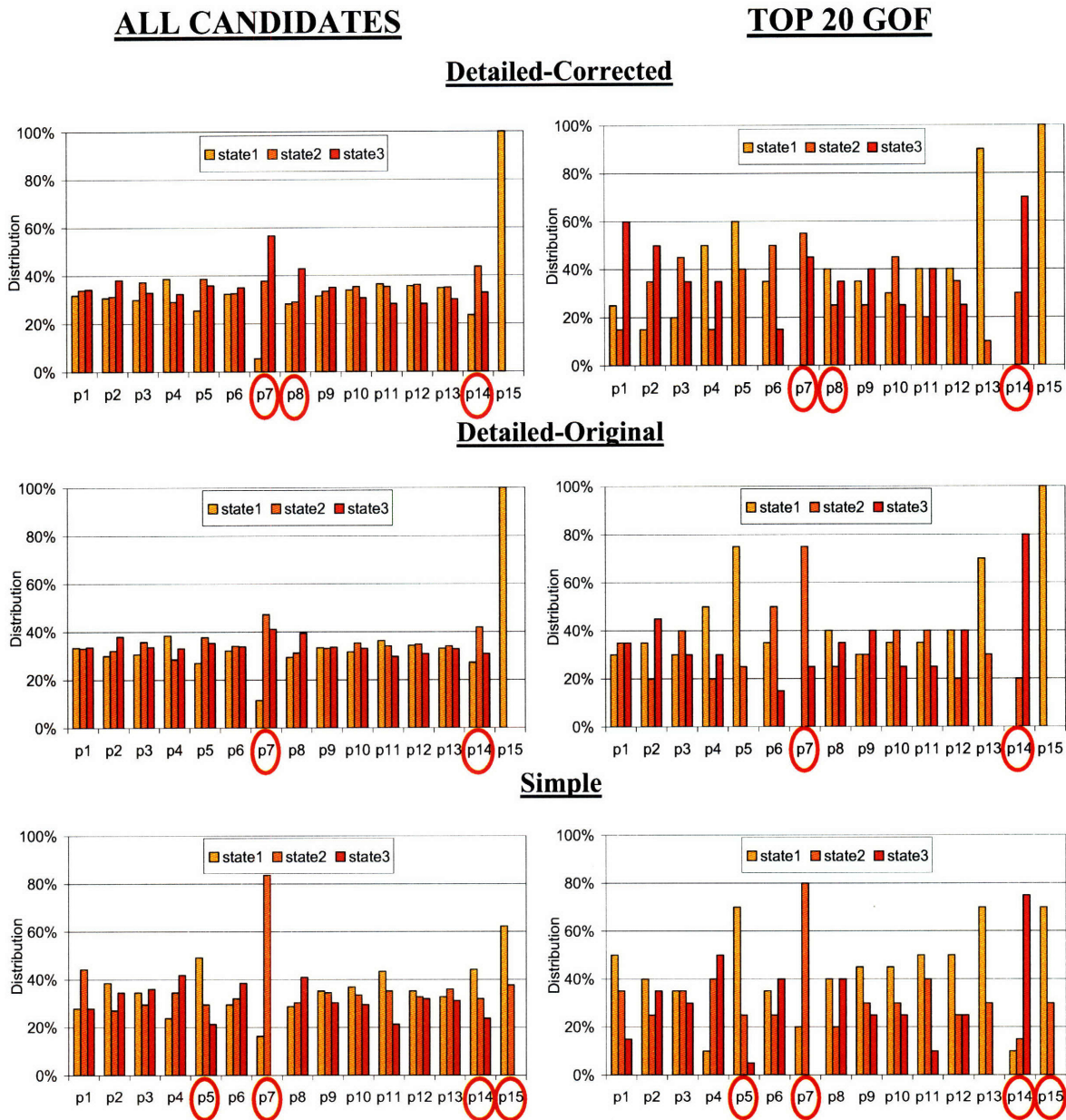


Figure 7-18: Distribution of parameter states for the Detailed-Corrected, Detailed-Original, and Simple LHMC calibrated models. The distribution of all of the calibrated candidates (“all candidates”, left graph) and Top 20 solutions (“Top 20 GOF”, right graph) are shown for each model. Results are from the 2000 LHMC runs.

It was not necessarily expected that the Top 20 solution set would identify the same strong parameters as the “all candidates” solution set; the number of candidates was simply too small and was much more likely to be affected by arbitrary parameter distributions. However, it might be expected that if a parameter is truly “strong” that it would show a bias toward the same values in the Top 20 solution set as the “all candidates” solution set. The later expectation was supported by the heat recovery effectiveness (p7) distribution in Figure 7-18, which showed a bias toward state 2 in both the “all candidates” solution set⁵ and in the Top 20 solution set for all three building models. Conversely, the temperature settings (p14) showed a strong bias toward state 2 (Detailed-Corrected and Detailed-Original) and state 1 (Simple) in the “all candidates” solution set and toward state 3 for all models in the Top 20 solution set. In this case, the results for the “all candidates” solution set matched with the expected values from conversations with building managers (state 2), while the Top 20 solutions did not.

The appearance of the schedules (p15) in state 1 for both the Detailed-Corrected and Detailed-Original models 100% of the time was imposed by the modeler based on the high level of certainty in the value of this input. However, in the semi-calibrated Simple model this parameter was permitted to vary between states 1 and 3. The results showed a strong bias toward state 1 for both the “all candidates” and Top 20 solution sets, as was expected.

Overall, the three models showed similar parameter distributions, especially when observing the strong parameters in the Top 20 solution sets. However, the Detailed-Corrected model highlighted both the Main building (p7) and Annex (p8) heat recovery effectiveness as strong parameters, and showed a bias toward high heat recovery effectiveness (state 3) in both models. This was contrary to the Detailed-Original and Simple models, which appeared with a bias toward a moderate (state 2) Main system heat recovery effectiveness (p7) and did not identify the Annex heat recovery efficiency (p8) as a strong parameter.

7.3.3.1 Manual Calibration: Fine grid MCA/Freezing strong parameters and other optional steps

The authors also explored the potential of two optional steps: the “freezing” of strong parameters and a fine grid search. In the Detailed-Original case, the parameters that appeared as strong after 2000 simulations were frozen at their dominant values and an additional batch of

⁵ Except the Detailed-Corrected model, which tends toward state 3 in the “all candidates” solution set.

simulations was run. This resulted in the identification of further strong parameters, but as a drawback also produced poorer (increased) GOF values, as shown in Table 7-7. The fine grid search, instead, resulted in only minor improvements in the GOF values for each of the four cases, again shown in Table 7-7.

7.3.4 LHMC Calibration: Lessons Learned

The proposed LHMC procedure has the potential to identify multiple calibrated solutions for a more robust analysis of energy conservation measures (ECMs), to save time in developing calibrated models, and to reduce modeler bias during calibration.

In this study, running the LHMC analysis on the manually calibrated Detailed-Original and Detailed-Corrected cases resulted in only a small improvement in the statistical fit between simulated and measured data, and identified a set of Top 20 candidate solutions. Similar results were observed for the semi-calibrated Simple case; the fit between simulated and measured data in this case was less accurate but still largely within the threshold values of the NMBE and CVRMSE that were defined in ASHRAE Guideline 14 [ASHRAE 14 2002].

The stabilization of strong parameters was suggested in RP-1051 [Reddy 2006] as the guide to determine the number of simulations to be run; here, this was found to be insufficient. No definitive criteria were found to unquestionably identify the optimal number of simulations for any case. Rather, the number of simulations (2000) was empirically recognized by observing the strong parameters, the goodness of fit, and the distribution of the solutions. Optional steps like the freezing of strong parameters or the fine grid search brought about only minor benefits.

The LHMC analysis accounts for model uncertainties by using the GOF statistic to identify a number of feasible candidate solutions, in which, the true solution is expected to lie. The ability of the LHMC to reach calibrated solutions appears to be strong; multiple solution vectors were identified in the case of the Detailed-Original, Detailed-Corrected, and Simple models. However, based on observed differences between the “all candidates” and Top 20 solution sets, the use of the monthly GOF as the metric for ranking the calibrated solutions appeared to be somewhat arbitrary.

The choice of the Top 20 solutions was also somewhat arbitrary, which is of consequence when one considers how computationally expensive it may be to run many simulations during the ECM energy savings analysis. As an example, if one were to run a parametric ECM analysis

with three ECMs, each with three states, this would require $3^3 = 27$ simulations when using a single calibrated solution. This number increases to more than $20 \times 27 = 540$ simulations when using the Top 20 solutions. The linearity of this relationship means that even reducing the number of Top solutions to 10 would decrease the computational time by half.

The Detailed-Original and Detailed-Corrected models showed similar levels of calibration. The Detailed-Original model obtained a slightly lower monthly GOF, while the Detailed-Corrected showed a tendency toward higher heat recovery effectiveness in its “all candidates” solutions. However, both models tended toward similar parameter distributions in their Top 20 solution sets, which was expected to be reflected in the retrofit analysis performed in Chapter 8.

7.4 Lessons Learned: Calibration

Both the manual and LHMC calibrations were able to identify models that achieved calibration on the basis of the monthly NMBE and CVRMSE statistics defined in ASHRAE Guideline 14 [ASHRAE 14 2002]; neither was able to achieve hourly calibration.

The LHMC was not able to identify the modeller errors highlighted in the adjusted manual calibration in section 7.2. This was because the LHMC was only able to identify strong parameters from amongst those inputs that were selected by the modeller to be varied during the LHMC. The modeller errors were only caught upon further review leading up to retrofit. It cannot be emphasized enough that all inputs must be justified prior to accepting a model to be calibrated.

The availability of hourly data and detailed input information made manual calibration a reasonable option for modelling the Steindal School. However, in models with less data availability, such as the Simple model, for which manual calibration tended to be more difficult, LHMC was capable of identifying calibrated solutions.

The GOF statistic used in the LHMC procedure recommended in RP-1051 [Reddy 2006] appeared to be somewhat arbitrary. However, it is beyond the scope of this work to devise an alternative method for highlighting the most well calibrated solutions, although suggested methods for further investigations include comparison against representative hourly profiles (as in work by Soebarto [Soebarto 1997]) or the application of a GOF that is weighted to account for variations in monthly utility billing (i.e. weighted to emphasize fit with the winter months).

RP-1051 [Reddy 2006] highlights the ability of the LHMC analysis to create multiple models for increasing the certainty in ECM savings prediction. This will be investigated in Chapter 8 on retrofit and compared against the predicted ECM savings for the Original and Corrected manually calibrated models. Additionally, the differences in the energy savings predictions of the Original and Corrected models were observed during retrofit (Chapter 8) to understand the implications of the differences in inputs that resulted from the manual calibration.

8 Retrofits

The retrofit analysis that was performed focused on decreasing the energy consumption in the Steindal School through the installation of retrofits, or Energy Conservation Measures (ECMs); the two terms will be used interchangeably in this work. Conversations with the Trondheim Municipality emphasized an interest in both reducing energy consumption and identifying alternatives to the current electric resistance heating system.

The retrofit analysis performed in this work followed the steps outlined in Figure 8-1.

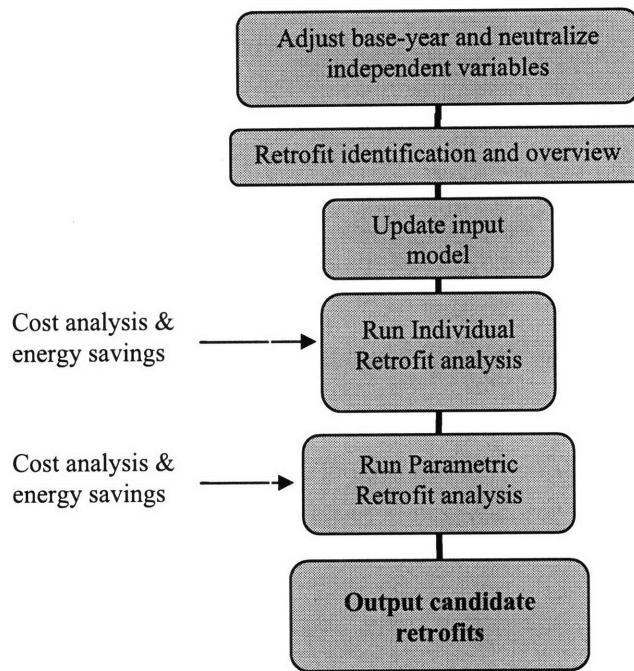


Figure 8-1: Steps followed in performing the retrofit analysis of the Steindal School.

First, base-year adjustments were made to incorporate changes to the building that occurred after the calibration period, in this case from January 2007 through January 2008. Additionally, independent variables, namely weather, were neutralized for both the pre-retrofit and post-retrofit models. This was done to ensure that changes in energy consumption were due only to the retrofits under consideration, not to differences in weather conditions between the base-year and retrofit simulations.

Two retrofit analyses were performed: an Individual Retrofit analysis and a Parametric Retrofit analysis. The Individual Retrofit analysis focused on the potential for energy savings in the Steindal School due to single component retrofits. The Parametric Retrofit analysis

investigated the potential for energy savings due to various retrofit combinations. These analyses focused on the following issues:

Individual Retrofit

- Predicted annual energy savings due to single component retrofits
- Quantifying uncertainty in energy savings predictions
- Differences in predicted energy savings between the manually and Latin Hypercube Monte Carlo (LHMC) calibrated models
- Differences in predicted energy savings between the Detailed and Simple models
- Evaluating the consequences of using fewer than the Top 20 LHMC candidates for retrofit evaluation
- Means of selecting cost effective retrofit options

Parametric Retrofit

- Obtainable Energy Performance in Building Directive (EBPD) ratings under various retrofit conditions
- Validity of estimating the energy savings from retrofit combinations by summing the energy savings from individual retrofit components

The Individual Retrofit analysis was performed with the five models listed in Table 8-1.

The Original and Corrected models were both manually calibrated and were examined to assess

LHMC (Top 20)	Detailed-Corrected Detailed-Original Simple
Manual	Original Corrected

Table 8-1: Calibrated models with which the retrofit analysis of the Steindal School was performed.

the influence of modeler errors on retrofit energy savings predictions. The Individual Retrofit analysis also considered all of the “Top 20 solutions” from three the LHMC calibrated models. The Detailed-Original and Detailed-Corrected models represented “well-calibrated”

models; the Simple model represented a “reasonably calibrated” model.

The Parametric Retrofit analysis was run only on the manually calibrated Corrected model. This was the model that had (1) the highest level of modeler confidence in its calibration and (2) was accepted as most representative of the conditions in the Steindal School. This is discussed further in section 8.4.

This work was performed in parallel with that by Sartori [Sartori 2008b], in which simulations were run to assess the potential for meeting the passive house [DHV 2006] standard through retrofit of the Steindal School. Additional information about the Passive House retrofit

of the Steindal School may be found in work by Sartori [Sartori 2008a] and Sartori and Wachenfeldt [Sartori 2008b].

8.1 Base-year Adjustments

Prior to running the retrofit analysis, the calibrated models were updated to include changes that were made to the Steindal School after the calibration year, starting in 2007. Conversations with building managers indicated that the only change was in the temperature setpoints in the 1st Floor classrooms and the Annex. These were increased from 20°C /18°C (occupied/unoccupied) to 21°C /19°C – the same temperature settings as in the Offices. No changes to the length or duration of the temperature schedules were made.

In the interest of generalizing the building model for any future year the schedule that was created during calibration to reduce the ventilation fan speed at extremely low outdoor temperatures ($T_{\text{outdoor}} < -6^{\circ}\text{C}$) was removed during the base-year adjustments. This schedule had been implemented for those periods with extremely low temperatures in 2006 and was specific to that year. No other schedule changes were made to the base-year model.

8.1.1 Comparison with Utility Data from 2007

Each of the five input models was then run with a modified IWEC Oslo weather file that included 2007 temperature data. The Top 20 solutions were run for each of the LHMC calibrated models; a single solution was run for each of the manually calibrated models. The results of these simulations were compared to utility data from 2007 that was available after the model calibration had been performed. The coefficient of variation of the root mean square error (CVRMSE), normal mean bias error (NMBE), and goodness of fit (GOF) were calculated on a monthly basis (Table 8-2) and those simulations with $\text{CVRMSE} \leq 15\%$ and $\text{NMBE} \leq 5\%$ were considered to be calibrated. The number of calibrated “candidates” is indicated in the far right column of Table 8-2 as a fraction of the maximum possible candidates (twenty in the LHMC calibrated models and one in the manually calibrated models). The CVRMSE and NMBE are shown for the simulation with the lowest GOF value. The minimum and maximum GOF of the Top 20 solutions is shown for the three LHMC calibrated models; the GOF of the single calibrated solution is shown for the two manually calibrated models.

2007 Data		Energy		Power		GOF	# Cand.
		NMBE	CVRMSE	NMBE	CVRMSE		
LHMC	<i>Detailed-Corrected</i>	4.68	12.77	2.70	11.43	8.99 -11.7	5 of 20
	<i>Detailed-Original</i>	0.89	11.03	-0.44	12.13	8.21 -10.71	4 of 20
	<i>Simple</i>	3.46	11.78	-0.23	12.58	9.15 -17.15	3 of 20
Manual	<i>Original</i>	1.02	11.92	-4.58	14.61	9.72	1 of 1
	<i>Corrected</i>	0.02	12.03	-5.75	15.40	10.2	0 of 1

Table 8-2: Monthly CVRSME, NMBE and GOF resulting from the comparison between the five 2006 calibrated models (with increased temperature setpoints) and the 2007 utility data.

Table 8-2 indicates that the LHMC models were able to identify between 3 and 5 calibrated models from amongst their Top 20 solutions. It was expected that with more specific daily schedules from 2007 a better fit with both measured energy consumption and peak power data would be achieved and a greater number of candidates would be found. However, recalibrating the models against 2007 data was outside of the scope of this work.

8.1.2 Neutralizing Weather Conditions

In the absence of a quality weather data from Trondheim depicting all of the weather conditions (solar radiation, temperature, wind, etc.) necessary to define an EnergyPlus weather file, the decision was made to use the unaltered International Weather for Energy Calculations (IWEC) weather file from Oslo, Norway to perform the retrofit analysis. It was recognized that differences existed in the seasonal temperature swings and solar exposure in Oslo and Trondheim, but in the absence of quality data from Trondheim these were taken to be acceptable.

8.1.3 Resolving the “baseload”

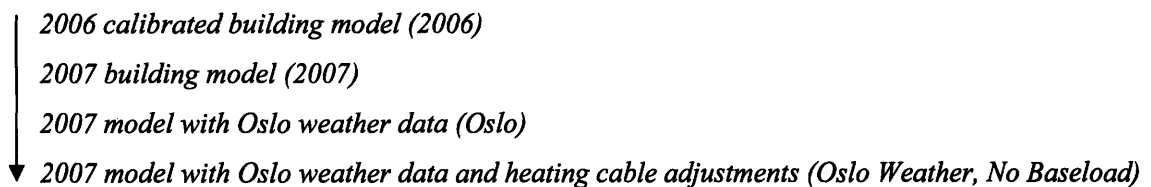
The final base-year adjustment altered the control of the electric resistance heating cables from a constant load to a temperature controlled load. This required that the electric resistance heating cables in the gym (5 kW) and wardrobes (6 kW) be properly controlled according to the indoor temperature setpoint. Additionally, the electric resistance heating cables in the bomb shelter (2 kW) and the offices (6 kW) were unnecessary and were disconnected. These changes resulted in an overall decrease in the annual energy consumption in the building of 16 kWh/m²/year, or 8%, of the building’s annual energy consumption. This difference was especially apparent during the summer when the electric resistance cables had previously been providing excess heating energy (Figure 8-2). Additionally, these base-year changes were the

first “retrofits” that were simulated, and it was assumed that these changes were made prior to moving forward with the Individual and Parametric Retrofit analyses.

8.1.4 Base-year Model: Monthly Energy Consumption

At this point all of the 2006 calibrated models: the Top 20 solution from the Detailed-Corrected, Detailed-Original, and Simple LHMC calibrated models and the single solution from the Corrected and Original models were at base-year conditions, and were considered ready for the retrofit analysis.

Figure 8-2 shows the monthly energy consumption of each simulation in the progression from the 2006 calibrated Corrected model to the base-year Corrected model. The 2006 and 2007 measured utility data from the Steindal School (2006 Utility Data and 2007 Utility Data) are also shown. The progression from the 2006 calibrated model to the base-year models was as follows:



All 2006 data is shown in green, all 2007 data is shown in blue/purple, and all Oslo weather file data is shown in orange/red. The base-year model is represented by the “Oslo Weather, No Baseload” data.

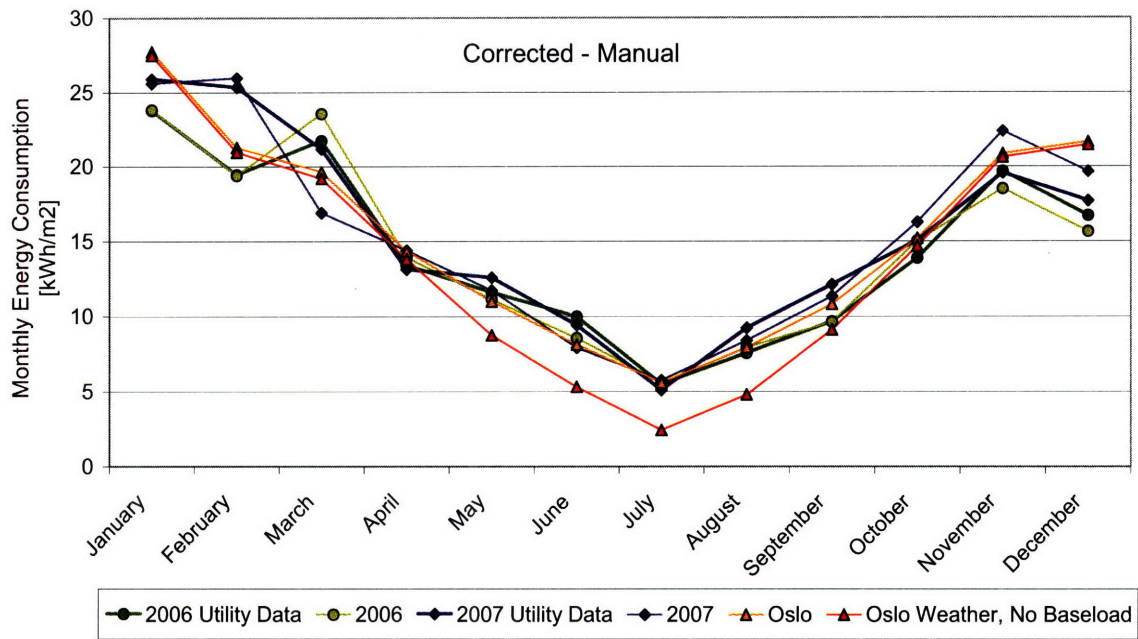


Figure 8-2: Monthly energy consumption of the four models that were developed in each step of the base-year model definition (kWh/m^2). The monthly utility data from 2006 and 2007 are also shown. The results are for the Corrected building model.

Figure 8-2 shows that the model with the unaltered IWEC Oslo weather file compares favorably with those models with the 2006 temperature and wind data from Trondheim, increasing the confidence that the Oslo weather file was an acceptable choice for neutralizing the weather conditions between the base-year and future retrofit simulations. Although Figure 8-2 only shows the results for the Corrected model, similar behaviors were observed for the Original, Detailed-Corrected, Detailed-Original, and Simple models when the progression from the 2006 model to the base-year model was plotted.

To summarize, the base-year changes that were made to the 2006 calibrated models included increases in temperature setpoints, the removal of the 2006 half fan speed ventilation schedule, and the adjustment of the “baseload” heating to operate according to temperature setpoints. Additionally, all retrofits were run with the IWEC Oslo weather file to neutralize the pre-retrofit and post-retrofit weather conditions.

8.2 Retrofit Identification and Overview

A list of potential retrofits (see Table 8-3) was generated for the retrofit analysis. Two sets of retrofits were simulated. The first set of retrofits was simulated in the interest of decreasing the energy consumption in the school (Energy Conservation Measures). The second set of retrofits included changes to the building's heating system to reduce the school's dependence on electricity for heating (Alternative Heating Supply Retrofits).

Unless otherwise specified, the energy referred to here, and in all future analyses, was the energy consumed at the building site.

Energy Conservation Measures	
HEATING & CONTROLS	
<ul style="list-style-type: none"> • Temperature Setback 	
VENTILATION	
<ul style="list-style-type: none"> • Heat Exchanger Effectiveness • Ventilation Flow Rate • Occupant Controlled Ventilation 	
ENVELOPE	
<ul style="list-style-type: none"> • Window U-value • Wall U-value • Ground U-value • Roof U-value • Infiltration Rate 	
TEMPERATURE INDEPENDENT LOADS	
<ul style="list-style-type: none"> • Lighting Density 	
Alternative Heating Supply Retrofits	
<ul style="list-style-type: none"> • Hydronic Heating w/Oil Boiler • Hydronic Heating w/District Heat 	

Table 8-3: List of candidate retrofits for possible installation in the Steindal School.

Each retrofit was assigned three discrete states: current, moderate, and low-energy. Where possible, the moderate state was equal to the value prescribed in the 2007 Norwegian Building Codes (NBC), while the low-energy state was equivalent to a value beyond the code requirements. The "current" value of each retrofit in section 8.2.1 corresponds to the input state from the manually calibrated Corrected model. However, it should be recognized that each of the five calibrated models assumed different input states for a number of the retrofit parameters (Chapter 7), and the retrofit energy savings were calculated accordingly. The consequences of this variation are discussed in the retrofit results in section 8.3.

The heating supply retrofits were only assigned a single retrofit value, equal to the required system capacity to meet the current heating demands in the building.

Unless otherwise noted, all cost data was taken from the Norwegian Holteprojeskt [Holte 2007], [FDV 2007] database (in Norwegian) and from the RS Means [Means Ass. 2007], [Means Fac. 2007], [Means LC 2007], [Means Mech. 2007], [Means SF 2007] database of United States construction costs. There was a high degree of uncertainty in the values of these costs stemming from:

1. Generalized costs

- For example, the Holteprojeskt database specified fan replacement costs for systems with 30,000 m³/hr and 60,000 m³/hr flow rates, but none of the values in between. In such cases interpolation was performed to find the cost of intermediate retrofits.

2. Conversion factors

- A conversion of six Norwegian Kroner (NOK) for each US dollar (USD) was used to convert the RS Means cost estimates to Norwegian cost estimates. Conversations with building managers indicated that this was likely to lead to an underestimate of the actual Norwegian costs [Arentz 2007].

3. Lack of data and differences in construction practice

- Data for certain retrofits were unavailable, especially when using the Holteprojeskt database.
- No cost data were available for the specific procedures followed in retrofitting the building envelope. Approximations were made according to the anticipated materials and labor hours necessary.
- Constructions in the US commonly use different materials than Norwegian constructions. For example, fiberglass insulation is the most typical insulation material in the US, while mineral wool insulation is more commonly used in Norway. In such cases approximations were made using the closest possible materials.

Therefore, costs from the US database were examined to assess the relative accuracy of the cost estimates from the Norwegian database.

8.2.1 Energy Conservation Measures

A brief description of each of the retrofits installed during the Individual Retrofit analysis follows. Included are justifications for each retrofit state, the anticipated costs of each retrofit, and the expected lifetime of each retrofit. The anticipated procedure for installing each retrofit is also discussed. All discussion of retrofit conditions and procedures refer to the EnergyPlus simulations that were run; none of these retrofits were actually installed in the Steindal School at the time of this analysis.

8.2.1.1 Heating & Controls

8.2.1.1.1 Temperature Setback

The current temperature setback in the school is equal to 2°C, which is roughly equivalent to that recommended in the 2007 Norwegian Building Codes (see Table 7 in Chapter 2).

The moderate 4°C temperature setback retrofit was taken as typical based on conversations with building managers at the Norwegian University of Science and Technology that indicated occupied/unoccupied temperature settings for university buildings that were equal to 23°C /19°C [Hansen 2007]. The low-energy retrofit had a temperature setback of 6°C, which reduced the unoccupied temperature in the school to 15°C, which was nearly equal to the vacation temperature setting of 14°C.

A ramping period was implemented during the morning hours on occupied weekdays to decrease the potential spikes in power resulting from the need to heat the building's thermal mass (see Appendix A) for additional information on thermal mass and temperature ramping). A 2°C per hour ramp was instituted with this retrofit and was automated to allow the building to reach the occupied temperature according to current schedules.

TEMPERATURE SETBACK	Degrees of Temperature Setback [°C]		
	Current	Moderate	Low-Energy
Temperature Setback (With ramping of 2°C/hour)	2	4	6

Table 8-4: Definition of the moderate and low-energy temperature setback retrofit with ramping. The ramping gradient was 2 degrees/hour.

This retrofit would be implemented by changing the temperature setpoints and schedules at the Trondheim Municipality's control center. Therefore, no demolition or removal would be

required to institute this retrofit. Additionally, the cost of this retrofit was assumed to be equal to the labor rate for the workers in the central control center, which was approximated as zero NOK.

8.2.1.2 Ventilation

8.2.1.2.1 Occupant Controlled Ventilation (OCV)

The current ventilation system is a constant air volume system with two air handlers supplying 100% outdoor air to two building zones. The ventilation is currently run from 6:00-16:00 in the Main building and 6:00-16:30 in the Annex on occupied days; there is no ventilation during unoccupied periods (nights and weekends). Ventilation is also available on select evenings when activities are going on in the school (see Table 5-22 in Chapter 5).

The OCV retrofit broke the building up into five ventilation zones: the Offices, 1st Floor, Bomb Shelter, Gymnasium, and Annex. The flow rate of air to each building zone was assigned based on the floor area and occupancy schedule of each space. Whenever a zone was occupied ventilation was supplied, when it was unoccupied no ventilation air was provided.

The moderate retrofit state instituted only a change in ventilation zone controls; the maximum air flow to the building when all zones were occupied was still equal to 2.9 L/m²/sec (46,800 m³/hr; 13m³/sec).

The low-energy retrofit instituted a change in the ventilation zone controls in addition to a reduction in the maximum ventilation air flow rate. The maximum ventilation air flow rate was reduced to the level required to meet the indoor air quality needs of the fewest number of occupants in a typical Norwegian building and was calculated according to Equation 8-1.

$$\dot{V}_{ventilation} = \frac{\dot{V}_{person} * n + \dot{V}_{materials} * A_{conditioned}}{A_{conditioned}} = \frac{4 * 340 + 0.8 * 4,400}{4,400} = 1.1 \frac{L}{m^2 s} \quad (8-1)$$

$\dot{V}_{ventilation}$	Ventilation air flow rate [L/m ² /sec]
\dot{V}_{person}	Outdoor air flow per person [L/person/sec]
$\dot{V}_{materials}$	Outdoor air flow for materials [L/m ² /sec]
$A_{conditioned}$	Conditioned floor area [m ²]
n	Maximum number of people [people]

The maximum ventilation flow rate ($V_{\text{ventilation}}$) with the low-energy retrofit was equal to 1.1 L/m²/sec (4.8 m³/sec) and was appropriate for a typical (non low-polluting) building (0.8 L/s/m²) with the fewest number of satisfied occupants (4 L/s/person) in Norway (see Table 2-3 in Chapter 2). In addition, the 1.1 L/m²/sec corresponded with the minimum outdoor air flow rate for “medium” air quality according to European Standard EN 13779 (Table 2-4 in Chapter 2, and the required outdoor air flow rate for acceptable air quality in classrooms in ASHRAE Standard 62 (Table 2-5 in Chapter 2).

VENTILATION SCHEDULES	Current	Moderate	Low-Energy
Flow Rate [L/m ² /sec]	2.9	2.9	1.1
Schedule	Always on	Zone occupancy	Zone occupancy

Table 8-5: Definition of the occupant controlled ventilation retrofit. Both the schedules of operation and maximum ventilation air flow rates (L/m²/sec) are shown.

The moderate retrofit state would allow for the ventilation system to continue operation with the current fans. However, dampers, damper motors, and damper controls would need to be installed at the inlet and return for each zone, and new fan controls would need to be installed to allow variable volumes of air flow.

The low-energy retrofit would require the installation of dampers and flow controls in the existing ventilation system. In addition, new fans with a lesser power consumption would need to be installed in the Main building to optimize the system efficiency at the lower air flow rates. Observation of performance curves for the existing ventilation fans indicated that the 4.8 m³/sec ventilation flow rate was at the lower end of their operable range, meaning that the fan efficiency was reduced to nearly 50% [Zhiel-Abegg 2008] at this flow rate. Additionally, because the flow rate was expected to dip below 4.8 m³/sec maximum during the occupant controlled operation of the system, it was anticipated that more appropriate ventilation fans would be necessary to enable the most effective operation of the ventilation system. To maintain consistency with the existing ventilation system the new fans would be centrifugal fans with 70%-73% total efficiency at a pressure drop between 600-900 Pa [Zhiel-Abegg 2008]. This would result in a power demand of approximately 4 kW per fan (calculated according to Equation 5-3 in Chapter 5).

In both the moderate and low-energy retrofits, the fans in the Annex were expected to remain unchanged except for the addition of occupant controlled ventilation “on-off” switches and controls.

Maintenance was expected to be limited for the occupant controlled ventilation retrofit. However, the installation of a sophisticated controls system would require that a specialized technician be hired to perform future system maintenance.

OCCUPANT CONTROLLED VENTILATION		Demolition and Removal	New Installations			Total Investment Cost	Lifetime [years]
Retrofit State	Source of Estimate	Fan removal	Dampers, motors, and damper controls	Fan controls	New fans		
Moderate	<i>RS Means</i>	X	<i>Included in fan controls</i>	17,800 USD	X	17,800 USD 106,800 NOK	10
	<i>Holte-projeskt</i>	X	25,000 NOK	24,200 NOK	X	49,200 NOK	18
Low-Energy	<i>RS Means</i>	4,150 USD	20,500 USD	17,800 USD	19,700 USD	62,150 USD 372,900 NOK	10
	<i>Holte-projeskt</i>	<i>Included in new fan costs</i>	25,000 NOK	7,900 NOK	132,700 NOK	165,600 NOK	18

Table 8-6: Estimated cost of installing the occupant controlled ventilation retrofit in the Steindal School. Cost estimates are shown from both US and Norwegian databases [Means Mech. 2007],[FDV 2007].

8.2.1.2.2 Ventilation Flow Rate

The existing ventilation system in the Steindal School supplies 100% outdoor air to the building. The current 2.9 L/m²/sec outdoor air flow rate from ventilation is well above the 1.1 L/m²/sec (4.7 m³/sec) that was calculated for a typical Norwegian building with the fewest number of satisfied occupants (see Table 2-3 in Chapter 2). As such, the moderate retrofit state adopted 1.1 L/m²/sec as the ventilation flow rate in the Steindal School.

The low-energy retrofit state corresponded to the lowest allowable ventilation rate for acceptable indoor air quality in a Norwegian building with low-polluting materials and the fewest number of satisfied occupants (see Table 2-3 in Chapter 2) and was equal to 0.7 L/m²/sec. This 0.7 L/m²/sec air flow rate also corresponded with the “acceptable” level of indoor air quality recommended in European Standard EN13779 in Table 2-4 in Chapter 2.

VENTILATION FLOW RATE	Current	Moderate	Low-Energy
Ventilation rate [L/m ² /s]	2.9	1.1	0.7

Table 8-7: Definition of the moderate and low-energy ventilation flow rate retrofit states (L/m²/sec).

In both the moderate and low-energy retrofit states the old fans should be removed and new fans should be installed to handle the more than 50% reduction in air flow rate. Although the existing fans are capable of handling the air flow rates at the moderate retrofit state, the

efficiency of the fans at this lower flow would be increased, meaning that the optimal energy savings would not be achieved. To obtain the greatest energy savings at the reduced flow rates new fans should be installed. The specifications for these fans were discussed with respect to the occupied ventilation retrofit, and would require approximately 4 kW of power per fan.

The estimated investment costs and service lifetime for the moderate and low-energy ventilation retrofits are given in Table 8-8.

VENTILATION FLOW RATE		Demolition and Removal	New Installations	Total Investment Cost	Lifetime [years]
Retrofit State	Source of Estimate	Fan Removal	New fans		
Moderate	RS Means	4,150 USD	19,700 USD	23,850 USD 143,100 NOK	10
	Holte-projekt	Included in new fan cost	132,700 NOK	132,700 NOK	18
Low-Energy	RS Means	4,150 USD	19,700 USD	23,850 USD 143,100 NOK	10
	Holte-projekt	Included in new fan cost	132,700 NOK	132,700 NOK	18

Table 8-8: Estimated cost of installing the ventilation rate retrofit in the Steindal School. Cost estimates are shown from both US and Norwegian databases [Means Fac. 2007],[FDV 2007].

8.2.1.2.3 Ventilation Heat Recovery Effectiveness

The current heat recovery effectiveness in the manually calibrated Corrected model is equal to 55%. The moderate ventilation heat recovery effectiveness retrofit was assigned according to the 2007 Norwegian Building Codes [BE 2008a] and was equal to 70%. The low-energy value corresponded to a typical rotary wheel heat recovery unit with an effectiveness just beyond code at 80% [Schild 2004].

VENTILATION HEAT RECOVERY EFFECTIVENESS	Current	Moderate	Low-Energy
Effectiveness, η [%]	55	70	80

Table 8-9: Definition of the moderate and low-energy heat recovery effectiveness retrofit values for the Main ventilation system (%).

The moderate retrofit case would require that the existing ventilation system to be cleaned and sealed to reduce leakage and improve heat transfer across the two rotary wheels. This should allow for an efficiency of 70% to be obtained and sustained with future maintenance.

In order to achieve and effectiveness of 80% in the low-energy retrofit the existing heat exchanger system must be upgraded. Manufacturer's data [NVP 1997] indicated a maximum efficiency of 75% for the existing system, making replacement necessary to reach the target

efficiency of 80% at the current ventilation flow rates. With improved maintenance and reduced ventilation flow rates it might be possible to achieve 80% heat recovery effectiveness with the existing system. However, the existing rotary wheels are from the 1978 construction and have been in use well beyond their expected lifetime of 16-20 years [FDV 2007]. Therefore, the low-energy retrofit in this analysis considered the replacement of these units. This would require the removal of the existing system and the installation of new controls, motors, and rotary wheels in the air handler.

HEAT RECOVERY EFFICIENCY		Demolition and Removal	Maintenance	New Installations	Total Investment Cost	Lifetime [years]
Retrofit State	Source of Estimate	Existing heat recovery system	Cleaning and Maintenance	Enthalpy wheel heat recovery and motor		
Moderate	<i>RS Means</i>	X	1,900 USD	X	1,900 USD 11,400 NOK	10
	<i>Holte-projeskt</i>	X	15,800 NOK	X	15,800 NOK	18
Low-Energy	<i>RS Means</i>	800 USD	X	27,700 USD	28,500 USD 171,000 NOK	10
	<i>Holte-projeskt</i>	<i>Included in new enthalpy wheel cost</i>	X	242,000 NOK	242,000 NOK	18

Table 8-10: Estimated cost of installing the heat recovery ventilation retrofit in the Steindal School. Cost estimates are shown from both US and Norwegian databases [Means Mech. 2007],[Means Fac. 2007],[FDV 2007].

8.2.1.3 Envelope

In making changes to the building envelope potential issues with moisture (condensation) will be neglected in this analysis. However, it is understood that this, in addition to high costs, is one of the major impediments to retrofitting the building envelope to very low U-values.

8.2.1.3.1 Window U-Value

The windows on the North façade of the Main building were installed in 1978, and have a manufacturer U-value equal to 2.9 W/m²K. Both the South windows in the Main building and the Annex windows were installed in 1997 and have manufacturer specified U-values equal to 1.1 W/m²K [Pilkington 2007]. These were the center of glazing U-values. The EnergyPlus simulations accounted for the window frame and the divider and had an increased U-value.

The moderate window retrofit corresponded to the U-value required in the 2007 Norwegian Building Code [BE 2008a] and was equal to 1.2 W/m²K. This U-value included the window glazing, frame, and dividers. The South windows in the Main building and the Annex

windows all had U-values near the code value, and were not retrofit in the moderate case. Only the North windows in the Main building were retrofit to meet the code U-value.

The low-energy window retrofit, with a center of glazing U-value equal to 0.8 W/m²K, corresponded to the lowest energy argon filled window supplied by Pilkington glass [Pilkington 2007], the manufacturer of the windows in both the Annex and the Main building. All of the windows were retrofit in the low-energy case.

It was assumed that the infiltration rate was unaffected by the change in windows and window frames for these retrofit states. This assumption was made to distinguish between energy savings resulting from improved window U-values and reduced infiltration, the latter of which was investigated as an independent retrofit.

WINDOW U-VALUE	Current	Moderate	Low-Energy
North [W/m ² K]	2.9	1.2	0.8
South/Annex [W/m ² K]	1.1	1.1	0.8

Table 8-11: Definition of the moderate and low-energy window U-value retrofit states (W/m²K).

In the moderate case new windows and frames would be installed for all windows on the North façade (160 windows) of the Main building. In the low-energy case all windows and frames on the North and South facades (249 windows) of the building would be replaced.

WINDOW U-VALUE		Demolition and Removal		New Installations		Total Investment Cost	Lifetime [years]
Retrofit State	Source of Estimate	Remove existing North windows	Remove existing South windows	North windows	South windows		
Moderate	RS Means	3,600 USD	N/A	76,150 USD	N/A	79,750 USD 478,500 NOK	40
	Holte-projekt	<i>Included in new window cost</i>	N/A	976,800 NOK	N/A	976,800 NOK	27
Low-Energy	RS Means	3,600 USD	2,000 USD	104,950 USD	56,500 USD	167,050 USD 1,002,300 NOK	40
	Holte-projekt	<i>Included in new window cost</i>	<i>Included in new window cost</i>	993,200 NOK	552,500 NOK	1,545,700 NOK	27

Table 8-12: Estimated cost of installing the window U-value retrofits in the Steindal School. Cost estimates are shown from both US and Norwegian databases [Means Mech. 2007],[Means Fac. 2007],[Means LC 2007],[FDV 2007].

8.2.1.3.2 Exterior Wall U-Value

The current U-value of the exterior walls varies between 0.25 W/m²K and 0.30 W/m²K in the Annex and the Main building, respectively. The moderate retrofit U-value was taken from the 2007 Norwegian Building Code [BE 2008a], and was equal to 0.18 W/m²K. The suggested low-energy U-value was taken to be lower than the code value, and was equal to 0.1 W/m²K [Engblom 2006].

EXTERIOR WALL U-VALUE	Current	Moderate	Low-energy
Main walls [W/m ² K]	0.30	0.18	0.1

Table 8-13: Definition of the moderate and low-energy wall U-value retrofit states (W/m²K).

The course of action in lowering the U-value of the walls was to install additional insulation and cladding on the exterior of the building, as per common practice in Norway [NBI Walls 2006].

In order to achieve the moderate retrofit an additional 9 cm of insulation would be installed at a conductivity of 0.043 W/mK. In the low-energy case, 29 cm of mineral wool insulation with a conductivity of 0.043 W/mK would be added, more than doubling the thickness of the exterior walls. Lower conductivity insulating materials would help to reduce the volume of required materials, but would also have a higher associated cost.

WALL U-VALUE		Demolition and Removal	New Installations		Total Investment Cost	Lifetime [years]
Retrofit State	Source of Estimate		9 cm of mineral wool, studs, and wood cladding	29 cm of mineral wool, studs, and wood cladding		
Moderate	<i>RS Means</i>	X	76,500 USD	X	76,500 USD 459,200 NOK	40
	<i>Holte-projeskt</i>	X	505,400 NOK	X	505,400 NOK	20-30
Low-Energy	<i>RS Means</i>	X	X	84,700 USD	84,700 USD 508,200 NOK	40
	<i>Holte-projeskt</i>	X	X	558,200 NOK	558,200 NOK	20-30

Table 8-14: Estimated cost of installing the wall U-value retrofit in the Steindal School. Cost estimates are shown from both US and Norwegian databases [Means Mech. 2007][Means Fac. 2007],[Means LC 2007],[FDV 2007].

8.2.1.3.3 Roof U-Value

The roof constructions in the South half of the Main building and the Annex are similar, both have a U-value equal to 0.18 W/m²K. However, the North roof above the Main building was separated from the conditioned 1st Floor by the open Underroof space. In order to provide a

conservative estimate of the U-value of the North roof, only the materials in the 1st Floor ceiling were accounted for in the calculation of the U-value; the insulating effect of the open Underroof space was neglected. This was done because there was no insulation in the Underroof space or in the roof structure above it, and so nearly all of the insulation between the heated portion of the building and the outdoor conditions was provided by the 15 cm of mineral wool in the 1st Floor ceiling.

The roof above the wardrobes constituted only a very small area compared to the Main building and Annex roofs, and was not considered for retrofit.

The moderate retrofit was defined according to the 2007 Norwegian Building Codes [BE 2008a] and was equal to 0.13 W/m²K, while the suggested low-energy U-value was taken to be lower than this, equal to 0.1 W/m²K [Engblom 2006].

ROOF U-VALUE	Current	Moderate	Low-Energy
Main building, South roof, and all Annex roofs [W/m ² K]	0.18	0.13	0.1
Main building, North roof [W/m ² K]	0.22	0.13	0.1

Table 8-15: Moderate and low-energy roof U-value retrofit states (W/m²K).

The U-value of the North roof would be reduced by adding insulation to the open Underroof space. The moderate retrofit would require that 17 cm of mineral wool be added, while the low-energy retrofit state would require that 27 cm of mineral wool be placed in the Underroof above the 1st Floor ceiling. The conductivity of the insulation was assumed to be 0.043 W/mK.

The South roof over the Main building and in the Annex roof would both require more drastic retrofit measures to achieve the moderate and low-energy U-values. Additional insulation would need to be installed on the roof's interior. The insulation added was assumed to be mineral wool with a conductivity of 0.043W/mK, and the amount of insulation added to the roof was equal to of 10 cm and 20 cm in the moderate and low-energy retrofit cases, respectively.

The moderate and low-energy retrofit would require that the existing ceiling tiles in the South half of the 1st Floor in the Main building and the entire Annex be removed and replaced to accommodate the additional insulation. No demolition would be necessary to retrofit the North roof above the Underroof in the Main building.

UNDERROOF		Demolition and Removal	New Installations		Total Investment Cost	Lifetime [Years]
Retrofit State	Source of Estimate		17 cm insulation	27 cm insulation		
Moderate	RS Means	X	8,400 USD	X	8,400 USD 50,400 NOK	40
	Holte-projeskt	X	109,400 NOK	X	109,400 NOK	20-30
Low-Energy	RS Means	X	X	11,700	11,700 70,200 NOK	40
	Holte-projeskt	X	X	143,100	143,100 NOK	20-30

Table 8-16: Estimated cost of installing the North roof in the Main building U-value retrofit in the Steindal School. Cost estimates are shown from both US and Norwegian databases [Means Mech. 2007],[Means Fac. 2007],[HOLTE 2007],[MEANS LC 2007].

ANNEX AND SOUTH ROOF		Demolition and Removal	New Installations		Total Investment Cost	Lifetime [years]
Retrofit State	Source of Estimate		10 cm insulation, studs and gypsum	20 cm insulation, studs and gypsum		
Moderate	RS Means	17,100 USD	50,050 USD	X	67,150 USD 402,900 NOK	40
	Holte-projeskt	<i>Included in new install. cost</i>	490,200 NOK	X	490,200 NOK	20-30
Low-Energy	RS Means	17,100 USD	X	65,500 USD	682,600 USD 495,600 NOK	40
	Holte-projeskt	<i>Included in new install. cost</i>	X	582,300 NOK	582,300 NOK	20-30

Table 8-17: Estimated cost of installing the South roof in the Main building and the Annex roof U-value retrofits in the Steindal School. Cost estimates are shown from both US and Norwegian databases [Means Mech. 2007],[Means Fac. 2007],[HOLTE 2007],[MEANS LC 2007].

ALL ROOFS		Demolition and Removal	New Installations		Total Investment Cost	Lifetime [years]
Retrofit State	Source of Estimate					
Moderate	RS Means	17,100 USD	58,450 USD	X	75,550 USD 453,300 NOK	40
	Holte-projeskt	<i>Included in new install. cost</i>	599,600 NOK	X	599,600 NOK	20-30
Low-Energy	RS Means	17,100 USD	X	77,200 USD	94,300 USD 565,800 NOK	40
	Holte-projeskt	<i>Included in new install. cost</i>	X	725,400 NOK	725,400 NOK	20-30

Table 8-18: Estimated cost of installing all roof U-value retrofits in the Steindal School. Cost estimates are shown from both US and Norwegian databases [Means Mech. 2007],[Means Fac. 2007],[HOLTE 2007],[MEANS LC 2007].

8.2.1.3.4 Ground Floor and Ground Wall U-Values

The current U-values of the ground floor and the ground wall were calculated with the materials supplied by the architect. These U-values are equal to 0.6 W/m²K and 1.14 W/m²K, respectively. The moderate retrofit U-value equaled 0.15 W/m²K and was the U-value required in the 2007 Norwegian Building Code (NBC) [BE 2008a] for ground floors and walls. The low-energy U-value was taken to be smaller than this, and equal to 0.1 W/m²K [Engblom 2006].

GROUND FLOOR AND WALL U-VALUES	Current	Moderate	Low-Energy
Ground Floor [W/m ² K]	0.67	0.15	0.1
Ground Wall [W/m ² K]	1.44	0.15	0.1

Table 8-19: Moderate and low-energy ground floor and ground wall U-value retrofit states (W/m²K).

Both the low-energy and moderate retrofit states would require that additional insulation be added to the interior of the ground floor and ground wall to reduce the U-value of these constructions. The most common insulation for these installations is expanded polystyrene (EPS). For reasons of moisture control, it would be preferable to place the additional insulation on the exterior of the ground slab and basement walls, but, due to the inaccessibility of these surfaces, interior insulation was the more likely retrofit for the Steindal School [UAF 2007].

The tiles and rugs on the ground floor would need to be removed and wooden studs and additionally insulation would need to be added to the ground floor of the building. The thickness of the expanded polystyrene insulation would be 18 cm and 29 cm in the moderate and low-energy cases, respectively.

No removal would be needed in the retrofit of the ground walls. These retrofits would require that 16 cm and 27 cm of expanded polystyrene insulation be added to the interior of the ground wall in the moderate and low-energy retrofits, respectively.

GROUND FLOOR		Demolition and Removal	New Installations		Total Investment Cost	Lifetime [years]
Retrofit State	Source of Estimate	Remove floor materials	Install 18 cm EPS on ground floor	Install 29cm EPS on ground floor		
Moderate	RS Means	2,600 USD	184,200 USD	X	186,800 USD 1,120,800 NOK	40
	Holte-projeskt	No information available	1,906,400 NOK	X	1,906,400 NOK	20-30
Low-Energy	RS Means	2,600 USD	X	236,700 USD	239,700 USD 1,438,200 NOK	40
	Holte-projeskt	No information available	X	1,989,000 NOK	1,989,010 NOK	20-30

Table 8-20: Estimated cost of installing the ground floor U-value retrofit in the Steindal School. Cost estimates are shown from both US and Norwegian databases [Means LC 2007],[Holte 2007].

GROUND WALL		Demolition and Removal	New Installations		Total Investment Cost	Lifetime
Retrofit State	Source of Estimate	Remove floor materials	16cm EPS on ground wall	27cm EPS on ground wall		
Moderate	RS Means	X	10,700 USD	X	10,700 USD 64,200 NOK	40
	Holte-projeskt	X	126,500 NOK	X	126,500 NOK	20-30
Low-Energy	RS Means	X	X	18,800 USD	18,800 USD 112,800 NOK	40
	Holte-projeskt	X	X	226,700 NOK	226,700 NOK	20-30

Table 8-21: Estimated cost of installing the ground wall U-value retrofit in the Steindal School. Cost estimates are shown from both US and Norwegian databases [Means Mech. 2007][Means LC 2007],[Holte 2007].

8.2.1.4 Infiltration Rate

The current infiltration rates in the building vary from 0.1 ACH to 0.3 ACH for each of the seven thermal zones (Table 5-10 in Chapter 5).

According to the 2007 NBC [BE 2008A] the nominal infiltration rate in new Norwegian buildings, measured under 50 Pa of pressure, should be less than 1.5 ACH. However, buildings do not operate under 50 Pa of pressure. At normal operating conditions, the 1.5 ACH that was measured under 50 Pa of pressure is equal to 0.15 ACH. This was calculated according to the 2007 release of NS3031 [NS3031 2007], which recommended the use of Equation 8-2 for converting from the infiltration rate at 50 Pa of pressure to the nominal operational infiltration rate. In performing this calculation it was assumed that the building was exposed to exterior

conditions on all four sides ($e = 0.1$) and had a balanced ventilation system ($V_1 - V_2 = 0$) (see Table 2-2 in section 2.5.2 of Chapter 2).

$$n_{infiltration} = \frac{n_{50}e}{1 + \frac{f}{e} \left(\frac{V_1 - V_2}{Vn_{50}} \right)} = \frac{1.5 * 0.1}{1} = 0.15 \quad (8-2)$$

Unfortunately, the 2007 release of NS3031 was not available until after the retrofit analysis was performed and a value of 0.2 ACH has been used for the moderate retrofit state. However, the 0.2 ACH that was applied during the retrofit analysis was within reason of the 0.15 ACH recommended in the 2007 NBC, and was acceptable in the absence of the 2007 NBC.

Additionally, the 0.1 ACH that was assigned for the low-energy retrofit was below the 2007 NBC value of 0.15 ACH and the 0.2 ACH that was assigned to the moderate retrofit, making it consistent with the pattern that was used in defining the low-energy states for other retrofits.

INFILTRATION RATE	Current	Moderate	Low-Energy
Infiltration Rate [ACH]	0.1-0.3	0.2	0.1

Table 8-22: Moderate and low-energy infiltration rate retrofit states (ACH).

In the moderate retrofit all windows, doors, and other exterior openings would be sealed to reduce outdoor air leakage. In the low-energy case all windows would be replaced with air-tight frames and then sealed to reduce the infiltration rate. These retrofit procedures were taken to be adequate for estimating the investment costs, but site visits would need to be made to verify that these installations would be capable of reducing the infiltration rates in the Steindal School to the desired levels.

The U-value of the retrofitted windows was taken to be equal to the current values in the building. This was done in the interest of maintaining independence between the predicted energy savings due to the infiltration and window retrofits.

INFILTRATION RATE		Demolition and Removal	New Installations		Total Investment Cost	Lifetime [years]
Retrofit State	Source of Estimate	Remove existing windows	Seal exterior openings	New Windows		
Moderate	RS Means	X	79,200	X	79,200 USD 475,200 NOK	15
	Holte-projeskt	X	129,100	X	129,100 NOK	6
Low-Energy	RS Means	<i>Included in new installation cost</i>	X	168,300	168,300 USD 1,009,800 NOK	40
	Holte-projeskt	<i>Included in new installation cost</i>	X	947,000	947,000 NOK	27

Table 8-23: Estimated cost of installing the infiltration rate retrofit in the Steindal School. Cost estimates are shown from both US and Norwegian databases [Means Mech. 2007][Means Fac. 2007],[FDV 2007].

8.2.1.5 Temperature Independent Loads: Installed Lighting Capacity

The current lighting layout in the school is subdivided into lighting zones serving classrooms, offices, gym spaces, and other areas of the building. The lights are overhead magnetic ballasts with T-12 fluorescent tubes and a total installed density of 13.4 W/ m².

The moderate retrofit to a lighting density of 10 W/m² was consistent with the expected values for newly constructed schools in Norway (Table 2-7 in Chapter 2). This was also the lighting density that corresponded to the installation of T-8 tubes and electronic ballasts in the school.

The low-energy retrofit to a lighting density of 9 W/m² maintained the T-8 tubes, but reduced the number of ballasts by 10% from the moderate retrofit case [DEER 2005].

LIGHTING DENSITY	Current	Moderate	Low-Energy
Lighting Density [W/m ²]	13.4	10	9

Table 8-24: Moderate and low-energy lighting density retrofit states (W/m²).

In order to reach the moderate retrofit state all existing fixtures would be replaced with T-8 tubes and electronic ballasts. In the low-energy retrofit the number of installed fixtures would be reduced by 10% over the moderate retrofit. All existing ballasts and lights would be removed and either reused, recycled, or properly disposed of.

LIGHTING DENSITY		Demolition and Removal	New Installations	Total Investment Cost	Lifetime [years]
Retrofit State	Source of Estimate	Remove existing bulbs and ballasts	Ballasts and bulbs		
Moderate	RS Means	249,300 USD		249,300 USD 1,495,900 NOK	20
	Holte-projeskt	1,246,400 NOK		1,246,400 NOK	15
Low-Energy	RS Means	224,400 USD		224,400 USD 1,346,300 NOK	20
	Holte-projeskt	1,146,200 NOK		1,146,200 NOK	15

Table 8-25: Estimated cost of installing the lighting density retrofit in the Steindal School. Cost estimates are shown from both US and Norwegian databases [Means Mech. 2007][Means Fac. 2007],[FDV 2007].

8.2.2 Alternative Heating Supply Retrofits

These retrofits are installed in the interest of reducing the consumption of electricity for heating in the school. This interest stems from a national initiative to reduce the electricity consumption for space and ventilation heating in Norwegian buildings [Arentz 2007].

8.2.2.1 Hydronic Heating System

8.2.2.1.1 Distribution

The intended heating retrofit was a hydronic heating system. Heat would be conveyed in this system via wall-mounted radiators with water as the heated fluid. The heat source would be either an oil boiler or district heating. The installed hydronic heating system would be sized appropriately to ensure that it was able to meet the heating demands in the school.

Currently, the installed space heating capacity, including the electric resistance heating cables in the gymnasium and wardrobes, is equal to 137 kW (see section 5.1.9 in Chapter 5 and section 7.2 in Chapter 7). Additionally, the installed heating capacity for ventilation and hot water is equal to 185 kW (see section 5.1.10 in Chapter 5). The total installed heating capacity in the Steindal School is currently equal to 322 kW.

Hydronic wall panel heaters should be installed in each zone according to the current installed heating capacity (defined in section 5.1.9 in Chapter 5 and section 7.2 in Chapter 7). In addition, thermostats, thermostat controlled valves, piping, pumps, and pipe insulation would need to be installed.

As-built documents indicated that there are approximately 170 electric resistance baseboard heaters currently installed in the Steindal School. Each of these should be removed to install the hydronic heating distribution system. Additionally, the existing 185 kW electric boiler

should be removed from the building and either reused or recycled, possibly even as an auxiliary boiler in another building.

8.2.2.1.2 Fuel Source: Oil Boiler

The oil boiler was sized to ensure it that would be able to meet the heating demands in the school; the installed heating capacity was 325 kW. The efficiency was taken to be 85% as per work performed by Wigenstad et al. [Wigenstad 2005].

OIL BOILER	Current	Retrofit
Installed Heating Capacity	325 kW	325 kW
Efficiency	~100 %	85%

Table 8-26: Required oil boiler retrofit heating capacity (kW) and efficiency (%).

The new oil boiler would be installed in the mechanical room of the school. In the analysis performed here, it was assumed that such an installation would fit in the space currently reserved for heating equipment and no major renovations to the space would be necessary.

OIL BOILER Source of Estimate	Demolition and Removal		New Installations			Total Investment Cost	Lifetime [years]
	Remove electric wall panels	Remove electric boiler	Hydronic distrib. system and controls	Oil boiler	Oil tank		
RS Means	8,900 USD	1,500 USD	516,750 USD	49,300 USD	20,000 USD	596,400 USD 3,578,700 NOK	30
Holte-projeskt	11,100 NOK	2,700 NOK	4,313,200 NOK	346,800 NOK	Include d in dist. & contr. cost	4,673,800 NOK	30

Table 8-27: Estimated cost of installing the oil boiler and hydronic heating system retrofit in the Steindal School. Cost estimates are shown from both US and Norwegian databases [Means SF 2007], [Arentz 2007]. [Means Mech. 2007],[DEER 2005].

8.2.2.1.3 Fuel Source: District Heating

District heating was considered for use in the Steindal School. The district heating capacity was taken to be 325 kW with an efficiency of 98%, as per Wigenstad et al. [Wigenstad 2005].

DISTRICT HEATING	Current	Low-Energy
Installed Heating Capacity	325 kW	325 kW
Efficiency	~100 %	98 %

Table 8-28: Required district heating retrofit heating capacity (kW) and efficiency (%).

District heating would require that piping be installed to connect to the main district heating supply line, the closest of which is approximately 0.5-1 km from the Steindal School.

Additionally, a controls and conversion system would be necessary to regulate the flow of heat from the grid into the building.

DISTRICT HEATING	Demolition and Removal		New Installations			Total Investment Cost	Lifetime [years]
	Remove electric wall panels	Remove electric boiler	Hydronic distrib. system	Connect to existing district heating mains	Install new district heating controls system		
RS Means	8,900 USD	1,500 USD	516,700 USD	33,000 USD	6,000 EURO (7,800 USD)	551,300 USD 3,307,800 NOK	30
Holte-projeskt	11,100 NOK	2,700 NOK	4,313,200 NOK	<i>included in dist. sys. And controls estimate</i>	6,000 EURO (46,800 NOK)	4,373,800 NOK	30

Table 8-29: Estimated cost of installing the district heating and hydronic heating system retrofit in the Steindal School. Cost estimates are shown from both US and Norwegian databases costs [Means SF 2007], [Arentz 2007],[GST 2007].

8.2.3 Other Potential Retrofits

Notable omissions from this list included schedules of operation for lighting and heating, indoor temperature setpoints, cooling retrofits, window shading, photovoltaics, and solar hot water heating.

Current schedules of operation for lighting and heating correspond to zone occupancy. As such, the energy savings from schedule changes was expected to be minimal. Similarly, temperature setpoints were not considered because the current values are already at acceptable lows [Arentz 2007],[BE 2008a].

The use window shading was not considered because of the low window area on the South façade and the absence of cooling in the building. The absence of occupants during the summer vacation made any excess solar gains during the summer months ineffective. The Municipality currently has no plans to install a cooling system in the school.

The use of photovoltaics would be most effective during the summer period when the electrical loads are at their lowest, and so would not be a cost effective solution. This same reasoning was applied to the use of solar hot water heating, which was also considered to be a relatively untested technology [Arentz 2007], and as such, was not considered suitable for retrofit of the school.

The use of a ground heat exchange water-to-water heat pump was considered, but conversations with building managers indicated that this was an unlikely candidate both because it was a relatively untested technology within the Trondheim Municipality, and because it was desirable to move away from electricity as the source of space heating.

8.2.4 Summary: Retrofit States and Investment Costs

The moderate and low-energy states for each of the retrofits to be analyzed are summarized in Table 8-30 and Table 8-31.

Energy Conservation Measures			
Retrofit	Current	Moderate	Low-Energy
CONTROLS			
Temperature Setback [°C]	2	4	6
VENTILATION			
Occupant Controlled Ventilation [L/m ² s]	Constant @ 2.9	Occupancy @ 2.9	Occupancy @ 1.1
Ventilation Rate [L/m ² s]	2.9	1.1	0.7
Ventilation Heat Recovery Efficiency [%]	55%	70%	80%
ENVELOPE			
U-Value Windows North [W/m ² K]	2.9	1.2	0.8
South/Annex [W/m ² K]	1.1	1.1	0.8
U-Value External Walls [W/m ² K]	0.30	0.18	0.1
U-Value Roof North [W/m ² K]	0.22	0.13	0.1
South [W/m ² K]	0.18	0.13	0.1
U-Value Ground Floor [W/m ² K]	0.67	0.15	0.1
Wall [W/m ² K]	1.44	0.15	0.1
Infiltration Rate [ach]	0.1-0.3	0.2	0.1
LIGHTING AND EQUIPMENT			
Lighting Density [W/m ²]	13.4	10	9

Table 8-30: Summary of moderate and low-energy retrofit states for all energy conservation retrofits.

Alternative Heating Supply Retrofits		
HEATING		
Hydronic Wall Panels [kW]	325 kW (heating) Electric Resistance Wall Panels & Electric Boiler	Yes
Oil Boilers [kW]		325 kW (heating) @ 85% η
District Heat [kW]		325 kW (heating) @ 98% η

Table 8-31: Summary of moderate and low-energy retrofit states for the hydronic heating retrofit with an oil boiler and district heating.

Table 8-32 and Table 8-33 present the total investment cost of the energy conservation measure and alternative heating supply retrofits, respectively. Costs from both US and Norwegian databases are shown. All of the costs are presented in Norwegian Kroners (NOK).

Energy Conservation Measures				
Retrofit		Moderate Investment Costs [NOK]	Low-Energy Investment Cost [NOK]	Lifetime [years]
CONTROLS				
Temperature Setback	US Data	0	0	X
	Norway Data	0	0	X
VENTILATION				
Occupant Controlled Ventilation	US Data	106,800	372,900	10
	Norway Data	49,200	165,600	18
Ventilation Rate	US Data	143,100	143,100	10
	Norway Data	132,700	132,700	18
Ventilation Heat Recovery Efficiency	US Data	11,400	171,100	10
	Norway Data	15,800	242,000	18
ENVELOPE				
U-Value Windows	US Data	478,500	1,002,300	40
	Norway Data	976,800	1,545,700	27
U-Value External Walls	US Data	459,200	508,200	40
	Norway Data	505,400	558,200	20
U-Value Roof	US Data	453,300	565,800	40
	Norway Data	599,600	725,400	20
U-Value Ground Floor	US Data	1,120,800	1,438,200	40
	Norway Data	1,906,400	1,989,000	20
U-Value Ground Wall	US Data	64,200	112,800	40
	Norway Data	126,500	226,700	20
Infiltration Rate	US Data	475,200	1,009,800	15(M)/40(L)
	Norway Data	129,100	947,000	6(M)/27(L)
LIGHTING AND EQUIPMENT				
Lighting Density	US Data	1,495,900	1,346,300	20
	Norway Data	1,246,400	1,146,200	15

Table 8-32 Summary of investment costs of all energy conservation measure retrofits. All costs are given in NOK. M and L are abbreviations for “moderate” and “low-energy”.

Alternative Heating Supply Retrofits			
HEATING			
Retrofit		Investment Cost [NOK]	Lifetime [years]
Hydronic Heating with Oil Boilers	US Data	3,578,700	30
	Norway Data	4,660,000	30
District Heat	US Data	3,307,800	30
	Norway Data	4,360,000	30

Table 8-33: Summary of investment and annual investment costs of alternative heating supply retrofits. All costs are given in NOK.

The total investment costs from the US Data and the Norwegian Data were generally within 50% of each other. The most notable deviation was in the moderate infiltration rate retrofit where the US costs were three times higher than the Norwegian costs. However, given that this was the most outstanding difference between the two datasets, the two cost estimates were taken to be reasonably similar. Therefore, the costs from the more general Norwegian resources were applied in moving forward with the retrofit analysis. This data was more likely to be used in investment cost analyses of Norwegian construction projects than the US data [Arentz 2007],[Nesje 2007].

There is still a fairly large amount of uncertainty associated with these investment costs, regardless of the compatibility that was observed between the US and Norwegian databases. However, this uncertainty was (1) difficult to quantify and (2) nearly impossible to alleviate without obtaining direct quotes from contractors and manufacturers. Recall that the focus of this work was on addressing simulated energy savings prediction uncertainty, not on assessing the accuracy of the cost estimates, which are known to be highly variable from project to project and database to database.

8.3 Individual Retrofit Analysis

The purpose of the Individual Retrofit analysis was to identify potential retrofits for the Steindal School. In performing this analysis (1) uncertainty in retrofit energy savings predictions were addressed, (2) differences between the predicted energy savings from the manually calibrated and Latin Hypercube Monte Carlo (LHMC) calibrated models were identified, (3) differences in predicted energy savings between the Detailed and Simple LHMC models were observed, (4) the consequences of using fewer than the Top 20 LHMC solutions to predict

retrofit energy savings were investigated, and (5) retrofit utility cost savings and annual investment costs were calculated.

8.3.1 Uncertainty in Retrofit Energy Savings Predictions

During data collection (Chapter 5) and calibration (Chapter 7) uncertainties were identified in both the calibrated EnergyPlus building model and its inputs. Consequently, some amount of uncertainty was expected to propagate into the retrofit energy savings predictions. This uncertainty is of consequence to project decision makers, including investors and building managers, who must select the most effective retrofits for the Steindal School on the basis of the predicted energy savings in this analysis. Therefore, two standards for identifying retrofits with acceptable levels of savings uncertainty were investigated during the Individual Retrofit analysis: the ASHRAE Guideline 14 method of quantifying uncertainty and the recommended energy savings values for identifying accurate predictions in RP-1051.

Additionally, means of quantifying the amount of uncertainty associated with energy savings predictions were investigated. In the LHMC calibrated models this uncertainty was approximated by the range of energy savings that were predicted by the Top 20 solutions from the Detailed-Corrected, Detailed-Original, and Simple models. However, the manually calibrated Corrected and Original models predicted only one energy savings value for each retrofit. Therefore, the equations for quantifying uncertainty that were suggested by ASHRAE Guideline 14 [ASHRAE 14 2002] and Reddy and Claridge [Reddy 2000] (section 3.2.5.3 of Chapter 3) were investigated as possible methods of quantifying the energy savings uncertainty associated with the manually calibrated models.

8.3.1.1 Quantifying Uncertainty

Recall that Reddy and Claridge [Reddy 2000] developed Equation 8-3 to evaluate the uncertainty, U , of an energy savings prediction, F , based on the coefficient of variation of the root mean square error (CVRMSE) of the calibrated model (see section 3.2.5.3 in Chapter 3 for more information).

$$U = \frac{\Delta E_{save,m}}{E_{save,m}} = t \cdot \frac{1.26 * CVRMSE [(1 + \frac{2}{n}) \frac{1}{m}]^{\frac{1}{2}}}{F} < 50\% \quad (8-3)$$

<i>U</i>	Uncertainty in predicted energy savings [%]
<i>F</i>	Predicted energy savings [%]
<i>CVRMSE</i>	Coefficient of variation of the root mean square error [%]
<i>n</i>	Number of data points in the calibration period
<i>m</i>	Number of data points in the retrofit period
<i>t</i>	t-statistic: expresses the desired level of confidence (see Table 3-9 in Chapter 3) in the accuracy of the energy savings prediction

The uncertainty defined in Equation 8-3 describes the likelihood that the predicted value of energy savings will be within some percentage of the real energy savings. For example, an uncertainty of 10% at a 90% confidence level means that 90% of the time the predicted value of energy savings would be expected to fall within 10% of the true value.

8.3.1.2 Threshold Values of Uncertainty

ASHRAE Guideline 14 [ASHRAE 14 2002] adopted the work by Reddy and Claridge [Reddy 2000] and recommended that only retrofits with CVRMSE and F values that allowed for $U < 50\%$ at a 68% confidence level ($t = 1$) be considered as plausible installations. This is illustrated in Figure 8-3, where Equation 8-3 has been rearranged to plot the values (black line) of the monthly CVRMSE and annual energy savings, F, that would be needed for a simulated energy savings prediction to meet the uncertainty criteria set forth in ASHRAE Guideline 14.

Also plotted in Figure 8-3 are the results of the Individual Retrofit analysis, as simulated with the manually calibrated Corrected model. Only the low-energy retrofit states are shown. Recall from Chapter 7 that ASHRAE Guideline 14 required a monthly CVRMSE $\leq 15\%$ to accept models to be calibrated. This is shown by the dashed red line in Figure 8-3. Figure 8-3 also plots the CVRMSE and F values that would be required if the uncertainty criteria were more rigorous than the 50% uncertainty at 68% confidence recommended in ASHRAE Guideline 14. The dashed grey line indicates 25% uncertainty at 68% confidence, while the solid grey line indicates 50% uncertainty at 95% confidence. Both uncertainty lines were calculated from Equation 8-3. The vertical orange and yellow lines represent the 5% (absolute minimum for acceptable uncertainty) and 10% (recommend value for acceptable uncertainty) energy savings thresholds that were suggested in RP-1051 [Reddy 2006] for identifying accurate retrofit energy

savings predictions. Increased energy savings are shown from left to right along the x-axis, while the quality of calibration increases with decreasing CVRMSE from the top to the bottom along the y-axis.

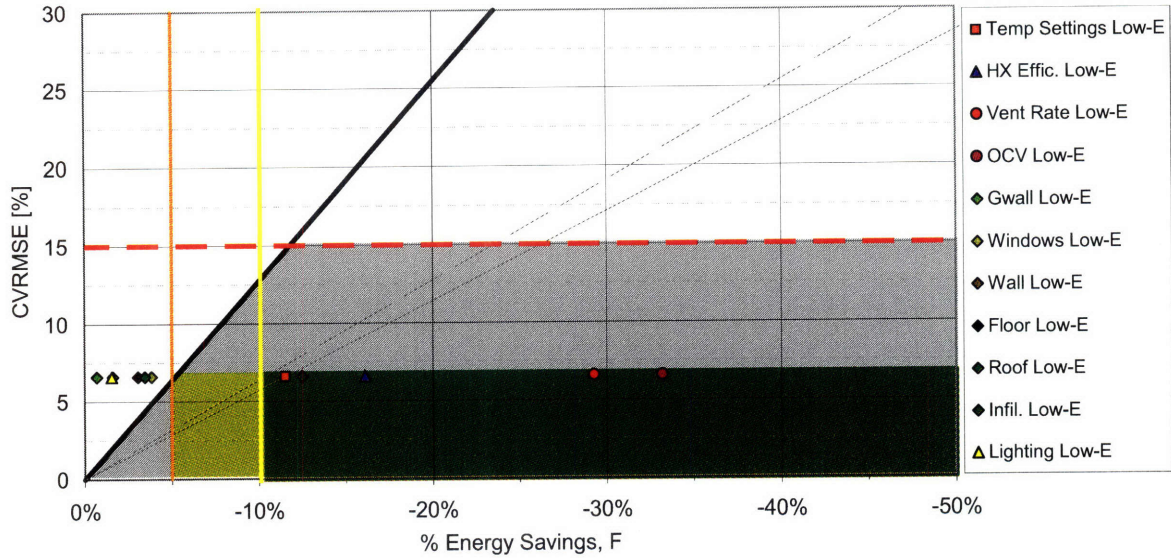


Figure 8-3: Monthly CVRMSE (%) vs. annual energy savings, F (%). The black line indicates combinations of the CVRMSE and F that result in 50% uncertainty in retrofit energy savings prediction at 68% confidence, as calculated with Equation 8-3. Similarly, the dashed grey line equates to 25% uncertainty at 68% confidence and the solid grey line represents 50% uncertainty at 95% confidence. The dashed red line indicates the threshold monthly CVRMSE for calibrated simulations, as per ASHRAE Guideline 14 [ASHRAE 14 2002]. The orange line indicates the 5% minimum energy savings required for acceptable retrofit energy savings in RP-1051 [Reddy 2006], while the yellow line indicates the recommended 10% energy savings for acceptable retrofit energy savings in RP-1051 [Reddy 2006]. The grey area highlights the plausible retrofit space defined in ASHRAE Guideline 14 [ASHRAE 14 2002], while the green areas indicate the plausible retrofit areas (light green – maximum solution space, dark green – recommended solution space) defined in RP-1051 [Reddy 2006]. The retrofit energy savings data points shown by the various colored diamonds, squares, circles, and triangles are from the low-energy Individual Retrofit of the Corrected model of the Steindal School.

Retrofits with energy savings predictions to the right of the black uncertainty line were considered accurate and accepted as plausible retrofit installations according to ASHRAE Guideline 14. All retrofits to the left of the black uncertainty line were too uncertain to be considered as possible installations. Note how the minimum savings fraction (F) required for models to obtain acceptable levels of uncertainty decreases linearly with increasing CVRMSE - the lower the quality of calibration (high CVRMSE), the higher the required energy savings (F) to obtain accurate energy savings predictions.

The area highlighted in grey to the right of the black uncertainty line and below the dashed red line at CVRMSE = 15% defines the plausible retrofit solution space that was

recommended for monthly calibrations by ASHRAE Guideline 14. Similarly, the area highlighted in green to the right of the vertical orange line at 5% energy savings and below $CVRMSE = 7\%$ defines the *maximum* plausible retrofit space that was recommended in RP-1051 (see section 3.2.5.3 in Chapter 3 for details about the recommended CVMRSE and F values from RP-1051). The *recommended* plausible retrofit space according to RP-1051 is defined by the dark green area lying to the right of the yellow line at 10% energy savings.

Note how the recommended plausible retrofit area (dark green area with energy savings $\geq 10\%$) in RP-1051 is a conservative subset of the retrofit space that was recommended in ASHRAE Guideline 14 (grey area). All retrofits that fell within the RP-1051 plausible retrofit space were also considered to meet the 50% uncertainty at 68% confidence criteria recommended in ASHRAE Guideline 14.

8.3.1.3 Variations in Required Uncertainty and Confidence

At higher confidence levels, like the 95% confidence level ($t = 1.98$, solid grey line) shown in Figure 8-3, the slope of the uncertainty line decreases, reducing the area in which retrofits with acceptable levels of energy savings might fall. A similar trend is observed when the acceptable level of uncertainty is decreased, as in the 25% uncertainty ($U = 25\%$, dashed grey line) shown in Figure 8-3. These two examples are intended to illustrate how more stringent uncertainty requirements lead to a reduction in the size of the plausible retrofit solution space.

Note that even at higher confidence levels and decreased uncertainty, the dark green area indicating the recommended retrofit space in RP-1051 is still considered a subset of the retrofit space defined by Equation 8-3 (below both grey lines). However, the maximum retrofit space defined in RP-1051, indicated by the light green area in Figure 8-3, is no longer a subset of the retrofit space defined by Equation 8-3 (below both grey lines). Therefore, when greater levels of certainty are desired, the plausible retrofit space should either be defined by energy savings $\geq 10\%$, or with Equation 8-3.

8.3.1.4 Retrofits with Acceptable Levels of Uncertainty

According to Figure 8-3 the retrofits satisfying the uncertainty criteria set forth by both ASHRAE Guideline 14 [ASHRAE 14 2002] and RP-1051 [Reddy 2006] were the low-energy temperature setback, ventilation rate, ventilation schedule, heat recovery effectiveness, and

infiltration rate retrofits that were simulated with the Corrected model. The moderate and low-energy retrofit results from the Corrected, Original, Detailed-Corrected, Detailed-Original, and Simple models are presented in Table 8-34 and Table 8-35.

On the basis of the observations that were made in the preceding sections it was suggested that the recommended uncertainty criteria from RP-1051 be used to approximate the uncertainty criteria from ASHRAE Guideline 14 with a series of “steps”. When the monthly CVRMSE of the calibrated models is less than 7%, the energy savings > 5% that defined the maximum acceptable retrofit space (green in Figure 8-3) in RP-1051 is suggested for identifying accurate energy savings predictions. When the monthly CVRMSE of the calibrated models is greater than 7%, but less than 15%, the energy savings greater than 10% that defined the recommended acceptable retrofit space in RP-1051 is suggested. Returning to Figure 8-3, it can be shown that adopting these two energy savings values as the minimum requirements at different CVRMSE values enables the 50% uncertainty at 68% confidence requirement from ASHRAE Guideline 14 to be approximated by two steps. However, this only applies when the desired uncertainty in the accuracy of the energy savings prediction is equal to 50% at 68% confidence. When greater confidence or less uncertainty is desired, Equation 8-3 should be applied.

8.3.1.5 Uncertainty in Hourly Calibrations

Thus far, the size of the plausible retrofit solution space has been investigated as a function of changes in the quality of calibration (CVRMSE), the value of predicted savings (F), the uncertainty (U), and the level of confidence (t) of monthly calibrated models. This investigation has covered all but two of the variables governing the behavior of Equation 8-3: the calibration time period (n) and the retrofit time period (m). Therefore, the implications of assessing uncertainty in models that are calibrated and retrofitted over hourly time periods were investigated.

Recall from section 3.2.5.3 in Chapter 3 that Reddy and Claridge [Reddy 2000] suggested the need to account for autocorrelation when assessing uncertainty in hourly calibrated models. Here, autocorrelation refers to data in which the value at one time step is dependent on the value at the previous time step. The method for calculating uncertainty in the presence of autocorrelation was discussed in Chapter 3, but the equation for performing the calculation,

along with the required values for each variable, are repeated in Equation 8-4 through Equation 8-6.

$$U = \frac{\Delta E_{save,m}}{E_{save,m}} = t \cdot \frac{1.26 \cdot CV \left[\frac{n}{n'} \left(1 + \frac{2}{n'} \right) \frac{1}{m} \right]^{1/2}}{F} \quad (8-4)$$

$$n' = n \cdot \frac{1 - \rho}{1 + \rho} \quad (8-5)$$

$$\rho = \sqrt{R^2} \quad (8-6)$$

The calculated values of ρ and n' with the hourly utility data from the Steindal School in 2006 were $\rho = 0.86$ and $n' = 318$, meaning that there were 318 independent data points in the data set. Reddy and Claridge suggested that data sets could be considered correlated when $\rho > 0.50$. Therefore, the 2006 hourly utility data from the Steindal School was considered to be subject to autocorrelation, and the predicted energy savings uncertainty was calculated accordingly (Equation 8-4).

Figure 8-4 plots the threshold value of the $CVRMSE \leq 30\%$ (dashed red line) for achieving hourly calibration from ASHRAE Guideline 14. Also shown are the 50% uncertainty at 68% confidence lines both with (grey line, calculated with Equation 8-4) and without (black line, calculated with Equation 8-3) allowances for autocorrelation.

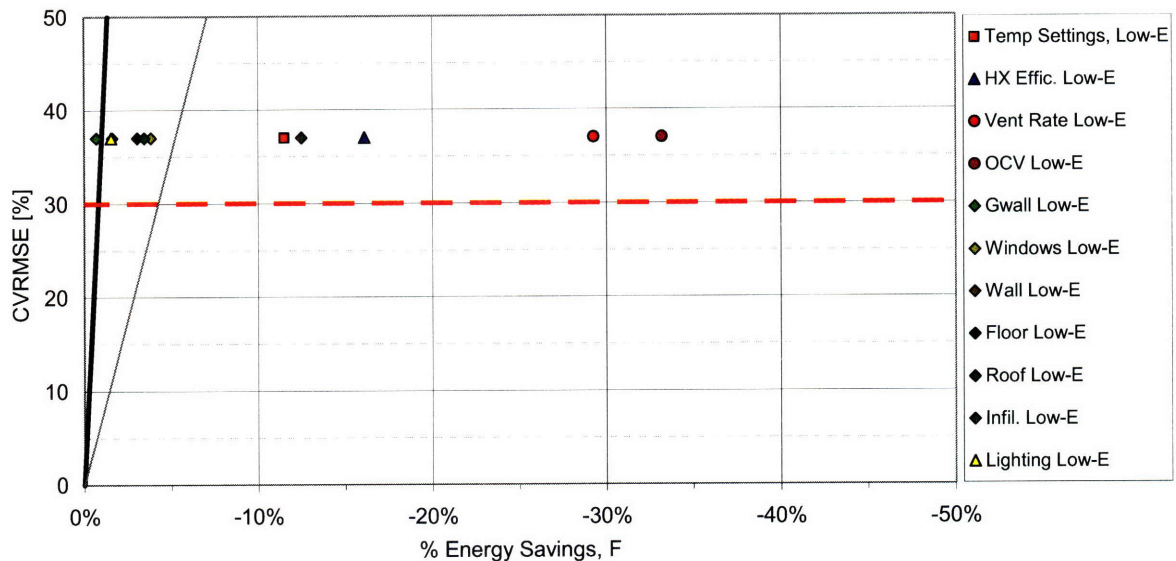


Figure 8-4: Hourly CVRMSE (%) vs. annual energy savings, F (%). The black line indicates combinations of the CVRMSE and F that result in 50% uncertainty in retrofit energy savings prediction at 68% confidence, as calculated with Equation 8-3. Similarly, the solid grey line represents 50% uncertainty at 68% confidence, as calculated with Equation 8-4 with n' equal to 318. The dashed red line indicates the threshold monthly CVRMSE for calibrated simulations, as per ASHRAE Guideline 14 [ASHRAE 14 2002]. The retrofit energy savings data points shown by the various colored diamonds, squares, circles, and triangles are from the low-energy Individual Retrofit of the Corrected model of the Steindal School.

Although the Corrected model did not satisfy the hourly calibration criteria ($CVRMSE \leq 30\%$) suggested in ASHRAE Guideline 14 [ASHRAE 14 2002], several of the retrofits that were simulated with the Corrected model were able to meet the energy savings uncertainty requirements from ASHRAE Guideline 14. The uncertainty line without allowances for autocorrelation identified nearly all of the retrofits as having acceptable levels of uncertainty, a result that was inconsistent with the results in the monthly uncertainty graph in Figure 8-3. When making allowances for autocorrelation, the only retrofits with acceptable levels of certainty were the temperature setback, ventilation rate, ventilation schedule, heat recovery effectiveness, and infiltration rates. This was similar to the result that was observed in the monthly uncertainty analysis. Therefore, when hourly calibration is performed, the 50% uncertainty at 68% confidence criteria recommended in ASHRAE Guideline 14 appears to be a more forgiving means of identifying calibrated simulations that the $CVRMSE \leq 30\%$.

8.3.1.6 Criteria for Assessing Uncertainty in the Individual Retrofit Analysis

In moving forward with the Individual Retrofit analysis the criteria that were suggested in RP-1051 were adopted to identify accurate energy savings predictions: at monthly CVRMSE < 7%, energy savings $\geq 5\%$ were considered acceptable and with $7\% \leq \text{CVRMSE} \leq 15\%$, energy savings greater than 10% were considered to be acceptable (see section 8.3.1.4).

Although the uncertainty criteria from RP-1051 were accepted as the standard for identifying accurate energy savings predictions, Equation 8-3 was still applied to calculate the uncertainty associated with each of the Individual Retrofit energy savings predictions from the manually calibrated Corrected and Original models. This calculation was performed with the CVRMSE values from the Corrected and Original building models at 68% confidence, and resulted in a variation in energy savings, equal to $U \cdot F$, for each model (Note that Equation 8-3 outputs the uncertainty, U , not the energy savings uncertainty, $U \cdot F$. $U \cdot F$ was calculated by multiplying Equation 8-3 by the energy savings, F . Therefore, all energy savings predictions shown in Table 8-34 and Table 8-35 for the Corrected and Original models are presented in terms of their simulated savings value and their predicted savings uncertainty, $U \cdot F$. The range of energy savings predicted by these models was then compared to the range of energy savings enclosed by the Top 20 solutions from the corresponding LHMC calibrated models. Equation 8-3 was used rather than Equation 8-4 because calibration was performed on a monthly basis.

8.3.2 Individual Retrofit Analysis: Energy and Peak Power Savings

8.3.2.1 Annual Energy Consumption Savings

The Individual Retrofit analysis investigated temperature setting, ventilation, envelope, and lighting retrofits. A summary of the resulting energy savings for all five of the input models identified in section 8.2 is shown in Table 8-34 and Table 8-35. The LHMC calibrated models are shown with their median value and standard deviation of their Top 20 solutions. The manually calibrated models are shown with their predicted energy savings, F , expressed as a percent, and their calculated savings uncertainty, $U \cdot F$, where $U \cdot F$ was calculated from Equation 8-3 at 68% confidence ($t = 1$) and with the appropriate monthly CVRMSE values for each of the manually calibrated models. Negative energy savings indicate a reduction from the base-year energy consumption.

	Manually Calibrated		Top 20 Solutions from LHMC		
	<i>Corrected</i>	<i>Original</i>	<i>Detailed-Corrected</i>	<i>Detailed-Original</i>	<i>Simple</i>
	Median +/- % savings	Median +/- % savings	Median +/- % savings	Median +/- % savings	Median +/- % savings
Moderate					
Heating and Controls					
Temperature Setback	-7% 3%	-7% 3%	-7% 0%	-7% 0%	-7% 1%
Ventilation					
Ventilation Rate	-24% 3%	-29% 3%	-25% 2%	-30% 2%	-31% 3%
Occupant Controlled Ventilation	-24% 3%	-28% 3%	-23% 2%	-29% 2%	-22% 3%
Heat Recovery Effectiveness	-10% 3%	-14% 3%	-9% 3%	-14% 3%	-8% 5%
Envelope					
Windows	-2% 3%	-2% 3%	-3% 1%	-2% 2%	-2% 1%
Exterior Wall	-1% 3%	-1% 3%	-1% 0%	-1% 0%	-1% 0%
Ground Wall	-1% 3%	-1% 3%	-1% 0%	-1% 0%	-1% 0%
Ground Floor	-3% 3%	-3% 3%	-4% 1%	-4% 1%	-3% 1%
Roof	-2% 3%	-2% 3%	-3% 1%	-3% 1%	-2% 1%
Infiltration Rate	-5% 3%	-5% 3%	2% 4%	3% 4%	1% 5%
Temperature Independent Loads					
Lighting Density	-1% 3%	-2% 3%	0% 0%	-1% 0%	-1% 0%

Table 8-34: Predicted energy savings from the Individual Retrofit analysis with all retrofits at their moderate retrofit state. The % +/- savings indicates the energy savings uncertainty as a percent of the base-year energy consumption. This was calculated from Equation 8-3 for the manually calibrated models and is equal to twice the standard deviation of the Top 20 solutions for each of the LHMC calibrated models.

	Manually Calibrated		Top 20 Solutions from LHMC		
	<i>Corrected</i>	<i>Original</i>	<i>Detailed-Corrected</i>	<i>Detailed-Original</i>	<i>Simple</i>
	Median +/- % savings				
Low-Energy					
Heating and Controls					
Temperature Setback	-12% 3%	-13% 3%	-12% 1%	-13% 0%	-12% 2%
Ventilation					
Ventilation Rate	-29% 3%	-34% 3%	-30% 2%	-35% 2%	-37% 3%
Occupant Controlled Ventilation	-33% 3%	-39% 3%	-33% 2%	-40% 2%	-39% 4%
Heat Recovery Effectiveness	-16% 3%	-20% 3%	-15% 3%	-20% 2%	-16% 5%
Envelope					
Windows	-4% 3%	-4% 3%	-5% 2%	-4% 2%	-4% 2%
Exterior Wall	-2% 3%	-2% 3%	-2% 0%	-2% 0%	-1% 0%
Ground Wall	-1% 3%	-1% 3%	-1% 0%	-1% 0%	-1% 0%
Ground Floor	-3% 3%	-3% 3%	-4% 2%	-4% 2%	-3% 1%
Roof	-3% 3%	-3% 3%	-4% 1%	-4% 1%	-3% 1%
Infiltration Rate	-12% 3%	-13% 3%	-6% 4%	-6% 3%	-8% 5%
Temperature Independent Loads					
Lighting Density	-2% 3%	-2% 3%	-1% 0%	-1% 0%	-1% 0%

Table 8-35: Predicted energy savings from the Individual Retrofit analysis with all retrofits at their low-energy retrofit state. The % +/- savings indicates the energy savings uncertainty as a percent of the base-year energy consumption. This was calculated from Equation 8-3 for the manually calibrated models and is equal to twice the standard deviation of the Top 20 solutions for each of the LHMC calibrated models.

Applying the criterion for retrofits with acceptable levels of uncertainty recommended by RP-1051, those retrofits with savings less than or equal to 5% were not considered for further analysis. Examining the retrofit results for all five building models in Table 8-35, the only retrofits consistently showing energy savings greater than or equal to 5% were the moderate and low-energy temperature setback, ventilation rate, occupant controlled ventilation, and heat recovery effectiveness. The infiltration rate shown mixed results. These are the same five retrofits that were identified as plausible on the basis of the ASHRAE Guideline 14 uncertainty criteria that was shown in Figure 8-3 in section 8.3.1 with the low-energy retrofits from the Corrected model.

The greatest potential for energy savings was shown by the ventilation rate retrofit, where up to 40% energy savings were observed in the Detailed-Original model. This was closely followed by the occupant controlled ventilation, which showed a maximum savings of 37%, again in the Detailed-Original model. Each of these retrofits is discussed in more detail in section 8.3.3.

It is worth commenting on the increase in energy consumption that was observed in the moderate infiltration rate retrofit for the three LHMC calibrated models. This occurred because the Top 20 calibrated solutions from each of these models tended toward low (< 0.2 ACH) infiltration rates during calibration, meaning that retrofitting the building to 0.2 ACH actually caused an increase in the overall infiltration rate.

8.3.2.2 Annual Peak Power Demand Savings

The peak power demand savings from all retrofits and models are shown in Appendix B, but a summary of the results for those retrofits with energy savings greater than or equal to 5% are shown in Table 8-36.

	Manually Calibrated		Top 20 Solutions from LHMC		
	<i>Corrected</i>	<i>Original</i>	<i>Detailed-Corrected</i>	<i>Detailed-Original</i>	<i>Simple</i>
	Median +/- % savings				
	Moderate				
Heating and Controls					
Temperature Setback	3% 3%	3% 3%	5% 2%	5% 2%	12% 2%
Ventilation					
Ventilation Rate	-10% 3%	-9% 3%	-10% 1%	-11% 1%	0% 1%
Occupant Controlled Ventilation	-32% 3%	-35% 3%	-31% 2%	-37% 3%	-37% 3%
Heat Recovery Effectiveness	-12% 3%	-16% 3%	-12% 4%	-18% 3%	-13% 4%

Table 8-36: Predicted peak annual power demand savings from the Individual Retrofit analysis at the moderate retrofit state. Only those retrofits with energy savings $\geq 5\%$ are shown. The % +/- savings indicates the energy savings uncertainty as a percent of the base-year energy consumption. This was calculated from Equation 8-3 for the manually calibrated models and is equal to twice the standard deviation of the Top 20 solutions for each of the LHMC calibrated models.

	Manually Calibrated		Top 20 Solutions from LHMC		
	<i>Corrected</i>	<i>Original</i>	<i>Detailed-Corrected</i>	<i>Detailed-Original</i>	<i>Simple</i>
	Median +/- % savings				
Heating and Controls	Low-Energy				
Temperature Setback	5% 3%	5% 3%	8% 13%	7% 2%	16% 4%
Ventilation					
Ventilation Rate	-36% 3%	-40% 3%	-34% 2%	-41% 2%	-37% 3%
Occupant Controlled Ventilation	-39% 3%	-42% 3%	-36% 2%	-45% 2%	-44% 3%
Heat Recovery Effectiveness	-23% 3%	-27% 3%	-22% 4%	-29% 3%	-27% 4%
Envelope					
Infiltration Rate	-9% 3%	-8% 3%	-4% 3%	-4% 2%	-5% 3%

Table 8-37: Predicted peak annual power demand savings from the Individual Retrofit analysis at the low-energy retrofit state. Only those retrofits with energy savings $\geq 5\%$ are shown. The % +/- savings indicates the energy savings uncertainty as a percent of the base-year energy consumption. This was calculated from Equation 8-3 for the manually calibrated models and is equal to twice the standard deviation of the Top 20 solutions for each of the LHMC calibrated models.

All of the retrofits under consideration resulted in a decrease in the peak power consumption except the temperature setback retrofit. The increase in peak power consumption for this retrofit was caused by the need to heat the building’s thermal mass very quickly (1-3 hours) when the temperature settings were increased from setback on cold mornings.

From this point forward the retrofit analysis will focus on the results of the temperature setback, occupant controlled ventilation, ventilation rate, heat recovery effectiveness, and infiltration rate retrofits.

8.3.3 Retrofit Energy Savings: Differences between Manual and Latin Hypercube Monte Carlo Calibrated Models

Figure 8-5 through Figure 8-11 show the predicted energy savings vs. calibration goodness of fit (GOF) for the moderate and low-energy temperature setback, ventilation rate, occupant controlled ventilation, heat recovery effectiveness, and infiltration rate retrofits. These retrofits were identified as having acceptable levels of uncertainty associated with their predicted energy savings values. The predicted energy savings are plotted in Figure 8-5 through Figure 8-11 for the Top 20 candidates from the LHMC calibrated Detailed-Corrected, Detailed-Original, and Simple models. Additionally, the predicted energy savings from the manually

calibrated Corrected and Original models are plotted and are bounded by the energy savings uncertainty, $U \cdot F$ that was calculated for each retrofit (see Table 8-34 for the calculated $U \cdot F$ values).

The focus was on assessing the range of energy savings predicted by each of the five models. Additionally, correlations between the distribution of strong parameters from Figure 7-18 in Chapter 7 and the predicted energy savings of each retrofit were investigated. The relationship between the goodness of fit (GOF) and predicted savings was also examined.

8.3.3.1 Heating and Controls Retrofits: Temperature Setback

The temperature setback retrofits are shown in Figure 8-5 for each of the five calibrated models. The Top 20 solutions are shown for the LHMC calibrated models and a single solution with calculated savings uncertainty is shown for each of the manually calibrated models. The low-energy retrofit state is indicated by the filled boxes for the LHMC models; the moderate energy state is indicated by unfilled boxes. The Simple model is shown in light orange, the Detailed-Original model in orange, and the Detailed-Corrected model in dark orange. The manually calibrated models are shown by x's and +'s, each with fill that is the same color as their corresponding LHMC calibrated model. The manually calibrated models are bounded by their savings uncertainty ($U \cdot F$). Increasingly negative energy savings indicate increased energy savings from the base-year.

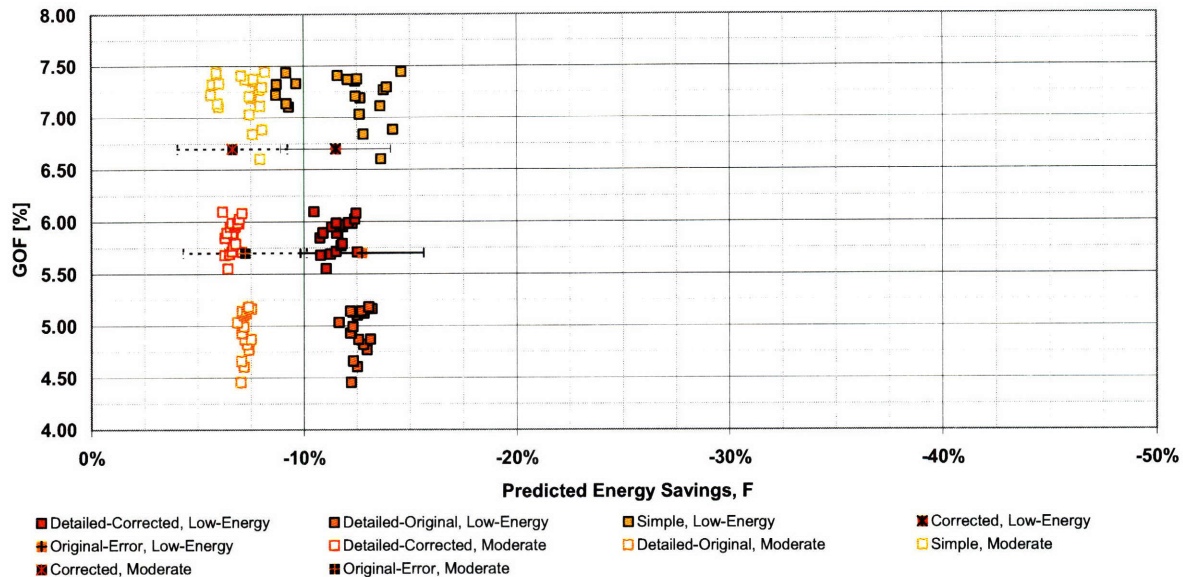


Figure 8-5: Monthly goodness-of-fit (%) vs. predicted annual energy savings (%) from the temperature setback retrofit, as simulated with the manually calibrated Original and Corrected models and the Top 20 solutions of the Detailed-Original, Detailed-Corrected, and Simple LHMC calibrated models. The manually calibrated models are bounded by their savings uncertainty ($U \cdot F$). Increasingly negative energy savings indicate increased energy savings from the base-year. Increasing GOF indicates a poorer fit between the calibrated model and measured utility data.

Figure 8-5 shows a tight cluster of predicted energy savings in both the low-energy and moderate temperature setback retrofits for each of the LHMC models. Both are tight enough to have all of their Top 20 solutions fall within the calculated savings variation for the manually calibrated models.

During calibration (see Chapter 7) the Simple model showed a greater variation in temperature schedules among its Top 20 solutions than the Detailed-Corrected or Detailed-Original models (see the schedule length parameter, p15, in Figure 7-18 in Chapter 7). This variation is reflected in Figure 8-5, where the median savings predicted by the Simple model is the same as the other four models, but the range of predicted savings is much greater. The tight clustering of predicted savings in the LHMC calibrated Detailed-Corrected and Detailed-Original models are likely due to the fact that the schedule lengths were the same for the Top 20 solutions for these two models and both tended toward the middle temperature settings during calibration.

There does not appear to be any correlation between the GOF and the value of predicted energy savings for any of the LHMC calibrated models. Reducing the number of Top solutions used to predicted energy savings for each of the LHMC calibrated models would not result in a change in the range of predicted energy savings.

8.3.3.2 Ventilation Retrofits: Ventilation Rate, Occupant Controlled Ventilation, and Heat Recovery Effectiveness

The ventilation rate, occupant controlled ventilation, and heat recovery effectiveness retrofit results are shown in Figure 8-6, Figure 8-7, and Figure 8-10 for each of the five calibrated models. The Top 20 solutions are shown for the LHMC calibrated models and a single solution with savings uncertainty ($U \cdot F$) is shown for each of the manually calibrated models. The low-energy retrofit state is indicated by the filled circles for the LHMC models; the moderate energy state is indicated by unfilled circles.

In Figure 8-6 (ventilation rate retrofit), the Simple model is shown in pink, the Detailed-Original model in magenta, and the Detailed-Corrected model in red. In Figure 8-7 (occupant controlled ventilation) the Simple model is shown in light purple, the Detailed-Original model in dark purple, and the Detailed-Corrected model in indigo. And, in Figure 8-10 (heat recovery effectiveness) the Simple model is shown in light blue, the Detailed-Corrected model in royal blue, and the Detailed-Original model in aqua blue. In all figures, increasingly negative energy savings indicate increased energy savings from the base-year.

In Figure 8-6, Figure 8-7, and Figure 8-10 the manually calibrated models are shown by boxes with x's for the low-energy state and +'s for the moderate state. The color of these +'s and x's matches the corresponding LHMC calibrated model.

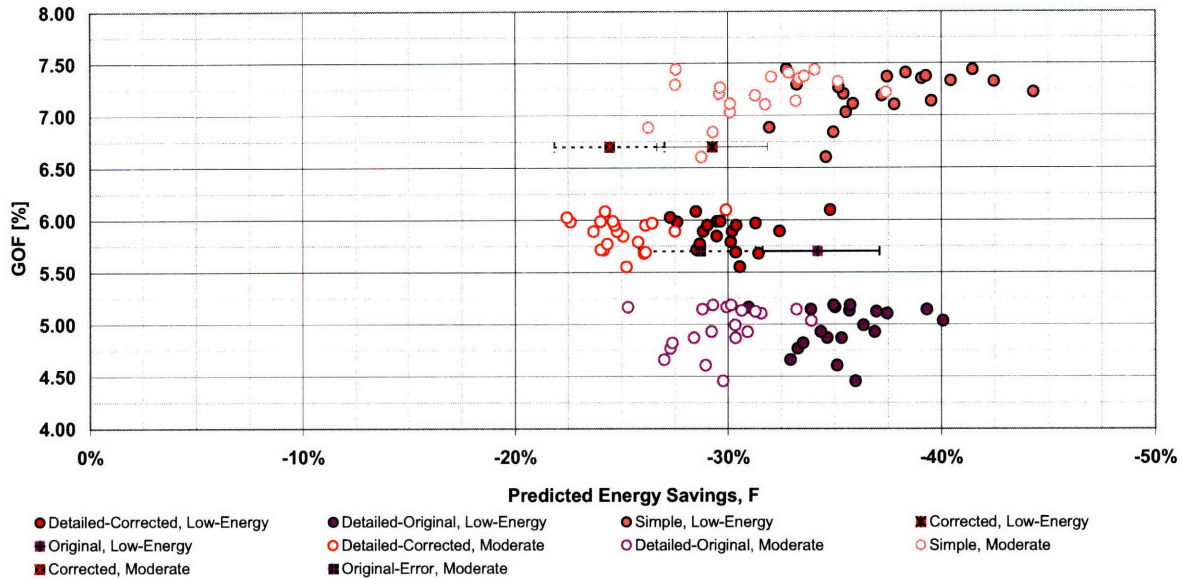


Figure 8-6: Monthly goodness-of-fit (%) vs. predicted annual energy savings (%) from the ventilation rate retrofit, as simulated with the manually calibrated Original and Corrected models and the Top 20 solutions of the Detailed-Original, Detailed-Corrected, and Simple LHMC calibrated models. The manually calibrated models are bounded by their savings uncertainty ($U \cdot F$). Increasingly negative energy savings indicate increased energy savings from the base-year. Increasing GOF indicates a poorer fit between the calibrated model and measured utility data.

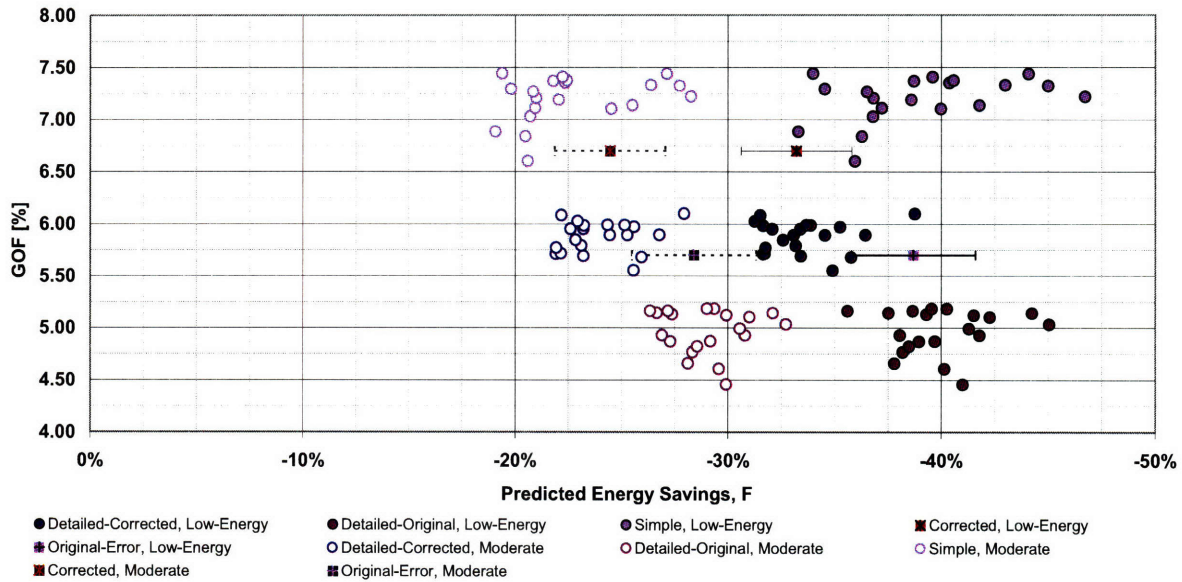


Figure 8-7: Monthly goodness-of-fit (%) vs. predicted annual energy savings (%) from the occupant controlled ventilation retrofit, as simulated with the manually calibrated Original and Corrected models and the Top 20 solutions of the Detailed-Original, Detailed-Corrected, and Simple LHMC calibrated models. The manually calibrated models are bounded by their savings uncertainty ($U \cdot F$). Increasingly negative energy savings indicate increased energy savings from the base-year. Increasing GOF indicates a poorer fit between the calibrated model and measured utility data.

Figure 8-6 and Figure 8-7 indicate that the calculated savings uncertainty ($U \cdot F$) for the manually calibrated Corrected and Original models are able to bound between 15-18 of the Top 20 solutions of their corresponding LHMC calibrated models.

The Simple model is observed to have a greater range of predicted energy savings than either of the other LHMC calibrated models in Figure 8-6 and Figure 8-7. This is due to the large variation in the values of both the heat recovery effectiveness and the specific fan power among the Top 20 calibrated solutions with the Simple model.

According to Figure 8-6 the LHMC calibrated Detailed-Original and Simple models predicted greater energy savings than the Detailed-Corrected model. This was due to the fact that the Detailed-Corrected model tended toward higher heat recovery effectivenesses (55%-65%) than the Simple (45%-60%) and Detailed-Original (50-60%) models during calibration (see Chapter 7). The higher heat recovery effectivenesses in the Detailed-Corrected model meant that less ventilation energy was available to be saved at lower ventilation rates, thus, a lower energy savings was observed. Additionally, the Simple model was known to have a higher calibrated fan energy (see the Pre-Retrofit, Simple bar in Figure 8-8), which led to greater energy savings from the low energy fans that were modeled with the low-energy ventilation retrofit.

Figure 8-7 presents the energy savings predicted for the occupant controlled ventilation retrofits. Here, the Detailed-Corrected model again shows lower energy savings than the Detailed-Original or Simple models at the low-energy retrofit state. This is due to the higher heat recovery effectivenesses in the Detailed-Corrected model. Additionally, the Simple model shows a significantly lower energy savings due to the moderate occupant controlled ventilation retrofit. This is due to the high specific fan power in the Simple model, which has a lower potential for decreased energy consumption at lower ventilation rates and shorter schedules (see the fan energy for the moderate retrofit in Figure 8-9).

Figure 8-8 and Figure 8-9 show the mean load distributions of the Top 20 solutions from both the Simple and Detailed-Original models. Both of these figures indicated that the Simple model had a significantly higher base-year fan power. This is the result of the LHMC calibration, in which the range of input values for the Simple model was centered on 1500 $W/m^3/sec$, as opposed to 1200 $W/m^3/sec$ for the Detailed-Original model (see Table 7-6 in Chapter 7). Figure 8-8 and Figure 8-9 also show the simulated mean annual load distributions of

the Top 20 solutions from the Simple and Detailed-Original models with the ventilation rate and occupant controlled ventilation retrofits.

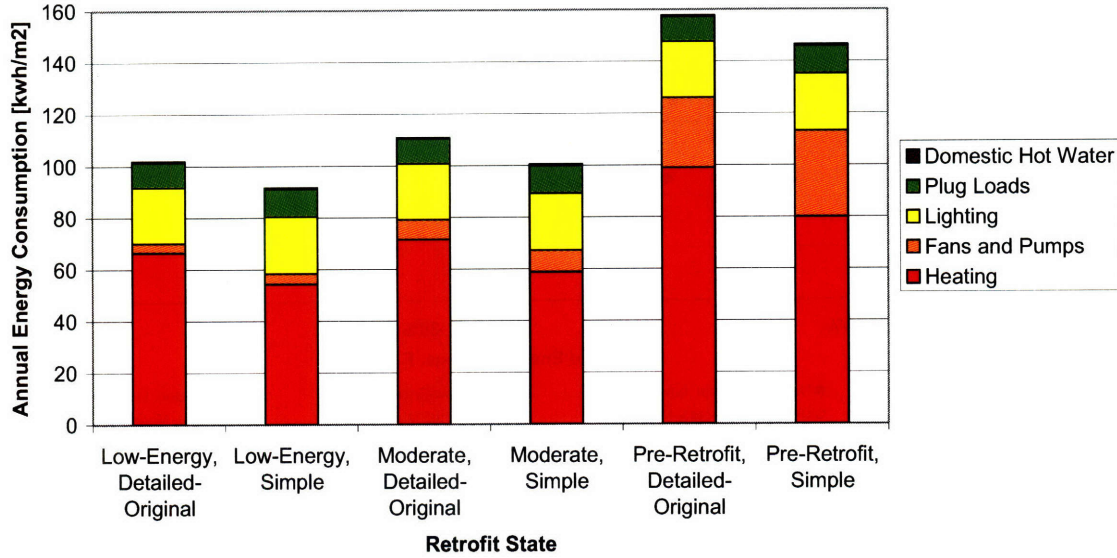


Figure 8-8: Ventilation rate retrofit annual energy consumption and load distribution (kWh/m2/year). The mean load distribution of the Top 20 solutions from the Simple and Detailed-Original LHC calibrated models are shown.

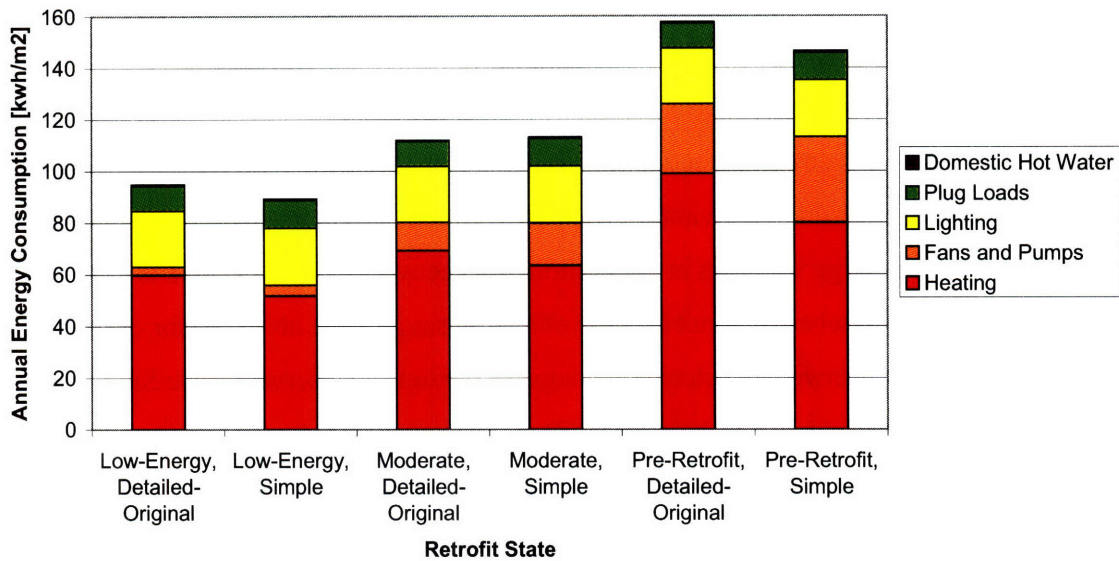


Figure 8-9: Occupant controlled ventilation retrofit annual energy consumption and load distribution (kWh/m2/year). The mean load distribution of the Top 20 solutions from the Simple and Detailed-Original LHC calibrated models are shown.

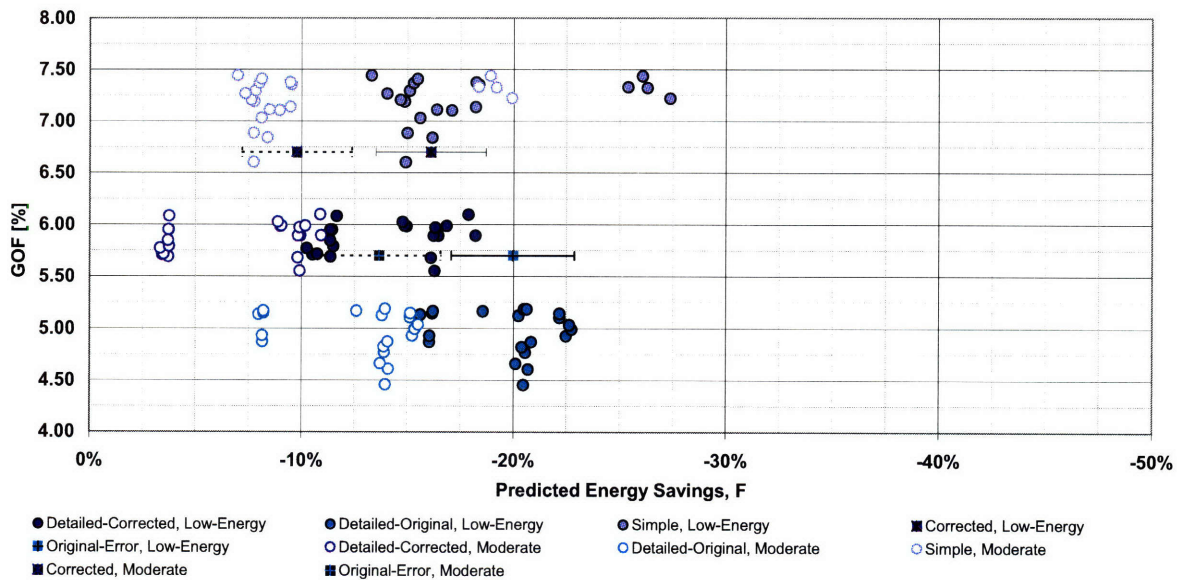


Figure 8-10: Monthly goodness-of-fit (%) vs. predicted annual energy savings (%) from the heat recovery effectiveness retrofit, as simulated with the manually calibrated Original and Corrected models and the Top 20 solutions of the Detailed-Original, Detailed-Corrected, and Simple LHC calibrated models. The manually calibrated models are bounded by their savings uncertainty ($U \cdot F$). Increasingly negative energy savings indicate increased energy savings from the base-year. Increasing GOF indicates a poorer fit between the calibrated model and measured utility data.

Observation of the heat recovery effectiveness parameter from the LHC calibration in Chapter 7 (Figure 7-18) showed that the Detailed-Original (50-60% heat recovery effectiveness) model tended toward heat recovery effectiveness values that were 5-15% less than the Detailed-Corrected (55-65% heat recovery effectiveness) model. The Simple (45-60% heat recovery effectiveness) model tended toward values that were between 5-20% less than the Detailed-Corrected model. The large variation in calibration heat recovery effectivenesses is easily observed in Figure 8-10, where distinct clusters of energy savings are observed for each LHC model. The largest gap between clusters of savings predictions is observed in the Simple model, most likely due to the large range of heat recovery effectivenesses, between 45% and 60%, that were observed in the Top 20 calibrated solutions from this model. The Detailed-Original and Detailed-Corrected models show much smaller gaps between clusters of predicted savings, which mirrors their smaller variation in calibrated heat recovery effectivenesses.

All three ventilation retrofits in Figure 8-6 through Figure 8-10 show a greater range of predicted savings with the Simple model than the Detailed-Corrected or Detailed-Original models. In all three retrofits – ventilation rate, occupant controlled ventilation, and heat recovery effectiveness - the calculated savings variation ($U \cdot F$) of the manually calibrated Corrected model

is able to bound 12-18 of the Top 20 solutions from the corresponding Detailed-Corrected model. Similarly, the Original model is able to bound 12-16 of the Top 20 solutions from the Detailed-Original model.

No patterns are observed between the GOF value and the predicted energy savings values. However, in all three retrofits, reducing the number of Top solutions used to predicted energy savings for each of the LHMC calibrated models results in a decrease in the interval of predicted energy savings.

8.3.3.3 Envelope Retrofits: Low-Energy Infiltration Rate

The low-energy infiltration retrofit results are shown in Figure 8-11 for each of the five calibrated models. The moderate infiltration retrofit results are not shown because their energy savings were less than 5%. The Top 20 solutions are shown for the LHMC calibrated models and a single solution with calculated savings variation ($U \cdot F$) is shown for each of the manually calibrated models. The low-energy retrofit state is indicated by the filled diamonds for the LHMC models. The Simple model is shown in sea green, the Detailed-Original model in olive green, and the Detailed-Corrected model in forest green. In Figure 8-11 the manually calibrated models are shown by boxes with x's for the low-energy state and +'s for the moderate state. The color of these +'s and x's matches the corresponding LHMC calibrated model. Increasingly negative energy savings indicate increased energy savings from the base-year.

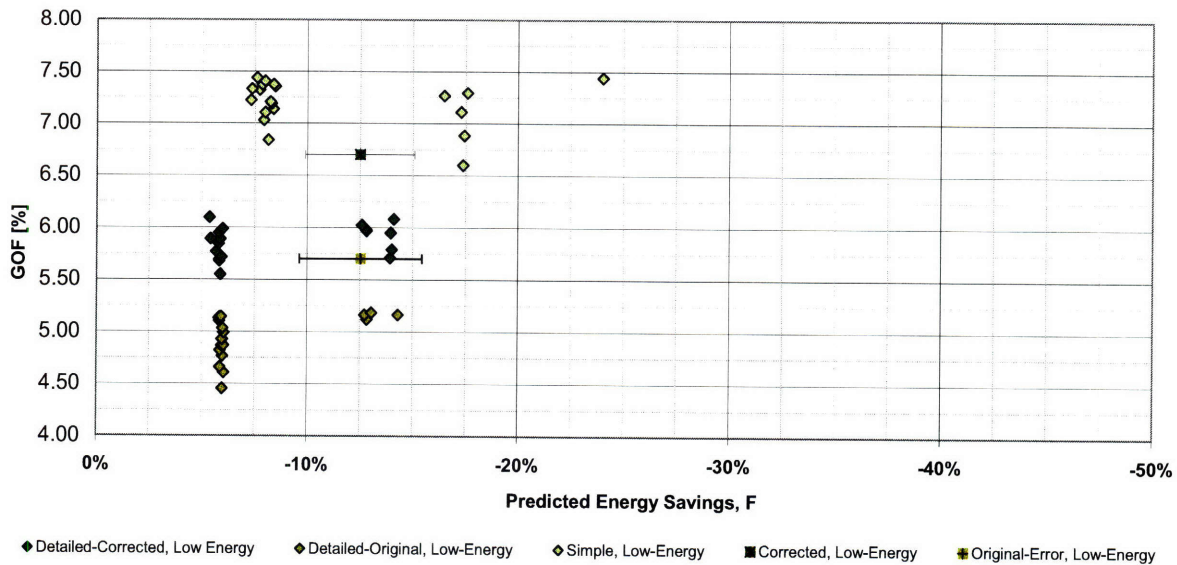


Figure 8-11: Monthly goodness-of-fit (%) vs. predicted annual energy savings (%) from the infiltration rate retrofit, as simulated with the manually calibrated Original and Corrected models and the Top 20 solutions of the Detailed-Original, Detailed-Corrected, and Simple LHMC calibrated models. The manually calibrated models are bounded by their savings uncertainty ($U \cdot F$). Increasingly negative energy savings indicate increased energy savings from the base-year. Increasing GOF indicates a poorer fit between the calibrated model and measured utility data.

All three LHMC calibrated models show similar distributions with a cluster of savings between 5-8% savings and again between 12-17% savings. In this case, the savings uncertainty of the manually calibrated models are only able to bound between 5 and 6 of the Top 20 solutions from the LHMC models.

Observation of the parameter distributions of the Top 20 solutions for each of the LHMC models from the calibration (see Figure 7-18 in Chapter 7) indicate a bias toward low (0.2 ACH) and moderate (0.3 ACH) infiltration rates in all three LHMC calibrated models. Conversely, both the Corrected and Original manually calibrated models were tuned to moderate infiltration rates of 0.3 ACH. As a result, the manually calibrated Corrected and Original models tend toward higher energy savings due to the installed retrofits, while the lower infiltration rates in the calibrated LHMC models lead to lower magnitudes of predicted energy savings. Additionally, the variation in calibration input states is apparent in the distinct clusters of predicted savings observed in each of the LHMC models.

No correlation between energy savings and GOF is observed. However, reducing the number of Top solutions used to predicted energy savings for each of the LHMC calibrated models would result in a decrease in the interval of predicted energy savings.

8.3.4 Summary of Observations: LHMC vs. Manually Calibrated Building Models

Observations of the predicted energy savings from the Individual Retrofits indicated five candidate retrofits with savings that achieved adequate levels of energy savings certainty (energy savings > 5% with a monthly CVRMSE \leq 7%). These retrofits were: increased temperature setback, decreased ventilation flow rates, occupant controlled ventilation, improved heat recovery effectiveness, and decreased infiltration rates. When examining the peak power demand savings, the temperature setback retrofit showed an increase in peak power demand. All other retrofits showed a decrease in both peak power and energy consumption.

The Corrected and Original models both predicted similar energy savings values for the temperature setback and infiltration retrofits, but showed differences of up to 10% in the predicted energy savings due to the three ventilation retrofits. These differences stemmed largely from variations in the heat recovery effectiveness of the two models. On the basis of these observations it was apparent that the errors that were made in accounting for the “baseload” in the Original model created a large degree of uncertainty in the predicted ventilation retrofit energy savings.

The Top 20 LHMC solutions from the Simple model predicted a greater range of energy savings than the Top 20 solutions from the Detailed-Corrected or Detailed-Original models. The Simple model was also more poorly calibrated statistically than either of the Detailed-Corrected or Detailed-Original models. However, regardless of the increased range of energy savings predictions, the Simple model predicted median energy savings values that were with 5%-10% of both of the Detailed LHMC calibrated models. Therefore, from the perspective of calibration, LHMC enabled the Simple model to be adequately calibrated for performing retrofit energy savings predictions with a minimal amount of modeler tuning and a limited amount of building data.

The manually calibrated Corrected and Original models with the calculated interval of savings uncertainty were consistently able to bound between 12 and 18 of the Top 20 LHMC solutions from their corresponding models. The exception to this was the low-energy infiltration retrofit, where the manually calibrated models were only able to bound between 5 and 6 of the Top 20 solutions.

No correlation was observed between solutions with low GOF values and a decrease in the range of predicted energy savings values. However, it was observed that using a larger number of Top solutions to perform the retrofit analysis did result in a larger interval of predicted savings.

On the basis of the above observations the Corrected model was taken as the baseline model for performing further retrofit analyses of the Steindal School. The Corrected model required only a single simulation to predict retrofit energy savings (as opposed to 20 for the LHMC calibrated models) and the modeler had the greatest amount of confidence in the accuracy of this model.

8.3.5 Retrofit Costs: Utility Billing and Total Annual Investment Costs

Recommended retrofits for the Steindal School were chosen on the basis of both energy savings and investment cost. Consequently, the annual utility cost, annual investment cost, and total annual cost were calculated for each retrofit. The total annual cost was the difference between the annual investment cost and the utility bill savings resulting from each retrofit; a negative total annual cost indicated that the utility bill savings were greater than the annual investment cost of the retrofit. Retrofits with negative total annual costs were considered as viable retrofit options for the Steindal School.

Methods for calculating the annual electricity, oil, and district heating costs in the Steindal School in addition to the total annual cost are all presented.

8.3.5.1 Utility Billing

Utility bills were charged on a monthly basis in the Steindal School and were calculated as a function of monthly energy consumption and annual peak power demand. Hot water billing was not included in this analysis.

8.3.5.1.1 Electricity

Electricity is currently the only energy carrier in the school, and the monthly utility bills are charged accordingly. The monthly electricity bill for the Steindal School is calculated as in Equation 8-7 through Equation 8-10, where tariffs (*Energy Tariff and Power Tariff*) are charged by both the production (*Charge from Producer*) and distribution (*Charge from Distributor*)

companies for monthly energy consumption and annual peak power demand. Additionally, a tariff is charged by the state energy fund (*Energy Fund Tariff*) for each kWh of energy consumed and a grid rent charge and fixed cost (*Fixed Annual Cost/12*) are charged each month. The total cost of energy (*Monthly Electricity Cost*) is the sum of the charges from the distributor, producer, and grid rent, multiplied by a state tax (*MVA*). The result is the monthly electricity bill for the school.

$$\text{Monthly Electricity Cost (NOK)} = (\text{Charge from Distributor} + \text{Charge from Producer} + \text{Grid Rent}) * \text{MVA} \quad (8-7)$$

$$\begin{aligned} \text{Charge from Distributor (NOK)} = & [\text{Energy Tariff (from distributor) (NOK/kWh)}] * [\text{Monthly Energy Consumption (kWh)}] + \\ & [\text{Power Tariff up to 200 kW (NOK/kW)}] * [200 \text{ kW}] + \\ & [\text{Power Tariff over 200 kW (NOK/kW)}] * [(\text{Peak Annual Power Demand (kW)} - 200 \text{ kW})] + \\ & [\text{Fixed Annual Cost (NOK)/12}] + \\ & [\text{Energy Fund Tariff (NOK/kWh)}] * [\text{Monthly Energy Consumption (kWh)}] \end{aligned} \quad (8-8)$$

$$\text{Charge from Producer (NOK)} = [\text{Energy Tariff (from producer) (NOK/kWh)}] * [\text{Monthly Energy Consumption (kWh)}] \quad (8-9)$$

$$\text{Grid Rent (NOK)} = [\text{Fixed charge for grid rent}] \quad (8-10)$$

Note that two different tariffs are applied to the annual peak power demand: a tariff for the first 200kW of peak power demand (*Power Tariff up to 200kW*) and a tariff for power demand in excess of 200 kW (*Power Tariff over 200kW*).

Table 8-38 summarizes the distribution tariffs and grid rent charges at the Steindal School from January 2005 through August 2007. The production tariffs are shown in Figure 8-12. Note the seasonal variation in the distribution energy tariff (Winter/Summer).

Year	Distribution					Other
	Energy*	Power < 200 kW**	Power > 200 kW	Fixed	**Cons. Tax	Grid Rent
	[NOK/kWh]	[NOK/kW]	[NOK/kW]	[NOK/month]	[NOK/kWh]	[NOK/month]
2004	0.042/0.027	41.66/46.67	25/28.33	666.67	0/0.0967	58.33
2005	0.042/0.027	46.67	28.33	666.67	0.0988	58.33
2006	0.04/0.025	44.17	27.50	666.67	0.1005	58.33
2007	0.055/0.025	42.5	25.83	666.67	0.1023	58.33

Table 8-38: Electricity billing distribution tariffs from the Steindal School for the periods from January 2004-August 2007 [Skjennald 2007]. **In 2004 the power tariffs and consumption tax increased starting with the August utility bill.

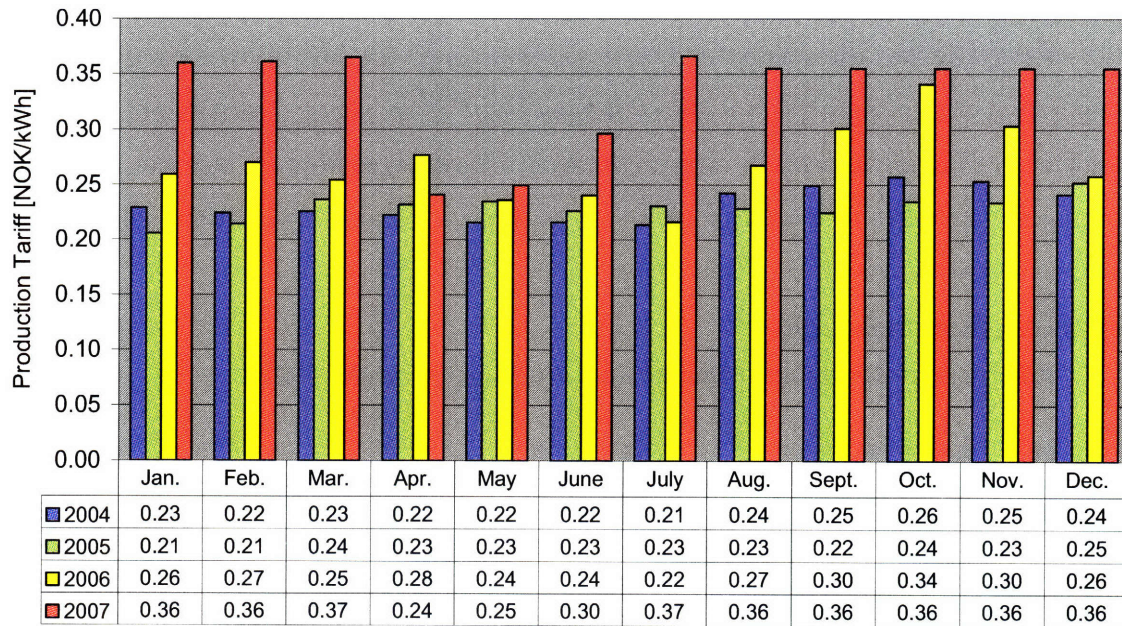


Figure 8-12: Electricity billing production tariffs from the Steindal School for the periods from January 2004-August 2007 (NOK/kWh) [Skjennald 2007].

In the absence of production tariff data for September through December 2007, an estimate of 0.36 NOK/kWh was made for these months.

Figure 8-13 summarizes the energy consumption and utility costs at the Steindal School from 2004 through 2007. These data were verified against collected utility bills for this period and an error of less than 1% was observed.

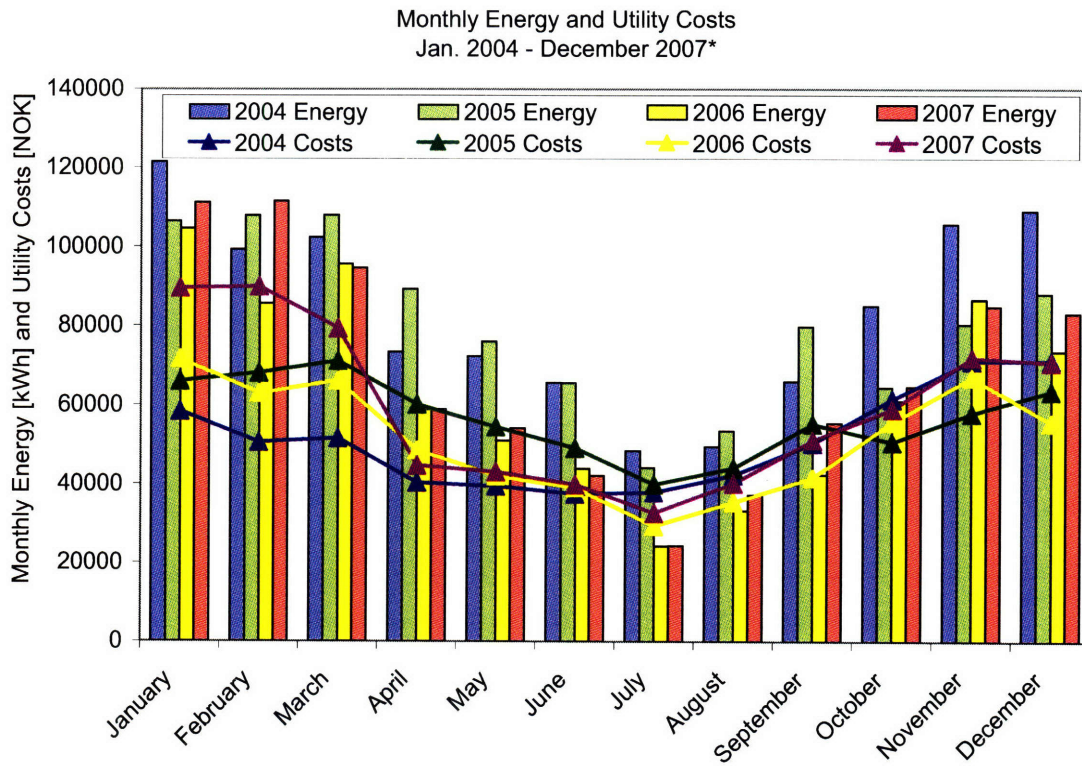


Figure 8-13: Monthly utility billing (NOK) and electricity consumption (kWh) from the Steindal School for the period from January 2004 through December 2007.

Of interest here is the influence of changes in tariffs from year to year. Two thousand and four is a particularly interesting year because it consistently shows the highest monthly energy consumption, but, due to the absence of an energy fund tariff from January through June, it also shows utility costs less than or equal to those observed in 2005, 2006, and 2007. Conversely, the 2006 data shows the lowest monthly energy consumption, but, due to the higher electricity tariffs during this year, shows similar utility costs to 2004, 2005, and 2007.

In each of the four years from 2004 through 2007 it was observed that 63%-65% of the annual utility costs (after tax) were due to energy tariffs, 34%-35% was attributed to peak power demand tariffs, and 1%-2% was due to fixed charges. Therefore, in assessing utility bill savings due to the simulated retrofits both the annual energy consumption and peak power demand were expected to be influential.

8.3.5.1.2 Oil

The calculation of heating oil billing in primary schools in Trondheim is as in Equation 8-11, where the cost of oil per kWh is equal to the sum of a fixed transportation charge

(*Transport Cost*) and variable oil cost (*Price of Oil*), multiplied by a state tax (*MVA*) and a seasonal cost factor (*Weight*). The division by 10,000 represents the energy (kWh) content per m³ of oil.

$$\text{Cost of Oil (NOK/kWh)} = \frac{[\text{Transport Cost (NOK/m}^3\text{)} + \text{Price of Oil (NOK/m}^3\text{)}] \cdot \text{MVA} \cdot \text{Weight}}{10,000} \quad (8-11)$$

In 2007 the transport cost was fixed at 79 NOK/m³, while the price of oil and seasonal cost factor varied from month to month, as shown in Table 8-39. The tax was constant and equal to 25% (*MVA* = 1.25).

2007 Oil Prices	Jan.	Feb.	Mar.	Apr.	May	June	July	Aug.	Sept.	Oct.*	Nov.*	Dec.*
Price of Oil [NOK/m ³]	3,800	3,900	4,000	3,900	4,200	4,200	4,300	4,300	4,000	4,100	4,000	3,800
Seasonal Cost Factor	0.8	0.8	0.8	0.7	0.7	0.7	0.7	0.7	0.8	0.8	0.8	0.8
Cost of Oil [NOK/kWh]	0.61	0.61	0.64	0.71	0.76	0.77	0.78	0.78	0.74	0.65	0.63	0.60

*estimated values

Table 8-39: Monthly oil tariffs (NOK/m³) and costs (NOK/kWh) and seasonal cost factors for schools in the Trondheim Municipality from January through September, 2007. The Cost of Oil includes the MVA, or tax.

Data for October-December were unavailable and were estimated based on observations of the costs in January – March of 2007.

The heating oil for schools in the Trondheim Municipality is supplied by Shell [Arentz 2007]. The seasonal cost factor accounted for the supplier’s increased cost to distribute oil during the non-peak season (summer).

8.3.5.1.3 District Heating

The fuel for district heating in the Trondheim municipally is a mix of garbage, oil, heat pumps, natural gas, propane/butane, bio-energy, and electricity [Arentz 2007].

Projections by the utility company [TEV 2007a] for 2008 anticipate that between 70% - 80% of the district heating fuel will be garbage.

District heating utility bills are charged as in Equation 8-12, where the price of district heating (*Price of District Heating*) varies from month to month and is given for 2007 in Table 8-40. The tax is fixed at 25% (*MVA* = 1.25).

$$\text{Cost of District Heating (NOK/kWh)} = \frac{\text{Price of District Heating (NOK/kWh)}}{MVA} \quad (8-12)$$

2007 District Heating Prices	Jan.	Feb.	Mar.	Apr.	May	June	July	Aug.	Sept.	Oct.*	Nov.*	Dec.*
Cost of District Heating [NOK/kWh]	0.83	0.72	0.69	0.56	0.56	0.54	0.60	0.59	0.59	0.75	0.89	1.00

*estimated values

Table 8-40: Monthly district heating tariffs (NOK/kWh) for schools in the Trondheim Municipality from January through September, 2007. The Cost of District Heating includes the MVA, or tax.

Once again, data for the final three months of 2007 were not available and were estimated from the observed patterns for the first several months of the year.

8.3.5.1.4 Summary of Utility Billing

Electricity, oil, and district heating utility rates were all available from the Trondheim Municipality in 2007. However, no oil or district heating utility billing data was available for 2004, 2005, or 2006. Therefore, in the interest of applying utility costs under similar annual conditions for all three energy supply types, 2007 data was applied in the retrofit analysis.

8.3.5.2 Annual Utility Costs

Table 8-41 presents the utility (all electricity) bill savings due to the simulated temperature setback, ventilation rate, occupant controlled ventilation, heat recovery effectiveness, and infiltration rate retrofits. These five retrofits all had acceptable levels of uncertainty in their energy savings predictions and were simulated with the Corrected building model. The predicted energy savings from the moderate infiltration retrofit was less than 5% of the base-year energy consumption and was omitted from the utility bill analysis. The total annual cost of electricity in the base-year Corrected model of the Steindal School was 631,752 NOK/year.

	<i>Corrected</i>
	Median +/- % savings
<u>Heating and Controls</u>	Moderate
Temperature Setback	-4% 3%
<u>Ventilation</u>	
Ventilation Rate	-20% 3%
Occupant Controlled Ventilation	-27% 3%
Heat Recovery Effectiveness	-10% 3%
<u>Heating and Controls</u>	Low-Energy
Temperature Setback	-7% 3%
<u>Ventilation</u>	
Ventilation Rate	-34% 3%
Occupant Controlled Ventilation	-32% 3%
Heat Recovery Effectiveness	-18% 3%
<u>Envelope</u>	
Infiltration Rate	-12% 3%

Table 8-41: Simulated utility bill savings, expressed as a percentage of the base-year utility costs, for the temperature setback, ventilation rate, occupant controlled ventilation, heat recovery effectiveness, and infiltration rate retrofits, as simulated with the Corrected building model. Negative savings equate to a decrease in utility costs from the base-year.

All of the retrofits under consideration showed reductions in their annual utility costs corresponding with the reduction in energy consumption that was observed in Table 8-34 and Table 8-35. However, the low-energy temperature setback retrofit, which showed greater than, or equivalent, energy savings to the moderate heat exchanger efficiency and low-energy infiltration retrofits in Table 8-34 and Table 8-35, showed lower utility bill savings than either of these retrofits. This was due to the increased peak power demand that resulted from the temperature setback retrofit (Table 8-36). Because the electricity cost is a function of both energy consumption and peak power demand, the increased power demand offsets the retrofit's energy savings and causes only moderate reductions in utility bill costs from the base-year. Therefore, in situations where the temperature setback retrofit was to be implemented, the installation of an oil boiler or district heating system was considered. These two alternative heating systems would reduce the peak electricity demand to the sum of the peak fan, pump,

lighting, and plug loads. In the Corrected base-year model the installation of an alternative heating system would decrease the peak electricity demand from 440 kW to 140 kW (not including the pumps for the hydronic heating system), a reduction of more than 68%.

8.3.5.3 Calculating Annualized Costs

The total annual cost that was applied in this retrofit analysis was chosen (1) for its simplicity and (2) because it allowed a direct comparison to be made between the annual utility bill savings and the investment cost of the retrofit.

The inclusion of environmental impacts is outside of the scope of the work performed here. Additionally, in the interest of simplicity, only the interest rate was factored into the annualized cost calculation.

The total annual cost (TC_{annual}) was equal to the difference between the annualized investment cost ($IC_{\text{total}} * a$) and the annual utility bill savings (ΔEC) and was calculated as in Equation 8-13 and Equation 8-14.

$$TC_{\text{annual}} = IC_{\text{total}} * a - \Delta EC \quad (8-13)$$

$$a = \frac{(1+i)^n * i}{(1+i)^n - 1} \quad (8-14)$$

a Annuity factor

i Interest rate

n Service lifetime

ΔEC Annual utility bill savings = annual utility costs in the base-year - annual utility cost after retrofit

A $TC_{\text{annual}} < 0$ indicates that the annual utility bill savings are greater than the annual investment costs, making the retrofit a cost effective option.

8.3.5.3.1.1 Total Annual Cost: Selecting an Appropriate Interest Rates

The total annual cost was calculated at interest rates of 1%, 2%, 4%, 7%, and 10%. The annual utility bill savings were calculated as the electricity cost savings from the Corrected building model. All investment costs were from Norwegian cost data.

The 7% interest rate was similar to that used by Statsbygg [Statsbygg 2007] in their investment analysis of a potential heat pump installation in a Norwegian building. The 2% interest rate was the lower bound of the expected lending rate from Norwegian banks; this was the lending rate through most of 2005 and into 2006 [Norges-Bank 2008]. The 4% was the

interest rate charged by Norwegian banks for most of 2007 [Norges-Bank 2008], and was also the interest rate that was applied to calculate the annual costs in work by Petersdorff et al. [Petersdorff 2005]. The 1% and 10% interest rates were intended to provide upper and lower bounds of the annualized investment costs.

Figure 8-14 and Figure 8-15 depict the total annual cost of each retrofit at varying interest rates. Although all of the retrofits that were simulated in the Individual Retrofit analysis are plotted, only those retrofits with annual energy savings > 5% were considered for installation in the Steindal School (see section 8.3.1 through 8.3.3). The remaining retrofits, those with annual energy savings $\leq 5\%$, are shown to give the overall cost vs. energy savings results from the Individual Retrofit analysis. The total annual cost (right hand side, y-axis) is graphed for each moderate and low-energy retrofit. A negative total annual cost indicates retrofits where the utility savings are greater than the annual investment cost, the opposite is true for retrofits with positive total annual costs.

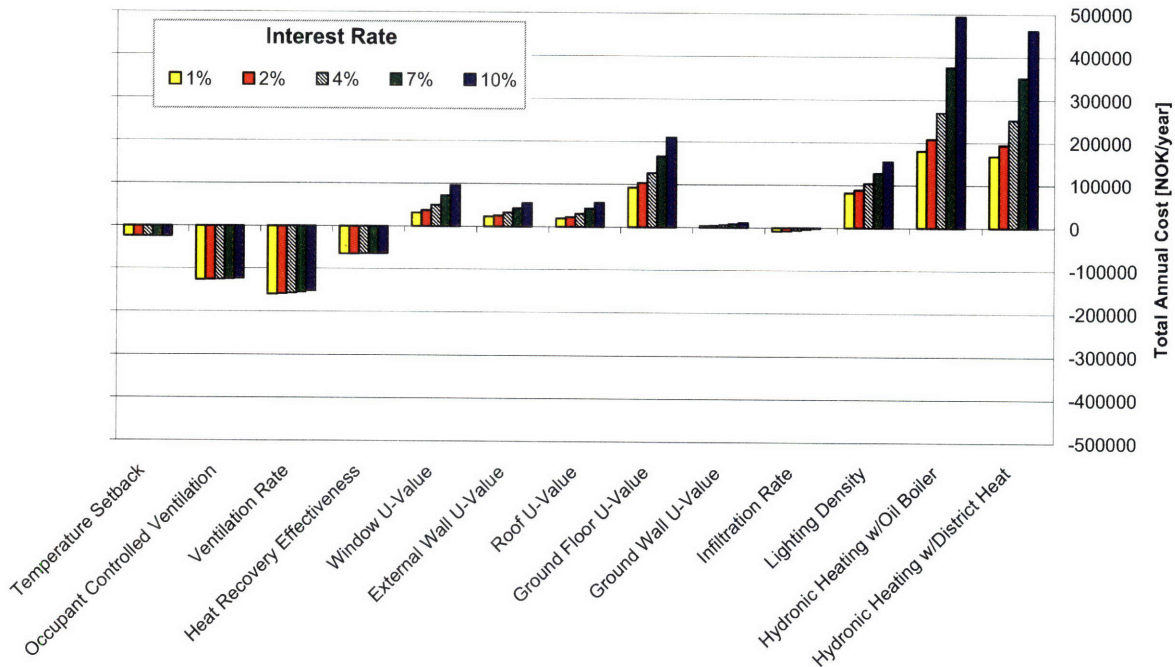


Figure 8-14: Total annual cost of all Individual Retrofits at their moderate retrofit state. Total annual costs are shown at a 1%, 2%, 4%, 7%, and 10% interest rate. All results are from the manually calibrated Corrected model (NOK/year).

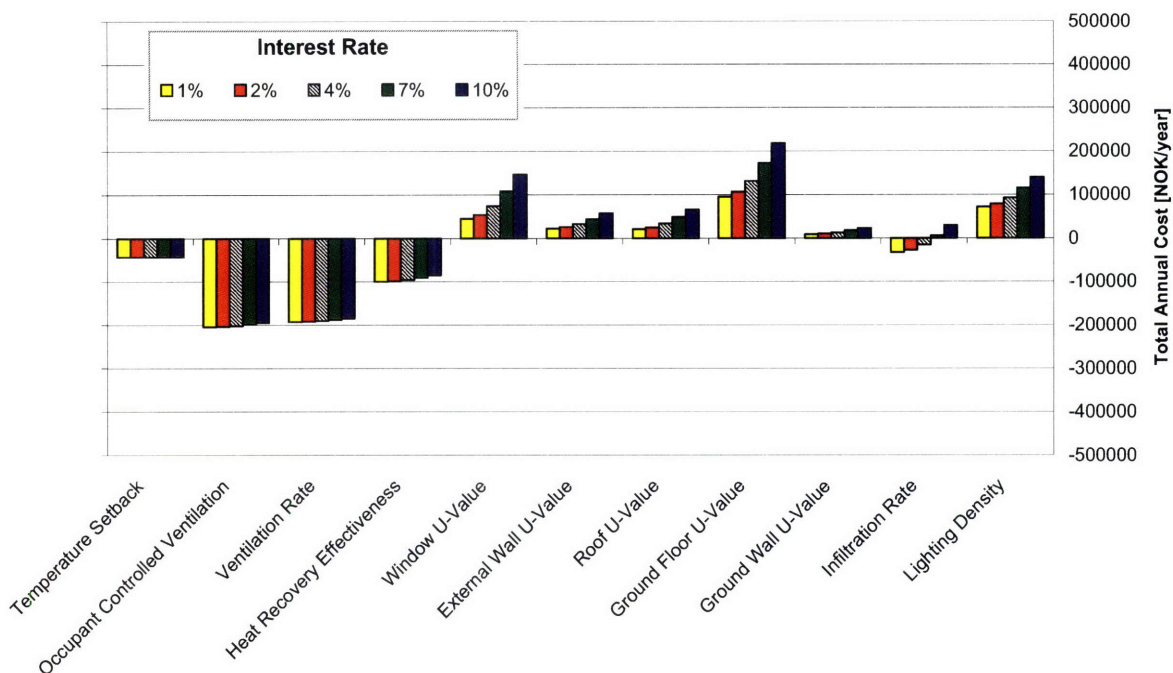


Figure 8-15 : Total annual cost of all Individual Retrofits at their low-energy retrofit state. Total annual costs are shown at a 1%, 2%, 4%, 7%, and 10% interest rate. All results are from the manually calibrated Corrected model (NOK/year).

Figure 8-14 and Figure 8-15 both indicate that the interest rate has almost no influence on the total annual cost of the temperature setback, occupant controlled ventilation, ventilation rate, and heat recovery effectiveness retrofits. This is because the annual utility bill savings for these retrofits are great enough to mask the variation in the annual investment cost at different interest rates.

Examining those retrofits with small energy savings and high annual investment costs (envelope, lighting, and heating system retrofits), the impact of changing the interest rate is much more pronounced. This is attributed to the fact the utility bill savings are almost negligible for these retrofits; their total annual costs are dominated by the annual investment cost of the retrofit, which is strongly influenced by the interest rate.

Perhaps the most interesting result of this portion of the retrofit analysis was the change in the total annual cost of the infiltration retrofit at varying interest rates. At low interest rates the total annual cost is less than zero, making this a cost effective retrofit option. However, at high interest rates the total annual cost of the infiltration retrofit becomes positive, making it too costly to consider for installation in the Steindal School. The 4% interest rate marked the

transition between positive and negative total annual costs. Consequently, it provided the most reasonable assessment of the total annual cost of the infiltration rate retrofit.

On the basis of the total annual investment costs shown in Figure 8-14 and Figure 8-15 the 4% interest rate was selected for performing all further total annual cost calculations. Subsequently, the total annual cost at a 4% interest rate was plotted coincidentally with the predicted energy savings from the Individual Retrofit analysis in Figure 8-16 and Figure 8-17. The annual energy savings (y-axis, left hand side, solid green bars) and total annual cost (y-axis, right hand side, hatched bars) are plotted. An energy savings < 0% indicates a reduction in energy consumption from the base-year and a total annual cost < 0 NOK/year indicates utility cost savings that exceeded the annualized investment cost of the retrofit. The black error bars that are associated with the predicted energy savings indicate the uncertainty in the savings value ($U \cdot F$), calculated according to Equation 8-3.

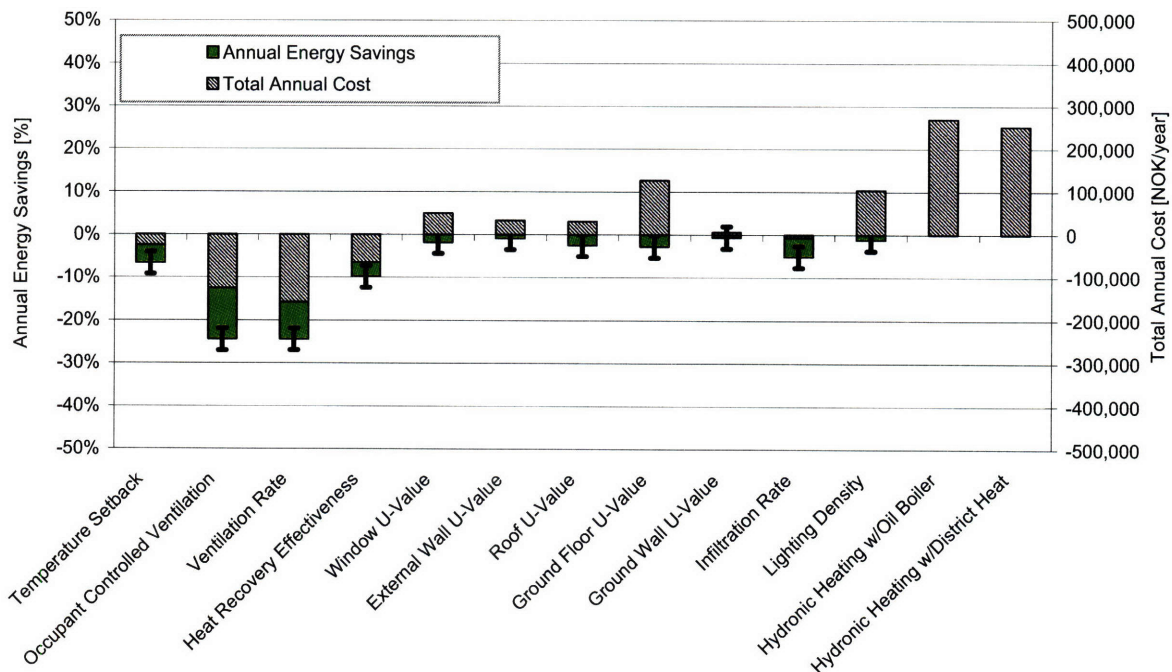


Figure 8-16: Annual energy savings (%) and total annual cost (NOK/year) of all Individual Retrofits at their moderate retrofit state. The interest rate was 4%; all results are from the Corrected model.

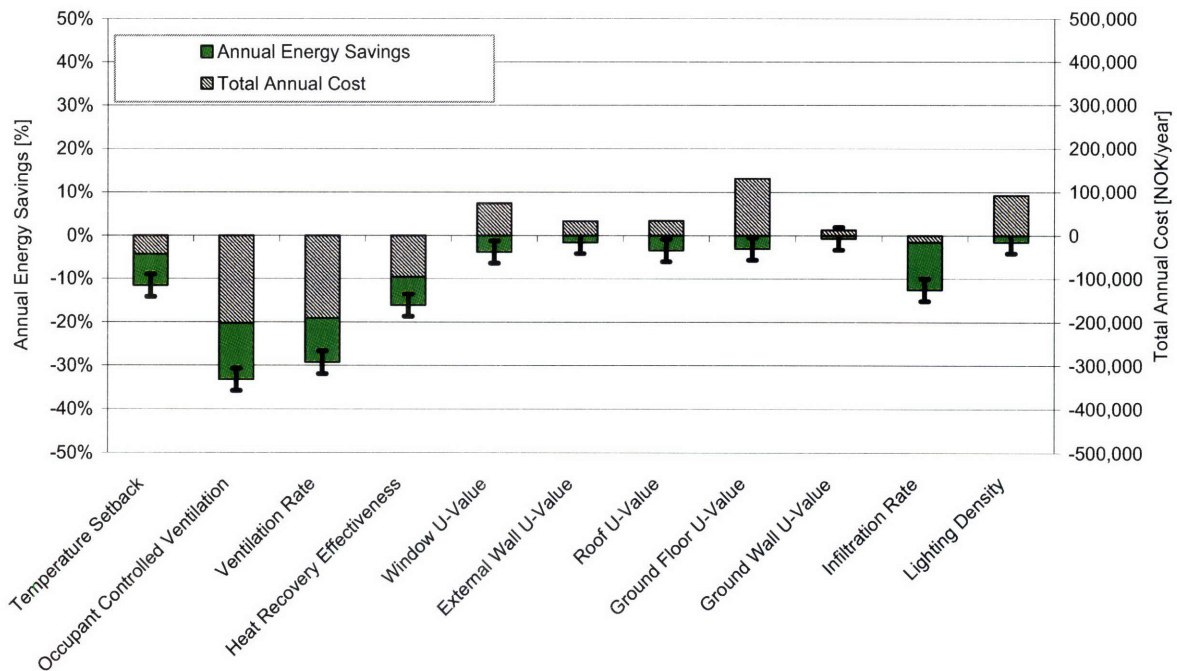


Figure 8-17: Annual energy savings (%) and total annual cost (NOK/year) of all Individual Retrofits at their low-energy retrofit state. The interest rate was 4%; all results are from the Corrected model.

According to Figure 8-16 and Figure 8-17 the only retrofits with total annual costs that were low enough to justify their installation were the temperature setback, ventilation rate, occupant controlled ventilation, heat recovery effectiveness, and infiltration rate. This result was consistent with uncertainty analysis that was performed previously and the results that were observed at varying interest rates in Figure 8-16 and Figure 8-17. Therefore, in moving forward with the analysis only the temperature setback, ventilation rate, occupant controlled ventilation, heat recovery effectiveness, and infiltration rate were considered as plausible energy conservation measures for the Steindal School.

8.4 Parametric Analysis

The parametric analysis examined all possible combinations of the five retrofits from the Individual Retrofit analysis that had predicted energy savings greater than 5%. This included the temperature setback, ventilation rate, occupant controlled ventilation, ventilation heat recovery effectiveness, and infiltration rate retrofits. The purpose of this parametric analysis was to identify the retrofit combination(s) with the greatest energy savings potential at the lowest total annual cost. Additionally, the Energy Performance in Buildings Directive (EPBD) rating was

calculated for each retrofit combination. The independence of retrofit savings predictions was also investigated.

The parametric analysis was performed with the manually calibrated Corrected model. EnergyPlus simulations were run with this model to calculate the energy savings for different retrofit combinations. The manually calibrated Corrected model was chosen in the interest of time. The parametric analysis discussed here required 162 simulations to be run:

$$\begin{aligned} \# \text{ Simulations} = & (3 \text{ temperature setback states} * 3 \text{ ventilation rate states} * \\ & 3 \text{ heat recovery efficiency states} * 3 \text{ infiltration rate states} * \\ & 2 \text{ occupant controlled ventilation states}) * 1 \text{ calibrated solution} \end{aligned}$$

The three retrofit states were the current, moderate, and low-energy retrofit states. Only two states were tested for the occupant controlled ventilation retrofit: on and off. Had the parametric analysis been run on the LHMC calibrated models with their Top 20 solutions the number of simulations would have been multiplied by 20, resulting in 3,240 simulations. At a run time between 1-2 minutes, 3,240 simulations would have required a minimum of 54 hours of runtime on a reasonably fast PC.

8.4.1 EPBD Rating Calculation

The method for calculating the EPBD rating for Norwegian buildings was presented in section 2.6 in Chapter 2, and will not be presented in its full form here. However, the equation for calculating a building's EPBD rating is shown in Equation 8-15. Additionally, the modification factors for different energy sources are shown in Table 8-42.

$$\text{Energy Rating} = \sum_{i=1}^N \frac{\text{Energy}_i}{\eta_{\text{production},i} * \eta_{\text{regulation},i} * \eta_{\text{distribution},i}} * IF_i \quad (8-15)$$

Energy_i	Energy consumption by each energy carrier in the building
IF_i	Influence factor for that energy carrier
$\eta_{\text{production},i}$	Efficiency of the energy produced at the building site for energy carrier i
$\eta_{\text{regulation},i}$	Efficiency of the building's control system for energy carrier i
$\eta_{\text{distribution},i}$	Efficiency of distribution of energy carrier i
N	Number of energy carriers in the building

Heat Source	Production Efficiency $\eta_{\text{production}}$	Regulation Efficiency $\eta_{\text{transformation}}$	Distribution Efficiency $\eta_{\text{distribution}}$	Total Efficiency $\eta_{\text{total}} = \eta_{\text{production}} + \eta_{\text{transformation}} + \eta_{\text{distribution}}$	Influence Factor IF	Total Modifier (IF/ η_{total})
Electricity	1.00	1.00	1.00	1.00	1.00	1.00
District Heat	0.98	0.95	0.95	0.88	0.55	0.625
Oil Boiler	0.85	0.95	0.95	0.77	1.00	1.30

Table 8-42: Modification factors for calculating the EPBD rating of Norwegian buildings. Modification factors for electricity, district heating, and an oil boiler are all given.

No additional EnergyPlus runs were performed to calculate the EPBD rating with different heating energy sources. Rather, the EPBD rating was calculated according to Equation 8-15, where oil, district heating, and electricity were all considered as potential energy carriers for heating the Steindal School; electricity was the only energy carrier considered for meeting the fan and pump, lighting, plug load, and hot water energy consumption in the school.

The modification factors presented in Table 8-42 were applied to differentiate between the three different heating energy carriers. These modification factors included the efficiency of on-site energy production in the oil boiler and district heating systems. No changes in annual energy consumption were made to account for pumps or other mechanical installations that would coincide with the installation of a hydronic heating system. The total annual cost of installing alternative heating systems was considered, including the annual investment and utility costs for each retrofit. The utility costs were appropriate for each heating energy supplier; equations and tariffs for calculating the cost of oil, district heating, and electricity were given in section 8.3.5.2.

8.4.2 Parametric Analysis Results

Figure 8-18 presents the results of the parametric analysis. The color-coded bands correspond to the levels of the EPBD for schools in Norway (Chapter 2) and are defined by the minimum and maximum energy savings required to reach each level. The required rating for existing buildings undergoing major retrofits is “C”. The results of the 162 parametric simulations with the existing electric resistance heating system (grey triangles), oil boiler (aqua diamonds), and district heating (pink circles) are all shown. The energy savings for the individual low-energy temperature setback, ventilation rate, heat recovery effectiveness, infiltration rate, and occupant controlled ventilation (OCV) retrofits are all highlighted and are bounded by the appropriate uncertainty bands (Equation 8-3). All retrofit results with the existing electric heating system are presented by triangles, the oil boiler is represented by

diamonds, and the district heating is represented by circles. Negative energy savings indicate a reduction in energy consumption from the base-year building conditions; a negative total annual cost indicates retrofits with utility bill savings that are greater than their annual investment cost. The base-year building conditions occur at the point with zero energy savings and zero total annual cost.

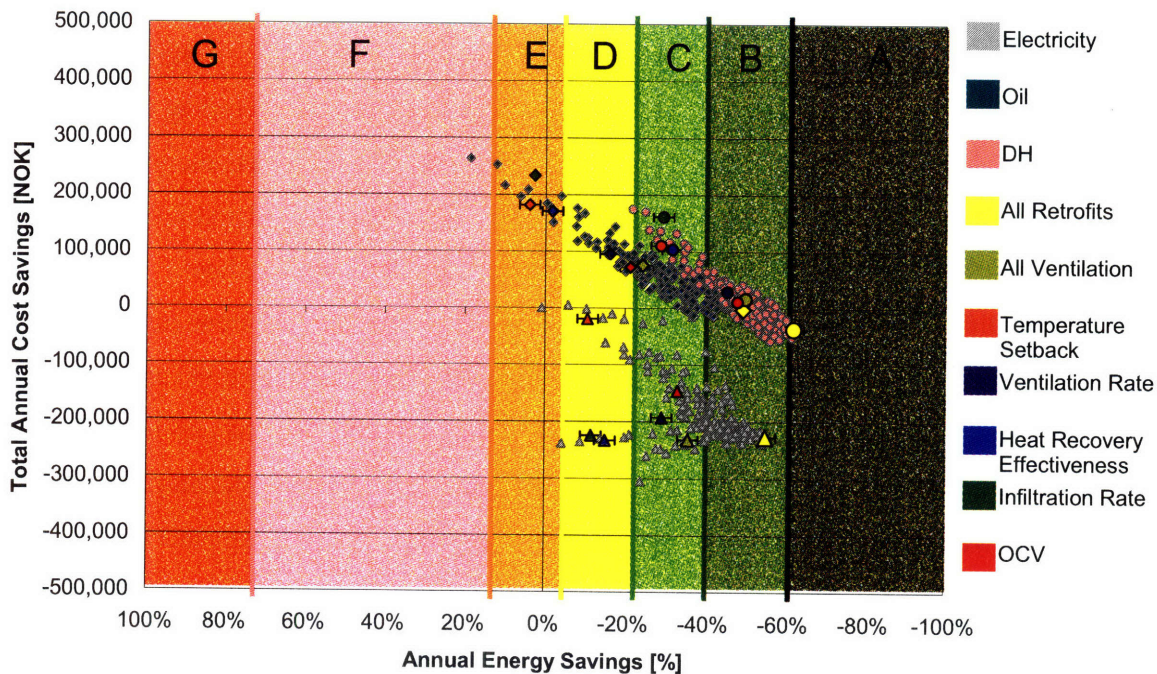


Figure 8-18: Results of the Parametric Retrofit analysis with the temperature setback, ventilation rate, occupant controlled ventilation, heat recovery effectiveness, and infiltration rates retrofits. All results are from the manually calibrated Corrected model.

The results of the parametric analysis with the existing electric resistance heating system showed a much greater spread in total annual costs than the oil boiler or district heating retrofits. This was because the very high investment costs of the oil boiler and district heating retrofits tended to damp out the variations in the total annual costs of the Parametric Retrofit combinations.

Recall from section 8.3.5 that the electricity utility bills were a function of three charges: energy, power, and a fixed cost. Additionally, recall that the moderate and low-energy temperature setback retrofits had a predicted energy savings of 7% and 12%, respectively, while the utility savings were only 4% and 7%, respectively. The moderate decrease in the utility costs from the base-year were the result of competing energy and power charges; the annual energy consumption was reduced, but the annual peak power demand was increased. Because the peak

power demand was strongly tied to the heating energy consumption in the building it was anticipated that the installation of a district heating or oil boiler system would make the temperature setback a more economically attractive retrofit for the school. Indeed, examining the electric resistance heating retrofits (triangles) in Figure 8-18 it may be noted that of the five low-energy retrofits that are highlighted, the temperature setback (orange triangle) has the highest total annual cost, despite the fact that it has essentially no investment cost. However, examining the oil boiler (diamonds) and district heating (circles) retrofits, the relative cost of the low-energy temperature setback is nearly the same as the heat recovery effectiveness, and is even lower than the infiltration rate retrofit. Consequently, the temperature setback retrofit was observed to be more cost effective when paired with the district heating or oil boiler systems. However, recall that the hydronic heating system pump demand was not included in the analysis that was performed here. It is anticipated that this pump will require additional power to meet the peak heating demands with the oil boiler and district heating systems, and will to some degree increase the peak electricity demand in the building. This was not quantified here, but it was important to recognize that this would have some impact on the peak power demand with increased temperature setback.

8.4.3 Achievable EPBD Ratings

Table 8-43 presents the EPBD levels that were achieved under a variety of retrofit conditions.

Retrofit					EPBD Rating		
Temp. Setback	OCV	Vent. Rate	Heat Recov. Effic.	Infil. Rate	Electricity	Oil	District Heating
Low-Energy	X	X	X	X	D	E	C
X	Low-Energy	X	X	X	C	D-C	B
X	X	Low-Energy	X	X	C	D	B
X	X	X	Low-Energy	X	D	E-D	C
X	X	X	X	Low-Energy	D	E	C
Low-Energy	Low-Energy	Low-Energy	Low-Energy	Low-Energy	B	B	B-A
X	Low-Energy	Low-Energy	Low-Energy	X	C	D-C	B
Low-Energy	Low-Energy	Low-Energy	Low-Energy	X	B	C-B	B

Table 8-43: EPBD ratings for various retrofits combinations from the Parametric Retrofit analysis. Ratings are shown with each of the three alternative heating systems: electricity, oil, and district heating.

The district heating had an equivalent or better EPBD rating than the existing electric resistance heating system for all of the low-energy Individual Retrofits (first five rows in Table 8-43); the oil boiler retrofit resulted in an equivalent or worse EPBD rating than the existing heating system.

The best possible EPBD rating was achieved when the temperature setback, occupant controlled ventilation (OCV), ventilation rate, heat recovery effectiveness, and infiltration rate were all retrofit to their low-energy states and a district heating system was installed. This retrofit combination brought the annual energy consumption in the Steindal School to the cusp of the level “A” rating, its uncertainty bars extended from level “B” into level “A”. Additionally, this retrofit was shown to be cost effective. The utility bill savings that resulted from the combination of the temperature setback, ventilation, and infiltration retrofits were able to justify the investment cost of the district heating system.

Other retrofit combinations of interest are summarized in Figure 8-19. All retrofits are shown with the existing electric resistance heating system. A brief description of each retrofit is provided and the annual energy consumption and total annual costs are shown. Scenarios #1

through #3 were only for the moderate retrofit states. Scenarios #4 through #6 were only for the low-energy retrofit states. The progression from Scenario #1 to #3 and from Scenario #4 to #6 started with the ventilation retrofits, then added the temperature controls retrofits, and finally simulated the infiltration rate retrofits.

- **Typical Norwegian School:** Energy consumption in typical Norwegian schools [Gustavsen 2007].
- **Base-year:** Simulated energy consumption from base-year Corrected building model.
- **Scenario #1:** OCV, ventilation rate, and heat recovery effectiveness at their moderate retrofit states.
- **Scenario #2:** OCV, ventilation rate, heat recovery effectiveness, and temperature setback at their moderate retrofit states.
- **Scenario #3:** All-retrofits at their moderate retrofit state: OCV, ventilation rate, heat recovery effectiveness, temperature setback, and infiltration rate at their moderate retrofit states.
- **Scenario #4:** OCV, ventilation rate, and heat recovery effectiveness at their low-energy retrofit states.
- **Scenario #5:** OCV, ventilation rate, heat recovery effectiveness, and temperature setback at their low-energy retrofit states.
- **Scenario #6:** All-retrofits at their low-energy retrofit state: OCV, ventilation rate, heat recovery effectiveness, temperature setback, and infiltration rate at their low-energy retrofit states.

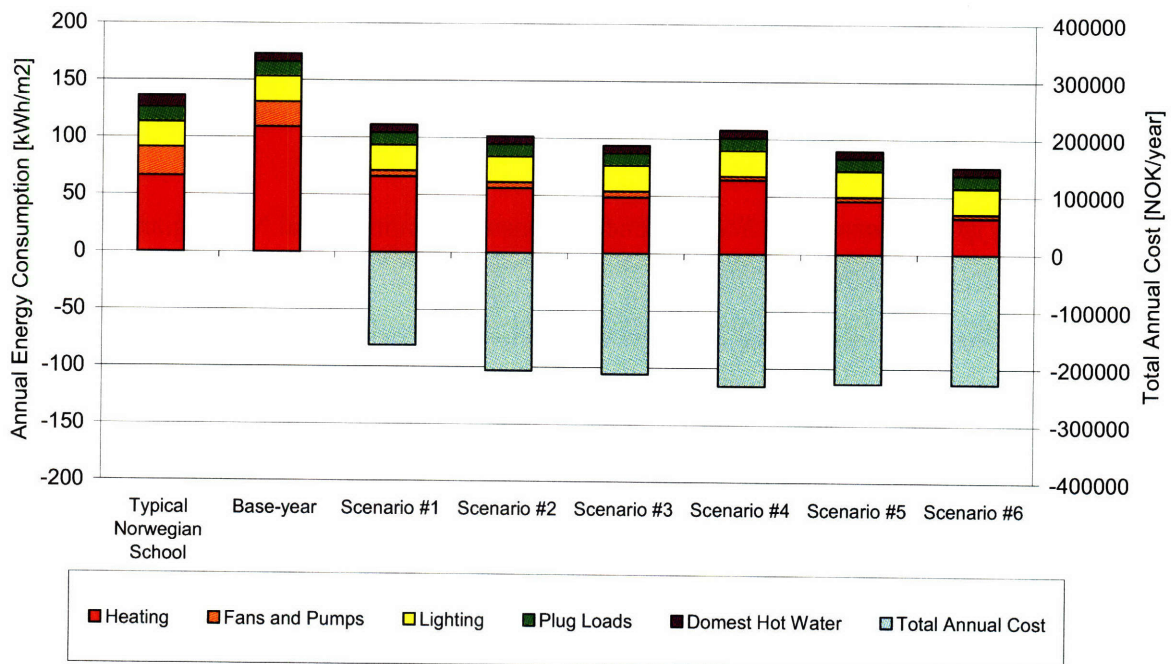


Figure 8-19: Annual energy consumption (kWh/m²/year) and total annual cost (NOK/year) for a number of retrofits from the Parametric Analysis. The annual energy consumption in the base-year of the Corrected model and a typical Norwegian school are also shown.

In all cases the ventilation retrofits were shown to be cost effective options. In combination (Scenario #1 and #4), the three ventilation retrofits were able to achieve an energy reduction of more than 30% over the base-year building conditions; the annual utility bill savings exceeded the annual investment cost by more than 200,000 NOK/year in both Scenario #1 and #4. Additionally, increasing the temperature setback in Scenarios #2 and #5 decreased the total annual energy consumption by more than 40% from the base-year. However, the increased temperature setback also resulted in an increase in total annual cost from Scenario #4 to Scenario #5. This increase in total annual cost was attributed to the fact that at low energy consumption (< 85 kWh/m²/year) the power tariffs tended to dominate the utility cost calculations.

Both Scenario #3 and #6 included reduced infiltration in addition to the ventilation and temperature setback retrofits in Scenario #2 and #5. Scenario #3 and #6 both showed the greatest potential for energy savings at their respective retrofit states (moderate and low-energy). However, neither of these scenarios showed an improvement in the total annual cost. The increased investment cost to implement the infiltration rate retrofit negated the utility bill savings with the reduced energy consumption.

In all six scenarios, retrofitting the ventilation system to improve the heat recovery effectiveness at decreased outdoor air flow rates with occupant control was shown to be an economically viable retrofit option. Additionally, combining the ventilation retrofits with increased temperature setback was shown to be economically viable in the moderate retrofit case, but not in the low-energy retrofit case.

8.4.4 Independence of retrofit energy savings predictions

It was also of interest to establish under what circumstances the energy savings from retrofit combinations could be estimated by the sum of the individual energy savings of each retrofit. For example, the temperature setback and ventilation retrofits were expected to be independent – schedules of operation dictated that these two retrofits were active during different parts of the day (ventilation during the day and temperature setback at night) and week (no ventilation on weekends, temperature setback on weekends). Additionally, these two retrofits impacted different building systems. The ventilation retrofits affected the ventilation system, while the temperature setback retrofits affected the space heating system. Given their anticipated independence, the simulated energy savings of the combination of these retrofits was expected to equal the sum of each individual retrofit’s energy savings.

Table 8-44 presents the **simulated** energy savings for any pair of retrofits at their low-energy states. The cells highlighted in grey are the energy savings for the individual retrofits. Pairings are indicated by the row and column headings for each cell.

Simulated Savings	Temperature Setback	OCV	Ventilation Rate	HRU Efficiency	Infiltration Rate
Temperature Setback	-11%				
OCV	-44%	-33%			
Ventilation Rate	-40%	-35%	-29%		
HRU Efficiency	-26%	-35%	-33%	-15%	
Infiltration Rate	-20%	-45%	-41%	-27%	-12%

Table 8-44: Calculated savings for two-retrofit, low-energy, combinations. Grey indicates Individual Retrofit results, while white indicates simulations with two retrofits in combination.

In order to **calculate the sum** of the energy savings of each individual retrofit (grey in Table 8-44) the following equation was applied: $|\% \text{ Savings, Retrofit } A| + |\% \text{ Savings, Retrofit } B| = |\% \text{ Savings, Total of } A \& B|$. The calculated energy savings for each retrofit combination is shown in Table 8-45.

Calculated Savings	Temperature Setback	OCV	Ventilation Rate	HRU Efficiency	Infiltration Rate
Temperature Setback	-11%				
OCV	-44%	-33%			
Ventilation Rate	-40%	-62%	-29%		
HRU Efficiency	-26%	-48%	-44%	-15%	
Infiltration Rate	-23%	-45%	-41%	-39%	-12%

Table 8-45: Calculated retrofits energy savings, equal to the sum of the energy savings of each Individual Retrofit.

In order to assess how well the sum of individual retrofit energy savings (Table 8-45) is able to estimate the simulated retrofit combination energy savings (Table 8-44) the error between the simulated and summed energy savings was calculated as $(\% Savings, Simulated - \% Savings, Calculated) / (\% Savings Simulated) = \% Error$. These errors are shown in Table 8-46.

% Error in simulated vs. additive savings	Temperature Setback	OCV	Ventilation Rate	HRU Efficiency	Infiltration Rate
Temperature Setback	0%				
OCV	0%	0%			
Ventilation Rate	1%	-79%	0%		
HRU Efficiency	1%	-39%	-33%	0%	
Infiltration Rate	-12%	1%	1%	-43%	0%

Table 8-46: % Error in the calculated vs. simulated savings for various retrofit pairings.

Table 8-46 shows that the sum of the individual retrofit savings provided good estimates ($\leq 1\%$ error) of the simulated energy savings when combining any one of the three ventilation retrofits with either the temperature setback or infiltration rate retrofit. This indicates that the ventilation retrofit energy savings were nearly independent from the infiltration or temperature setback energy savings. However, the combination of multiple ventilation retrofits shows a highly non-linear relationship, with errors of up to 79% when using the simple summation to estimate the combined savings. The combination of the temperature setback and infiltration retrofit had an error of 12%; the simulated 20% energy savings was 3% less than the sum of the individual retrofit energy savings.

Recognizing that the relationship between the energy savings of the three ventilation retrofits was highly non-linear, but that they were all independent from the temperature setback and infiltration retrofits, the simulated energy savings for all three ventilation retrofits was summed with the individual temperature setback and infiltration retrofit energy savings to estimate the savings for the combination of all low-energy retrofits:

$$-11\% + -12\% + -36\% = -59\% \text{ calculated vs. } -55\% \text{ simulated, a } 7\% \text{ error}$$

This resulted in a reasonable match with the simulated data, and further supports the independence of the temperature setback and infiltration retrofits from the ventilation retrofits.

Based on the parametric study performed above it was suggested that retrofits that affect different building systems, as in the temperature setback and ventilation retrofits in this analysis, show linearity in the prediction of their combined savings. However, retrofits that affect similar systems and that are known to be highly interactive, as in the ventilation retrofits, have highly non-linear relationships, and their combined savings are not easily estimated with a quick summation.

8.4.4.1 Infiltration and Windows

Recall from the Individual Retrofit analysis that all retrofits were considered to be independent. Under this assumption only five of the ten retrofit options that were modeled were considered to have acceptable levels of uncertainty in their predicted energy savings. As a result, only the temperature setback, ventilation rate, occupant controlled ventilation, heat recovery effectiveness, and infiltration rate were taken to be candidate retrofits. However, what was not investigated was the potential for reasonable energy savings when these five retrofits were paired with those five retrofits that were considered to be uncertain. For example, the benefits of retrofitting the ventilation system in conjunction with the building's windows were not investigated. The investigation into these combinations would have been exhaustive, and the cost analysis indicated that all of the building envelope retrofits had high total annual costs, and would have been difficult installations to justify. However, one potential combination that was both reasonable and potentially cost effective was the low-energy infiltration retrofit and the low-energy window retrofit. The low-energy infiltration retrofit would be implemented by installing new windows and frames, making it an opportune time to upgrade the windows in the Steindal School.

Individually, the predicted energy savings for the infiltration and window U-value retrofits, when simulated with the manually calibrated Corrected model, were 12% and 4% with a total investment cost of 947,000 NOK/year and 1,545,700 NOK/year, respectively. The uncertainty associated with each of these energy savings predictions was equal to 3%. Recalling the relationships observed in the previous section, a first approximation of the upper bound of the energy savings resulting from the combination of these two retrofits was equal to $12\% + 4\% =$

16%. This was confirmed through a simulation with the manually calibrated Corrected model, where the two low-energy retrofits were run simultaneously. The resulting energy savings were equal to 16%. Additionally, the investment cost of such a retrofit was equal to the low-energy window installation cost, or 1,545,700 NOK. Annually, this was equivalent to an investment cost of 95,000 NOK/year at an interest rate of 4%. However, this annual investment cost was well in excess of the 30,000 NOK/year of utility cost savings that were simulated for this retrofit combination. Therefore, although the combination of the low-energy window and infiltration rate was able to obtain a greater energy savings than either of the two retrofits alone, the increase in the investment cost of the retrofit led to a the total annual cost greater than zero. This retrofit combination was too expensive to be considered an economically viable option.

8.5 Lessons Learned

The retrofit analysis performed above indicated that the greatest energy savings were achieved by the ventilation retrofits, which show savings on the order of 20-30% and 30-40% for their moderate and low-energy states, respectively. Additionally, both the temperature setback and infiltration rate retrofits were observed to have energy savings that were greater than, or equal to, the 5-10% that were recommended for identifying accurate energy savings predictions. These are also the five retrofits with the lowest total annual cost, making them cost effective retrofit possibilities for installation in the Steindal School.

Equations developed by Reddy and Claridge [Reddy 2000] for estimating the uncertainty in the energy savings prediction of a single simulation were applied to the manually calibrated Corrected and Original models and were able to bound between 15-18 of the Top 20 solutions in the corresponding LHMC calibrated models for the ventilation rate, occupant controlled ventilation, heat recovery effectiveness, and temperature setback retrofits. Additionally, the Simple model, which was the most poorly calibrated of the five models examined in this analysis, consistently showed a wider range of predicted energy savings than the other four calibrated models. However, no two models showed a variation in their median energy savings that was greater than 7%, and this occurred in the ventilation retrofits, where the predicted savings were typically between 25-40%.

Performing a parametric analysis with the temperature setback, ventilation rate, occupant controlled ventilation, heat recovery efficiency, and infiltration rate retrofits indicated that the

greatest possible energy savings of 55% was achieved when all of these retrofits were at their low-energy states with the existing electric resistance heating system. This corresponds to a category “B” EPBD rating. Additionally, when installed with a district heating system, this retrofit combination was able to reach the cusp of the “A” EPBD rating at a negative total annual cost.

The calculated EPBD rating for the Steindal School with electricity as the only energy supplier ranged from category “D” to “B”. Installing an oil boiler and applying the modification factors recommended in the work performed by Wigenstad et al. [Wigenstad 2005] caused the range of predicted energy savings to shift to poorer (“E” to “F”) EPBD ratings at higher total annual costs. Conversely, the range of predicted energy savings shifted to better (“A” to “B”) EPBD ratings at a higher total annual cost when installing a district heating system. The best possible rating for the oil boiler was a “C” rating, while the district heating was consistently able to achieve a rating of “B”. The required rating for major renovations is “C”.

Linear relationships were observed between the calculated energy savings from the temperature setback and ventilation retrofits and the infiltration rate and ventilation retrofits. However, the ventilation retrofits showed a high degree of non-linearity in their combined savings.

On the basis of this analysis the recommended retrofit for the Steindal School was a reduction in ventilation rates with occupant control and improved heat recovery effectiveness. Additionally, with the installation of a hydronic heating system, the temperature setback retrofit was shown to be cost effective.

9 Conclusions

On the basis of the observations made in Chapters 5 through 8 a number of recommendations were made for performing future retrofit energy savings analyses.

- ***Retrofit selection*** (Chapter 8): Potential retrofits for the building should be defined before selecting the method of energy savings assessment (i.e. simple estimates or computer simulations). Retrofits should be chosen from typical practice and conversations with building managers and should represent the most likely renovations for the building of interest. This enables potentially important building characteristics to be identified prior to selecting the retrofit evaluation method.
- ***Method of retrofit analysis*** (Chapters 6 and 7): Calibrated simulations are useful when analyzing building systems with complex interactions. Examples of such systems include the building envelope, space heating, lighting, and plug loads. In systems whose energy consumption can be isolated from the whole-building energy consumption, like the domestic hot water and ventilation in the Steindal School, much simpler calculation procedures (i.e. measurements and spreadsheet analysis) may be appropriate for predicting retrofit energy savings. However, these simple procedures are only valid if detailed system data are available. When key system characteristics are not well defined or are difficult to measure, calibrated simulations are useful for identifying the most likely values of these characteristics. This was the case with the heat recovery effectiveness in the Steindal School, for which accurate measurements were not available and calibrated simulations were utilized to estimate the most likely value of this system characteristic.

The remainder of these recommendations will focus on the use of calibrated simulations, as this was the method applied in this work.

- ***Resources for defining the energy use in buildings*** (Chapters 5 and 6): Resources and methods for describing the building's energy use include as-built documents, site visits, conversations with building managers, and measurements. Here, it is useful to think of the resources for data collected in terms of the six levels defined in RP-1051 [Reddy 2006], which were shown in Table 3-5 of Chapter 3.

- As-built documents, site visits, and conversations with building managers were easiest to come by and defined levels 1 through 3 in Table 3-5. These levels were defined as having “low data availability”; levels 4 through 6 included more detailed building information including measurements and hourly energy consumption data and were defined as having “high data availability”.
 - Higher levels of data collection tend to increase model accuracy, but also imply higher costs. The modeler, investors, and building managers should decide which level of data collection is most appropriate to the needs of a specific retrofit project.
- In this work, simple annual energy estimates were found to be useful in estimating unknown inputs and establishing a first estimate of the building’s end-use energy consumption distribution. Because they are simple to perform and are capable of providing valuable information prior to model calibration, simple energy estimates are recommended for future calibrated simulation analyses.
- **Methods for calibrating building energy models** (Chapter 7): Two methods for calibrating building energy simulations were investigated in this work (Chapter 7): manual and Latin Hypercube Monte Carlo Analysis (LHMC). Both of these techniques enable influential inputs to be isolated from other input variables, but the two were found to be most effective under different model input conditions. In this work, it was found that the LHMC calibration was most appropriate for buildings with “low data availability” (see “Resources for defining the energy use in buildings” heading, above), while the manual calibration was most appropriate for buildings with “high data availability” (see “Resources for defining the energy use in buildings” heading, above). Additionally, in this work, running the LHMC on models that had already been calibrated manually showed little to no improvement in the fit between the simulated energy consumption and the measured utility data.
 - Automated calibration techniques, like LHMC, are not a replacement for modeler experience. A lack of experience leads to modeler errors, which may or may not be caught during calibration.
- **Calibration metrics** (Chapter 7): The quality of the fit between simulated and measured building energy data should be quantified statistically and graphically. In this work, the coefficient of variation of the root mean square error (CVRMSE), normal mean bias error

(NMBE), and goodness of fit (GOF) were calculated (see Equations 7-1, 7-2, and 7-3 in Chapter 7). Additionally, the resulting power and energy consumptions were graphed against the measured utility data to visually inspect the two data sets. The statistics provided threshold values for accepting models to be “calibrated” against monthly utility data, while the graphs of the predicted and measured data allowed those areas where discrepancies occurred to be isolated and the appropriate inputs to be tuned to improve the quality of the calibration. Therefore, both statistical and graphical calibration metrics are suggested for future analyses.

- Calibrations should be performed against a full year of uninterrupted utility data (12 consecutive months). Where hourly utility data is available, hourly calibration should be performed; monthly calibration is an acceptable alternative.
- In this work, the threshold values of CVRMSE and NMBE from ASHRAE Guideline 14 [ASHRAE 14 2002] (section 7.1.2 in Chapter 7) were acceptable when calibrating on a monthly basis ($\text{CVRMSE} \leq 15\%$ and $\text{NMBE} \leq 5\%$), but not on an hourly basis ($\text{CVRMSE} \leq 30\%$ and $\text{NMBE} \leq 10\%$). On an hourly basis, the uncertainty criteria recommended by Reddy and Claridge [Reddy 2000] (Equation 3-4 in Chapter 3) were found to be a more appropriate metric for accepting models as calibrated.
 - Hourly calibrations are subject to inaccuracies stemming from inconsistencies in the behavior of building occupants and systems, making it difficult to match the hourly calibration criteria set forth in ASHRAE Guideline 14 [ASHRAE 14 2002] ($\text{CVRMSE} \leq 30\%$ and $\text{NMBE} \leq 10\%$).
 - The uncertainty criteria recommended by Reddy and Claridge [Reddy 2000] are also recommended when the investors, building managers, or modeler require that the level of confidence in the predicted retrofit energy savings be increased beyond the standard 50% uncertainty at 68% confidence recommended in ASHRAE Guideline 14 [ASHRAE 14 2002].
- ***Uncertainty in retrofit energy savings predictions*** (Chapter 8): During LHMC the energy savings uncertainty should be defined by the range of predicted savings of the Top 20 calibrated solutions, while uncertainty should be defined using equations from Reddy and Claridge [Reddy 2000] when using manually calibrated models for retrofit energy savings prediction.

- ***Independence of retrofit energy savings predictions*** (Chapter 8): In the work performed here it was found that when retrofits influence different building systems, i.e. the space heating and ventilation systems in the Steindal School, the energy savings from the combination of these retrofit may be approximated as the sum of their individual energy savings. This was not the case with retrofits that influence the same system, as with multiple ventilation retrofits in this work.
- ***Retrofit cost assessments*** (Chapter 8): A simple cost assessment is useful in identifying retrofits whose utility bill savings justify their investment costs. The cost analysis performed in this work provided an easy means of comparing a number of retrofit options, and may be thought of as a method of narrowing the potential retrofits to a handful of candidates for which a more accurate cost analysis could be performed. In cases where a more precise cost analysis is desired, manufacturers and contractors should be contacted to obtain quotes for specific retrofit procedures. Additionally, escalation and inflation rates should be considered in addition to the interest rate that was considered in this analysis.

On the basis of these observations the manually calibrated Corrected model was considered to be the most accurate and appropriate for the Steindal School. This model had a higher level of modeler confidence in its inputs than the Original model, and similar CVRMSE and NMBE values to the Original model (Chapter 7). The application of LHMC to the manually calibrated Corrected model proved to be extraneous – it provided only minor improvements in the statistical fit with measured data. Additionally, when bounded by the energy savings uncertainty bands calculated according to ASHRAE Guideline 14 [ASHRAE 14 2002] and in work by Reddy and Claridge [Reddy 2000] (Equation 8-3 in Chapter 8), the Corrected model provided a good approximation of the range of energy savings values that were predicted with the Top 20 solutions from the Detailed-Corrected LHMC model. Thus, the Corrected model was able to quantify the uncertainty in retrofit energy savings predictions without performing an LHMC analysis.

9.1 Steindal School Case Study: Implications of Energy Savings Results

The recommended course of action for the Steindal School is to first improve the controls and the electric resistance heating that constituted the “baseload” in the building. Second, the ventilation system should be retrofit to reduce the ventilation rates, institute occupant control, and improve the heat recovery effectiveness. Additionally, the temperature setback should be increased to reduce the annual energy consumption in the school. After these retrofits have been performed a district heating system retrofit may be considered for installation in the Steindal School. The simple cost analysis showed that the district heating system was a cost effective retrofit when installed coincidentally with the ventilation system and temperature setback retrofits, but not as a stand-alone system.

The first energy conservation measure that is suggested for the Steindal School is the adjustment of the 20 kW “baseload” that was identified during calibration in Chapter 7. Installing thermostat controls on the electric resistance heating that contributed the majority of this load would result in an 8% reduction in the annual energy consumption compared to the current conditions in the school. Additionally, this retrofit would require only minor controls changes at essentially no cost (Chapter 8).

The second energy conservation measure that is suggested for the Steindal School is the retrofit of the ventilation system (decreased ventilation rates with improved heat recovery effectiveness and occupant controlled schedules of operation) and temperature setback (Chapter 8). Simulation of these measures showed that 46%⁺/_{-3%} of the current annual energy consumption in the Steindal School could be saved. The total investment cost of this retrofit scenario was estimated to be 424,000 NOK; at an annual utility bill savings of 260,000 NOK/year this retrofit would quickly pay for itself. With a district heating system, the total investment cost was increased to the sum of the district heating (4,500,000 NOK) and ventilation and temperature setback retrofits (424,000 NOK), or nearly 5,000,000 NOK. However, this increase in investment cost was offset somewhat by an increase in utility bill savings to 330,000 NOK/year. Over a 15-16 year period, the utility bill savings would be capable of paying back the 5,000,000 NOK investment cost of the district heating system, ventilation system, and temperature setback retrofits.

Retrofitting only the ventilation system and temperature setback with the existing heating system would bring the building from an Energy Performance in Buildings Directive (EPBD) rating of “E/D” to “B” – one level better than the “C” rating (equivalent to an annual energy consumption between 101-130 kWh/m²/year) required for existing buildings undergoing a major renovation (Chapter 8). With the district heating system, the EPBD rating would be shifted to the cusp of the “A” rating (equivalent to an annual energy consumption between < 65 kWh/m²/year).

10 General Procedure for Performing Energy Conservation Measure (ECM) Evaluations with Calibrated Simulations

On the basis of the conclusions that were made in Chapter 9 a general procedure was proposed for performing future retrofit analyses with calibrated simulations. This procedure is outlined in

Figure 10-1 and includes steps for collecting building data (Input), generating a calibrated model (Calibration), and performing retrofit analyses (Retrofit). This procedure is considered to be general because it relies on a series of observations and decisions that are based on the available data, modeler experience, costs, and the desired level of retrofit energy savings. Thus, it is not a concrete series of steps, but rather a recommended train of thought for moving forward with retrofit energy savings evaluations with calibrated simulations.

Retrofits should be identified prior to data collection. This enables the modeler to focus their attention on the inputs that are most likely to influence both the level of calibration of the model and the accuracy of the retrofit energy savings predictions. The choice of which building components to retrofit may be based on the modeler's observation of existing conditions, the desires of building managers or project investors, or on typical retrofits for similar buildings.

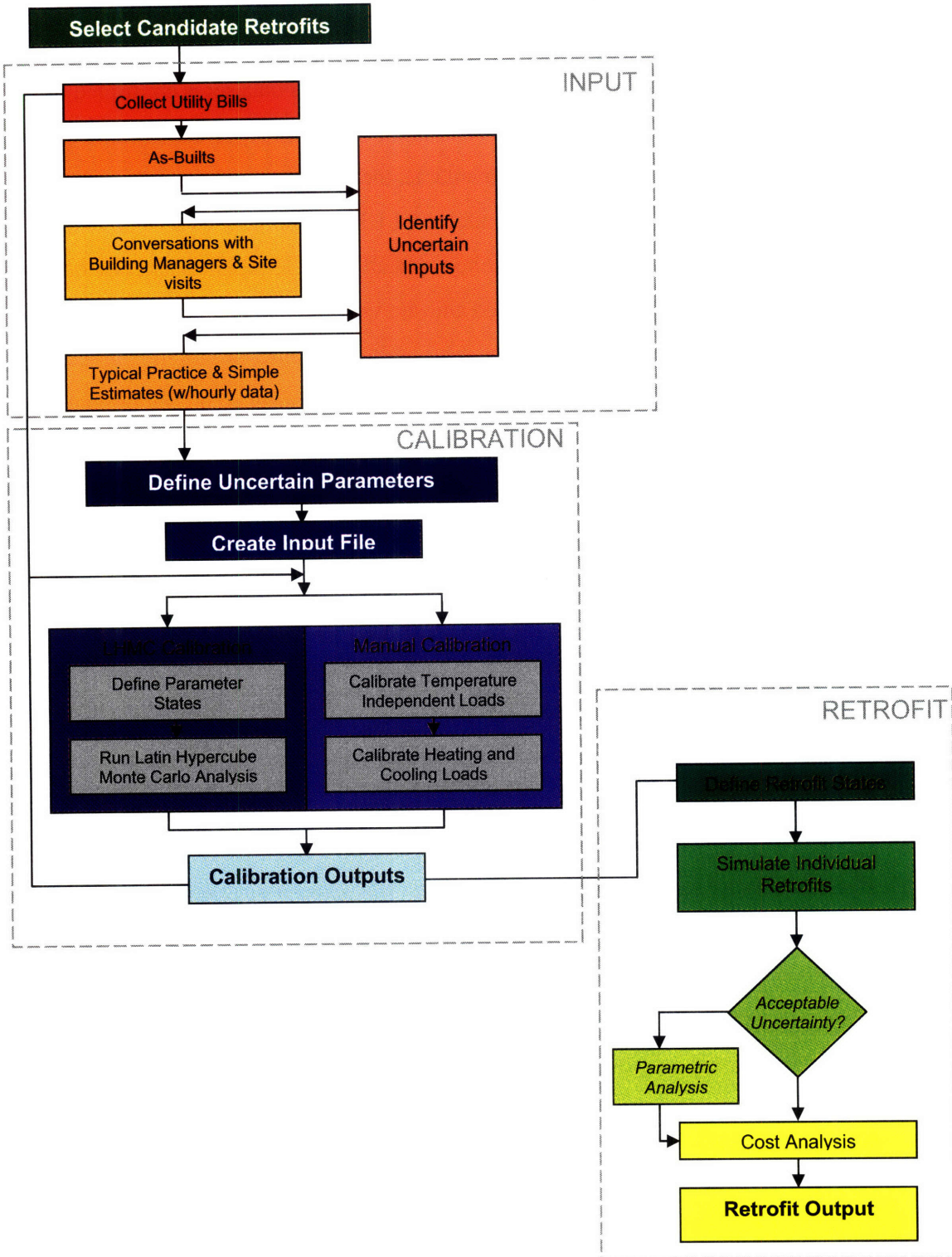


Figure 10-1: Recommended procedure for performing future retrofit analyses

10.1 Input

First, utility data should be collected. This data should be examined for any inconsistencies or outliers in the data set. After the accuracy of this data set is confirmed the modeler may decide to perform either a manual calibration or a Latin Hypercube Monte Carlo (LHMC) analysis calibration. If hourly data is available, then a manual calibration is recommended; if only monthly utility data is available a LHMC calibration is recommended.

As-built documents should then be consulted, and all possible building inputs should be defined. All uncertain inputs should be identified and site visits should be made to verify these inputs. Simple measurements of ventilation flow rates, air temperature, or building dimensions should be made during this site visit. Building managers may be consulted during the site visit, or may be contacted later. If the conversations with building managers occur after the site visit a list of uncertain and unknown inputs should be compiled after the site visit and before the conversations with building managers. This iterative process allows for the most efficient definition of the building characteristics.

After as-builts, site visits, and conversations with building managers have been completed a decision must be made by the modeler – should detailed measurements be made to verify uncertain inputs, or are a combination of typical values, simple estimates, and calibration acceptable? The work performed here showed the ventilation and heating loads to be important to accurately define the model of the Steindal School. Thus, for buildings in Norway, if the input is either unknown, or highly uncertain, and is concerned with the heating or ventilation systems, it is suggested that detailed measurements be performed. However, if detailed measurements have a high cost associated with their application, it is suggested that the modeler very carefully weigh their necessity against the uncertainty that would be generated by using typical values and simple estimates. Additionally, on/off tests like those used by Soebarto might be used. On/off tests were not utilized in this case study, but they are one simple method of isolating unknown building loads.

10.2 Calibration

After all inputs are verified against available data a list of inputs that are considered to be both uncertain and potentially influential to the accuracy of the calibration and retrofit should be generated. This list of uncertain inputs is passed to calibration, and is combined with knowledge

of the available utility data to decide whether a manual or LHMC calibration is most appropriate. If the quality of the available data is low, i.e. no hourly data are available or there are a large number of uncertain inputs (10-20), then LHMC is recommended. However, if the quality of the input data is high, manual calibration is recommended. In either case, the expected range of values for each uncertain input should be defined.

The metrics for calibration may either be based on retrofit uncertainty [Reddy 2000] or the coefficient of variation of the root mean square error (CVRMSE) and the normal mean bias error (NMBE) [ASHRAE 14 2002]. The NMBE and CVRMSE statistics from ASHRAE Guideline 14 [ASHRAE 14 2002] would be recommended unless conversations with investors or building managers indicate a desired retrofit energy savings uncertainty that is greater than that recommended in ASHRAE Guideline 14 (50% uncertainty at 68% confidence). For example, if the project's investors desire that the predicted energy savings be within 10% of the actual retrofit energy savings 90% of the time, the uncertainty criteria recommended by Reddy and Claridge [Reddy 2000] would be recommended for identifying calibrated model with an uncertainty of 10% at a 90% confidence level.

These metrics may be applied on a monthly, weekly, daily, or hourly basis. As a rule of thumb, the calibration should first be evaluated against the highest resolution data available. This means that where only monthly utility billing is available, monthly calibration should be performed ($NMBE \leq 5\%$ and $CVRMSE \leq 15\%$). Similarly, when hourly utility data is available, hourly calibration should be performed. However, when calibrating on an hourly basis the threshold statistics ($NMBE \leq 10\%$ and $CVRMSE \leq 30\%$) from ASHRAE Guideline 14 [ASHRAE 14 2002] were found to be difficult to attain in this case study, whereas, a number of retrofits were able to meet the uncertainty criteria recommended by Reddy and Claridge [Reddy 2000]. If the calibration statistics from ASHRAE Guideline 14 [ASHRAE 14 2002] cannot be met with hourly data then a lower resolution calibration may be performed, but the goal should still be to minimize the simulated error in order to increase the certainty in the accuracy of the model.

At this point the modeler may perform either a manual calibration or a LHMC calibration. As mentioned previously, the manual calibration is recommended when high resolution, high quality data, are available and a limited number (5-10) of uncertain inputs need to be investigated. The manual calibration utilizes the available hourly utility data to first tune

the building's temperature independent loads, then the building's heating and cooling loads. This enables the temperature independent, heating, and cooling loads to be isolated, enabling sources of model inaccuracies to be more easily identified. However, when lower resolution, lower quality data with a higher number of uncertain inputs are available, LHMC calibration is recommended. The number of runs for the LHMC calibration is dependent on the case study performed. Here, 2000 simulations were found to be adequate. One guideline for selecting the number of simulations to perform, recommended by RP-1051 [Reddy 2006], is to run iteratively higher numbers of LHMC simulations. If the same strong parameters are identified in consecutive sequences of simulations, then the method may be considered to have converged. However, the work performed here did not match this definition of convergence, and so its validity is still in question. Therefore, it is at the discretion of the modeler to judge whether or not enough simulations have been run. Here, the decision to stop running further simulations was made when no further improvements in the goodness-of-fit (GOF) value of the Top 20 calibrated models was made. Therefore, where "convergence" as defined by RP-1051 is not achieved, the stabilization of the GOF value may be used to select a stopping point. Once a reasonable number of simulations has been run the modeler may choose to analyze a number of top solutions during retrofit analysis. Here, the Top 20 solutions were found to be more than adequate, meaning that the Top 10 or 15 solutions may also have been accepted without compromising the accuracy of the energy savings predictions with the LHMC calibrated models.

At the conclusion of calibration it may be found that one particular input has a high degree of uncertainty and a strong influence on the quality of the calibration. Should this occur, the modeler should return to data collection to refine the definition of this input. This may be done by uncovering previously unavailable as-built documents, making simple measurements, or by performing detailed measurements. However, the use of detailed measurements should be weighed against the anticipated influence of the input. If the input is to be assessed during retrofit analysis, then it may be cost effective to verify its value with detailed measurements. After the uncertain inputs have been resolved the calibration should be rerun and the resulting calibrated model(s) should be passed to the retrofit analysis.

10.3 Retrofit

The first step in the retrofit analysis is to discretize the retrofits that were identified at the start of the procedure into a number of states. In this analysis each retrofit was assigned two states— moderate and low-energy. The moderate state generally corresponded with the most recent building code values, while the low-energy values were intended to represent greater energy savings, but also had higher costs.

Prior to performing the retrofit analysis all independent variables, i.e. weather, should be neutralized for both the pre-retrofit and post-retrofit building simulations. This ensures that all predicted energy savings are due to the retrofits of interest, and not differences in weather conditions between the two simulations.

After all retrofits states are defined an Individual Retrofit analysis should be performed. This analysis tests each retrofit independently at all possible states. The total number of simulations in this retrofit analysis is equal to $s*r*n$, where s is the number of solutions from calibration (i.e. 20 from LHMC and 1 from manual calibration), r is the number of retrofits, and n is the number of retrofit states.

The results of the Individual Retrofit analysis should then be examined to identify retrofits with acceptable levels of energy savings to be considered “certain”. Here, the equation defined by Reddy and Claridge [Reddy 2000] (Equation 8-3 in Chapter 8), is applied to define those retrofits with acceptable levels of predicted savings (50% uncertainty at 68% confidence). Retrofits that meet the uncertainty criteria should be evaluated for their utility and investment cost. The total annualized cost was used in the case study performed here, although a number of other investment cost metrics may also be appropriate.

Optionally, a parametric analysis may be performed to assess potential combinations of the individual retrofits that were considered to meet the uncertainty criterion. The choice of whether or not to run the parametric analysis should be based on the number of simulations and the amount of time required to perform the analysis. For example, to run a parametric analysis on five retrofits, r , each with three states, n , using the Top 20 solutions from the LHMC calibration, s , the total number of simulations would be equal to $s*n^r$, or 4,860 simulations. At 65-90 seconds per simulation (the time required for the Detailed-Corrected model) this amounts to 88-122 hours of simulations! Work performed here also showed that when the retrofits of interest in the parametric analysis influence independent building systems, i.e. space heating and

ventilation, then the total energy saved by performing both retrofits may be approximated by the sum of the energy saved by each individual retrofit. However, when two retrofits are not independent, i.e. space heating and lighting, this is not the case, and a linear approximation is not appropriate. However, in retrofits with small predicted energy savings, the total retrofit energy savings from their combination may be estimated by the sum of their individual retrofit savings. This approximation was shown to be valid with the infiltration and window U-value retrofits in section 8.4.4.1 of Chapter 8. However, no clear definition of “small predicted energy savings” was established. Consequently, linear energy savings estimates should be made with extreme caution.

The result of the retrofit analysis should be a recommended course of action for performing cost effective retrofits in the building of interest. This should be presented as a range of possible values, either with the Top 20 LHMC solutions, or using the uncertainty equations suggested by Reddy and Claridge [Reddy 2000]. In this way the modeler is able to acknowledge that the predicted retrofit energy savings were dependent on the amount of uncertainty present in the building model. Additionally, with the new EPBD regulations going into effect by 2010, the predicted energy savings should be presented in terms of the anticipated EPBD rating for the building.

11 Future Work

In future work, it would be useful to assess the accuracy of approximating unknown or uncertain inputs during calibration. The accuracy of this input definition method should be examined by performing detailed measurements to verify uncertain calibrated inputs. For example, in the Steindal School case study, it would be of interest to measure the heat recovery effectiveness of the ventilation system to verify the value that was accepted during calibration was accurate. This would provide a better understanding of the uncertainty associated with estimating retrofit energy savings with calibrated building models. Additionally, this would provide insight into the circumstances under which detailed measurements need to be made.

It would also be of interest to investigate methods of quantifying modeler bias in future work. Under what circumstances does it arise, and what influence does it have on model calibration and retrofit energy savings predictions? Developing answers to these questions would enable the accuracy of manually calibrated building models to be better understood.

The need for complicated calibrations with detailed computer software, like EnergyPlus, should be more explicitly contrasted against the much simpler building energy evaluation methods presented in Norwegian Standard 3031 [NS3031 2007]. Various building types with a number of constructions should be assessed with both modeling methods to establish when each method is most appropriate, and what kind of energy savings prediction accuracy could be expected with each.

The integration of calibration techniques and uncertainty quantification into retrofit energy savings software would enable a more fluid implementation of these procedures during retrofit evaluation. This software would be important to enabling project investors and building managers to assess the risk associated with a number of retrofit alternatives before selecting the most appropriate candidate for installation. This would also allow project decision makers to quantify their desired level of uncertainty prior to developing calibrated building energy models.

It is recommended that a more refined statistic than the goodness-of-fit (GOF) be developed for ranking calibrated simulations during Latin Hypercube Monte Carlo analysis. Here, the GOF was shown to be somewhat arbitrary, and did not necessarily output a set of “Top 20” solutions that were representative of the entire calibrated solution set.

Appendix A Considerations in Building Energy Simulation: Steady-state vs. Transient Building Models

Work performed by Engblom [Engblom 2006] used a steady-state building energy simulation program to perform a retrofit analysis of office buildings in Norway. The purpose of the work by Engblom was to determine the most cost effective course of action to implement retrofits in the Norwegian office building stock.

The purpose of this appendix was to evaluate the validity of using steady-state calculations to estimate the energy consumption in Norwegian buildings. Therefore, a comparison was made between the calculated energy consumption in a generic Norwegian office building with steady-state and transient building energy models. All building energy calculations were performed with the EnergyPlus simulation software.

A.1 Thermal Mass Analysis

Two scenarios were investigated: a building with and without thermal mass. The building without thermal mass was considered to be a steady-state model; the building with thermal mass was considered to be transient. In addition to simply assessing the difference between simulations with and without thermal mass, the following simulation inputs were varied in a parametric analysis:

- (1) Properties of the building **envelope and equipment**
- (2) **Temperature controls** strategy

The permissible states for each of these parameters and the thermal mass are shown in Table A-1.

Parameter	Options
Thermal Mass	<ul style="list-style-type: none">• Yes• No
Envelope and Equipment	<ul style="list-style-type: none">• Old• New
Temperature Controls	<ul style="list-style-type: none">• Fixed temperature• Variable temperature

Table A-1: Overview of variables for thermal mass analysis.

Running a parametric analysis with these parameters at their given states resulted in 2 Envelope and Equipment Parameters x 2 Temperature Controls Strategies x 2 Thermal Mass Parameters = 8 simulations. All weather conditions were those for a typical meteorological year in Oslo,

Norway. In addition, to this parametric analysis increased temperature setback and varied thicknesses of thermal mass were also investigated.

All energy discussed in this chapter refers to the site energy consumed at the building.

A.1.1 Inputs

The building geometry remained fixed in all cases except for changes to the percent of the façade that was glazed. The building had a square footprint (19.36 m x 19.36 m) with four floors, each 3m in height, and a total building floor area of 1500 m². Glazings were evenly distributed between floors and façades, and were centered on the midpoint of each surface (Figure A-1). The ground temperature was held at the EnergyPlus default value of 18°C.

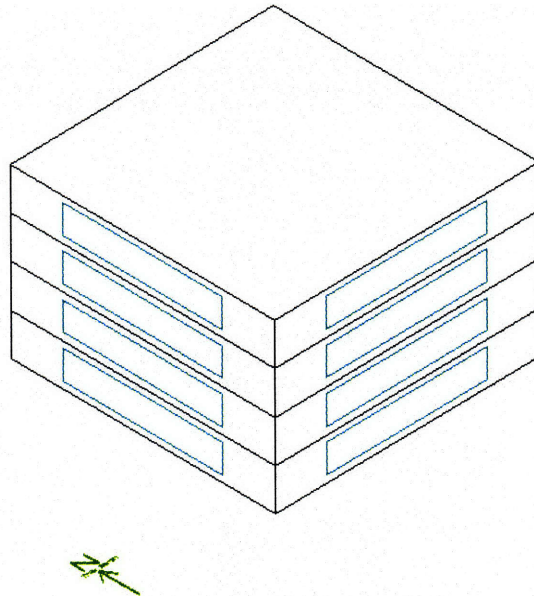


Figure A-1: Geometry of building for thermal mass analysis.

Table A-1 and Figure A-2 summarize the inputs to the parametric analysis. Table A-1 provides a broad overview, while Figure A-2 focuses on the characteristics of the building façade.

Envelope and Equipment		Old	New
U-Values		Poor thermal properties	Excellent thermal properties
Windows	<i>Materials</i>	1 Pane, Clear Glass	Winter: 3 panes, 1 low-e, argon
	<i>% Floor Area</i>	12.5%	25%
Internal Gains [kWh/m ² /year]		Lighting = 35 Equipment = 38 Hot Water = 10	Lighting = 28 Equipment = 17 Hot Water = 10
Infiltration [ACH]		0.3	0.1
Specific Fan Power [W/m ³ /sec]		2120	1000
Heat Recovery Effectiveness		60%	80%
Occupied Vent. Rate [L/m ² s]		3	1.5
Unoccupied Vent. Rate [L/m ² s]		1	0.5
Temperature Controls		Fixed Temperature	Variable Temperature
T_{in}, heating [°C]		23	21
T_{in}, cooling [°C]		23	25
ΔT Setback [°C]		0	2
Thermal Mass		Without Thermal Mass in the Building	With Thermal Mass in the Building
Thermal Mass		No	Yes, 20cm internal surfaces incl. ceilings

Table A-2: Summary of inputs to the thermal mass analysis.

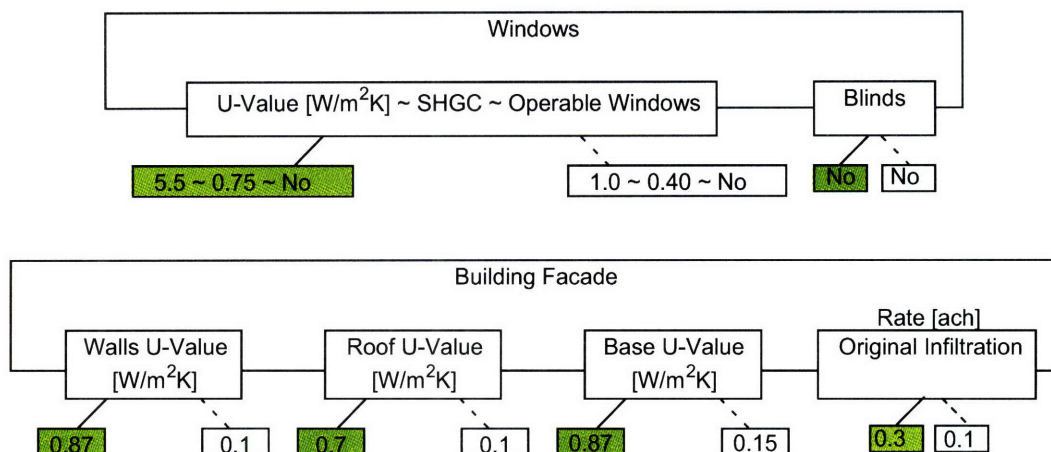


Figure A-2: Summary of input conditions for the building façade in the thermal mass analysis. The green values are for the poor energy performance, or “Old”, scenario; the white boxes highlight the excellent energy performance, or “New”, scenario.

A.1.1.1 Building Envelope and Equipment Parameters

The building's envelope and equipment parameters, identified in Table A-1, Table A-2, and Figure A-2 were concerned with the properties of the building envelope, internal gains, and heating, ventilation, and air conditioning (HVAC) equipment. These values were defined according to the work by Engblom [Engblom 2006], and corresponded to building designs with poor envelope and equipment energy performance in the “Old” category and excellent envelope and equipment energy performance in the “New” category. The “Old” and “New” thermal properties were presented in Figure A-2. The “Old” properties appear in green and the “New” properties appear in white.

The inputs for the thermal properties of the exterior of the building were assigned according to the 1987 release of Norwegian Standard 3031 (NS3031) [NS3031 1987], where the U-Values of each building component were defined as in Figure A-2. All surface constructions were assigned using a combination of mineral wool for insulation and heavyweight concrete for thermal mass and structure. This was a simplified model of the construction, but was sufficient for the parametric analysis that was performed. The U-Values for these composite walls were defined according to Equation A-1.

$$U = \frac{1}{\frac{1}{h_{in}} + \sum \frac{t}{k} + \frac{1}{h_{out}}} \quad (A-1)$$

Where $h_{in} = 7.7 \text{ W/m}^2\text{K}$ and $h_{out} = 25 \text{ W/m}^2\text{K}$ were taken from NS3031, and the t/k value for each building surface was extracted from the known U-value. h_{in} and h_{out} accounted for both convection and radiation on the interior and exterior of each building surface, respectively; no differentiation was made between walls and roofs. These t/k values were then kept constant during simulation while the convection coefficients were permitted to vary dynamically according to the wind and temperature conditions at the building.

The window design in the “New” case was a triple glazing with argon fill and a single low-e coating. The windows in the “Old” case had a single clear glazing.

Ventilation was available during all hours of the year; occupied ventilation rates were applied from 7 a.m. to 7 p.m. on weekdays, unoccupied ventilation rates were applied during all other times. The ventilation rates in the “Old” case were for a pre-1969 office building in Norway, as defined in the work by Engblom [Engblom 2006]. The “New” case had ventilation

flow rates that were two times lower than the “Old” case. The ventilation system included an economizer that provided free cooling during the building’s occupied hours when the outdoor temperature was no more than 4°C below the indoor setpoint.

All people, lighting, and equipment was available on weekdays from 7 a.m. to 7 p.m. and was unavailable on weekends.

The remainder of the envelope and equipment parameters were defined according to the information presented in the work by Engblom [Engblom 2006] and are shown in Figure A-2.

A.1.1.2 Controls Parameters

The temperature controls parameters defined the temperature controls strategies that were implemented when heating and cooling the building. The fixed temperature strategy had a fixed indoor temperature of 23°C for both heating and cooling; the variable temperature strategy had $T_{\text{heating}} = 21^{\circ}\text{C}$ and $T_{\text{cooling}} = 25^{\circ}\text{C}$, with a temperature setback of 2°C during unoccupied periods. Increased temperature setback was examined in section A.1.2.2. The occupied temperature setpoint was met from 9 a.m. to 7 p.m. on weekdays. It shall be noted that when simulating the control strategy with temperature setback, the morning heating setpoint ramped between the initial and final values in a time span of four hours – starting at 5:00 a.m. and reaching the final setpoint by 9:00 a.m. This was done to avoid iniquitous results in the power figures for simulations with thermal mass.

Heating and cooling were supplied to maintain the interior building temperature. These loads were modeled in EnergyPlus with simple Purchased Air objects, which supplied heating or cooling in response to the conditions on the interior of the building. The zone supply air humidity ratios were maintained between eight and nine grams of water per kilogram of air. Additionally, both heating and cooling were made available year-round. This was not typical practice in Norwegian buildings, but was implemented to assess the demand for cooling or heating with very good (“New” case) and bad (“Old” case) building envelopes.

A.1.1.3 Thermal Mass Parameters

The thermal mass parameters refer to a building with and without thermal mass. The reduction of the thermal mass was achieved by lowering the thickness of the concrete in the building to 0.002 m (2 mm), while the thermally massive case was achieved by increasing this

thickness to 0.2 m (20 cm). The thermal mass that was used in this construction was a heavyweight concrete with a density (ρ) of 2243 kg/m³ and a specific heat (C_p) of 837 J/kgK. This thermal mass was installed in the walls, floor, and ceilings of the building, and in the case of the exterior walls, and roof it was taken as the interior of the two envelope layers. All of the ceilings and floors were exposed concrete surfaces.

A.1.1.4 Climate Parameters

All weather data was taken from the EnergyPlus website [EPlus 2007b]. These were hourly weather files with International Weather for Energy Calculations (IWEC) data from Oslo, Norway. Oslo data was considered to be representative of the conditions in Norway and was applied to all simulations.

A.1.2 Results

A.1.2.1 Results of the Parametric Analysis

The results presented in this section focus on the difference between simulations that considered thermal mass (a dynamic analysis) and simulations that did not consider thermal mass (steady-state analysis). All simulations were run in EnergyPlus and were modeled with the inputs described in section A.1.1. Recall that the only difference between the simulations with and without thermal mass the thickness of the building's concrete.

Figure A-3 shows the behavior of indoor temperature on the third floor of the building (as an example) with and without thermal mass. The outdoor temperature is also superimposed to give a sense of the driving force behind the indoor temperature changes. Solar radiation and internal gains also influence the indoor temperature. The two data sets shown in Figure A-3 represent the combination of parameters that gives the best energy performance (the least energy consumption) both with and without thermal mass in the Oslo climate. Specifically, the parameters correspond to the “New” envelope and equipment (excellent thermal properties) case with variable temperature controls. The last parameter, thermal mass, was the object of comparison in this and the following graphs.

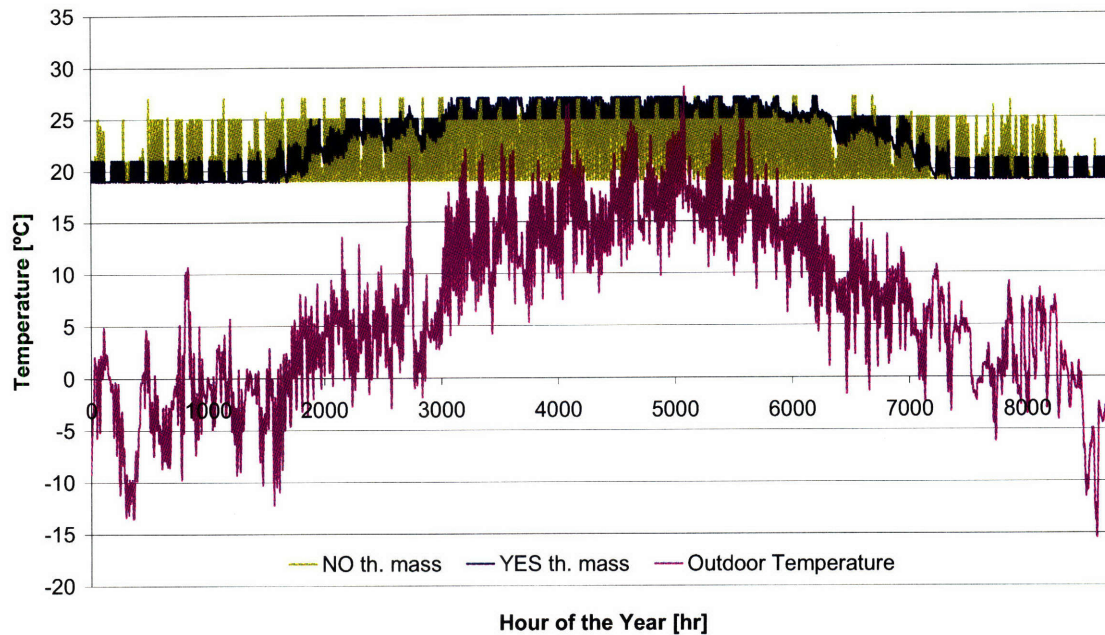


Figure A-3: Outdoor temperature and indoor temperature variation, with vs. without thermal mass.

The indoor temperature was observed to be sensitive to changes in outdoor temperature when simulating without thermal mass (green line). In this case, the indoor temperature follows the swings of the outdoor temperature. Additionally, in the extremely well insulated building with no thermal mass, the solar radiation, lighting, equipment, people actually contribute enough internal gain to raise the indoor temperature above the *cooling* temperature setpoint during the winter.

The thermal mass (blue line) acts to reduce the impact of the internal gains and attenuates the oscillations in the indoor temperature. The model with thermal mass has a slower and delayed response to internal gains and outdoor temperature changes; as a result the behavior of the indoor temperature appears more “realistic”, with no demand for cooling in winter. Similar behaviors were observed with lower envelope and equipment quality and fixed temperature settings.

The next graph, Figure A-4, summarizes the specific energy demand (per square meter per year) of each of the eight parametric analysis scenarios. The labels on the x-axis indicate what combination of parameters applies to each situation. The first four bars on the left all had “New” (excellent thermal properties) equipment and envelope characteristics. The four bars on the right had “Old” equipment and envelope characteristics. Each pair of bars had either variable

temperature controls or fixed temperature controls. One bar in each pair had thermal mass, the other did not.

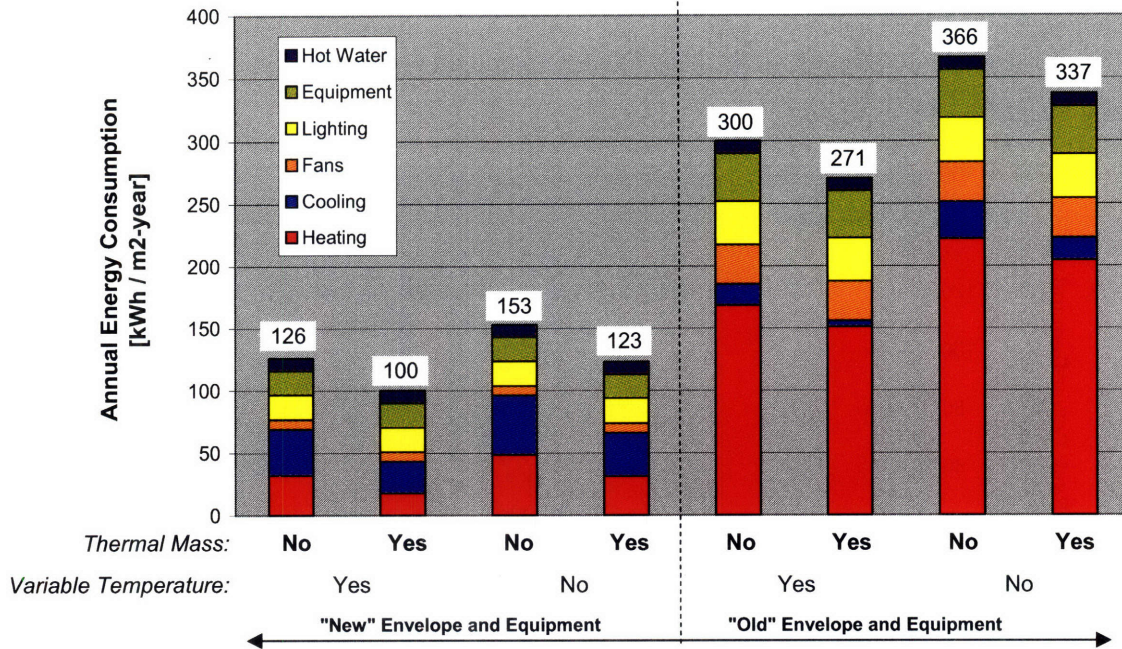


Figure A-4: Total energy consumption resulting from the thermal mass analysis.

Not surprisingly, the two groups with “Old” and “New” envelope and equipment properties showed the greatest discrepancies in energy consumption (with all other conditions at parity). Less striking differences were observed for the other parameters. In particular, variations in thermal mass brought about changes in energy consumption of up to 30 kWh/m²/year. In the scenario with fixed indoor temperatures and “New” envelope and equipment properties the case with thermal mass had an annual energy consumption that was 20% less than the same scenario without thermal mass. Overall, the inclusion of thermal mass decreased the annual energy consumption in the test building by between 8% and 21% compared to a building with all other conditions at parity.

The peak power demand was also strongly influenced by the amount of thermal mass in the building. In buildings with temperature setback, as in the variable temperature scenario that was examined in the parametric analysis, large volumes of thermal mass resulted in high power demands. Power spikes are observed when the building attempts to heat up from the unoccupied to the occupied temperature setpoint, as a large amount of energy is required to raise the temperature of the thermal mass. The peak power demand from each of the eight simulations

that were run in the parametric analysis is shown in Figure A-5. Once again, the first four bars on the left all had “New” (excellent thermal properties) equipment and envelope characteristics. The four bars on the right had “Old” equipment and envelope characteristics. Each pair of bars had either variable temperature controls or fixed temperature controls. One bar in each pair had thermal mass, the other did not.

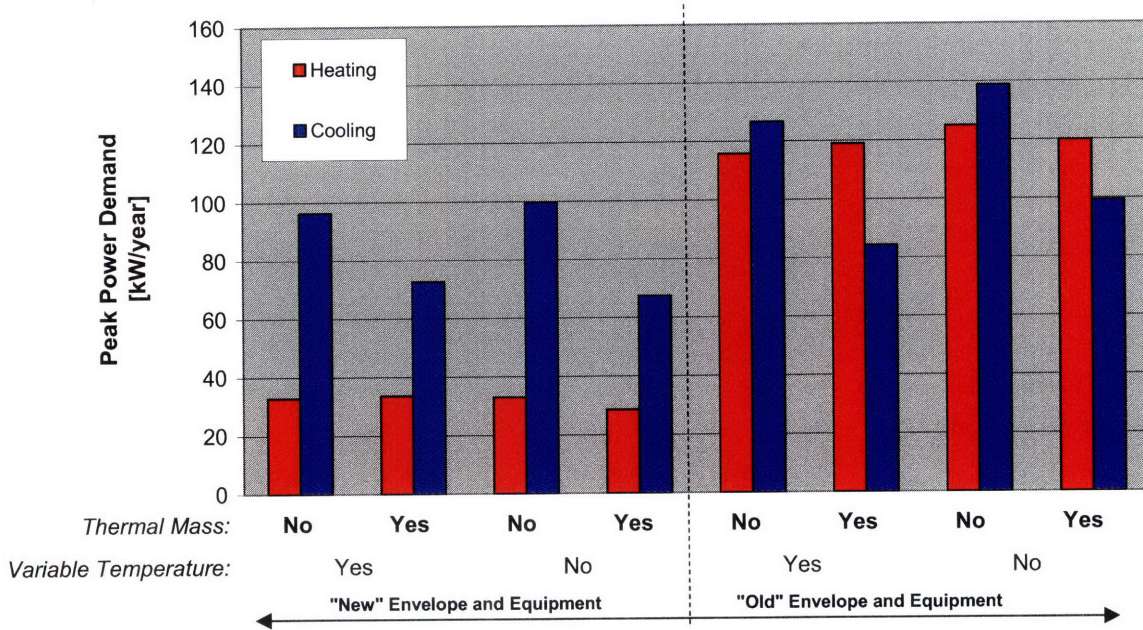


Figure A-5: Difference in the required power for heating and cooling in the thermal mass analysis.

To assess the influence of thermal mass the eight bars in Figure A-5 should be examined in pairs. While peak heating demand shows mixed results, the peak cooling demand always appears significantly lower with thermal mass than without it.

In the cases with variable temperature control, the buildings with thermal mass tended to have a higher peak heating demands, while the opposite was true in buildings with fixed temperatures. The greatest difference occurred in the building with “New” envelope and equipment and fixed temperatures. In this case, the building without thermal mass had a peak power demand that was 14% greater than the building with thermal mass. Conversely, the case with “Old” envelope and equipment and variable temperatures required 3% less heating energy with thermal mass than without it.

The higher peak heating demand with thermal mass and variable temperatures resulted from the need to heat the thermal mass from the setback to the occupied temperature on cool weekday mornings. The temperature ramping was intended to eliminate this effect, but the

results above indicate that the ramping period was too abrupt. With fixed temperatures the thermal mass stored the heat gains from solar radiation, people, lights, and equipment gains throughout the day and the released this energy at high. Because the coolest temperatures occurred overnight, the peak heating demand was decreased as the thermal mass released the heating energy that it had stored over the course of the day.

With thermal mass, the peak cooling demand was reduced by between -24% and -34%. This was because the peak in cooling demand tended to occur during the middle of the day, when solar, occupant, lighting, and equipment gains were greatest. The thermal mass absorbed some of the heating energy from these gains, reducing the instantaneous cooling load that was required to maintain the indoor temperature setpoint. Therefore, a lower peak cooling demand was observed with thermal mass than without it.

A.1.2.2 Increased temperature setback in Oslo

This simulation analyzed the effect of introducing a wider range of temperature settings in Oslo. It was assumed that in winter, during unoccupied hours, the temperature control was setback to 15 °C instead of 19 °C. This quite radical assumption stressed the potential for energy savings that might take place in a light construction with virtually no thermal mass; while the same potential was likely to be “obscured” in a building with a thermally massive construction. Along with increasing the temperature step, the ramp for morning warming up was extended to go from 3:00am to 9:00am. Figure A-6 shows temperature behaviors for a thermally massive building with the original temperature setback to 19°C (green line) and the increased temperature setback to 15°C (blue line). The outdoor temperature is shown in pink.

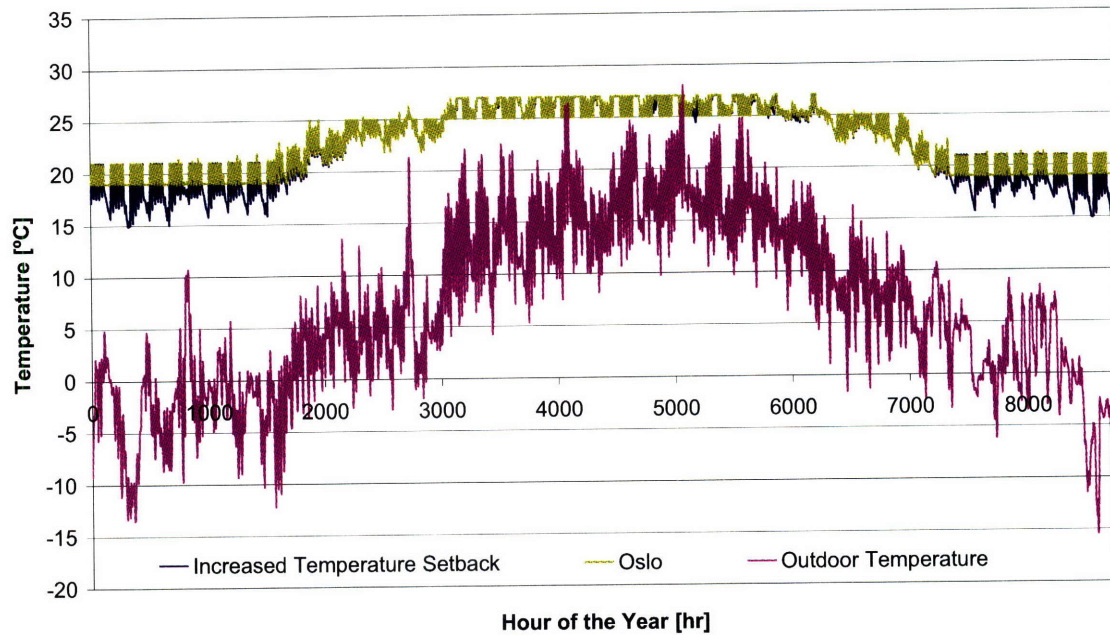


Figure A-6: Change in indoor temperature due to increased temperature setback (from 2 to 6 °C). The graph refers to the case with thermal mass.

In winter time, the setback to a lower indoor reduced the energy consumed to heat the building. The consequences on the annual specific energy demand for heating were as in Figure A-7. The y-axis expresses the amount of energy consumed with increased temperature setback. The cases with increased temperature setback (6°C) are indicated by the hatched bars; the cases with the typical (2°C) temperature setback are indicated by red bars. The presence of thermal mass is indicated along the x-axis by either “yes” if thermal mass was included, or “no” if thermal mass was not included in the simulation. The “New” and “Old” envelope conditions are also indicated on the left and right hand sides of the x-axis.

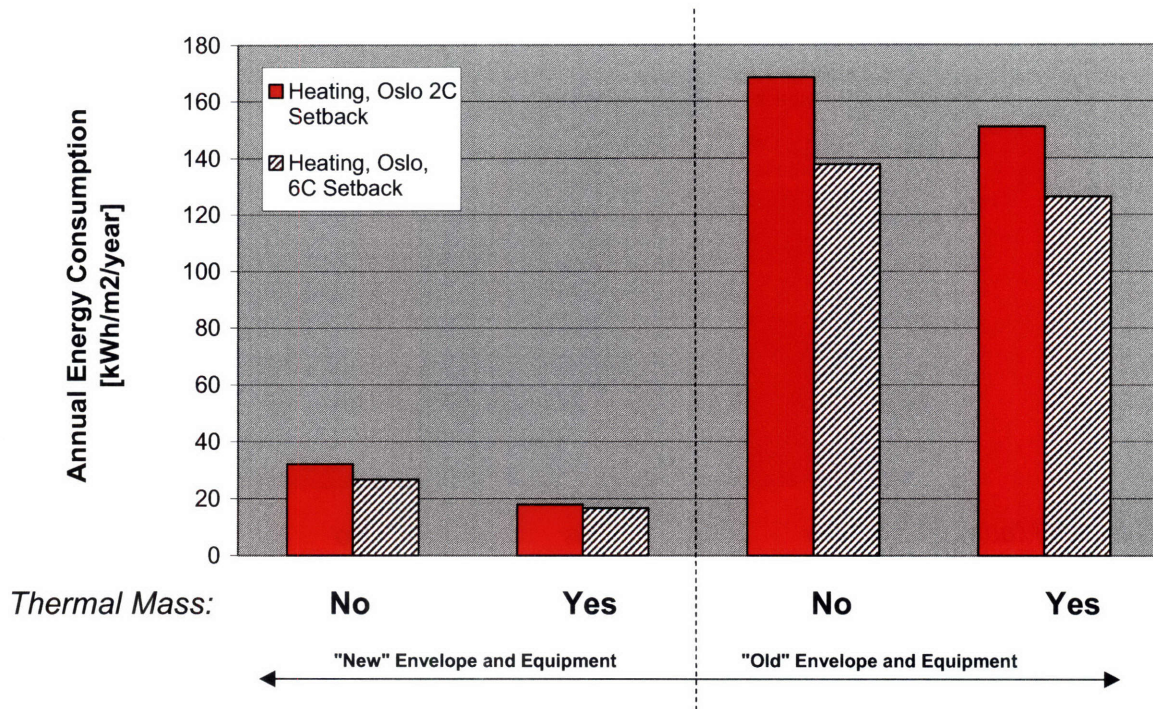


Figure A-7: Change in heating energy due to increased temperature setback (from 2 to 6 °C).

As expected, the reduced annual energy consumption from increased setback continued for both the cases with and without thermal mass (Figure A-7). However, the consequence of a widened range of temperature is that of an increase in required power, depicted graphically in Figure A-8. The cases with increased temperature setback are indicated by the hatched bars; the cases with the typical temperature setback are indicated by red bars. The presence of thermal mass is indicated along the x-axis by either “yes” if thermal mass was included, or “no” if thermal mass was not included in the simulation. The “New” and “Old” envelope conditions are also indicated on the left and right hand sides of the x-axis.

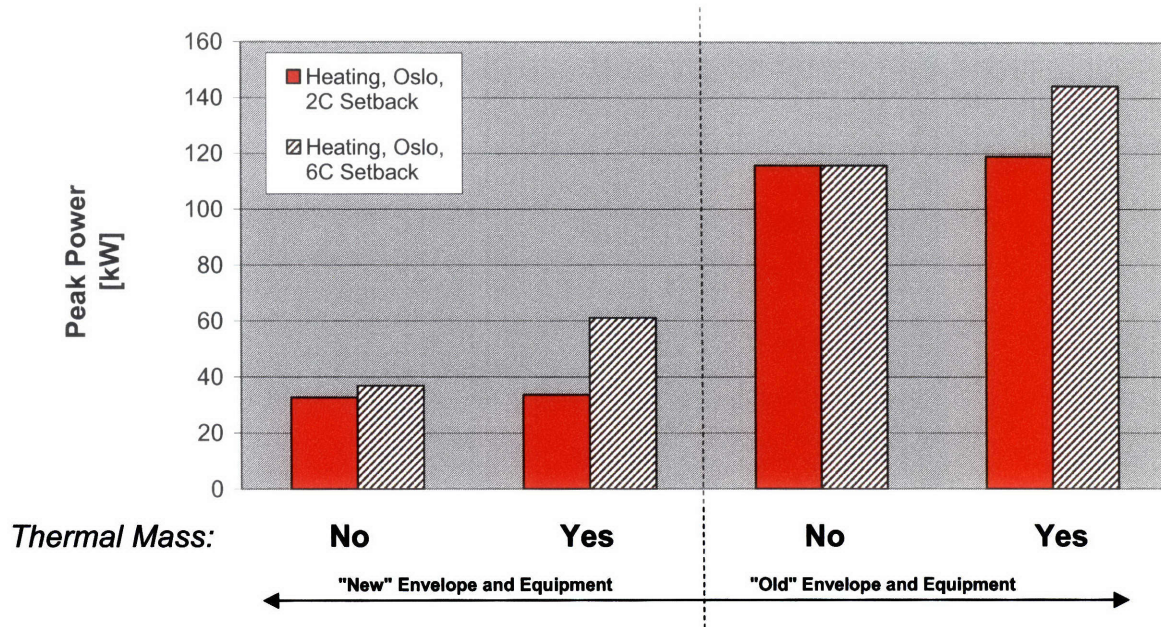


Figure A-8: Change in heating power demand due to increased temperature setback (from 2 to 6 °C). Those cases with thermal mass showed a much stronger (> 20 kW) increase in peak heating power with increased temperature setback than did those cases without thermal mass. Only small differences (less than 5 kW) were observed when comparing the energy consumption with and without increased temperature setback under “New” and “Old” envelope conditions.

Recall that the peak cooling demand occurred during occupied hours, and was not influenced by increased temperature setback. Additionally, the majority of the annual cooling energy consumption occurred during occupied hours, again negating the influence of increased temperature setback. Therefore, the cooling energy and power were not presented as the increased temperature setback had little to no influence on the peak cooling demand or the annual cooling energy consumption.

A.1.2.3 Variation in Thermal Mass

In order to understand the effect of variations in the volume of thermal mass in the best performing building (“New” envelope and equipment with variable temperature controls) a simple comparison was made in which the thickness of the thermal mass was varied between 0.02 cm (same as no thermal mass), 2 cm, 10 cm, 20 cm (same as simulations in previous sections), and 30 cm. A thickness of 30 cm was the maximum thickness expected in Norwegian office buildings.

Figure A-9 and Figure A-10 show the difference in the annual heating and cooling energy consumption and peak power demand, respectively. Only heating and cooling are shown because they are the two building loads that are directly affected by changes in the thickness of thermal mass.

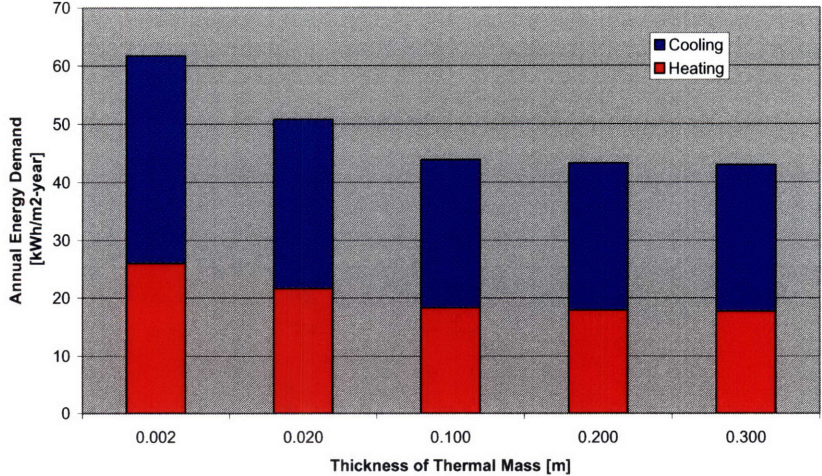


Figure A-9: Change in heating and cooling energy with variation of thermal mass. Changes to thermal mass are made in the thickness.

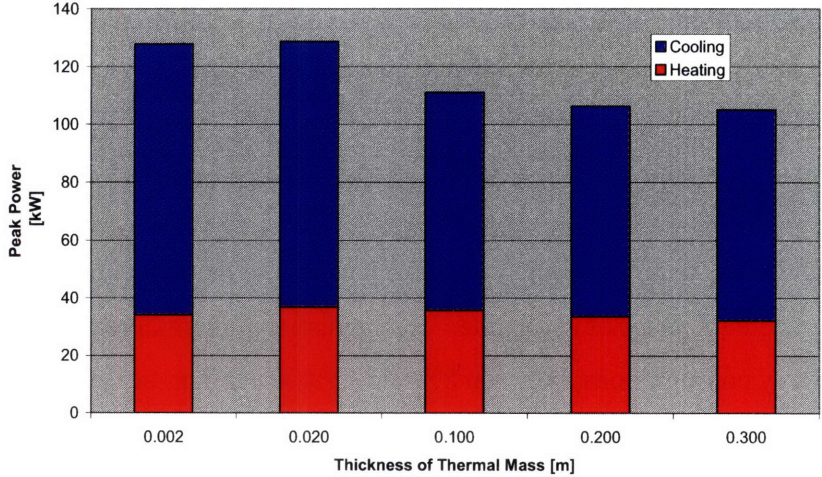


Figure A-10: Change in heating and cooling peak power demand with variation of thermal mass. Changes to thermal mass are made in the thickness.

It is apparent from Figure A-9 and Figure A-10 that the thickness of the thermal mass only has a significant effect when changes on the order of 10 x to 100 x are made. When varied between 10, 20 or 30 cm only minor changes in annual energy consumption and peak power demand are observed.

Figure A-11 shows the variation of the indoor temperature in zone three (a middle zone) of the building over the course of the year and with varying thicknesses of thermal mass. This graph shows that the affect of small changes in thermal mass (10 cm – 30 cm) are most significant in the spring and fall when the outdoor temperatures are mild. This graph also shows more dramatic temperature swings with much smaller thicknesses of thermal mass and more stable indoor temperatures with increased thermal mass, as would be expected.

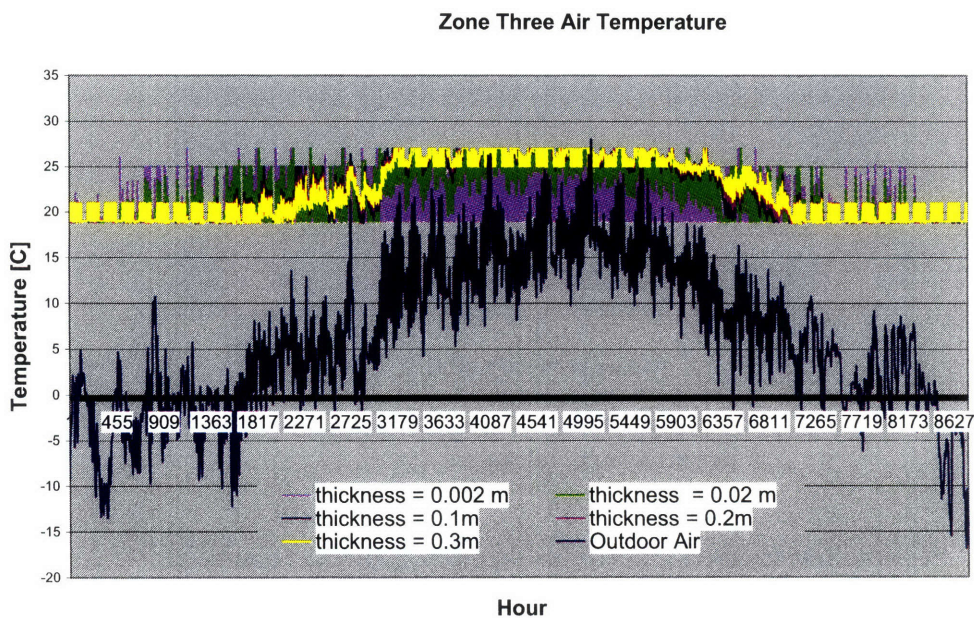


Figure A-11: Indoor air temperature for various volumes of thermal mass.

A.2 Lessons Learned

The results of the parametric analysis make it clear that the influence of thermal mass in building energy calculations is not negligible. The inclusion of thermal mass predicts much lower annual energy consumptions, between 8% and 21% lower than the same building without thermal mass. The required power for heating and cooling the building is also affected by the presence of thermal mass in the simulation. The decrease in required power varied between -3% and +14% for heating and -24% and -34% for cooling. It is apparent from these results that the influence of thermal mass in building energy simulations in climates like those found in Norway is not negligible, and must be considered to obtain more accurate predictions of building energy loads.

Appendix B Supplementary Information

B.1 Preliminary EPBD Certification Values

	A	B	C	D	E	F	G
Offices	≤ 80	81-120	121-160	161-190	191-225	226-335	> 335
Kindergartens	≤ 80	81-120	121-160	161-190	191-225	226-335	> 335
Schools	≤ 65	66-100	101-130	131-160	161-190	191-290	> 290
Hospitals	≤ 160	161-240	241-320	321-345	346-365	366-545	> 545
Nursing Homes	≤ 110	111-165	166-220	221-250	251-275	276-415	> 415
Hotels	≤ 115	116 -175	176-230	231-260	261-290	291-435	> 435
Restaurants	≤ 115	116 -175	176-230	231-260	261-290	291-435	> 435
Gymnasiums	≤ 95	96-145	146-190	191-230	231-275	276-410	> 410
Business	≤ 265	266-400	401-530	531-605	606-680	681-1020	> 1020
Building	≤ 145	146-220	221-290	291-340	341-390	391-585	> 585
Cultural	≤ 85	86-130	131-170	171-180	181-190	191-280	> 280
Industrial	≤ 80	81-120	121-160	161-220	221-280	281-415	> 415

Table 11-1: EPBD energy rating values for different building types [Wigenstad 2005]

B.2 Additional Retrofit Results

	Manually Calibrated		Top 20 Solutions from LHMC		
	Corrected	Original	Detailed-Corrected	Detailed-Original	Simple
	Median +/- % savings	Median +/- % savings	Median +/- % savings	Median +/- % savings	Median +/- % savings
Moderate					
Heating and Controls					
Temperature Setback	3% 3%	3% 3%	5% 2%	5% 2%	12% 2%
Ventilation					
Occupant Controlled Ventilation	-10% 3%	-9% 3%	-10% 1%	-11% 1%	0% 1%
Ventilation Rate	-32% 3%	-35% 3%	-31% 2%	-37% 3%	-37% 3%
Heat Recovery Effectiveness	-12% 3%	-16% 3%	-12% 4%	-18% 3%	-13% 4%
Envelope					
Windows	-1% 3%	-1% 3%	-2% 1%	-1% 2%	-1% 1%
Exterior Wall	0% 3%	0% 3%	0% 0%	-1% 0%	0% 0%
Ground Wall	0% 3%	0% 3%	0% 0%	0% 0%	0% 0%
Ground Floor	-1% 3%	-1% 3%	-1% 0%	-1% 0%	-1% 0%
Roof	-1% 3%	-1% 3%	-1% 1%	-1% 1%	-1% 1%
Infiltration Rate	-4% 3%	-3% 3%	0% 3%	1% 2%	0% 3%
Temperature Independent Loads					
Lighting Density	-2% 3%	-2% 3%	0% 0%	-1% 1%	0% 0%

Table B-1: Annual peak power demand savings under moderate retrofit conditions from the Individual Retrofit analysis in Chapter 8 .

	Manually Calibrated		Top 20 Solutions from LHMC		
	<i>Corrected</i>	<i>Original</i>	<i>Detailed-Corrected</i>	<i>Detailed-Original</i>	<i>Simple</i>
	Median +/- % savings	Median +/- % savings	Median +/- % savings	Median +/- % savings	Median +/- % savings
<u>Heating and Controls</u>	<u>Low-Energy</u>				
Temperature Setback	5% 3%	5% 3%	8% 13%	7% 2%	16% 4%
<u>Ventilation</u>					
Occupant Controlled Ventilation	-36% 3%	-40% 3%	-34% 2%	-41% 2%	-37% 3%
Ventilation Rate	-39% 3%	-42% 3%	-36% 2%	-45% 2%	-44% 3%
Heat Recovery Effectiveness	-23% 3%	-27% 3%	-22% 4%	-29% 3%	-27% 4%
<u>Envelope</u>					
Windows	-2% 3%	-1% 3%	-2% 1%	-1% 1%	-2% 1%
Exterior Wall	-1% 3%	-1% 3%	-1% 0%	-1% 0%	-1% 0%
Ground Wall	0% 3%	0% 3%	0% 0%	0% 0%	0% 0%
Ground Floor	-1% 3%	-1% 3%	-1% 1%	-1% 1%	-1% 0%
Roof	-2% 3%	-1% 3%	-2% 1%	-2% 1%	-2% 1%
Infiltration Rate	-9% 3%	-8% 3%	-4% 3%	-4% 2%	-5% 3%
<u>Temperature Independent Loads</u>					
Lighting Density	-2% 3%	-3% 3%	-1% 0%	-2% 1%	0% 0%

Table B-2: Annual peak power demand savings under low-energy retrofit conditions from the Individual Retrofit analysis in Chapter 8.

	Manually Calibrated		Top 20 Solutions from LHMC		
	<i>Corrected</i>	<i>Original</i>	<i>Detailed-Corrected</i>	<i>Detailed-Original</i>	<i>Simple</i>
	Median +/- % savings				
<u>Moderate</u>					
Heating and Controls					
Temperature Setback	-4% 3%	-4% 3%	-3% 1%	-4% 1%	-2% 1%
Ventilation					
Occupant Controlled Ventilation	-20% 3%	-23% 3%	-20% 2%	-24% 2%	-16% 2%
Ventilation Rate	-27% 3%	-30% 3%	-26% 2%	-32% 2%	-33% 3%
Heat Recovery Effectiveness	-10% 3%	-14% 3%	-10% 4%	-15% 3%	-10% 4%
Envelope					
Windows	-2% 3%	-2% 3%	-2% 1%	-2% 4%	-2% 4%
Exterior Wall	-1% 3%	-1% 3%	-1% 0%	-1% 0%	-1% 0%
Ground Wall	-1% 3%	0% 3%	-1% 0%	-1% 0%	-1% 0%
Ground Floor	-2% 3%	-2% 3%	-3% 1%	-3% 1%	-2% 1%
Roof	-2% 3%	-2% 3%	-3% 1%	-2% 1%	-2% 1%
Infiltration Rate	-5% 3%	-5% 3%	2% 4%	2% 3%	1% 5%
Temperature Independent Loads					
Lighting Density	-1% 3%	-2% 3%	0% 0%	-1% 0%	-1% 0%

Table B-3: Utility bill savings under moderate retrofit conditions from the Individual Retrofit analysis in Chapter 8.

	Manually Calibrated		Top 20 Solutions from LHMC		
	<i>Corrected</i>	<i>Original</i>	<i>Detailed-Corrected</i>	<i>Detailed-Original</i>	<i>Simple</i>
	Median +/- % savings				
<u>Low-Energy</u>					
Heating and Controls					
Temperature Setback	-7% 3%	-8% 3%	-6% 1%	-7% 1%	-4% 2%
Ventilation					
Occupant Controlled Ventilation	-34% 3%	-39% 3%	-34% 2%	-40% 2%	-38% 3%
Ventilation Rate	-32% 3%	-36% 3%	-31% 2%	-37% 2%	-39% 3%
Heat Recovery Effectiveness	-18% 3%	-22% 3%	-17% 3%	-23% 3%	-19% 4%
Envelope					
Windows	-3% 3%	-3% 3%	-5% 2%	-4% 2%	-3% 2%
Exterior Wall	-1% 3%	-1% 3%	-2% 0%	-2% 0%	-1% 0%
Ground Wall	-1% 3%	-1% 3%	-1% 0%	-1% 0%	-1% 0%
Ground Floor	-2% 3%	-2% 3%	-3% 1%	-4% 1%	-2% 1%
Roof	-3% 3%	-3% 3%	-4% 1%	-3% 1%	-3% 1%
Infiltration Rate	-12% 3%	-11% 3%	-6% 4%	-5% 3%	-7% 4%
Temperature Independent Loads					
Lighting Density	-2% 3%	-2% 3%	-1% 0%	-1% 0%	-1% 0%

Table B-4: Utility bill savings under low-energy retrofit conditions from the Individual Retrofit analysis in Chapter 8.

Appendix C Calculations

C.1 UA-Value of the heating coil

This section applied equations for calculating the heat transferred between two unmixed fluids in a cross flow heat exchanger to estimate the UA-value of the heating coil in the Main ventilation system of the Steindal School. The two fluids were water and air. Water was supplied to the coil by the 185 kW boiler in the basement of the school. The air entered the coil from the supply side of the heat recovery unit. Additional information about the ventilation systems in the Steindal School was provided during data collation in Chapter 5.

Site visits indicated that the water was supplied at a mass flow rate of 2.8 kg/sec and a temperature of 65°C. However, it was unknown if these were the design conditions under which the coil was installed. To account for this, a supply temperature of 70°C was also tested. Additionally, in the absence of design data for the temperature drop across the heat exchanger coils, members of SINTEF research were consulted; the recommended temperature drop across the coils was 15°C. The ventilation air was assumed to enter the heat exchanger at a temperature of 5°C⁶ and left the heat exchanger at the ventilation setpoint temperature of 18°C. The air flow rate in the Main ventilation system was equal to 11 m³/sec as per section 5.1.10.

The UA-value of the coil was then calculated according to the procedure for a cross flow heat exchanger with unmixed fluid streams from Incropera and Dewitt [Incropera 2001].

Given:

$$T_{water,in}=65^{\circ}C \ \& \ 70^{\circ}C$$

$$T_{water,out}=50^{\circ}C \ \& \ 55^{\circ}C$$

$$T_{air,in}=18^{\circ}C$$

$$T_{air,out}=5^{\circ}C$$

$$m_{water}=2.8 \text{ kg/sec}$$

$$m_{air}=V_{air}\rho_{air}=11*1.2=13.2\text{kg/sec}$$

$$Cp_{water}=4212 \text{ J/kgK}$$

$$Cp_{air}=1000 \text{ J/kgK}$$

⁶ This corresponded to an outdoor temperature of -8°C, with a heat recovery effectiveness of 50% and a return air temperature of 18°C.

Calculating:

$$Q_{water} = m_{water} \cdot Cp_{water} (T_{water,in} - T_{water,out}) \quad (C-1)$$

$$Q_{air} = m_{air} \cdot Cp_{air} (T_{air,out} - T_{air,in}) \quad (C-2)$$

$$Q_{water} = Q_{air} \quad (C-3)$$

$$\Delta T_{lnm} = \frac{(T_{water,out} - T_{air,in}) - (T_{water,in} - T_{air,out})}{\ln\left(\frac{T_{water,out} - T_{air,in}}{T_{water,in} - T_{air,out}}\right)} * F \quad (C-4)$$

$$UA_{coil} = \frac{Q_{water}}{(\Delta T_{ln,m})} = \frac{Q_{air}}{(\Delta T_{ln,m})} \quad (C-5)$$

Results:

$$UA_{coil}(60^{\circ}C) = 4,000 \text{ W/K}$$

$$UA_{coil}(70^{\circ}C) = 3,500 \text{ W/K}$$

Consequently, 3,750 W/K was the estimated UA-value of the Main ventilation heating coil.

C.2 Heating Contribution from Thermal Mass

The rate of decay of the heat loss from the internal mass in the Steindal School was estimated to identify when the building was undergoing steady-state heat transfer. The motivation for this calculation was discussed in Chapter 6.

C.2.3 Surface Descriptions

C.2.3.1 Interior Building Surfaces

The internal mass that was present in the Steindal School is summarized in Table C-1. Brief descriptions of each surface are also given. Unless otherwise indicated, all surfaces were located inside of the building.

		Interior Partitions								
		Ceilings & Floors Between Zones		Walls Between Zones			Walls Internal to Zones		Internal Mass	
		Offices and Bomb Shelter to 1 st Floor	1 st floor to Under-roof (Ceiling)	Bomb Shelter to Offices	1 st Floor to Under-roof (Wall)	Gym to 1 st Floor	Main Building to Annex	Gymnasium to Locker-rooms	Dividing wall in 1 st Floor Class-rooms and Annex	Internal Mass – wooden chairs, desks, etc.
Construction Materials	Surface #1	False Ceiling Board	False Ceiling Board	50 cm HW Concrete	15 cm HW Concrete	20 cm HW Concrete	15 cm HW Concrete	20 cm HW Concrete	11cm Brick	2.54 cm Wood
		Ceiling Air Space	Ceiling Air Space		5 cm Mineral Wool		13 cm Mineral Wool		3 cm Air Gap	
		15 cm HW Concrete	15cm HW concrete		11 cm Brick	11 cm Brick	11 cm Brick		11 cm Brick	
	Surface #2	Linoleum Floor Tile	15 cm Mineral Wool							

Table C-1: Internal ceiling, floor, and thermal mass constructions.

Descriptions of each of the building surfaces in Table C-1 are provided below:

C.2.3.1.1 Ceilings and Floors

- **Offices and Bomb Shelter to 1st Floor** was the interior ceiling that separated the ground floor from the 1st Floor. It ran the full length and width of the Main building and was composed of concrete. There was no insulation in this ceiling.
- **1st Floor to Underroof (ceiling)** was the concrete ceiling that separated the North half of the heated 1st Floor from the unheated Underroof space. This ceiling included a layer of insulation that separated the concrete from the Underroof zone.

C.2.3.1.2 Interior Walls Separating Zones

- **Bomb Shelter to Offices** was the wall that separated the heated Offices from the unheated Bomb Shelter. The heavy concrete construction of this wall was attributed to the fact that it was a part of the school's Bomb Shelter. There was no insulation on this wall.
- **1st Floor to Underroof (wall)** was the wall that ran along the South ridge of the Main building and separated the heated 1st Floor from the unheated Underroof zone. There was no insulation on this wall.
- **Gym to 1st Floor** were the two walls that separated the heated Gymnasium from the heated 1st Floor Classrooms. These were a heavyweight concrete and brick construction.
- **Main Building to Annex** was originally an exterior wall before the Annex was built in 1997. The concrete and brick were separated by a layer of insulation; the concrete faced the Main Building and the brick faced the Annex. Both spaces were heated.

C.2.3.1.3 Internal Walls Within Heated Zones

- **Gymnasium to Lockerrooms** was the dividing wall between the gymnasium and the locker rooms in the Gym zone. This was a heavyweight concrete wall with no insulation. Both spaces were heated.
- **Dividing Wall in 1st Floor Classrooms and Annex** was the wall that ran from East to West and divided both the Main Building and the Annex into two sections: North and South. This wall was composed of a brick and air gap construction. There was no insulation in this wall.

C.2.3.1.4 Internal Mass

- **Internal Mass** was composed of wooden chairs, desks, and shelving throughout the school.

C.2.3.2 Exterior Building Surfaces

Several of the exterior walls in the Main Building of the Steindal School had materials on the interior of the wall that contributed thermal mass to the inside of the building. These thermally massive materials were separated from the outdoors by a layer of insulation.

- **North & South Wall, Main Building** was made of brick and composed the interior surface of the North and South walls on the 1st Floor in the Main Building. A layer of insulation separated these walls from the exterior environment.
- **West Wall, Main Building** was a concrete wall that composed the interior surface of the West wall in the Main Building. This surface abutted the 1st Floor, Offices, and Bomb Shelter. A layer of insulation separated this wall from the exterior environment.
- **Ground Floor** was the floor slab in the Offices and Bomb Shelter of the building. This slab was insulated from the ground by a layer of insulation.

C.2.4 Calculation Method

The first term approximation of the infinite series solution for plane walls was applied to calculate the rate of decay of the heating contribution from the thermal mass in the Steindal School, as per Equations C-6 through C-10 and with the input data from Table C-1.

C.2.4.1 Interior Building Surfaces: Boundary Conditions

C.2.4.1.1 Ceilings and Floors

The concrete in the **Offices and Bomb Shelter to 1st Floor** was assumed to have a plane of symmetry about its center, i.e. equal amounts of heat were released to the 1st Floor zone above the ceiling and the Office and Bomb Shelter below the ceiling.

The concrete in the **1st Floor to Underroof (ceiling)** was assumed to be adiabatic on its upper surface. This was in response to the presence of insulation above the concrete and assumed that all heat was released from the concrete into the 1st Floor of the building.

C.2.4.1.2 Interior Walls Separating Zones

The concrete wall that separated the **Bomb Shelter to Offices** was assumed to have a plane of symmetry about its center, i.e. equal amount of heat were released from the wall into the heated Offices and unheated Bomb Shelter.

The concrete in the **1st Floor to Underroof (wall)** wall was assumed to have an adiabatic surface facing the Underroof, meaning that all heating energy from this thermal mass was released into the 1st Floor classrooms.

The concrete and brick in the **Gym to 1st Floor** wall were both assumed to have adiabatic surfaces on their inner wall surface (the surface *inside* of the wall). Therefore, all stored heating energy was released into the heated building space.

The concrete and brick in the **Main Building to Annex** wall were both assumed to have adiabatic surfaces on their inner wall surface (the surface *inside* of the wall); all stored heating energy was released into the heated building space.

C.2.4.1.3 Internal Walls Within Heated Zones

The concrete wall in the **Gymnasium to Lockerrooms** was assumed to have a plane of symmetry about its center and released heat into the heated portion of the building.

The brick **Dividing Wall in 1st Floor Classrooms and Annex** wall was assumed to have adiabatic surfaces on the inner wall surface (the surface *inside* of the wall) of each layer of brick; all stored heating energy was released into the heated building space.

C.2.4.2 Internal Mass

The wooden chairs, desks, and shelving that comprised the **Internal Mass** contributed 100% heat gain to the building.

C.2.4.3 Exterior Surfaces: Boundary Conditions

The brick in the North & South Wall, Main Building were assumed to have an adiabatic surface on their exterior, therefore they contributed heat only to the interior of the building, not to the exterior.

The concrete in the **West Wall, Main Building** was assumed to have an adiabatic surface on its exterior, therefore all of its stored heat was contributed to the interior of the building.

The concrete in the **Ground Floor** was assumed to have an adiabatic surface on its exterior. Therefore, all of its stored heat was contributed to the interior of the building.

C.2.4.4 Summary of Boundary Conditions

The boundary conditions that were assigned to each thermally massive building element were conservative. For example, the 50 cm concrete wall that separated the heated Offices from the unheated Bomb Shelter was assumed to have a plane of symmetry about its center, meaning that it released equal amounts of energy to both the Office and the Bomb Shelter. In reality, a

large amount of heating energy was likely to be released into the unheated Bomb Shelter, making the energy contributed to the Offices small. Another example was the Ground Floor, which was assumed to have an adiabatic surface on its exterior, and thus contributed all of its internal mass to the interior of the building. It was more likely that much of the stored energy in the floor was transferred to the cool ground, not the warm heated space. The conservative nature of these assumptions made the rate of decay observed in Figure C-1 appear much longer than expected. However, this approximation provided a first estimate of the influence of thermal mass on the heating energy demand on weekends when heating was required.

C.2.4.5 Equations

Incropera and Dewitt [Incropera 2001] provided equations for calculating the rate of decay of the heating energy released by a plane wall. These equations, as well as the constants necessary to calculate the heat transfer, Q , are given in Equations C-6 through C-10 and in Table C-2 and Table C-3.

The dimensionless Biot number is calculated as in Equation C-6

$$Bi = \frac{hL_c}{k} \quad (C-6)$$

Where $Bi > 0.1$ then the error associated with the simple lumped capacitance method [Incropera 2001] is too large, making more accurate models necessary. In this case, the infinite series solution for plane walls was applied. When the dimensionless Fourier number is greater than 0.2 ($Fo > 0.2$) the 1st term of the series solution may be used to approximate the total series with little to no loss in accuracy.

$$Fo = \frac{\alpha t}{L_c^2} \quad (C-7)$$

The internal mass in the Steindal School nearly always had $Fo > 0.2$, making the first term approximation of the series solutions appropriate for calculating the heat storage capacity of the internal mass. The time constant for each surface was then calculated as in Equation C-8.

$$\tau = \frac{L_c^2}{\alpha * \zeta_1} \quad (C-8)$$

Where ζ_1 was a constant and was taken from Table C-2. The total heat storage capacity was calculated according to Equation C-9.

$$Q_o = \rho CV(T_i - T_\infty) \quad (C-9)$$

Where ρ and C were the density and specific heat of the material, respectively, T_i was the initial temperature of the mass, and T_∞ was the ambient temperature. The heat released from the thermal mass at any time, t (in seconds), was then calculated as in Equation C-10.

$$Q = Q_o \left(1 - \frac{\sin(\zeta_1)}{\zeta_1} * C_1 e^{-\zeta_1^2 * Fo} \right) \quad (C-10)$$

The total heating contribution from the building's thermal mass was calculated by summing the heating energy from each thermally massive building surface from hour to hour. The result of this summation is shown in Figure C-1.

Table C-2 provides the necessary constants for performing the calculations in Equation C-6 through Equation C-10.

Bi	ζ_1	C₁
0.2	0.4328	1.0311
0.25	0.4801	1.0382
0.3	0.5218	1.0450
0.4	0.5932	1.0580
0.5	0.6533	1.0701
0.6	0.7051	1.0814
0.7	0.7506	1.0919
0.8	0.7910	1.1016
0.9	0.8274	1.1107
1	0.8603	1.1891
2	1.0769	1.1795

Table C-2: Values of ζ_1 and C_1 for the 1st term approximation of heat transfer in a plane wall [Incropera 2001].

Table C-3 summarizes the characteristics of each building surface, as well as the Bi , τ , and Q_o that were calculated for each. The Fo varied with time and is not shown. Note how $Bi > 0.1$ for all building surfaces except the internal mass.

INTERIOR			Material Properties					Dimensions						
Surface Type	Boundary Cond.	Materials	k [W/mK]	rho [kg/m3]	Cp [J/kgK]	alpha [m2/sec]	Lc [m]	A heat transfer [m2]	V [m3]	h [W/m2K]	Ti-Tinf [°C]	Biot	Tau [hrs]	Qo [MJ]
Office South - Bomb Shelter North	Wall	symmetric about the center 50 cm HW Concrete	1.73	2243	837	9.21E-07	0.25	468.8	117	7.7	2	1.11	24	440
Office East - Gym West	Wall	abiatatic surfaces on inside of brick and concrete 20 cm Concrete	1.73	2243	837	9.21E-07	0.2	65.2	13	7.7	2	0.89	18	49
		11 cm Brick	1.31	2083	920	6.84E-07	0.11	65.2	7	7.7	2	0.65	9	27
Gym South - Locker Room North	Wall	symmetric about the center 20 cm HW Concrete	1.73	2243	837	9.21E-07	0.1	130.6	13	7.7	2	0.45	8	49
1st Floor North-South Divider	Wall	abiatatic surfaces on inside of brick and concrete 11 cm Brick	1.31	2083	920	6.84E-07	0.11	698	77	7.7	2	0.65	9	294
		11 cm Brick	1.31	2083	920	6.84E-07	0.11	698	77	7.7	2	0.65	9	294
1st Floor East - Annex West	Wall	abiatatic surfaces on inside of brick and concrete 20 cm HW Concrete	1.73	2243	837	9.21E-07	0.2	91.2	18	7.7	2	0.89	18	68
		11 cm Brick	1.31	2083	920	6.84E-07	0.11	91.2	10	7.7	2	0.65	9	38
Gym East and South - 1st Floor West and North	Wall	abiatatic surfaces on inside of brick and concrete 20 cm Concrete	1.73	2243	837	9.21E-07	0.2	160	32	7.7	2	0.89	17	120
		11 cm Brick	1.31	2083	920	6.84E-07	0.11	160	18	7.7	2	0.65	9	67
Ground Ceiling - 1st Floor Floor	Ceiling/Floor	symmetric about the center 15 cm HW Concrete	1.73	2243	837	9.21E-07	0.08	3864.2	290	7.7	2	0.33	6	1088
1st Floor Ceiling - Underroof	Ceiling	abiatatic on upper surface 15 cm HW Concrete	1.73	2243	837	9.21E-07	0.15	1018	153	7.7	2	0.67	13	573
Additional Wooden Internal Mass	Other	symmetric about the center Wood	1.73	593	2510	1.16E-06	0.01	1600	20	7.7	2	0.06	1.342	60

EXTERIOR			Material Properties					Dimensions						
Surface Type	Boundary Cond.	Materials	k [W/mK]	rho [kg/m3]	Cp [J/kgK]	alpha [m2/sec]	Lc [m]	A heat transfer [m2]	V [m3]	h [W/m2K]	Ti-Tinf [°C]	Biot	Tau [hrs]	Qo [MJ]
North & South Wall, Main Building	Exterior Wall	abiatatic surfaces on inside of brick and concrete 11 cm Brick only in Main	1.31	2083	920	6.84E-07	0.11	283	31	7.7	2	0.85	9	119
West Wall, Main Building	Exterior Wall	abiatatic surfaces on inside of brick and concrete 15 cm HW Concrete	1.73	2243	837	9.21E-07	0.15	139	21	7.7	2	0.67	13	78
Ground Floor	Ground Floor	abiatatic surfaces on inside of brick and concrete Wood	1.73	2243	837	9.21E-07	0.1	2426	243	7.7	2	0.45	8	911

Table C-3: Inputs for calculating the heating energy in the thermal mass in the Steindal School.

C.2.5 Results

Figure C-1 shows the rate of decay of the amount of heat released from the thermal mass into the building. The thermal mass is assumed to begin at the occupied temperature of 20C, and is exposed to a temperature of 18°C when the interior temperature is setback to the unoccupied setpoint.

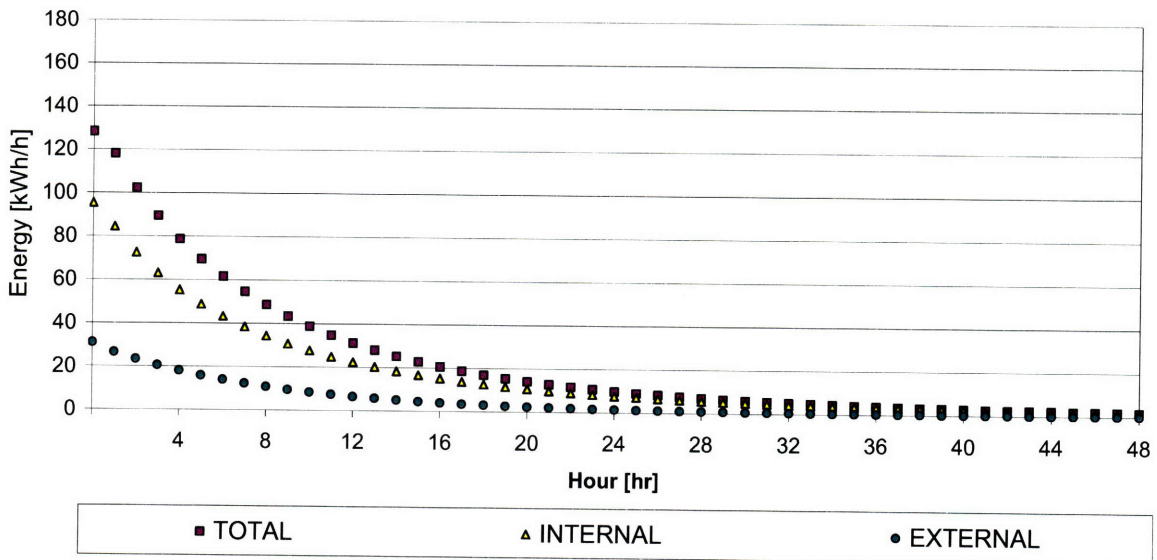


Figure C-1: Heating contribution of the internal thermal mass in the Steindal School, expressed as energy released (kWh) vs. time (hr). “INTERNAL” represents the heating contribution from internal building surfaces, while “EXTERNAL” represents the heating contribution from all exterior building surfaces. “TOTAL” is the sum of the two heating contributions.

Looking at the total energy released by the thermal mass in the building each hour, it takes more than 24 hours for the heating contribution to drop below 10kWh. During weekends in the Steindal School this would roughly coincide with Saturday evening. The implication of this result was discussed in Chapter 6.

This approximation has no direct influence on the calibration of the EnergyPlus building model; EnergyPlus calculates the influence of thermal mass dynamically within the software. However, it was useful in getting of the heating contribution from the building’s thermal mass.

C.3 Ground Heat Loss Calculation

The ASHRAE Handbook of Fundamentals [ASHRAE 2005], Chapter 32, describes a method for assessing the thermal performance of basement and slab on grade constructions. This method is a simplified calculation based on work performed by Krarti and Chuangchid [Krarti 1999] and is intended for estimating the heat transfer between the ground and basements and slab foundations. Required inputs for performing the heat transfer calculation in this method include the thermal resistances of the basement and slab materials, the thermal properties of the soil, the geometry of the building foundation, and the indoor and outdoor temperatures.

Three surfaces abutted the ground in the Steindal School: the east wall of the Gym on the ground level, the south wall of the Bomb Shelter on the ground level, and the ground floor slab. The two walls had similar constructions and were accounted for as a single surface. Consequently, two ground surfaces were accounted for in the ground heat transfer calculation that was performed.

According to the ASHRAE Handbook of Fundamentals, the annual heat transfer between the building and the ground was calculated as:

$$Q_{annual} = \frac{(q_{mean} + q_{amp}) * 8760}{1000} \quad (C-11)$$

where Q_{annual} is the heat loss (kWh) from the foundation over the course of the year, q_{mean} is the average heat loss or gain from the building (W), q_{amp} is the amplitude of the heat loss or gain in the building (W), 8,760 accounts for the 8,760 hours in the year, and 1,000 is a conversion factor. The required information for performing the calculation of Q_{annual} are given in Table C-3. These values were appropriate for the conditions at the Steindal School.

	Floor, Main & Annex	Main Building Wall, South & East
Conductivity of the Soil, k_s [W/mK]	1.21	1.21
Thermal Diffusivity of Soil, α_s [m ² /sec]	4.47E-07	4.47E-07
Thermal Resistance of Insulation (R_i) [m ² K/W]	1.43	0.00
Thermal Resistance of Concrete Slab (R_f) [m ² K/W]	0.06	0.69
Average Outdoor Temperature, $T_a = T_{out,ave}$ [°C]	6.50	6.50
Average indoor temperature, $T_r = T_{in,ave}$ [°C]	18.60	10.00
Annual temperature amplitude, T_{amp} [°C]	13.50	13.50
Height of Wall, B (zero for slabs) [m]	0.00	0.30
Length, L [m]	118.30	114.75
Width, W [m]	20.50	3.18
Area, A [m ²]	2425.15	364.91
Perimeter [m]	277.60	235.86
A/P [m]	8.74	1.55

Table C-4: Inputs for ground heat transfer calculation [ASHRAE 2005].

Then the equations required to calculate Q_{annual} were as follows:

$$U_o = \frac{k_s}{(A/P)_b} \quad (C-12)$$

Where k_s is the soil conductivity, $(A/P)_b$ is the area to perimeter ratio for the wall and slab configuration was given in Table C-4.

$$b_{eff} = \frac{B}{(A/P)_b} \quad (C-13)$$

Where B is the basement depth (B = 0 for slab on grade configurations).

$$R_{eq} = R_f + R_i \quad (C-14)$$

Where R_i is the resistance of insulation in the floor or wall construction, R_f is the resistance of the concrete in the floor or wall construction, and R_{eq} is the equivalent resistance of the floor or wall construction.

$$H_b = \frac{(A/P)_b}{k_s R_{eq}} \quad (C-15)$$

$$(A/P)_{eff,b,mean} = [1 + b_{eff}(-0.4 + e^{-H_{b,mean}})](A/P)_b \quad (C-16)$$

$$(A/P)_{eff,b,amp} = (1 + b_{eff} e^{-H_{b,amp}})(A/P)_b \quad (C-17)$$

$$G = k_s R_{eq} \sqrt{\frac{\omega}{\alpha_s}} \quad (C-18)$$

Where ω is the angular resistance and is equal to $1.992 \cdot 10^{-7}$ rad/sec, α_s is the thermal diffusivity of the soil and is taken as $4.47 \cdot 10^{-7}$ m²/s, as per Table C-4.

$$H_{mean} = \frac{(A/P)_{eff,b,mean}}{k_s R_{eq}} \quad (C-19)$$

$$H_{amp} = \frac{(A/P)_{eff,b,amp}}{k_s R_{eq}} \quad (C-20)$$

$$D_{mean} = \ln \left[(1 + H_{mean}) \left(1 + \frac{1}{H_{mean}} \right)^{H_{mean}} \right] \quad (C-21)$$

$$D_{amp} = \ln \left[(1 + H_{amp}) \left(1 + \frac{1}{H_{amp}} \right)^{H_{amp}} \right] \quad (C-22)$$

The effective mean and amplitude heat transfer coefficients for calculating the heat loss to the ground were then equal to:

$$U_{eff,mean} = m U_o D_{mean} \quad (C-23)$$

$$U_{eff,amp} = a U_o D_{amp}^{0.16} G^{-0.6} \quad (C-24)$$

Where **m** and **a** were defined in the ASHRAE Handbook of Fundamentals [ASHRAE 2005] for horizontal and vertical insulation placements.

And the mean heat loss per hour was equal to:

$$q_{mean} = U_{eff,mean} A (T_{in,ave} - T_{out,ave}) \quad (C-25)$$

$$q_{amp} = U_{eff,amp} A T_{amp} \quad (C-26)$$

$$q(\theta) = q_{mean} + q_{amp} \quad (C-27)$$

Multiplying by 8760 hours per year, and dividing by 1000W/kW, the total annual heat loss was calculated as:

$$q(\theta) = \frac{(q_{mean} + q_{amp}) * 8760}{1000} \quad (C-27)$$

Inputting the specifications from Table C-4 into Table C-5 for the floor and basement walls of the Steindal School:

	Floor: Main & Annex	Main Building Wall, South & East
U_o	0.14	0.78
$(A/P)_{mean}$	8.74	1.47
$(A/P)_{amp}$	8.74	1.59
H_b	4.85	1.85
b_{eff}	0.00	0.19
G	1.20	0.56
R_{eq}	1.49	0.69
H_{mean}	4.85	1.77
H_{amp}	4.85	1.91
D_{mean}	2.67	1.81
D_{amp}	2.67	1.87
m	0.40	0.40
a	0.25	0.25
U_{mean}	0.15	0.57
U_{amp}	0.04	0.31
Q_{mean} (W)	4349	723
Q_{amp} (W)	1187	1512
q (W)	5536	2235
Q_{total} , Annual (kWh)	48494	19581
Q_{TOTAL} (kWh)	68075	

Table C-5: Calculation of ground heat transfer in the Steindal School.

The total energy transferred from the school to the ground was estimated to be 68,075 kWh/year.

References

- [Arentz 2007] Conversations with Jørgen Arentz of the Trondheim Municipality, Trondheim, Norway, February-September, 2007
- [AS MOE 1997] Measurements by AS Moe, ventilation contractor, 1997. Taken from documents at the Steindal School, accessed February-April 2007 (In Norwegian)
- [ASHRAE 1997] ASHRAE Handbook of Fundamentals, American Society of Heating, Refrigerating, and Air-Conditioning Engineers, Atlanta, GA: 1997
- [ASHRAE 2005] ASHRAE Handbook of Fundamentals, American Society of Heating, Refrigerating, and Air-Conditioning Engineers, Atlanta, GA: 2005
- [ASHRAE 14 2002] Reeves, G. et al (2002) ASHRAE Guideline 14-2002: Measurement of energy and demand savings American Society of Heating, Refrigerating, and Air-Conditioning Engineers, Atlanta, GA: 2002
- [ASHRAE 62 2004] ASHRAE 62.1-2004: Ventilation for Acceptable Indoor Air Quality, American Society of Heating, Refrigeration and Air Conditioning Engineers, Atlanta, GA: 2004
- [BE 2008a] Technical Building Codes, National Office of Building Technology and Administration, accessed January 2008. Available at: www.be.no (In Norwegian)
- [BE 2008b] Energi07, National Office of Building Technology and Administration, accessed January 2008. Available at: www.be.no (In Norwegian)

- [Bioforsk 2007] Norwegian Institute for Agricultural and Environmental Research (Bioforsk), accessed February-March, 2007. Available at: www.bioforsk.no (In Norwegian)
- [Bou Saada 1995] Bou Saada, T. Haberl, J. (1995) "A weather-daytyping procedure for disaggregating hourly end-use loads in an electrically heated and cooled building from whole-building hourly data" *IECEC Paper No. ES-197 ASME* 1995, p349-355.
- [Box 2005] Box, George E.P., Hunter, Stuart, Hunter, William G., (2005) "Statistics for experimenters: design, discovery, and innovation" John Wiley and Sons Hoboken, NJ
- [Christensen 2003] Christensen, Craig, Stoltenberg, B., Barker, G. (2003) "An Optimization of building thermal design and control by multi-criterion genetic algorithm." *Proceedings of ISEC 2003*, Hawaii, USA, 2003, p93-100
- [De Wilde 2004] De Wilde, P. and van der Voorden, M. (2004) "Providing computational support for the selection of energy saving building components" *Energy and Buildings*, v36, p749-758
- [De Wit 2002] De Wit, S. and Augenbroe, G. (2002) "Analysis of uncertainty in building design evaluations and its implications" *Energy and Buildings* v34, p951-958
- [DEER 2005] DEER Database, accessed March 2008: www.energy.ca.gov/deer
- [DHV 2006] "Norway: The Passive House" Created by DHV as part of the European Promotion of European Passive House (PEP) project. Available at: <http://www.europeanpassivehouses.org/>
- [EC 2008] European Commission Homepage, External Relations, Norway, accessed January 2008. Available at: http://ec.europa.eu/external_relations/norway/

- [EC Dahls 2007] EC Dahls Homepage, accessed January 2007. Available at: www.ecde.no
- [EERE 2008a] Simulation Tools Directory, *United States Department of Energy*, accessed January, 2008. Available at: www.eere.energy.gov/building/tools_directory
- [EERE 2008b] “How to Buy Energy-Efficient Fluorescent Tube Lamps”, *U.S. Department of Energy*, accessed June, 2007. Available at: www1.eere.energy.gov/femp/pdfs/fluor_lamps.pdf
- [EPlus 2007a] EnergyPlus Input/Output Manual, *University of Illinois and the University of California*, 2007, accessed January 2008. Available at: <http://www.energyplus.gov>
- [EPlus 2007b] EnergyPlus website, *United States Department of Energy*, accessed January 2008. Available at: <http://www.energyplus.gov>
- [EPlus 2007c] EnergyPlus Auxiliary Programs, *University of Illinois and the University of California*, 2007. Accessed January 2008
- [EPlus 2007d] EnergyPlus Engineering Reference, *University of Illinois and the University of California*, 2007. Accessed January 2008
- [EPlus 2007e] EnergyPlus Materials Database, *University of Illinois and the University of California*, 2007, accessed January 2008. Available at: <http://www.energyplus.gov>
- [EN13779 2004] Ventilation for non-residential buildings. Performance requirements for ventilation and room-conditioning systems, EN Standards: EN13779:2004, Published June, 2005.

- [Engblom 2006] Engblom et al. (2006) “Scenario Analysis of Retrofit Strategies for Reducing Energy Consumption in Norwegian Office Buildings” Masters Thesis, Massachusetts Institute of Technology, 2006.
- [ENOVA 2007] Enova website: www.enova.no, accessed May 2007
- [ENOVA 2005] “Bygningsnettverkets Energistatistikk 2005” *ENOVA Bygningsnettverk*, ENOVA Rapport 2005. (In Norwegian)
- [Entra 2007] Entra Energi: www.entra.no, accessed February 2007 (In Norwegian).
- [EPBD 2008NO] *Norwegian Building Energy Directive*, accessed January 2008. Available at: www.bygningsenergidirektivet.no (In Norwegian).
- [EPBD 2006] Energy performance of buildings - Assessment of energy use and definition of energy ratings, *CEN, prEN 15203/15315*, Brussels, 2006.
- [EPBD 2002] Directive 2002/91/EC of the European parliament and of the council of 16 December 2002 on the energy performance of buildings, *Official Journal of the European Communities*, 2002.
- [Factbook 2008a] CIA World Factbook (2008) “Norway”, accessed January 2008. Available at: <https://www.cia.gov/library/publications/the-world-factbook/geos/no.html>
- [Factbook 2008b] CIA World Factbook (2008) “Rank Order - GDP - per capita”, accessed January 2008, Available at: <https://www.cia.gov/library/publications/the-world-factbook/rankorder/2004rank.html>

- [FDV 2007] FDV-nøkkelen, *HolteProsjekt*, accessed May 2007. Available from www.holtebyggsafe.no (In Norwegian).
- [Fürbringer 1995] Fürbringer, J.M., Roulet, C.A. (1995) "Comparison and Combination of Factorial and Monte-Carlo Design in Sensitivity Analysis" *Building and Environment* v30 p505-519
- [Fürbringer 1999] Fürbringer, J.M., Roulet, C.A. (1999) "Confidence in simulation results: put a sensitivity analysis module in your MODEL. The IEA-ECBCS Annex 23 experience of model evaluation" *Energy and Buildings* v30 p61-71.
- [GenOpt 2004] GenOpt webpage: <http://gundog.lbl.gov/GO/>, accessed August 2007.
- [GoogleMaps 2007] GoogleMaps: www.maps.google.com, accessed December 2007.
- [Gorgolewski 1995] Gorgolewski, M. (1995) "Optimizing renovation strategies for energy conservation in housing" *Building and Environment* v30, p583-589.
- [Griffith 2007] Conversations with Brent Griffith, June 2007
- [GST 2007] Quote from Eriki Eklund, *GST Group*, May, 2007.
- [Gustafsson 2001] Gustafsson, S.I.(2001) "Optimal fenestration retrofits by use of MILP programming technique" *Energy and Buildings* v33 p843-851.
- [Gustavsen 2007] Gustavsen, A. (2007), "Heat Insulation, windows, air tightness and measures for increasing the energy efficiency", Lecture, Norwegian University of Science and Technology, unpublished.

- [Hansen 2007] Conversations with Geir Hansen, Facilities Manager, Norwegian University of Science and Technology, May 2007.
- [Hanssen 2007] Hanssen, S.O. (2007), "Indoor Environment Guidelines and Recommendations", Lecture, Norwegian University of Science and Technology, unpublished.
- [Harhoff 2006] Harhoff, J. Mathews, E.H. (2006) "A Monte Carlo method for thermal building simulations" *Energy and Buildings* v38 p1395-1399.
- [Hestnes 2007a] Hestnes, Anne Grete (2007) "Sustainable Buildings", Lecture, Norwegian University of Science and Technology, unpublished.
- [Hestnes 2007b] PowerPoint provided by Professor Anne Grete Hestnes, Accessed February 2007.
- [Hobber 2007] Conversations with Mats Hobber, manager of schools for the Trondheim Municipality, February 2007.
- [Holte 2007] HolteProsjekt Building Construction Cost Database Software
HolteProjekt:2007. Available at: www.holtebyggsafe.no (In Norwegian).
- [Incropera 2001] Incropera, Frank P. and Dewitt, David P., "Fundamentals of heat and mass transfer, 5th ed." John Wiley and Sons, USA:2001.
- [IPMVP 2002] International Performance Measurement and Verification Protocol: Concepts and Options for Determining Energy and Water Savings, Volume 1 International Performance Measurement & Verification Protocol Committee, U.S. Department of Energy, USA:2002.

- [Jokisalo 2007] Jokisalo, J. and Kurnitski, J. (2007) "Performance of EN ISO 13790 utilization factor heat demand calculation method in a cold climate" *Energy and Buildings* v39, p236-247.
- [Krarti 1999] Krarti, M. and Chuangchid, P. (1999) "Cooler floor heat gain for refrigerated structures" Final Report, ASHRAE Research Project TRP-953
- [Kringstad 2007] Conversations with Bård Kringstad, teacher at the Steindal School, February through March, 2007.
- [Lam 1996] Lam, J.C., Hui, S.C.M. (1996) "Sensitivity Analysis of Energy Performance of Office Buildings" *Building and Environment* v31, p27-39.
- [Liu 1960] Liu, B. Y. H., and Jordan, R.C. (1960) "The Interrelationship and Characteristic Distribution of Direct, Diffuse and Total Solar Radiation," *Solar Energy*, v4, p1-19.
- [Lomas 1992] Lomas, K.J., Eppel, H. (1992) "Sensitivity analysis techniques for building thermal simulation programs" *Energy and Buildings*, v19, p21-44.
- [Macdonald 1999] Macdonald I A, Clarke J A and Strachan P. (1999) "Assessing Uncertainty in Building Simulation", *Proceedings of Building Simulation 1999*, Kyoto, Japan, p683-690.
- [Målfrid 2007] Conversations with Rustad Målfrid at Trondheim Energi, September 2007.
- [Means Ass. 2007] Assemblies Cost Data/RS Means, Kingston, MA: RS Means 2007.

- [Means Fac. 2007] Facilities Maintenance and Repair Cost Data//RS Means, Kingston, MA: RS Means 2007.
- [Means LC 2007] Light Commercial Cost Data//RS Means, Kingston, MA: RS Means 2007.
- [Means Mech. 2007] Mechanical Cost Data//RS Means, Kingston, MA: RS Means 2007.
- [Means SF 2007] Square Foot Cost Data//RS Means, Kingston, MA: RS Means 2007.
- [MET 2007] Norwegian Meteorological Institute climate database: www.met.no, accessed February and March 2007 (In Norwegian).
- [Municipality 2007a] As-built building documents provided by the Trondheim Municipality, accessed February-May, 2007.
- [Municipality 2007b] Heat recovery effectiveness measurements from the Trondheim Municipality, accessed February – March 2007 and September 2007.
- [Myhre 2000] Myhre, Lars (2000) “Towards Sustainability in the Residential Sector: A Study of the Future of Energy Use in the Norwegian Dwelling Stock” *Norwegian Building Research Institute:2000*
- [NBI Walls 2006] Norwegian Guidelines for Retrofitting Existing Concrete and Masonry Building Walls, University of Alaska at Fairbanks, 2006. Available at: www.uaf.edu/ces/publications/freepubs/HCM-01553.pdf
- [NBI Roof 2006] Norwegian Guidelines for Retrofitting Building Roofs, University of Alaska at Fairbanks, 2006. Available at: www.uaf.edu/ces/publications/freepubs/HCM-01552.pdf

- [NBI Floor 2006] Norwegian Guidelines for Retrofitting Building Floors and Foundations, University of Alaska at Fairbanks, 2006. Available at: www.uaf.edu/ces/publications/freepubs/HCM-01555.pdf
- [Nesje 2007] Conversations with Arne Nesje of SINTEF Buildings and Infrastructure, May 2007.
- [Noren 1998] Noren, C., Pyrko, J. (1998) "Typical load shapes for Swedish schools and hotels" *Energy and Buildings*. v28, p145-157.
- [Norford 1994] Norford, L.K., Socolow, R.H., Hseih, E.S., Spadaro, G.V. (1994) "Two-to-one discrepancy between measured and predicted performance of a 'low-energy' office building: insights from a reconciliation based on DOE-2 model" *Energy and Buildings*, v21, p121-131.
- [Norges-Bank 2008] Norges Bank: www.norges-bank.no, accessed March, 2007.
- [NREL 1995] Short, W., Packey, D., Holt, T. (1995) "A Manual for the Economic Evaluation of Energy Efficiency and Renewable Energy Technologies." *National Renewable Energy Laboratory*, Golden, CO.
- [NS3031 1987] NS3031: Thermal Insulation: Calculation of the energy and power demand for heating and ventilation in buildings Standard Norge, 1987 (In Norwegian).
- [NS3031 2007] NS3031: Calculation of energy performance of buildings, Method and Data Standard Norge, 2007 (In Norwegian).
- [NVP 1997] Measurements by Norske Ventilasjon Produkts, ventilation contractor, in 1997. Taken from documents at the Steindal School, accessed February-April 2007 (In Norwegian).

- [Pan 2006] Pan, Y., Huang, Z., Wu, G. (2006) "Calibrated building energy simulation and its application in a high-rise commercial building in Shanghai" *Energy and Buildings*, v.39, p351-357
- [Pedrini 2002] Pedrini, A., Westphal, F.S., Lamberts, R. (2002) "A methodology for building energy modeling and calibration in warm climates" *Building and Environment*, v.37, p903-912.
- [Petersdorff 2005] Petersdorff, C. et al. "Cost-Effective Climate Protection in the EU Building Stock", Report by ECOFYS and EURIMA, Germany: 2005
- [Pilkington 2007] Pilkington glass datasheet, taken from documents at the Steindal School, accessed February-April, 2007.
- [Reddy 2006] Reddy, A.T., Maor, I. (2006) "RP-1051: Procedures for Reconciling Computer-Calculated Results With Measured Energy Data" American Society of Heating, Refrigerating, and Air-Conditioning Engineers, Atlanta, GA:2006
- [Reddy 2000] Reddy, T.A., Claridge, D.E. (2000) 'Uncertainty of "Measured" Energy Savings from Statistical Baseline Models.' *HVAC&R Research*, v.6, p.3-20.
- [Rivås 1996] Ventilation layout from Rivås, ventilation contractor, in 1996. Taken from documents at the Steindal School, accessed February-April 2007 (In Norwegian).
- [Saltelli 2004] Saltelli, A. (2004) "Sensitivity analysis in practice: a guide to assessing scientific models", Wiley, Hoboken, NJ:2004.
- [Sartori 2008a] PhD work by Igor Sartori, Norwegian University of Science and Technology, 2008.

- [Sartori 2008b] Sartori, I. and Wachenfeldt, B. (2008) "Case study on retrofit of a Norwegian school: possible to achieve the passive house standard?" Proceedings of the PassivHus Norden Conference, Trondheim, Norway, April 2008.
- [Schild 2004] Schild, Peter (2004) "Air-to-Air Heat Recovery in Ventilation Systems", AIVC Ventilation Information Paper. Available at: www.aivc.org.
- [Simmonsens 2007] Conversations with Gunnar Simmonsens, manager of the Steindal School, February-April 2007.
- [SINTEF 2007] SINTEF: www.sintef.no, accessed March, 2007.
- [Skjennald 2007] Correspondence with Margareth Skjennald, secretary at the Steindal School, February-August 2007.
- [Soebarto 1997] Soebarto, V.I. (1997) "Calibration of hourly energy simulations using hourly data and monthly utility records for two case study buildings" *Proceedings of building simulation '97*, Prague:1997, p411-419.
- [Statbank 2007] Statistics Norway, Statbank: <http://statbank.ssb.no//statistikbanken/>, accessed December, 2007 (In Norwegian).
- [Statsbygg 2007] Statsbygg: www.statsbygg.no, accessed May, 2007.
- [Steindal 2007] As-built building documents provided by the Steindal School, accessed February-May, 2007.
- [Tamburrini 2003] Tamburrini, M., Palmer, D., Macdonald, I. (2003) "Calibrating Models for Simulation Use in Design Practices" *Proceedings of the Eighth International IBPSA Conference* Eindhoven, Netherlands:2003, p1273-1278.

- [TEV 2007a] District heating statistics from Trondheim Energi: www.tev.no, accessed January, 2008 (In Norwegian).
- [TEV 2007b] Trondheim Energi Website: www.tev.no, accessed February, 2007 (In Norwegian).
- [Thiel 1971] Thiel, H (1971) "Principles of Econometrics" *John Wiley & Sons*, New York:1971
- [UAF 2007] Seifert, Richard D. (2007) "Building in Alaska: Tips on Insulating an Existing House", University of Alaska at Fairbanks, 2007. Available at: www.uaf.edu/ces/publications/freepubs/EEM-04452.pdf
- [Waltz 2000] Waltz, J.P. (2000) "Computerized building energy simulation handbook" *Fairmont Press*, Lulburn, GA:2000.
- [Wang 2006] Wang, Fan (2006) "Modeling sheltering effects of trees on reducing space heating in office buildings in a windy city" *Energy and Buildings*, v.38, p1443-1454.
- [Westphal 2005] Westphal, F.S., Lampberts, R. (2005) "Building Simulation Calibration Using Sensitivity Analysis Building Simulation" *IBPSA Conference 2005* Montreal, Canada, p1331–1338.
- [Wigenstad 2005] Wigenstad, T., Holge Dokka, T., Pettersen, T.D., Myhre, L., (2005) "Energimerking av næringsbygg", SINTEF Report. Available at: <http://www.bygningsenergidirektivet.no/> (In Norwegian).
- [Yoon 2003] Yoon, J. Lee, E.J., Claridge, D.E. (August, 2003) "Calibrated Procedure for Energy Performance Simulation of a Commercial Building" *Journal of Solar Energy Engineering*, v.125, p251-257

[Zhiel-Abegg 2008] Data from Zhiel-Abegg, fan manufacturer: www.ziehl-abegg.com, accessed February-April 2007.

[Zhu 2006] Zhu, Y. (2006) "Applying computer-based simulation to energy auditing: A case study" *Energy and Buildings*, v.38, p421-428.